Universidade da Coruña

Doctoral Thesis

A general formulation for computational design of grounding systems in underground electrical substations

Author:

Raquel Guizán Roca

Supervisors:

Dr. José París López
Dr. Ignasi Colominas Ezponda

Programa de doctorado en Ingeniería Civil
Febrero 2018

Abstract

Electricity has become an essential element in our lives, which is necessary in our daily routine to do basic tasks as work or communicate. This makes the correct supply of electricity a fundamental issue. One of the elements in charge of the electricity supply is the electrical substations. As a consequence of the considerable population growth in cities and the increasing demand for power and power supply have caused the construction of new electrical substations in urban areas. However, this construction has become in a challenge because of factors as the limited availability of space or the cost of urban land. Consequently, engineers developed the underground electrical substations, which consist of compact solutions buried in the ground.

A key element to keep in mind in electrical substations is safety, especially during a fault condition. Grounding systems are the devices in charge of guaranteeing the proper functioning of electrical substations and the safety conditions for people in these situations. The correct design and analysis of grounding grids have become an essential procedure in the underground electrical substations, since they are located in urban areas. A grounding grid is mainly characterised by the ground resistance, the ground potential rise, and the step, touch and mesh voltages.

In this thesis a general formulation to design and analyse properly grounding systems of underground electrical substations has been developed, which allows to represent a realistic soil structure in order to calculate with a good accuracy their main parameters. The function of a grounding system is to carry and dissipate the fault electric current into the ground, causing the appearance of potential gradients within and around substations. To achieve the formulation, the physical phenomenon of a fault current derivation into the ground through a grounding system was study by means of the Maxwell's Equations. Thus, a mathematical approach based on the steady-state behaviour of the general equations of electromagnetism has been carried out in order to model this derivation of electric current. The procedure to obtain this mathematical model was to study each conductive domain that formed the soil structure, a uniform soil and a non-homogeneous finite volume, as if they were separated from each other, and then coupled for their resolution. After that, two systems of equations defined by potential functions are obtained, which are related between them by the compatibility conditions applied on the surface of the enclosure. To achieve a problem which can be solved by numerical techniques, the mathematical approach was recast into three boundary integral equations by means of the concepts of potential theory. The nu-

merical technique chosen to solve these boundary integral equations is the Boundary Element Method (BEM), since it is the appropriate method to solve the governing equations proposed to model the electric current derivation to an infinity domain like the ground. Before applying this technique, the strong form of the boundary integral equations are reformulated in their weak form from which accurate approximate solutions can be calculated by means of the weighted residual methods. Thus, two numerical approaches are carried out to solve the boundary integral equations, one based on the Point Collocation and other on the Bubnov-Galerkin Method. The results obtained from the resolution of both numerical approaches allows to calculate the values of the leakage current densities emanating from the surface of the grounding grid to the ground, as well as the current densities and electric potential distributions on the substation enclosure. Therefore, the electrical potential at any point in the ground can be calculated, and so the earth surface potential distribution. Then, from this surface distribution, the main parameters that characterised a grounding system can be calculated.

Finally, the general formulation developed is applied to analyse grounding systems for real underground electrical substations. The model shows excellent results for these analyses and proves that the formulation allows to calculate the main parameters of these facilities with good accuracy.

Contents

List of Figures

List of Tables

Chapter 1

Introduction

1.1 Motivation

Since electricity was introduced into technology in the early 1800s, it has become a basic element in our lives. The discovery of electricity, and the subsequent studies and inventions, changed and are still changing and improving our lifestyle. Nowadays, electricity is necessary to do many tasks in our daily routine and it is indispensable to work, communicate, transport or even cook. Thus, nowadays, we cannot imagine the world without it.

At present, the electric power industry is in charge of supplying electricity to industrial, commercial and residential areas. It is principally formed by three activities: generation, which produces electricity from sources of primary energy; transmission, which allows delivering the electricity produced to the consumption areas; and distribution, which carries electricity from the transmission systems to consumers.

On the interface between these activities there is an essential element which makes possible the electricity supply system, the electrical substations. But technically, *what is an electric substation?* According to several definitions proposed in [IEEE 100, 2000], an electrical substation is: "An area or group of equipment containing switches, circuit breakers, buses, and transformers for switching power circuits and to transform power from one voltage to another or from one system to another".

In general, three kinds of substations can be differentiated: the step-up substations, which raise the voltage circuit with the purpose to transmit electricity more efficiently; the step-down substations, which reduce the voltage circuit from transmission lines to subtransmission voltage; and the distribution substations, which reduce the subtransmission voltage to one lower that can be used to supply industrial, commercial and residential needs by the distribution activity. Normally, the step-up substations are near to power plants and far away from residential areas, and the step-down and distribution substations are located near to consumption areas.

Traditionally, electrical substations are industrial units located above ground that require large areas of land for their electrical equipment (Figure 1.1). Among their characteristics, it can be underlined that they are unsightly and noisy, and they usually present permanent environmental impacts over their location.

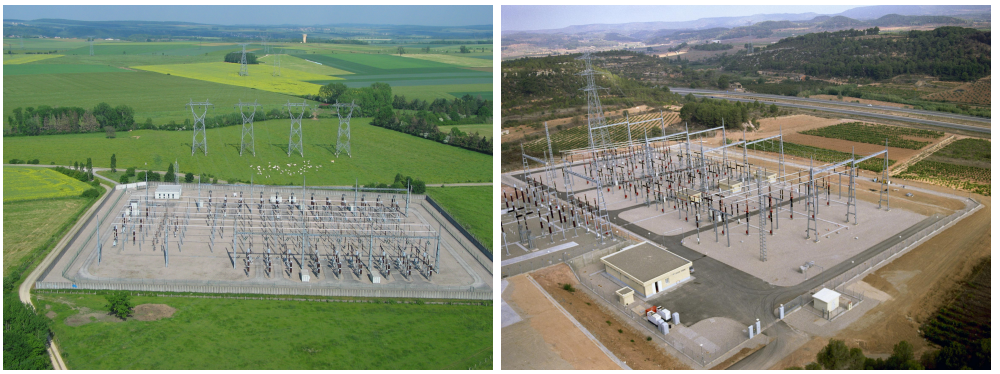

Figure 1.1. Above ground electrical substations. (Sources: blog.formatis, semi)

As it is known, the majority of electricity customers live and work at cities. In the last decades, most urban areas have experienced considerable population growth with the direct consequences of an increasing demand for power and power supply, the need to transmit electricity at high voltage levels to the bustling urban centres, and guarantee in every moment the electricity supply. Thus, in order to achieve these purposes, the construction of new electrical substations or an extension of the existing facilities is needed. However, these new substations can neither be installed in the outskirts nor be built as an extension of current substations since, with the population growth, the suburbs and industrial areas have been transformed into new residential and commercial zones. As a result, building new electrical substations in urban areas or expanding the existing installations has been converted in a challenge due to factors as the limited availability of space, the cost of land, the noise and visual restrictions, the very high security measures, or the low acceptance by citizens.

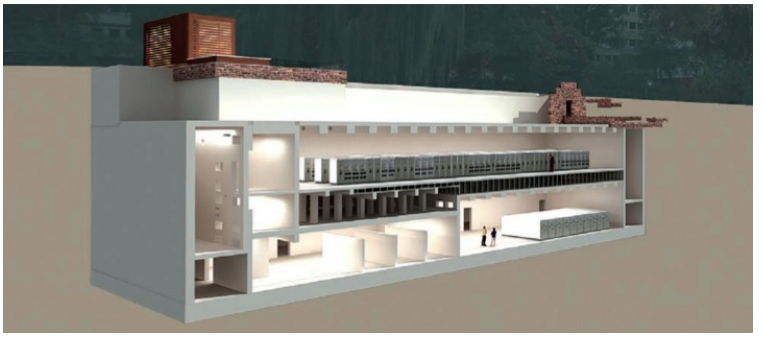

Figure 1.2. Underground electrical substation. (Source: elp)

In view of this situation, engineers developed a new design concept of substation, the underground electrical substations (Figure 1.2). In general, these substations consist of compact solutions where all electrical equipment is placed underground inside precast concrete enclosures (Figure 1.3).

(a) Prefabricated enclosure with vertical ventilation. (Source: ectricol)

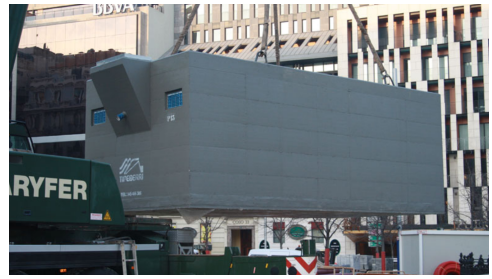

(b) Prefabricated enclosure with horizontal ventilation. (Source: tipeberri)

Figure 1.3. Undreground compact transformer substations.

An important characteristic is that they are almost unnoticeable since the area occupied above ground is minimum, which makes them suitable for zones with limited surface space. They are also almost imperceptible to general public (Figure 1.4). Therefore, the free surface area is open for other purposes such as commercial areas, parks or even residential buildings. In addition, the underground substations meet the environmental requirements since they operate silently, so their neighbourhoods can live with them peacefully.

Figure 1.4. Examples of underground compact substations in urban areas. (Sources: grupolekunbide, inst-morenoygonzalez)

It is important to note that, against traditional above ground substations, which are characterised to be unsightly, underground substations are not. The visible parts of these substations are usually the vents, especially in the vertical ventilation configurations. Even though, the precast enclosures bring the ventilation ducts with an industrial form by default, they can be designed to fit perfectly with the landscape if the surrounding architecture or scenery requires. An example is the underground

substation installed at Paternoster Square in London, in which their industrial vents where changed into a sculpture designed by Thomas Heatherwick known as Angel's Wings (Figure 1.5). This example shows that underground substations can be perfectly integrated in cities, meeting the urban restrictions, fitting with the surrounding sceneries, creating new areas with additional value for people and, what is more important, bringing the power supply into the city centres and neighbourhoods.

Figure 1.5. Cooling system of underground substation at Paternoster Square (London). (Source: heatherwick)

An essential aspect to keep in mind in electrical substations is safety, especially when fault conditions occur. During a fault condition, care must be taken to ensure the proper functioning of the electrical equipment in order to minimize faults and assure the continuity of electricity supply, as well as the safety of people in the vicinity areas. In the electrical substations, the grounding system is the one in charge of guaranteeing the safety conditions for people and the proper functioning of the facility by means of conducting the fault current into the ground.

These protection systems have always had an important role in the electrical substations. However, with the emergence of underground electrical substations and their urban character where they are surrounded by residential buildings, green areas, parks or commercial areas, the grounding systems have become an essential element to design and analyse.

1.2 Background

As it was stated, safety in electrical substations has always been a key element in order to properly design the devices while able to guarantee their functioning and security conditions. Therefore, the design and analysis of grounding systems are important steps since the fault currents in electrical substations can be quite high, as well as the damages due to these currents.

This section presents briefly what is a grounding system and their main parameters. Then, a review of the most fundamental researches and improvements in the design and analysis of grounding grids will be summarised.

1.2.1 What is a grounding system?

A grounding system, also called grounding grid, can be defined as: "A system of horizontal ground electrodes that consists of a number of interconnected bare conductors buried in the earth, providing a common ground for electrical devices or metallic structures, usually in one specific location" [IEEE 100, 2000]. In general, grids are added to ground rods and may be further connected to auxiliary ground electrodes to lower its resistance with respect to remote earth.

These systems have principally two objectives: to carry and dissipate electric currents into the ground under normal or fault conditions in order to not exceed the operating and equipment limits and affect the continuity of service, and to guarantee the security of people in the vicinity of electrical installations to avoid critical electric shocks.

The flow of the currents into the ground causes the appearance of potential gradients within and around substations. As a consequence, maximum potential gradients may appear in some areas high enough to endanger a person in the vicinity who could suffer an electric shock accident. The main sources of electric shock accidents possible are described in [IEEE Std 80, 2013]. It should be noted that the number of critical electric accidents is low since all circumstances that cause an electric shock do not usually happen at the same time. Thus, grounding grids are designed having in mind the low probabilities to cause a critical electric shock which allow to establish tolerable voltages for the safety of a person.

To this end, it is necessary to characterise the principal electrical parameters of human body involved in grounding system analysis, which can be summarised in resistance, tolerable body current limit and safety limit of potential differences. Since 1940s, several studies have investigated and identified the effects of electric shocks, as well as the limits of allowable leakage currents. Among the papers published about these studies, the following are noteworthy: [Dalziel, 1946, 1953; Kouwenhoven et al., 1959; Dalziel & Lee, 1969; Dalziel, 1972; Dawalibi et al., 1990; Freschi & Mitolo, 2017]. As a result, these investigations conclude that the effects of an electric current passing through a human body and their vital parts depend on the duration, magnitude and frequency of the current. As it might be expected, the most dangerous consequence of

electric shocks is the death, which can be caused by ventricular fibrillation, respiratory arrest or asphyxia [Lee, 1966]. Nowadays, international standards as [IEC TS 60479-1, 2016; IEC TS 60479-2, 2017] provide a basic guidance on the effects of electric shocks.

During a fault condition, mainly two electric shock situations involving a person and grounding facilities might happen. These are the foot-to-foot contact and hand-to-feet contact. The foot-to-foot contact occurs when the current flowing through the ground generates a surface potential, and consequently person's feet may come in contact with points at different potential. This difference is known as step voltage, and it is one of the main parameters that characterises grounding systems in terms of safety. In general, the step voltage is defined as the potential difference between two points on the ground's surface separated by 1 m. The hand-to-feet contact is caused by the difference generated in the potential distribution between the device and the ground when some of the current dissipated into the ground flows back to the facility. Thus, if a person, who is standing on the ground, touches the installation, a potential difference between its hand and feet occurs. This difference is called touch voltage and it is another main parameter of grounding systems. It can be defined as the potential difference between the ground potential rise (GPR) and the potential on the ground's surface where a person is standing while at the same time having a hand in contact with the electrical installation. The maximum touch voltage that is developed in the grid of the grounding system is called mesh voltage. The GPR is the maximum potential that a grounding grid may reach relative to a distant grounding point which is assumed to be at the potential of remote earth. This is another main parameter characteristic of grounding systems, which can be calculated as the product of the grid resistance and the maximum grid current. These electric shock situations are depicted in Figure 1.6, as well as the step, touch and mesh voltage.

The safe limits for these voltages are calculated using the formulas given by the standards, such as [IEEE Std 80, 2013] and [RD 337/2014, 2014] (Spanish standard), which provide guidance to design safe grounding systems. Therefore, for each grounding system analysis, the step and touch voltage values have to be checked against the maximum tolerable voltages in order to guarantee the safety of people and animals.

1.2.2 State of the art

Grounding system analysis has always been an important issue for engineers in order to properly design electrical substations and to guarantee safety conditions. As shown before, the main parameters that characterise a grounding grid are the ground potential rise, and the step, touch and mesh voltages. Since the beginning of electrical substations development, engineers have been concerned with the research and elaboration of suitable techniques to calculate these parameters.

The first steps in grounding system analysis were based on experimental and theoretical investigations which derived in analytical expressions to calculate their parameters. The first researches were focused on calculating the ground resistance. This is an important parameter since it determines the potential level of the grid when a fault

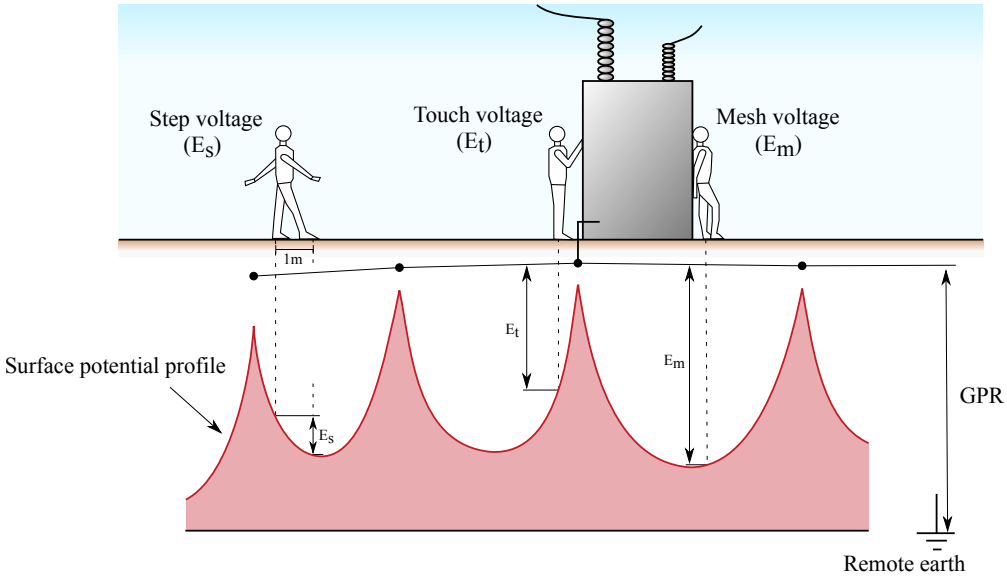

Figure 1.6. Electric shock situations. (Adapted from [IEEE Std 80, 2013])

condition occurs and it affects the fault current distribution. One of the first formulas to calculate the ground resistance were posed by [Dwight, 1936]. There, he presented some analytical expressions to calculate the ground resistance for different arrangements of ground conductors in uniform soil conditions, and their practical applications. After that work, many formulas have been proposed to calculate this parameter. Between them, it can be highlighted for their accuracy, the set of equations presented in [Schwarz, 1954] for uniform soil, which years later was improved and expanded in [Nahman & Salamon, 1984] to include two-layer soil models, and the formula proposed by [Dawalibi & Mukhedkar, 1977], based on the average potential method and valid for uniform and two-layer soil models.

The other major concern for engineers was the study of safety in grounding systems and the development of equations to establish the safe limits for potential differences based on experimental studies. In this context, noteworthy researches were presented in [Sverak et al., 1981]. In his work, Sverak described the conditions and factors encountered during a fault condition in electrical substations, and characterised the effects of an electric current passing through a human body. As a result, he posed the expressions to calculate the step and touch voltage limits. The contents of this article were included in the standard IEEE Std 80 (1986), extending and modifying the 1976 version [Sverak, 1998].

Nowadays, all expressions developed in these researches are collected in standards as [IEEE Std 80, 2013]. They provide engineers a simple and quick method to evaluate initial designs of grounding grids and a guidance to analyse and guarantee safety conditions for grounding systems.

However, these analytical and empirical formulas are unsuitable to design real grounding systems buried in complex soil structures due to their intricacy and excessive study cost. Therefore, the need arose to develop more sophisticated techniques to analyse real grounding grids with a good accuracy and which can be implemented in computers in order to improve the efficiency of grounding system analysis. One of the first computer-aided techniques was performed by Dawalibi [Dawalibi & Mukhedkar, 1976], who introduced two methods, the Multi Step method and the Iterative method, based on analytical expressions which can be implemented to calculate the ground resistance and current distribution of grounding electrodes. Based on these methods, in 1979 Dawalibi presented a study about how the length, location and number of ground rods affect the main parameters of grounding systems [Dawalibi & Mukhedkar, 1979]. This study could not be possible until that moment, since the simplified formulas were not able to describe accurately the influence of ground rods in grounding grids, especially when they are buried in two-layer soils.

After these advances, in the 90s the first computer programs for grounding systems analysis appeared [Dawalibi & Donoso, 1993; Melipoulos et al., 1993]. These computer models allow engineers not only to calculate the grounding resistance and current distributions, but also the step and touch voltages, potential distributions on the ground surface and voltage profiles, which can be plotted in 2D and 3D. The methodologies developed in these software programmes were applicable to simple or complex grounding systems buried in uniform or two-layer soil models with accuracy. Despite these models were a great advance in grounding analysis, most of them were based on semi-empirical expressions or numerical treatments in which electrodes were discretised. The effect of these segments was analysed through matrix techniques [Dawalibi & Mukhedkar, 1975]. Thus, at the end of the 90s engineers started to study and develop new techniques based on numerical methods which can tackle the problem considering the conductors and the ground rods as entire elements. These new numerical approaches are mainly based on techniques as Boundary Element Method [Colominas et al., 1999, 2007], Finite Element Method [Trlep et al., 1998; Güemes-Alonso & Hernando-Fernández, 2004; Güemes-Alonso et al., 2006], or hybrid models of these two methods [Trlep et al., 2003]. These methods allow to analyse and design grounding systems for cases with different soil properties and arbitrary arrangements and combinations of grounding grid elements. Although most approaches are based on common computational methods, semianalytical and analytical methods are still carried out [Freschi et al., 2013; Ghoneim & Shoush, 2013; Ghoneim, 2013]. There, the authors propose expressions to calculate the grounding parameters and verify the obtained results with FEM and BEM techniques.

All the methods presented until now were carried out to design grounding systems buried in uniform and two-layer soil models. In general, two-layer soils can represent with good precision the majority of real soil structures, and so the values of ground resistance, step and touch voltages obtained with these models are closer to reality than those obtained with uniform soil models. The literature shows that grounding system analysis is heavily dependent on soil structure and in some cases two-layer soil models

are not precise enough to represent it. As a result, multilayer soil models (more than two layers) were developed. The first analyses of multilayer soil structures were presented in [Dawalibi et al., 1994]. There, the authors present a parametric analysis based on the Method of Moments and the method of images. The results proved the influence of the soil structure in the parameters of grounding systems. Subsequent researches, based on the same approach, analysed the effects of soil structure in grounding analysis in depth comparing the results obtained with uniform, two-layer and multilayer soils. The results obtained confirmed the differences among the models [Ma et al., 1996; Lee et al., 1998]. Numerical approaches based on techniques as direct Boundary Element Method have also been posed to analyse grounding grids in multilayer soil models, as the formulation proposed in [Colominas et al., 2002].

The approaches presented are basically applied to horizontal soil structures; that is, the layers are located in horizontal and parallel stratums. But in some analysis, it can be interesting to represent vertical layers to model the soil structure, especially in urban areas where engineers can find constructions as underground car parks or slurry walls, and so the soil properties change in vertical stratums. In order to undertake these particularities, numerical approaches to design grounding grids were carried out [Colominas et al., 2001; Li et al., 2007].

Furthermore, soil heterogeneities can appear in some soil structures, and grounding grids can be buried near or inside these volumes. This type of soil cannot be modelled with uniform or multilayer soils, and numerical approaches are usually needed due to the geometrical shape of the outlines of heterogeneity. Thus, new approaches were carried out to obtain a good representation of these soils. The first researches considering these soil conditions were posed by Ma and Dawalibi [Ma et al., 1993]. They propose a numerical approach based on the Method of Moments to analyse grounding grids which can be buried inside or near to a heterogeneous volume having hemispherical shape, which is embedded into a uniform soil and its flat side is in contact with the air-soil interface. These models try to represent situations as depressions in soils, lakes or open mines. The results obtained for grid resistance and earth surface potential show that these heterogeneities have a significant influence on grounding designs. Years later, these researches were further extended to other geometries as cylindrical [Ma & Dawalibi, 2000] and hemispheroidal [Hajiaboli et al., 2015] soil volumes. In some soil structures, the heterogeneities can be totally embedded within soil. In [Ma & Dawalibi, 2002], the authors developed a formulation using the boundary element method to analyse grounding systems in these types of soil, which were extended in [Fortin et al., 2015] to calculate grounding grids buried in horizontal multilayer soils with finite heterogeneities located totally in one of the layers.

An example of this last soil condition is the underground electrical substations. However, any specific approach has been developed to design and analyse their grounding grids. In these facilities, in addition to calculate the ground resistance, the step and touch voltages, and the earth surface potential, it may be useful to know the voltage and current density distribution over underground enclosures with the purposes

of guaranteeing safety conditions for workers and could improve the enclosure design. Thus, these grounding systems analyses need a formulation with a realistic approximation to soil structure, a numerical approach with at least linear order interpolation to represent with a good accuracy the physical phenomenon, and be able to calculate the electrical distributions over the enclosure.

1.3 Research objective

The objective of this thesis is to carry out a mathematical and numerical formulation to design and analyse properly grounding systems for underground electrical substations. The formulation is based on the general equations of electromagnetism in order to study and simulate the phenomenon of electric current derivation to the ground through earthing grids. The particularity of the model developed is that it allows to introduce the geometrical and electrical properties of substation enclosures in a uniform soil model.

In order to achieve this aim, a series of specific objectives are needed:

- Understand the physics of the underlying problem.
- Develop a reliable model to simulate the physical phenomenon in a complex soil model.
- Define a mathematical model by means of the most appropriate techniques to recast the potential problems obtained as a result of the study of the physical phenomenon.
- Determine and develop the suitable numerical techniques to solve the problem in real time according to the characteristics of the mathematical formulation.
- Validate the computational model proposed with several test cases, and solve some real examples to verify the utility of the whole formulation.

1.4 Thesis overview

This document is organised in six chapters. Following this introduction, in Chapter 2 the mathematical equations to model the physical phenomenon of electric current derivation to ground through a grounding system are introduced. This model presents the equations for a soil structure formed by a uniform soil which contains a finite volume with different electrical properties, the underground enclosure. As a result, two potential problems with a series of boundary conditions are obtained. In Chapter 3, these potential problems are recast into a system of boundary integral equations through the application of Green's Identities. Chapter 4 describes the numerical methods chosen to solve the problem, which are based on the Boundary Element Method and the weighted residual techniques of point collocation and Bubnov-Galerkin method. In Chapter 5,

several validation examples are presented, as well as a comparison between the proposed numerical approaches, and the industrial applications. The principal application of this development is the grounding system analysis for underground electrical substations. Finally, Chapter 6 presents the conclusions and further research lines.

At the end of this document, the reader will find the appendices and the bibliographical references.

Chapter 2

Physical and Mathematical Model

2.1 Introduction

Safety has always had an important role in electrical substations. In these facilities, grounding systems are the devices required to ensure the proper functioning of electrical equipment and the safety of people and animals if a fault condition occurs. During a fault situation, grounding grid is in charge of conducting the fault current into the ground so as to dissipate it. As a consequence, this current flowing often causes potential gradients within and around the electrical substation, which can present in some areas a sufficient magnitude to endanger people and animals.

Since the early days of electrical substations, engineers have been concerned with the design and analysis of suitable grounding systems, as well as to establish limits of allowable leakage currents and potential differences in order to avoid electric shock situations. For this aim, several empirical formulas and numerical approaches were carried out to analyse these protection systems and calculate their main parameters, which are mainly the ground resistance and the step and touch voltages.

An important point in grounding analysis is to have approaches that allow to represent the soil structures where the grid is buried as realistic as possible. Thus, in order to analyse the grounding systems of underground electrical substations it is necessary to develop a formulation that represents the complexity of the soil model. In this thesis, the soil model will consist of a uniform soil which contains inside a finite volume with different electrical properties to represent the prefabricated enclosure.

In order to carry out this formulation, this chapter presents the physical model that represents the performance of grounding systems when fault conditions occur. To this end, first the general approach of the phenomenon is presented, as well as the hypotheses stated. Then, the mathematical equations that govern the problem are obtained through the application of the general equations of electromagnetism, and the formulation is simplified applying the conditions considered for conductive media.

Finally, the relation between the model results and the main parameters of grounding systems is introduced.

2.2 General approach to the problem

When a fault situation occurs in an electrical substation, the fault current originated is conducted by the grounding system into the ground, and consequently to the surrounding area of the facility producing a potential field and potential gradients. Figure 2.1 depicts this fault situation, in which an electric current, denoted as I_G, is derived from the underground electrical substation (Ω_I) to a conductor of the grounding grid (Ω_G). This electric current energizes the electrode to a potential V_G, which is the ground potential rise (GPR), and subsequently, the current densities that emanate from the conductor surface are discharged into the ground (Ω).

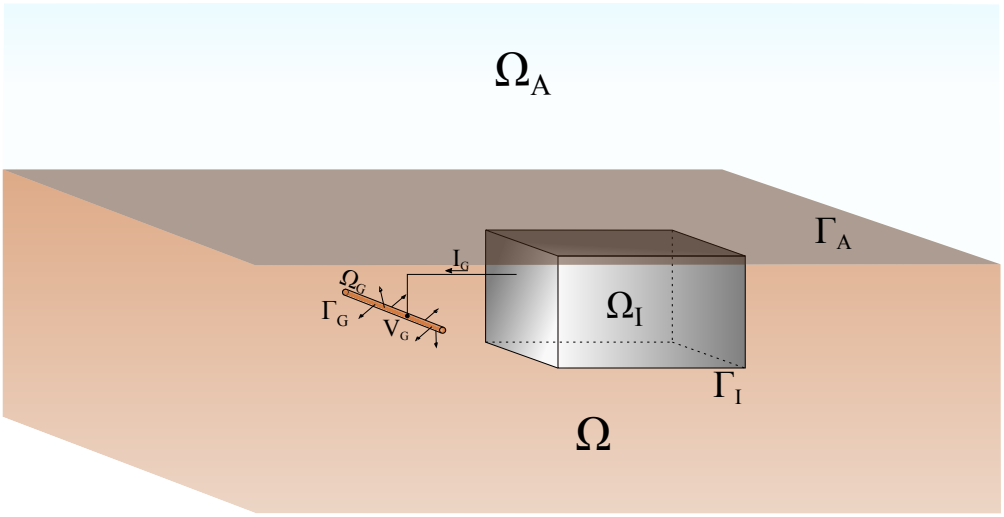

Figure 2.1. Schematic representation of the electric current transmision from a protection system to the ground.

The notation used throughout this chapter to denote the different domains and their boundaries is:

Ω 3D domain corresponding to the infinite conductive medium where the fault current is dissipated (the ground).

Ω_A 3D domain corresponding to the insulating medium (the atmosphere).

Γ_A Boundary that separates the conductive medium Ω and the insulating medium Ω_A (the ground surface).

Ω_I 3D domain corresponding to the conductive medium embedded in Ω, with finite dimensions and equal or different electrical properties (the underground electrical substation).

Γ_I Boundary that surrounds the finite conductive medium Ω_I (the underground electrical substation surface).

Ω_G 3D domain corresponding to the generator medium of electric current (the grounding grid).

Γ_G Boundary that surrounds the generator medium Ω_G (the grounding grid surface).

The main parameters that characterise a grounding system are mainly the grid resistance, the step, touch and mesh voltages, and the earth surface potential. Thus, to properly design and analyse grounding grids, it is necessary to determine their values and check that the safe limits are not exceeded.

In order to calculate these parameters for underground electrical substations, a formulation will be carried out. The developed approach will be stated according to the hypotheses that the atmosphere (Ω_A) is a perfect insulator, so its conductivity is zero, and the grounding grid (Ω_G) is formed by perfect conductors, therefore it is treated as infinitely conductive. The ground conductors will be energized with a direct current and the electromotive force ($V_G - V_0$) of the generator medium Ω_G will be assumed constant. The soil configuration has to represent the prefabricated enclosure buried inside the ground, so the developed soil model will consist of a uniform soil with a conductivity γ, that contains a finite heterogeneity with a conductivity γ_I inside. Moreover, the geometrical characteristics of the precast enclosure and the spatial arrangement and dimensions of the grounding grid will be required to analyse the grounding grids.

As a result, the developed approach will allow to obtain the leakage current densities emanating from the surface of the grounding grid to the ground (σ_G), the current densities (σ_I) between the soil and the enclosure, and the electric potential distributions on the enclosure surface (V_I). Based on these results, the ground resistance, the step and touch voltages, and the earth surface potential can be calculated. Thus, the grounding system analysis can be done.

2.3 Physical model equations

In this section the equations required to mathematically model the physical phenomenon depicted in Figure 2.1 are presented. First of all, the general equations of electromagnetism are introduced. These equations define the behaviour of an electric current flow in a 3D domain and in the boundaries which separate media with different conductivities. Afterwards, the previous equations will be characterized for the steady-state behaviour. Finally, these formulas will be used to obtain the mathematical approach to analyse grounding systems in underground electrical substations.

2.3.1 The general equations of electromagnetism

The behaviour of an electric current flow in a 3D generic domain Ω is defined by the general equations of electromagnetism, also known as Maxwell's Equations [Lorrain et al., 1988]. These are formed by four laws:

1. Gauss's Law for Electric Field, which states that the electric flux through a closed surface is proportional to the charge enclosed,

$$\mathbf{div}(\boldsymbol{E}) = \frac{q_v}{\epsilon_0} \quad \text{in} \quad \Omega \tag{2.1}$$

   where $\boldsymbol{E}$ is the electric field, q_v is the electric charge density and ϵ_0 is the vacuum permittivity ($8.8542 \cdot 10^{-12}$ [F m^{-1}]).

2. Gauss' Law for Magnetic Field, which formulates that the total magnetic flux through a closed surface is zero,

$$\mathbf{div}(\boldsymbol{B}) = 0 \quad \text{in} \quad \Omega \tag{2.2}$$

   where $\boldsymbol{B}$ is the magnetic flux density.

3. Faraday's Law of Induction, which shows that changes in the magnetic flux produce an electric field,

$$\mathbf{rot}(\boldsymbol{E}) = -\frac{\partial \boldsymbol{B}}{\partial t} \quad \text{in} \quad \Omega \tag{2.3}$$

   where t is the time.

4. Ampère's Law, which states that electric current and changes in the electric flux produce a magnetic field,

$$\mathbf{rot}(\boldsymbol{B}) = \mu_0 \left[\boldsymbol{\sigma} + \epsilon_0 \frac{\partial \boldsymbol{E}}{\partial t}\right] \quad \text{in} \quad \Omega \tag{2.4}$$

   where μ_0 is the vacuum permeability ($4\pi \cdot 10^{-7}$ [H m^{-1}]) and $\boldsymbol{\sigma}$ is the electric current density.

These are the four fundamental equations of the electromagnetism in their differential form (equations (2.1) to (2.4)).

In addition to the previous laws, the constitutive equation or Ohm's Law of electric conduction in the continuous form is needed to study this problem, which is formulated as:

$$\boldsymbol{\sigma} = \boldsymbol{\gamma}\, \boldsymbol{E} \quad \text{in} \quad \Omega \tag{2.5}$$

where the current density $\boldsymbol{\sigma}$ is related with the electric field $\boldsymbol{E}$ through the conductivity tensor $\boldsymbol{\gamma}$.

To complete Maxwell's Equations, it is necessary to introduce the conservation law of electric charge, also known as the continuity equation. This law is defined by an

expression which is obtained by combining equations (2.1) and (2.4). To do so, first the divergence of Ampère's Law (equation (2.4)) is calculated:

$$\mathbf{div}(\mathbf{rot}(\boldsymbol{B})) = \mathbf{div}(\mu_0 \left[\boldsymbol{\sigma} + \epsilon_0 \frac{\partial \boldsymbol{E}}{\partial t}\right]) \quad \text{in} \quad \Omega \tag{2.6}$$

Then, if it is accepted that $\boldsymbol{B}$ is a function of C^2 in Ω, $\mathbf{div}(\mathbf{rot}(\boldsymbol{B})) = 0$ is verified, and so the following expression is obtained:

$$0 = \mathbf{div}(\mu_0 \left[\boldsymbol{\sigma} + \epsilon_0 \frac{\partial \boldsymbol{E}}{\partial t}\right]) \quad \text{in} \quad \Omega \tag{2.7}$$

Finally, reversing the sequence of the derivatives:

$$\mathbf{div}(\boldsymbol{\sigma}) + \frac{\partial}{\partial t}\mathbf{div}(\epsilon_0 \boldsymbol{E}) = 0 \quad \text{in} \quad \Omega \tag{2.8}$$

and applying Gauss's Law for Electric Field (equation (2.1)), the continuity equation in differential form is obtained as:

$$\mathbf{div}(\boldsymbol{\sigma}) + \frac{\partial q_v}{\partial t} = 0 \quad \text{in} \quad \Omega \tag{2.9}$$

This equation shows that, whatever the circumstances, the net electric charge of a closed domain is constant.

The previous set of equations defines the behaviour of electromagnetic fields in a generic domain Ω. However, to determine the behaviour of electromagnetic fields between two domains with different electrical properties (Ω_1 and Ω_2), it is necessary to establish these equations on the interface between them ($\partial\Omega$) (Figure 2.2).

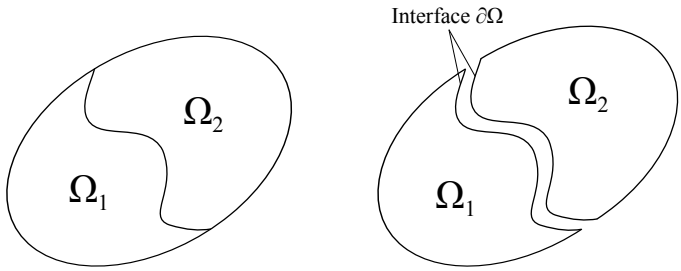

Figure 2.2. Schematic representation of a non-homogeneous region.

In order to obtain these boundary conditions, the integral form of Maxwell's Equations should be used. The integral forms are obtained through the application of the divergence theorem in equations (2.1) and (2.2) and Stoke's theorem in equations (2.3) and (2.4) [Staelin, 2011]. Therefore, Maxwell's Equations on the interface between two domains with different electrical properties are formulated as:

1. Gauss's Law for Electric Field

$$\boldsymbol{n} \cdot (\boldsymbol{E}_2 - \boldsymbol{E}_1) = \frac{q_s}{\epsilon_0} \quad \text{in} \quad \partial\Omega \tag{2.10}$$

where $\boldsymbol{n}$ is the unit vector normal to the boundary $\partial\Omega$, $\boldsymbol{E}_2$ is the electric field in Ω_2, $\boldsymbol{E}_1$ is the electric field in Ω_1 and q_s is the surface electric charge density.

2. Gauss' Law for Magnetic Field

$$\boldsymbol{n} \cdot (\boldsymbol{B}_2 - \boldsymbol{B}_1) = 0 \quad \text{in} \quad \partial\Omega \tag{2.11}$$

where $\boldsymbol{B}_2$ is the magnetic flux density in Ω_2 and $\boldsymbol{B}_1$ is the magnetic flux density in Ω_1.

3. Faraday's Law of Induction

$$\boldsymbol{n} \times (\boldsymbol{E}_2 - \boldsymbol{E}_1) = \boldsymbol{0} \quad \text{in} \quad \partial\Omega \tag{2.12}$$

4. Ampère's Law

$$\boldsymbol{n} \times (\boldsymbol{B}_2 - \boldsymbol{B}_1) = \mu_0 \boldsymbol{k} \quad \text{in} \quad \partial\Omega \tag{2.13}$$

where $\boldsymbol{k}$ is the lineal electric current density.

The same procedure should be used with the continuity equation to obtain its expression on the interface $\partial\Omega$, which after the transformation is given by

$$\boldsymbol{n} \cdot (\boldsymbol{\sigma}_2 - \boldsymbol{\sigma}_1) + \frac{\partial q_s}{\partial t} = 0 \quad \text{in} \quad \partial\Omega \tag{2.14}$$

where $\boldsymbol{\sigma}_2$ is the electric current density in Ω_2 and $\boldsymbol{\sigma}_1$ is the electric current density in Ω_1.

2.3.2 General equations for the hypothesis of steady-state model

In this approach, the study of fault current discharges into the ground through a grounding system will be limited to the steady-state behaviour, and so the transient period will be neglected since it is extremely short in comparison with the fault duration [IEEE Std 80, 2013]. The steady-state behaviour allows to decouple Maxwell's Equations and to study the electric phenomenon isolated from the magnetic one. Thus, the general equations of electromagnetism introduced in Subsection 2.3.1 are reformulated for the steady-state behaviour as:

- Coulomb's equations, which are formed by Gauss's Law for Electric Field (equations (2.1) and (2.10)) and Faraday's Law of Induction (equations (2.3) and (2.12)). These equations for a generic domain Ω are defined as

$$\begin{aligned} \mathbf{div}(\boldsymbol{E}) &= \frac{q_v}{\epsilon_0} \quad \text{in} \quad \Omega \\ \mathbf{rot}(\boldsymbol{E}) &= \boldsymbol{0} \quad \text{in} \quad \Omega \end{aligned} \tag{2.15}$$

and for the boundary $\partial\Omega$ between two domains with different electrical properties are

$$\begin{aligned} \boldsymbol{n}\cdot(\boldsymbol{E}_2-\boldsymbol{E}_1) &= \frac{q_s}{\epsilon_0} \quad \text{in} \quad \partial\Omega \\ \boldsymbol{n}\times(\boldsymbol{E}_2-\boldsymbol{E}_1) &= \boldsymbol{0} \quad \text{in} \quad \partial\Omega \end{aligned} \tag{2.16}$$

Note that the steady-state behaviour affects Faraday's Law, and so the equation term $\frac{\partial \boldsymbol{B}}{\partial t}$ will be equal to zero.

- Ampère's Laws, which consist of Gauss's Law for Magnetic Field (equations (2.2) and (2.11)) and Ampère's Law (equations (2.4) and (2.13)). The mathematical expressions for a generic domain Ω are

$$\begin{aligned} \mathbf{div}(\boldsymbol{B}) &= 0 \quad \text{in} \quad \Omega \\ \mathbf{rot}(\boldsymbol{B}) &= \mu_0\boldsymbol{\sigma} \quad \text{in} \quad \Omega \end{aligned} \tag{2.17}$$

and for the boundary $\partial\Omega$ between two domains with different electrical properties are

$$\begin{aligned} \boldsymbol{n}\cdot(\boldsymbol{B}_2-\boldsymbol{B}_1) &= 0 \quad \text{in} \quad \partial\Omega \\ \boldsymbol{n}\times(\boldsymbol{B}_2-\boldsymbol{B}_1) &= \mu_0\boldsymbol{k} \quad \text{in} \quad \partial\Omega \end{aligned} \tag{2.18}$$

Likewise, the steady-state behaviour affects Ampere's Law and the equation term $\frac{\partial \boldsymbol{E}}{\partial t}$ will be equal to zero.

- The continuity equation. In it, the steady-state behaviour reduces the terms $\frac{\partial q_v}{\partial t}$ and $\frac{\partial q_s}{\partial t}$ in equations (2.9) and (2.14), and so the continuity equation for a generic domain Ω and for the interface $\partial\Omega$ between two different domains are given by

$$\begin{aligned} \mathbf{div}(\boldsymbol{\sigma}) &= 0 \quad \text{in} \quad \Omega \\ \boldsymbol{n}\cdot(\boldsymbol{\sigma}_2-\boldsymbol{\sigma}_1) &= 0 \quad \text{in} \quad \partial\Omega \end{aligned} \tag{2.19}$$

- The constitutive equation, which for a generic domain Ω is

$$\boldsymbol{\sigma} = \boldsymbol{\gamma}\,\boldsymbol{E} \quad \text{in} \quad \Omega \tag{2.20}$$

In order to carry out a mathematical formulation that allows to perform the physical phenomenon of a fault current discharged into the ground through a grounding system, only the equations that govern the electric phenomenon are necessary. Note that in this approach the magnitudes that will be required to analyse a grounding grid are the leakage current density emanating from the grounding grid, and the current densities and electric potential on the prefabricated enclosure surface. Thus, the Ampère's Laws (equations (2.17) and (2.18)) will not be used in this development, since they are not necessary to calculate those magnitudes.

Therefore, the general equations that define the physical phenomenon of electric current derivation in a generic conductive medium and in the interface of a non-homogenous region are:

- Coulomb's equations

$$\begin{aligned} \mathbf{div}(\boldsymbol{E}) &= \frac{q_v}{\epsilon_0} \quad \text{in} \quad \Omega \\ \mathbf{rot}(\boldsymbol{E}) &= \mathbf{0} \quad \text{in} \quad \Omega \\ \boldsymbol{n} \cdot (\boldsymbol{E}_2 - \boldsymbol{E}_1) &= \frac{q_s}{\epsilon_0} \quad \text{in} \quad \partial\Omega \\ \boldsymbol{n} \times (\boldsymbol{E}_2 - \boldsymbol{E}_1) &= \mathbf{0} \quad \text{in} \quad \partial\Omega \end{aligned} \tag{2.21}$$

- The continuity equation

$$\begin{aligned} \mathbf{div}(\boldsymbol{\sigma}) &= 0 \quad \text{in} \quad \Omega \\ \boldsymbol{n} \cdot (\boldsymbol{\sigma}_2 - \boldsymbol{\sigma}_1) &= 0 \quad \text{in} \quad \partial\Omega \end{aligned} \tag{2.22}$$

- The constitutive equation

$$\boldsymbol{\sigma} = \boldsymbol{\gamma}\ \boldsymbol{E} \quad \text{in} \quad \Omega \tag{2.23}$$

2.3.3 Mathematical model of the problem

The mathematical approach to design and analyse grounding systems for underground electrical substations will be obtained by means of the application of equations (2.21) to (2.23) at each domain and boundary defined in this problem. As shown in Figure 2.1, four domains with different electrical properties can be identified in the studied physical phenomenon: the surrounding atmosphere (Ω_A), the ground (Ω), the underground electrical substation (Ω_I), and the grounding grid (Ω_G). These domains are delimited among them for three boundaries, which are the ground surface (Γ_A), the enclosure surface (Γ_I) and the conductor surfaces (Γ_G).

After the application of these equations at each domain, the following set of expressions is obtained for:
The insulating medium Ω_A (the atmosphere):

$$\mathbf{div}(\boldsymbol{E}_A) = \frac{q_{v_A}}{\epsilon_0} \quad \text{in} \quad \Omega_A \tag{2.24a}$$

$$\mathbf{rot}(\boldsymbol{E}_A) = \mathbf{0} \quad \text{in} \quad \Omega_A \tag{2.24b}$$

$$\mathbf{div}(\boldsymbol{\sigma}_A) = 0 \quad \text{in} \quad \Omega_A \tag{2.24c}$$

$$\boldsymbol{\sigma}_A = \boldsymbol{\gamma}_A\ \boldsymbol{E}_A \quad \text{in} \quad \Omega_A \tag{2.24d}$$

The conductive medium Ω (the ground):

$$\mathbf{div}(\boldsymbol{E}) = \frac{q_v}{\epsilon_0} \quad \text{in} \quad \Omega \tag{2.25a}$$

$$\mathbf{rot}(\boldsymbol{E}) = \mathbf{0} \quad \text{in} \quad \Omega \tag{2.25b}$$

$$\mathbf{div}(\boldsymbol{\sigma}) = 0 \quad \text{in} \quad \Omega \tag{2.25c}$$

$$\boldsymbol{\sigma} = \boldsymbol{\gamma}\ \boldsymbol{E} \quad \text{in} \quad \Omega \tag{2.25d}$$

The conductive medium Ω_I (the underground electrical substation):

$$\mathbf{div}(\boldsymbol{E}_I) = \frac{q_{v_I}}{\epsilon_0} \quad \text{in} \quad \Omega_I \tag{2.26a}$$

$$\mathbf{rot}(\boldsymbol{E}_I) = \mathbf{0} \quad \text{in} \quad \Omega_I \tag{2.26b}$$

$$\mathbf{div}(\boldsymbol{\sigma}_I) = 0 \quad \text{in} \quad \Omega_I \tag{2.26c}$$

$$\boldsymbol{\sigma}_I = \boldsymbol{\gamma}_I \; \boldsymbol{E}_I \quad \text{in} \quad \Omega_I \tag{2.26d}$$

The generator medium Ω_G (the grounding grid):

$$\mathbf{div}(\boldsymbol{E}_G) = \frac{q_{v_G}}{\epsilon_0} \quad \text{in} \quad \Omega_G \tag{2.27a}$$

$$\mathbf{rot}(\boldsymbol{E}_G) = \mathbf{0} \quad \text{in} \quad \Omega_G \tag{2.27b}$$

$$\mathbf{div}(\boldsymbol{\sigma}_G) = 0 \quad \text{in} \quad \Omega_G \tag{2.27c}$$

$$\boldsymbol{\sigma}_G = \boldsymbol{\gamma}_G \; \boldsymbol{E}_G \quad \text{in} \quad \Omega_G \tag{2.27d}$$

The boundary between the conductive medium Ω and the insulating medium Ω_A, Γ_A (the ground surface):

$$\boldsymbol{n} \cdot (\boldsymbol{E}_A - \boldsymbol{E}) = \frac{q_{s_A}}{\epsilon_0} \quad \text{in} \quad \Gamma_A \tag{2.28a}$$

$$\boldsymbol{n} \times (\boldsymbol{E}_A - \boldsymbol{E}) = \mathbf{0} \quad \text{in} \quad \Gamma_A \tag{2.28b}$$

$$\boldsymbol{n} \cdot (\boldsymbol{\sigma}_A - \boldsymbol{\sigma}) = 0 \quad \text{in} \quad \Gamma_A \tag{2.28c}$$

The boundary of the finite conductive medium Ω_I, Γ_I (the enclosure surface):

$$\boldsymbol{n} \cdot (\boldsymbol{E}_I - \boldsymbol{E}) = \frac{q_{s_I}}{\epsilon_0} \quad \text{in} \quad \Gamma_I \tag{2.29a}$$

$$\boldsymbol{n} \times (\boldsymbol{E}_I - \boldsymbol{E}) = \mathbf{0} \quad \text{in} \quad \Gamma_I \tag{2.29b}$$

$$\boldsymbol{n} \cdot (\boldsymbol{\sigma}_I - \boldsymbol{\sigma}) = 0 \quad \text{in} \quad \Gamma_I \tag{2.29c}$$

And the boundary between the conductive medium Ω and the generator medium Ω_G, Γ_G (the conductor surfaces):

$$\boldsymbol{n} \cdot (\boldsymbol{E}_G - \boldsymbol{E}) = \frac{q_{s_G}}{\epsilon_0} \quad \text{in} \quad \Gamma_G \tag{2.30a}$$

$$\boldsymbol{n} \times (\boldsymbol{E}_G - \boldsymbol{E}) = \mathbf{0} \quad \text{in} \quad \Gamma_G \tag{2.30b}$$

$$\boldsymbol{n} \cdot (\boldsymbol{\sigma}_G - \boldsymbol{\sigma}) = 0 \quad \text{in} \quad \Gamma_G \tag{2.30c}$$

As it was stated in Section 2.2, this approach will be formulated according to the hypotheses that the atmosphere is a perfect insulator, so its conductivity is zero ($\boldsymbol{\gamma}_A = \hat{\gamma}_A \boldsymbol{I}$, where $\hat{\gamma}_A = 0$), and the grounding grid is formed by perfect conductors, which means that it has an infinite conductivity ($\boldsymbol{\gamma}_G = \hat{\gamma}_G \boldsymbol{I}$, where $\hat{\gamma}_G \to \infty$). Introducing the first hypothesis in the constitutive equation (2.24d), it is obtained that the value of electric current density $\boldsymbol{\sigma}_A$ is zero. Therefore, it can be affirmed that

the normal component of the current density to the earth surface is zero and there is no electric current flux through the ground surface. Similarly, if the hypothesis about the grounding grid is introduced in equation (2.27d), it can be deduced that the value of field $\boldsymbol{E}_G$ have to be zero, since otherwise the electric current density $\boldsymbol{\sigma}_G$ will be enormous. As a result, it can be stated that the tangential component of the electric field $\boldsymbol{E}_G$ to the electrode surface is zero.

These hypotheses allow to decouple the equations of the ground and the underground electrical substation from the expressions related to the grounding grid and the atmosphere. Therefore, the approach can be focused on the study of fault current flowing in the conductive media.

In this problem, there are two conductive domains since the soil structure consists of a uniform soil, the ground (Ω), which has a non-homogenous finite volume inside it, the underground electrical substation (Ω_I). Thus, the procedure to obtain the mathematical model will be to study each conductive subregion as if they were separated from each other, and then the equations will be coupled for their resolution. In order to link them, it will be necessary to define the compatibility conditions on the boundary Γ_I. Next, the equations that govern each conductive medium and the compatibility conditions between them are presented.

Subregion 1: Conductive medium Ω

First, the mathematical model that performs the phenomenon of a fault current derivation to the ground (Ω) through the grounding grid (Ω_G) is obtained. Here, the ground is assumed as a uniform soil. As Figure 2.3 depicts, in this phenomenon the fault current resulting from a fault situation in an electrical substation is discharged at a point of the electrode, and consequently current densities emanate from the conductor surface (Γ_G) to the ground.

This phenomenon is mathematically defined by the set of equations presented in (2.25). The first equation (2.25a) is the Gauss's Law for Electric Field, which allows to calculate volumetric density of charges in conductive medium from electric field. For this approach, this equation is not necessary to analyse grounding systems, and so it can be neglected. The second expression (2.25b) indicates that $\boldsymbol{E}$ is a irrotational field, which means that the electric field admits a potential scalar V like $\boldsymbol{E} = -\nabla V$. This expression can be introduced into the constitutive equation (2.25d), and thus the set of equations defined for the conductive medium Ω is reduced to

$$\begin{aligned} \mathbf{div}(\boldsymbol{\sigma}) &= 0 && \text{in } \Omega \\ \boldsymbol{\sigma} &= -\boldsymbol{\gamma}\,\nabla V && \text{in } \Omega \end{aligned} \tag{2.31}$$

Figure 2.3 shows that there are two boundaries in this subregion: Γ_G and Γ_A. The equations that govern the boundary Γ_G are (2.30). These expressions can be reduced by means of the hypothesis that the grounding grid is formed by perfect conductors, which states that $\hat{\gamma}_G \to \infty$, and so $\boldsymbol{E}_G = 0$. Thus, the set of equation can be rewritten

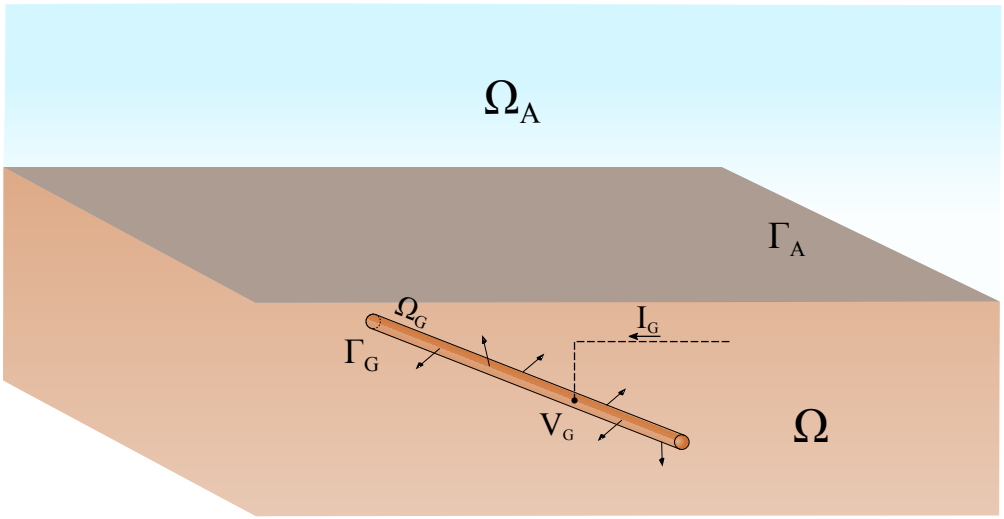

Figure 2.3. Schematic representation of the phenomenon studied in Subregion 1.

as

$$\boldsymbol{n} \cdot \boldsymbol{E} = \frac{q_{s_G}}{\epsilon_0} \quad \text{in} \quad \Gamma_G \tag{2.32a}$$

$$\boldsymbol{n} \times \boldsymbol{E} = \boldsymbol{0} \quad \text{in} \quad \Gamma_G \tag{2.32b}$$

$$\boldsymbol{n} \cdot (\boldsymbol{\sigma}_G - \boldsymbol{\sigma}) = 0 \quad \text{in} \quad \Gamma_G \tag{2.32c}$$

where equation (2.32a) can be neglected as it was done in the conductive medium Ω and the equation required to solve this problem is (2.32b), since it is focused on the study of electric current dissipation into the ground. As it was indicated previously, $\boldsymbol{E}$ is an irrotational field, and so, the boundary equation Γ_G can be restated as

$$\boldsymbol{n} \times \nabla V = \boldsymbol{0} \quad \text{in} \quad \Gamma_G \tag{2.33}$$

This equation indicates that vectors $\boldsymbol{n}$ and ∇V are parallel, and thus, the value of the potential V is constant in the electrode surface. Due to electrodes are considered perfect conductors, the value of V will be equal to the potential that is discharged at the electrode, which is the Ground Potential Rise (V_G). Therefore, this boundary condition is formulated as

$$V = V_G \quad \text{in} \quad \Gamma_G \tag{2.34}$$

The boundary Γ_A is governed by the set of equations (2.28). As it was done in Γ_G, the hypothesis that the surrounding atmosphere is a perfect insulator allows to reduce these equations since $\hat{\gamma}_A = 0$, and so $\boldsymbol{\sigma}_A = 0$. Thus, the equations for boundary Γ_A are given by

$$\boldsymbol{n} \cdot (\boldsymbol{E}_A - \boldsymbol{E}) = \frac{q_{s_A}}{\epsilon_0} \quad \text{in} \quad \Gamma_A \tag{2.35a}$$

$$\boldsymbol{n} \times (\boldsymbol{E}_A - \boldsymbol{E}) = \boldsymbol{0} \quad \text{in} \quad \Gamma_A \tag{2.35b}$$

$$\boldsymbol{n} \cdot \boldsymbol{\sigma} = 0 \quad \text{in} \quad \Gamma_A \tag{2.35c}$$

where Gauss's Law for Electric Field (equation (2.35a)) will be neglected, as previously indicated, and equation (2.35b) is not necessary to analyse the electric current dissipation into the ground. Consequently, the boundary equations in Γ_A are simplified to

$$\boldsymbol{n} \cdot \boldsymbol{\sigma} = 0 \quad \text{in} \quad \Gamma_A \tag{2.36}$$

As a result, it is obtained that the physical phenomenon of a fault current derivation to a uniform soil through a grounding grid is governed by the following set of equations

$$\mathbf{div}(\boldsymbol{\sigma}) = 0 \quad \text{in} \quad \Omega \tag{2.37a}$$

$$\boldsymbol{\sigma} = -\boldsymbol{\gamma}\, \nabla V \quad \text{in} \quad \Omega \tag{2.37b}$$

$$\boldsymbol{n} \cdot \boldsymbol{\sigma} = 0 \quad \text{in} \quad \Gamma_A \tag{2.37c}$$

$$V = V_G \quad \text{in} \quad \Gamma_G \tag{2.37d}$$

Subregion 2: Conductive medium Ω_I

Now, the second part of the problem will be analysed. Here, the phenomenon that will be mathematically modelled addresses how the current densities emanating from the grounding grid (Ω_G) to the ground (Ω) affect the non-homogeneous finite volume, which represents the precast enclosure (Ω_I).

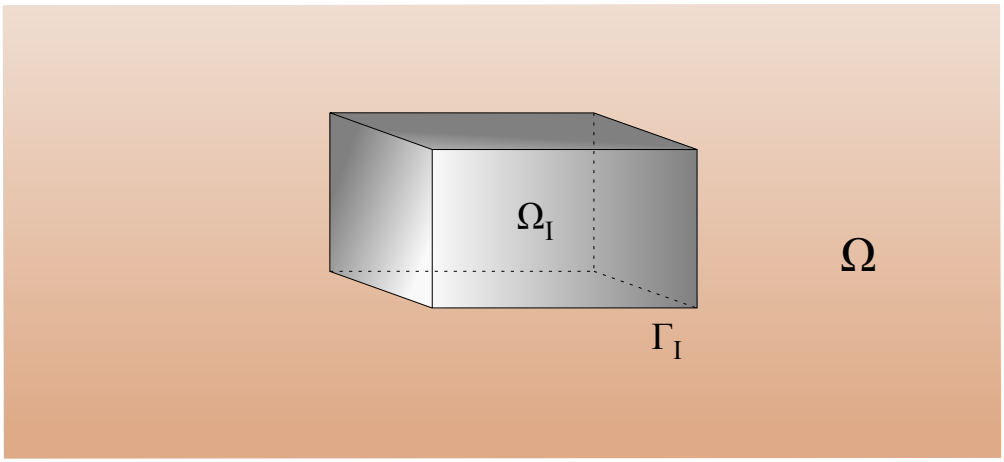

Figure 2.4. Schematic representation of Subregion 2 which is inside Subregion 1.

The equations that govern the physical phenomenon of electric current derivation in the conductive medium Ω_I have been presented in (2.26). Following the same procedure as in Subregion 1, equation (2.26a) can be neglected since it is a secondary result for

this problem and equation (2.26b) allows to state that $\boldsymbol{E}_I$ is an irrotational field, and so, it has associated a potential scalar V_I like $\boldsymbol{E}_I = -\nabla V_I$. Therefore, the equations that mathematically define the physical phenomenon in this subregion can be reduced to

$$\mathbf{div}(\boldsymbol{\sigma}_I) = 0 \qquad \text{in} \quad \Omega_I \tag{2.38a}$$

$$\boldsymbol{\sigma}_I = -\,\boldsymbol{\gamma}_I\,\nabla V_I \qquad \text{in} \quad \Omega_I \tag{2.38b}$$

Compatibility conditions: Boundary Γ_I

As Figure 2.4 shows, Γ_I is the boundary between Subregion 1 and 2, which is the enclosure surface. The expressions that govern Γ_I are defined in (2.29). Again, Gauss's Law for Electric Field will be neglected for the same reasons stated before, and so the boundary conditions Γ_I are given by

$$\boldsymbol{n} \times (\boldsymbol{E}_I - \boldsymbol{E}) = \mathbf{0} \quad \text{in} \quad \Gamma_I \tag{2.39}$$

$$\boldsymbol{n} \cdot (\boldsymbol{\sigma}_I - \boldsymbol{\sigma}) = 0 \quad \text{in} \quad \Gamma_I \tag{2.40}$$

where equation (2.39) can be rewritten as

$$\boldsymbol{n} \times (-\,\nabla V_I + \nabla V) = \mathbf{0} \quad \text{in} \quad \Gamma_I \tag{2.41}$$

since $\boldsymbol{E}$ and $\boldsymbol{E}_I$ have been previously stated as irrotational fields, and so they can be expressed as potential scalars V and V_I.

Consequently, the compatibility conditions are defined as

$$\boldsymbol{n} \times (-\,\nabla V_I + \nabla V) = \mathbf{0} \qquad \text{in} \quad \Gamma_I \tag{2.42a}$$

$$\boldsymbol{n} \cdot (\boldsymbol{\sigma}_I - \boldsymbol{\sigma}) = 0 \qquad \text{in} \quad \Gamma_I \tag{2.42b}$$

2.4 Conductive media characteristics

In grounding system analysis, the study of soil resistivity in a substation site is essential in order to determine the general soil composition and its degree of homogeneity. In this problem, there are two conductive media, and so, two different resistivities: the soil resistivity and the precast enclosure resistivity.

Rigorously, the resistivity can be mathematically represented as a tensor which assigns this parameter at different points and directions. This measure of how much the conductivity medium resists the flow of electricity affects the ground resistance and potential gradients originated due to fault situations. Therefore, an important step in the design and analysis of grounding grids is to determine the range of resistivities in the substation site and, additionally for this problem, the concrete resistivity of the underground enclosure.

In the literature, there are a number of tables showing the range of resistivities for different soils and composite materials as concrete. The simplest tabulation was

posed by [Rüdenberg, 1945]. More detailed tables can be found in standards as [IEEE Std 80, 2013] and [RD 337/2014, 2014] and in handbooks. However, sometimes more precise estimations may be required since this measure used to vary with depth. In [IEEE Std 81, 2012], a series of practical test methods and techniques for measuring soil resistivity is presented, being the most commonly used technique the Wenner four-pin method [Wenner, 1916]. The interpretation of this measure had led to a number of publications, among which the following should be highlighted: [Dawalibi & Blattner, 1984; Meliopoulos & Papalexpoulos, 1986; Nahman & Salamon, 1988; Lagace et al., 1996, 2006; Southey et al., 2015].

For this approach, the ground and the concrete of the enclosure will be assumed as isotropic and homogeneous media. Therefore, a unique value of resistivity for each medium will be considered.

2.4.1 Isotropic and homogeneous conductive medium

The assumption of considering conductive media as isotropic and homogenous allows to simplify the set of equations that govern the phenomenon presented. Thus, with the isotropic assumption the conductivity tensors can be replaced by scalar conductivities that vary only with position, $\boldsymbol{\gamma} = \hat{\gamma}\boldsymbol{I}$ and $\boldsymbol{\gamma}_I = \hat{\gamma}_I\boldsymbol{I}$. At the same time, these scalars conductivities will be substituted with the homogeneous assumption by apparent scalar conductivies, $\hat{\gamma} \to \gamma$ and $\hat{\gamma_I} \to \gamma_I$. This last assumption states that the ground and the concrete of the enclosure will have the same electric properties at every point and at every direction.

Introducing these apparent scalar conductivities in equations (2.37), (2.38) and (2.42), the mathematical approach can be rewritten as follows:

Subregion 1: Isotropic and homogeneous conductivity γ

$$\mathbf{div}(\boldsymbol{\sigma}) = 0 \qquad \text{in} \quad \Omega \tag{2.43a}$$

$$\boldsymbol{\sigma} = -\,\gamma\,\nabla V \qquad \text{in} \quad \Omega \tag{2.43b}$$

$$\boldsymbol{n}\cdot\boldsymbol{\sigma} = 0 \qquad \text{in} \quad \Gamma_A \tag{2.43c}$$

$$V = V_G \qquad \text{in} \quad \Gamma_G \tag{2.43d}$$

where equation (2.43a) and equation (2.43b) can be combined, and so, the expression that govern the phenomenon of electric current derivation in the conductive medium Ω is reduced to

$$\gamma\ \mathbf{div}(\nabla V) = 0 \quad \text{in} \quad \Omega \tag{2.44}$$

The expression $\mathbf{div}(\nabla V)$ can be formulated based on the Laplace-Beltrami operator as $\nabla^2 V = \Delta V$.

Likewise, equation (2.43a) can be substituted into the boundary equation Γ_A, and thus, equation (2.43c) is restated as

$$\boldsymbol{n}\cdot(\boldsymbol{\sigma}) = -\gamma\ \boldsymbol{n}\cdot\nabla V = 0 \tag{2.45}$$

where the assumptions allow to write it in terms of directional derivative with respect to the unit vector normal $\boldsymbol{n}$ to the boundary Γ_A.

Additionally, potential V satisfies regularity conditions at infinity since all intensity sources are enclosed in a region of space (the grounding grid) [Colominas, 1995].

Subregion 2: Isotropic and homogeneous conductivity γ_I

$$\mathbf{div}(\boldsymbol{\sigma}_I) = 0 \qquad \text{in} \quad \Omega_I \tag{2.46a}$$

$$\boldsymbol{\sigma}_I = -\,\gamma_I\,\nabla V_I \qquad \text{in} \quad \Omega_I \tag{2.46b}$$

where, as in Subregion 1, the equation that govern the physical phenomenon in the conductive medium Ω_I can be reduced if equation (2.46a) and equation (2.46b) are combined. As a result, the following equation is obtained

$$\gamma_I\ \mathbf{div}(\nabla V_I) = 0 \quad \text{in} \ \ \Omega_I \tag{2.47}$$

where $\mathbf{div}(\nabla V_I)$ can be analogously formulated as ΔV_I.

Compatibility conditions

$$\boldsymbol{n} \times (-\,\nabla V_I + \nabla V) = \mathbf{0} \qquad \text{in} \quad \Gamma_I \tag{2.48a}$$

$$\boldsymbol{n} \cdot (\boldsymbol{\sigma}_I - \boldsymbol{\sigma}) = 0 \qquad \text{in} \quad \Gamma_I \tag{2.48b}$$

where equation (2.43b) and equation (2.46b) can be introduced into the boundary expression (2.48b) which is rewritten as

$$\boldsymbol{n} \cdot (-\,\gamma_I\,\nabla V_I + \,\gamma\,\nabla V) = 0 \quad \text{in} \ \ \Gamma_I \tag{2.49}$$

It should be noted that equations (2.48a) and (2.49) are also the compatibility conditions between both subregions. These expressions are formed by three vectors: the unit vector normal $\boldsymbol{n}$ to boundary Γ_I, and the gradient vectors ∇V and ∇V_I. Taking into account that $\boldsymbol{n}$ is a non zero vector, ∇V have to be equal to ∇V_I in order to satisfy equations (2.48a) and (2.49) simultaneously. In addition, equation (2.48a) establishes that vector $(\nabla V - \nabla V_I)$ is parallel to vector $\boldsymbol{n}$, so it will satisfy the condition that the value of potential V and V_I have to be constant. Thus, the relation that V and V_I are equal and constant for every point of surface Γ_I is obtained.

Consequently, the compatibility conditions can be reduce to

$$V_I = V \quad \text{in} \ \ \Gamma_I \tag{2.50}$$

$$\boldsymbol{n} \cdot \boldsymbol{\sigma}_I = \boldsymbol{n} \cdot \boldsymbol{\sigma} \quad \text{in} \ \ \Gamma_I \tag{2.51}$$

where V_I and $\boldsymbol{\sigma}_I$ are variables that belong to Subregion 2, and V and $\boldsymbol{\sigma}$ to Subregion 1.

2.5 Horizontal ground surface

As it was presented in Chapter 1, the underground electrical substations are usually located in urban areas like streets, squares or parks, so the ground where they are installed is perfectly regularised. Therefore, the ground surface can be considered as horizontal.

This assumption allows to convert the developed approach into an equivalent one easier to solve by means of the application of the method of images [Maxwell, 1873; Lorrain et al., 1988; Colominas, 1995]. Thus, assuming that the ground surface is horizontal, the boundary equation (2.45), which belongs to the ground surface, can be replaced through the method of images. In this problem, this method will consist of reproducing symmetrically the domain Ω with all domains that are inside it (the grounding grid and the underground electrical substations) above the plane of surface Γ_A, as shown in Figure 2.5. Consequently, Ω is modified into a semi-infinite region, and so, the effort involved in solving the problem is considerably reduced. New boundary conditions will be applied over boundaries $\Gamma_G^{'}$ and $\Gamma_I^{'}$ and they will be equal to the conditions of their images boundaries.

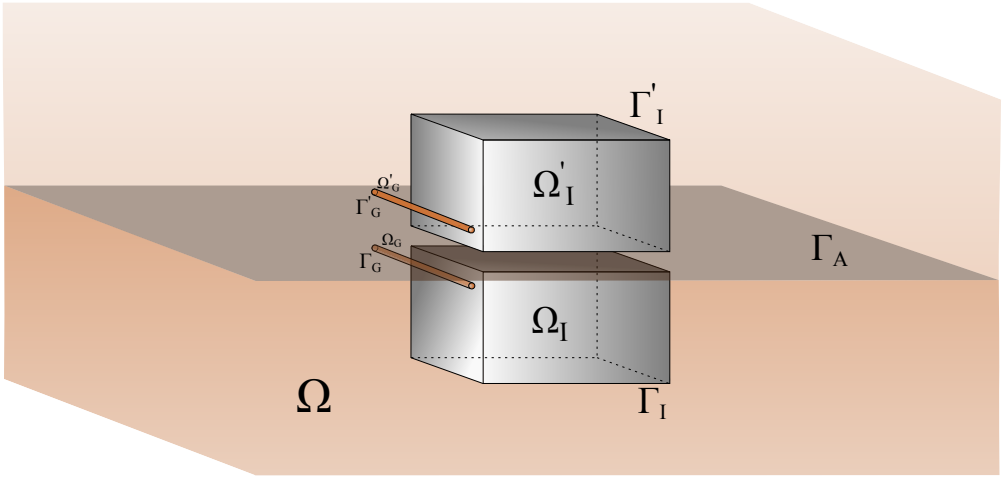

Figure 2.5. Schematic representation of the method of images

As a result, the equations that define mathematically the physical phenomenon of a fault situation in an underground electrical substation, where a fault current is conducted by the grounding grid into the ground, are given by:
An exterior Dirichlet problem in Ω with boundary conditions in Γ_G and $\Gamma_G^{'}$:

$$\boxed{\begin{array}{rcl} \Delta V & = & 0 \quad \text{in} \quad \Omega \\ V & = & V_G \quad \text{in} \quad \Gamma_G \quad \text{and} \quad \Gamma_G^{'} \end{array}} \tag{2.52}$$

where potential V satisfies regularity conditions at infinity.

Two interior problems in Ω_I and $\Omega_I^{'}$:

$$\boxed{\Delta V_I = 0 \qquad \text{in} \quad \Omega_I \quad \text{and} \quad \Omega_I^{'}} \tag{2.53}$$

And the boundary conditions in Γ_I and $\Gamma_I^{'}$, which are the compatibility conditions between the exterior and the interior problems:

$$\boxed{\begin{array}{rcl} V_I & = & V \qquad \text{in} \quad \Gamma_I \quad \text{and} \quad \Gamma_I^{'} \\ \boldsymbol{n} \cdot \boldsymbol{\sigma}_I & = & \boldsymbol{n} \cdot \boldsymbol{\sigma} \quad \text{in} \quad \Gamma_I \quad \text{and} \quad \Gamma_I^{'} \end{array}} \tag{2.54}$$

2.6 Relation between the model unknowns and the main parameters of grounding systems

The mathematical model to analyse grounding systems of underground electrical substations has been carried out throughout this chapter. This model allows to obtain the values of the leakage current densities (σ_G) emanating from the surface of the grounding grid to the ground, as well as the current densities (σ_I) and electric potential (V_I) distributions on the substations enclosure. However, from an engineering point of view, the main parameters that characterise a grounding system are the ground resistance, the step, touch and mesh voltages, and the earth surface potential distribution. Therefore, it is necessary to relate the model results with these parameters.

The ground resistance can be defined as the quotient between the Ground Potential Rise (V_G) and the maximum grid current (I_G). This grid current can be calculated by means of the leakage current densities (σ_G) integrating them on the conductor surface Γ_G:

$$I_G = \iint_{\Gamma_G} \sigma_G \, \mathrm{d}\Gamma_G \tag{2.55}$$

where $\sigma_G = \boldsymbol{n} \cdot \boldsymbol{\sigma}$ in Γ_G.

And so

$$R_G = \frac{V_G}{I_G} \tag{2.56}$$

On the other hand, after solving the problem, the electrical potential at any point in the ground can be calculated, and so it is possible to obtain the earth surface potential distribution. From this surface distribution, the step, touch and mesh voltages will be got. Thus, the step voltage will be calculated as the surface potential difference between two points separated 1 m; the touch voltage will be obtained as the difference between the Ground Potential Rise and the surface potential at a point; and, the mesh voltage is the maximum touch voltage.

Therefore, from the leakage current densities (σ_G) and the earth surface potential distribution, the main parameters of a grounding system can be obtained.

2.7 Conclusions

The proper design and analysis of grounding systems are an important step in electrical substations. In this chapter, a physical and mathematical model that performs the functioning of grounding systems of underground electrical substations has been deduced. In order to carry out this model, Maxwell's Equations, the conservation charge equation and the constitutive equation of a conductive medium have been used. First, these expressions have been obtained for a homogenous conductive domain, and then the formulas that define the behaviour of electromagnetic fields on the interface between two domains with different electrical properties have been presented. This set of equations has been simplified after considering the hypotheses of steady-state behaviour, isotropic and homogenous conductive media, horizontal ground surface, grounding grid as a perfect conductor and the atmosphere as a perfect insulator. As a result, the equations that govern the physical phenomenon that occurs during a fault situation in an underground electrical substation are obtained. This mathematical approach has been formulated as an exterior Dirichlet problem and two interior problems with the compatibility conditions between them.

The resolution of this approach allows to calculate the main parameters that characterise a grounding system, which are principally the ground resistance, the step and touch voltages, and the earth surface potential. In the next chapter, the most suitable technique to solve the proposed equations formulated by potential functions will be presented.

Chapter 3

Boundary Integral Equations of Potential Problems

3.1 Introduction

The equations that model the phenomenon of a fault current derivation into the ground through an earthing system of an underground electrical substation were presented in Chapter 2. This mathematical approach has been obtained by the application of the general equations of the electromagnetism. For this problem, these equations have been reformulated by means of the following assumptions: steady-state behaviour, isotropic and homogeneous conductive media, horizontal ground surface, and grounding grid considered as a perfect conductor, so the potential value is constant in the ground conductor surfaces. As a result, a mathematical approach formed by an exterior Dirichlet problem and two interior problems have been formulated to determine the main parameters that characterise a grounding grid.

These problems constitute a system of coupled equations that has to be solved together. For the exterior Dirichlet problem, the potential value V at any point in the ground is the unknown, which has to verify the Laplace equation in the ground domain. Its boundary conditions state that the potential value on the surface of the electrodes is constant and equal to the Ground Potential Rise (V_G), and function V satisfies regularity conditions at infinity. Likewise, in the interior problems, the unknown values are the potential V_I and the current densities σ_I at any point on the enclosure surface, which have to verify the Laplace equation in domain Ω_I. In this case, the boundary conditions in Γ_I are at the same time the compatibility conditions between the exterior and the interior problems. Such conditions indicate that at the same point of the enclosure surface the potential and current density of the exterior problem must be equal to the values of the interior problem.

This system of equations is described by potential functions which satisfy the Laplace equation. This mathematical approach can be recast as integral equations relating only boundary values, since they offer a more practical point of view for the subsequent numerical analysis. These boundary integral equations will be formulated through the application of Green's Identities, which provide the starting point to solve the potential problems by the Boundary Element Method.

This chapter presents the transformation of these potential problems into boundary integral equations. In order to achieve this objective, the basic concepts to formulate a boundary integral equation are introduced in Section 3.2, and the transformation of the differential problems into boundary integral equations in Section 3.3. These equations are summarised in Section 3.4. Finally, the boundary integral equation to calculate the potential value at any point in the ground is presented in Section 3.5.

3.2 Basic concepts

In this section, some basic concepts of potential theory used to transform the differential problems into integral equations are introduced. These will be the fundamental solution of the Laplace equation in three dimensions, the Divergence Theorem and Green's Identities, and other fundamental definitions.

3.2.1 C^k and harmonic functions

C^k functions

According to [Hughes, 1987] a C^k function can be defined as:

- Let us consider a function in an open domain: f: $\Omega \rightarrow \mathbb{R}$. The function f is said to be class C^k (let k be a non-negative integer) if the derivatives $f^{'}$, $f^{''}$,...$f^{(k}$ exist and are continuous, so function f is k-times continuously differentiable. Class C^0 indicates that a function is continuous and class C^∞ states that a function has derivatives of all orders and they are continuous.

- Let us consider a function which is bounded in the domain: $|f(x)| < \alpha$, where α is a constant for all $x \in \Omega$. If this function is a class C^k function, its nomenclature will be C_b^k.

C^k and C_b^k functions, with $k > 1$, up to ∞, are called smooth functions. If domain Ω is a closed domain instead of being an open one, the difference between C^k and C_b^k disappears, reducing to C^k functions.

Harmonic functions

As stated in [Kellogg, 1929], a real function F is said to be harmonic at a point $x \in \mathbb{R}$ if its second derivatives exist and are continuous ($F \in C^2$) and satisfy the Laplace equation $\Delta F = 0$ throughout the neighbourhood of x. Additionally, a function F is

said to be *harmonic in a domain* if it is harmonic at all the points of that domain, and F is said to be *harmonic in closed region* if it is continuous in the domain with its boundary and harmonic at all interior points of the domain. For infinite domains, a supplementary condition, which states that F satisfies regularity conditions at infinity, will be imposed.

3.2.2 Fundamental solution of the Laplace equation

The fundamental solution of the Laplace equation can be defined as a function $\phi^*(\boldsymbol{x}, \boldsymbol{y})$ at least C^2 which satisfies

$$\Delta\phi^*(\boldsymbol{x}, \boldsymbol{y}) + \delta(\boldsymbol{x} - \boldsymbol{y}) = 0, \quad \forall \boldsymbol{x},\, \boldsymbol{y} \in \mathbb{R}^3 \tag{3.1}$$

where $\delta(\boldsymbol{x}-\boldsymbol{y})$ is the Dirac Delta function, and function $\phi^*(\boldsymbol{x}, \boldsymbol{y})$ represents the response at field point $\boldsymbol{y}$ generated by a concentrated unit charge acting at point $\boldsymbol{x}$ (source point).

For a three-dimensional potential problem defined over a homogeneous and isotropic medium, the fundamental solution of the Laplace equation is

$$\phi^*(\boldsymbol{x}, \boldsymbol{y}) = \frac{1}{4\pi\, r(\boldsymbol{x}, \boldsymbol{y})} \tag{3.2}$$

where $r(\boldsymbol{x}, \boldsymbol{y})$ is the distance between the source point $\boldsymbol{x}$ and the field point $\boldsymbol{y}$.

3.2.3 Divergence Theorem and Green's Identities

Divergence Theorem and its corollaries, known as Green's Identities, are the basic concepts used to recast potential problems into integral equations. Therefore, their expressions and principal properties are presented here. The main properties of potential functions can be derived from these concepts.

Divergence Theorem

The divergence theorem, also known as Gauss's theorem, can be mathematically formulated as

$$\iiint_{\mathrm{V}} \mathbf{div}(\boldsymbol{F})\, \mathrm{dV} = \iint_{\mathrm{S}} (\boldsymbol{F} \cdot \boldsymbol{n})\, \mathrm{dS} \tag{3.3}$$

where V is a domain in $\mathbb{R}^3$ bounded by a closed surface S, $\boldsymbol{F}$ is a continuously differentiable vector field defined in V, and $\boldsymbol{n}$ is the outward unit vector normal to the boundary S.

Flux conservation for potential flows

If the vector field $\boldsymbol{F}$ is substituted for $\boldsymbol{F} = \nabla\phi$ in the Gauss's Theorem, being ϕ a harmonic function, equation (3.3) is restated as

$$\iiint_{\mathrm{V}} \mathbf{div}(\nabla\phi)\, \mathrm{dV} = \iint_{\mathrm{S}} (\nabla\phi \cdot \boldsymbol{n})\, \mathrm{dS} \tag{3.4}$$

where $\mathbf{div}(\nabla\phi)$ can be rewritten as $\Delta\phi$ and reduced to zero, since ϕ satisfies the Laplace equation.

Thus, if ϕ is a potential function, the divergence theorem can be reduced to

$$\iint_{\mathrm{S}} (\nabla\phi \cdot \boldsymbol{n})\,\mathrm{dS} = 0 \tag{3.5}$$

This expression states that, in a potential problem without internal sources, the net flux across the surface must vanish [Wrobel, 2002].

Green's first identity

The expression for Green's first identity is obtained from Gauss's Theorem by means of substituting the vector field $\boldsymbol{F}$ for a regular vector field defined as $\boldsymbol{F} = \phi\,\nabla\psi$. As a result, the equation of Green's first identity is given by

$$\iiint_{\mathrm{V}} (\nabla\phi \cdot \nabla\psi + \phi\Delta\psi)\,\mathrm{dV} = \iint_{\mathrm{S}} (\phi\,\nabla\psi \cdot \boldsymbol{n})\,\mathrm{dS} \tag{3.6}$$

where ϕ is a C^1 function defined in V, and ψ is a C^2 function defined in V.

Green's second identity

Green's second identity is obtained from Green's first identity. This identity is mathematically defined by

$$\iiint_{\mathrm{V}} (\phi\Delta\psi - \psi\Delta\phi)\,\mathrm{dV} = \iint_{\mathrm{S}} (\phi\,\nabla\psi \cdot \boldsymbol{n} - \psi\,\nabla\phi \cdot \boldsymbol{n})\,\mathrm{dS} \tag{3.7}$$

where ϕ and ψ are C^2 functions defined in V.

If ϕ and ψ are harmonic and continuously differentiable in the closed regular region V, it can be stated that:

$$\iint_{\mathrm{S}} (\phi\,\nabla\psi \cdot \boldsymbol{n} - \psi\,\nabla\phi \cdot \boldsymbol{n})\,\mathrm{dS} = 0 \tag{3.8}$$

where S is the boundary of V [Kellogg, 1929].

3.3 Boundary Integral Equations

The technique chosen to solve the potential problems deduced in Chapter 2 will consist in recasting the exterior Dirichlet problem and the interior problems to boundary integral equations (BIEs). In order to do this transformation the basic concepts presented in the previous section will be used.

Once the potential problems are formulated as integral equations, the boundary and compatibility conditions will be applied to obtain the equations that define the mathematical model.

3.3.1 Boundary integral equation of the exterior Dirichlet problem

Differential form of the exterior Dirichlet problem

The equations that govern the phenomenon of a fault current discharged into the ground (Ω) through a grounding grid (Ω_G) have been carried out in the previous chapter. These are given by

$$\begin{aligned} \Delta V &= 0 \quad \text{in} \quad \Omega \\ V &= V_G \quad \text{in} \quad \Gamma_G \quad \text{and} \quad \Gamma_G^{'} \end{aligned} \tag{3.9}$$

where V satisfies regularity conditions at infinity.

The aim of this problem is to obtain the potential field V, which is a harmonic function in Ω, since it satisfies the Laplace equation and it is a C^2 function. For domains Γ_G and $\Gamma_G^{'}$, V will be a C^1 function.

Boundary integral equation: Formulation

In order to transform the exterior Dirichlet problem into an integral equation, it is necessary to remind the concepts introduced in Section 3.2 about the fundamental solution of the Laplace equation in three dimensions, the harmonic functions and the equation of Green's second identity.

In Section 2.5, the exterior problem was reduced into an equivalent one (equation (3.9)) which is defined over a semi-infinite region Ω after introducing the assumption of horizontal ground surface and applying the method of images. Thus, this potential problem can be transformed into a boundary integral equation in which Ω is a bounded region and the regularity conditions to function V are applied on a boundary $\Gamma_{\Omega(R)}$ which is infinitely distant (Figure 3.1).

The development of the boundary integral equations for this problem starts from the expression that mathematically defined the Green's second identity (3.7). In this expression, functions ϕ and ψ will be substituted for the potential field V and the fundamental solution of the Laplace equation ϕ^*, respectively. As a result, the exterior Dirichlet problem can be written as

$$\iiint_{\Omega} (V\Delta\phi^* - \phi^*\Delta V)\,\mathrm{d}\Omega = \iint_{\Gamma_{\Omega(R)}} (V\,\nabla\phi^* \cdot \boldsymbol{n} - \phi^*\,\nabla V \cdot \boldsymbol{n})\,\mathrm{d}\Gamma_{\Omega(R)} \tag{3.10}$$

where Ω is a domain in $\mathbb{R}^3$ bounded by a closed surface $\Gamma_{\Omega(R)}$, and $\boldsymbol{n}$ is the outward unit vector normal to the boundary $\Gamma_{\Omega(R)}$.

In this equation the fundamental solution of the Laplace equation ϕ^* is singular at the source point $\boldsymbol{x}$, so it is necessary to remove this point from the domain Ω isolating it by a sphere $B(\boldsymbol{x},\epsilon)$ centred at $\boldsymbol{x}$ with a radius ϵ and a boundary $\Gamma_{B(\boldsymbol{x},\epsilon)}$. Therefore, if the source point $\boldsymbol{x}$ is removed from Ω, the integral equation (3.10) can be restated as

$$\iiint_{\Omega - B(\boldsymbol{x},\epsilon)} (V\Delta\phi^* - \phi^*\Delta V)\,\mathrm{d}\Omega = \iint_{\Gamma - \Gamma_{B(\boldsymbol{x},\epsilon)}} (V\,\nabla\phi^* \cdot \boldsymbol{n} - \phi^*\,\nabla V \cdot \boldsymbol{n})\,\mathrm{d}\Gamma \tag{3.11}$$

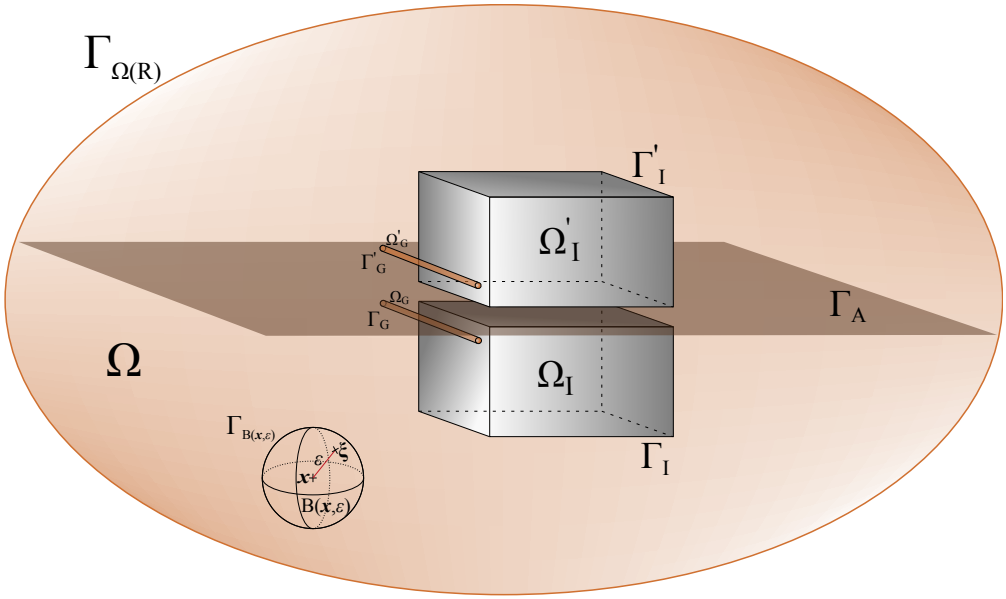

Figure 3.1. Schematic representation of the new bounded region.

where $\nabla(\bullet)\cdot\boldsymbol{n}$ represents a directional derivative.

Figure 3.1 shows that the surfaces that bound the region $\Omega - B(\boldsymbol{x},\epsilon)$ are $\Gamma_{\Omega(R)} \cup \Gamma_{B(\boldsymbol{x},\epsilon)} \cup \Gamma_G \cup \Gamma_G^{'} \cup \Gamma_I \cup \Gamma_I^{'}$, where $\Gamma_{\Omega(R)}$ is the external boundary and the rest are internal boundaries. Consequently, equation (3.11) can be split as

$$\begin{aligned}
\iiint_{\Omega - B(\boldsymbol{x},\epsilon)} (V\Delta\phi^* - \phi^*\Delta V)\,\mathrm{d}\Omega \;=\; & \iint_{\Gamma_{\Omega(R)}} (V\,\nabla\phi^*\cdot\boldsymbol{n} - \phi^*\,\nabla V\cdot\boldsymbol{n})\,\mathrm{d}\Gamma_{\Omega(R)} \\
+ & \iint_{\Gamma_{B(\boldsymbol{x},\epsilon)}} (V\,\nabla\phi^*\cdot\boldsymbol{n} - \phi^*\,\nabla V\cdot\boldsymbol{n})\,\mathrm{d}\Gamma_{B(\boldsymbol{x},\epsilon)} \\
+ & \iint_{\Gamma_G} (V\,\nabla\phi^*\cdot\boldsymbol{n} - \phi^*\,\nabla V\cdot\boldsymbol{n})\,\mathrm{d}\Gamma_G \\
+ & \iint_{\Gamma_G^{'}} (V\,\nabla\phi^*\cdot\boldsymbol{n} - \phi^*\,\nabla V\cdot\boldsymbol{n})\,\mathrm{d}\Gamma_G^{'} \\
+ & \iint_{\Gamma_I} (V\,\nabla\phi^*\cdot\boldsymbol{n} - \phi^*\,\nabla V\cdot\boldsymbol{n})\,\mathrm{d}\Gamma_I \\
+ & \iint_{\Gamma_I^{'}} (V\,\nabla\phi^*\cdot\boldsymbol{n} - \phi^*\,\nabla V\cdot\boldsymbol{n})\,\mathrm{d}\Gamma_I^{'}
\end{aligned} \tag{3.12}$$

Next, all terms of equation (3.12) will be analysed.

Volume integral $\Omega - B(\boldsymbol{x}, \epsilon)$

This integral is defined as

$$I(\boldsymbol{x}, \epsilon) = \iiint_{\Omega - B(\boldsymbol{x}, \epsilon)} (V \Delta \phi^* - \phi^* \Delta V) \, \mathrm{d}\Omega \tag{3.13}$$

Given that V and ϕ^* are defined in the domain $\Omega - B(\boldsymbol{x}, \epsilon)$ and they are harmonic functions, the volume integral is zero. This way, the original domain is recovered by taking the improper integral of equation (3.13):

$$\lim_{\epsilon \to 0} I(\boldsymbol{x}, \epsilon) = 0 \tag{3.14}$$

Boundary integral $\Gamma_{\Omega(R)}$

As it was stated, Ω is a semi-infinite region bounded by $\Gamma_{\Omega(R)}$. Thus, let $\boldsymbol{x}$ be a source point on an arbitrary location in Ω and $\Gamma_{\Omega(R)}$ be a spherical surface centred at $\boldsymbol{x}$ (Figure 3.2). Taking this into account, the first integral on the right-hand side of equation (3.12) can be formulated as

$$\begin{aligned} I(\boldsymbol{x}, R) &= \iint_{\boldsymbol{\xi} \in \Gamma_{\Omega(R)}} \Big(V(\boldsymbol{\xi}) \, \nabla \phi^*(\boldsymbol{x}, \boldsymbol{\xi}) \cdot \boldsymbol{n}(\boldsymbol{\xi}) - \phi^*(\boldsymbol{x}, \boldsymbol{\xi}) \, \nabla V(\boldsymbol{\xi}) \cdot \boldsymbol{n}(\boldsymbol{\xi}) \Big) \, \mathrm{d}\Gamma_{\Omega(R)} \\ &= \iint_{\boldsymbol{\xi} \in \Gamma_{\Omega(R)}} \Big(V(\boldsymbol{\xi}) \, \nabla \Big(\frac{1}{4\pi \, r(\boldsymbol{x}, \boldsymbol{\xi})} \Big) \cdot \boldsymbol{n}(\boldsymbol{\xi}) - \Big(\frac{1}{4\pi \, r(\boldsymbol{x}, \boldsymbol{\xi})} \Big) \nabla V(\boldsymbol{\xi}) \cdot \boldsymbol{n}(\boldsymbol{\xi}) \Big) \, \mathrm{d}\Gamma_{\Omega(R)} \end{aligned} \tag{3.15}$$

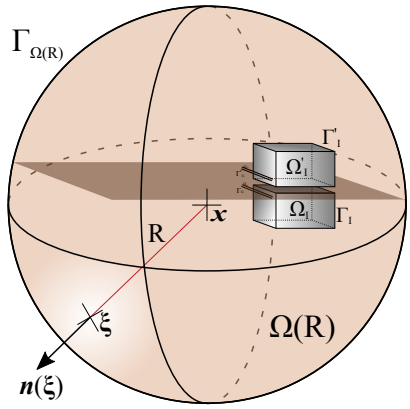

Figure 3.2. Domain of the boundary integral $\Gamma_{\Omega(R)}$.

The above expression can be written as an improper integral when R tends to infinity giving:

$$\lim_{R \to \infty} \iint_{\boldsymbol{\xi} \in \Gamma_{\Omega(R)}} \Big(V(\boldsymbol{\xi}) \, \nabla \Big(\frac{1}{4\pi \, r(\boldsymbol{x}, \boldsymbol{\xi})} \Big) \cdot \boldsymbol{n}(\boldsymbol{\xi}) - \Big(\frac{1}{4\pi \, r(\boldsymbol{x}, \boldsymbol{\xi})} \Big) \nabla V(\boldsymbol{\xi}) \cdot \boldsymbol{n}(\boldsymbol{\xi}) \Big) \, \mathrm{d}\Gamma_{\Omega(R)} \tag{3.16}$$

Thus, it can be stated that the asymptotic behaviour of the function ϕ^* in the second term of equation (3.16) is $O(r^{-1})$ and the asymptotic behaviour of the function $\nabla\phi^*$ in the first term is $O(r^{-2})$. These are the regularity conditions at infinity, so it can be asserted that the behaviour of equation (3.16) is at most $O(r^{-1})$ [Wrobel, 2002]. Consequently, the boundary integral $\Gamma_{\Omega(R)}$ is zero when R tends to infinity:

$$\lim_{R\to\infty} I(\boldsymbol{x}, R) = 0 \tag{3.17}$$

Boundary integral $\Gamma_{B(\boldsymbol{x},\epsilon)}$

This boundary integral appears due to the necessity of removing the source point $\boldsymbol{x}$ of the Laplace equation when it is singular, which means that the source point and the field point are the same. The solution proposed in the majority of books is to isolate the source point by a sphere $B(\boldsymbol{x}, \epsilon)$ centred at $\boldsymbol{x}$ with a radius ϵ and a boundary $\Gamma_{B(\boldsymbol{x},\epsilon)}$, as shown in Figure 3.3.

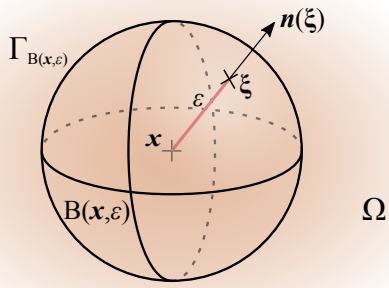

Figure 3.3. Sphere $B(\boldsymbol{x}, \epsilon)$ centred at $\boldsymbol{x}$ in the domain Ω.

In order to analyse this boundary integral, the approach proposed in the Boundary Element books [Brebbia & Dominguez, 1992; Beer, 2001; Wrobel, 2002; Liu, 2009] will be applied.

The analysed boundary integral is:

$$\begin{aligned} I(\boldsymbol{x},\epsilon) &= \iint_{\boldsymbol{\xi}\in\Gamma_{B(\boldsymbol{x},\epsilon)}} \Big(V(\boldsymbol{\xi})\ \nabla\phi^*(\boldsymbol{x},\boldsymbol{\xi})\cdot\boldsymbol{n}(\boldsymbol{\xi}) - \phi^*(\boldsymbol{x},\boldsymbol{\xi})\ \nabla V(\boldsymbol{\xi})\cdot\boldsymbol{n}(\boldsymbol{\xi})\Big)\,\mathrm{d}\Gamma_{B(\boldsymbol{x},\epsilon)} \\ &= \iint_{\boldsymbol{\xi}\in\Gamma_{B(\boldsymbol{x},\epsilon)}} \Big(V(\boldsymbol{\xi})\ \nabla\Big(\frac{1}{4\pi\, r(\boldsymbol{x},\boldsymbol{\xi})}\Big)\cdot\boldsymbol{n}(\boldsymbol{\xi}) - \Big(\frac{1}{4\pi\, r(\boldsymbol{x},\boldsymbol{\xi})}\Big)\ \nabla V(\boldsymbol{\xi})\cdot\boldsymbol{n}(\boldsymbol{\xi})\Big)\,\mathrm{d}\Gamma_{B(\boldsymbol{x},\epsilon)} \end{aligned} \tag{3.18}$$

First, the term

$$\iint_{\boldsymbol{\xi}\in\Gamma_{B(\boldsymbol{x},\epsilon)}} V(\boldsymbol{\xi})\,\nabla\Big(\frac{1}{4\pi\, r(\boldsymbol{x},\boldsymbol{\xi})}\Big)\cdot\boldsymbol{n}(\boldsymbol{\xi})\,\mathrm{d}\Gamma_{B(\boldsymbol{x},\epsilon)} \tag{3.19}$$

will be analysed.

Initially, the value $V(\boldsymbol{x})$ is subtracted from and added to the value of $V(\boldsymbol{\xi})$ to obtain

$$\begin{aligned} &\iint_{\boldsymbol{\xi}\in\Gamma_{B(\boldsymbol{x},\epsilon)}} V(\boldsymbol{\xi})\,\nabla\Big(\frac{1}{4\pi\, r(\boldsymbol{x},\boldsymbol{\xi})}\Big)\cdot\boldsymbol{n}(\boldsymbol{\xi})\,\mathrm{d}\Gamma_{B(\boldsymbol{x},\epsilon)} = \\ &= \iint_{\boldsymbol{\xi}\in\Gamma_{B(\boldsymbol{x},\epsilon)}} [V(\boldsymbol{\xi}) - V(\boldsymbol{x})]\,\nabla\Big(\frac{1}{4\pi\, r(\boldsymbol{x},\boldsymbol{\xi})}\Big)\cdot\boldsymbol{n}(\boldsymbol{\xi})\,\mathrm{d}\Gamma_{B(\boldsymbol{x},\epsilon)} \\ &+ V(\boldsymbol{x}) \iint_{\boldsymbol{\xi}\in\Gamma_{B(\boldsymbol{x},\epsilon)}} \nabla\Big(\frac{1}{4\pi\, r(\boldsymbol{x},\boldsymbol{\xi})}\Big)\cdot\boldsymbol{n}(\boldsymbol{\xi})\,\mathrm{d}\Gamma_{B(\boldsymbol{x},\epsilon)} \end{aligned} \tag{3.20}$$

Now, the second integral on the right-hand side of equation (3.20) will be calculated. To do it, it is necessary to obtain the value of the directional derivative:

$$\nabla\Big(\frac{1}{4\pi\, r(\boldsymbol{x},\boldsymbol{\xi})}\Big)\cdot\boldsymbol{n}(\boldsymbol{\xi}) = -\frac{1}{4\pi\,(r(\boldsymbol{x},\boldsymbol{\xi}))^2}\,\nabla\big(r(\boldsymbol{x},\boldsymbol{\xi})\big)\cdot\boldsymbol{n}(\boldsymbol{\xi}) \tag{3.21}$$

where $r(\boldsymbol{x},\boldsymbol{\xi})$ is the distance between the source and the field points, and $\boldsymbol{n}(\boldsymbol{\xi})$ is the outward unit vector normal to the boundary $\Gamma_{B(\boldsymbol{x},\epsilon)}$. In a sphere, the term $\nabla\big(r(\boldsymbol{x},\boldsymbol{\xi})\big)\cdot\boldsymbol{n}(\boldsymbol{\xi})$ is equal to 1. As a result, the directional derivative (3.21) is equal to

$$\nabla\Big(\frac{1}{4\pi\, r(\boldsymbol{x},\boldsymbol{\xi})}\Big)\cdot\boldsymbol{n}(\boldsymbol{\xi}) = -\frac{1}{4\pi\,(r(\boldsymbol{x},\boldsymbol{\xi}))^2} \tag{3.22}$$

The analysed integral can be written in spherical coordinates according to Figure 3.4. Thus,

$$\mathrm{d}\Gamma_{B(\boldsymbol{x},\epsilon)} = \epsilon^2 \sin(\Theta)\,\mathrm{d}\Theta\,\mathrm{d}\varphi$$

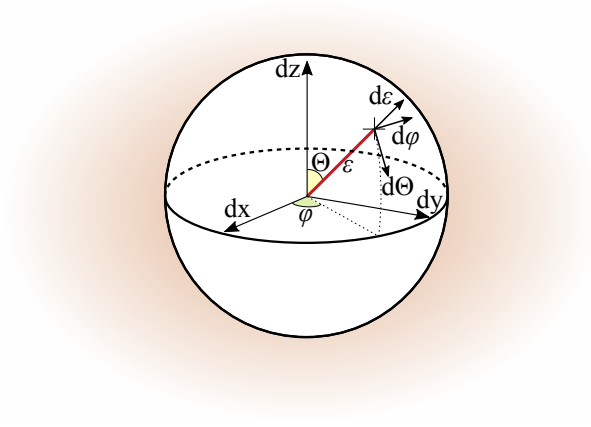

Figure 3.4. Spherical coordinates used in the boundary integral $\Gamma_{B(\boldsymbol{x},\epsilon)}$. ***In this case the sphere is totally included in the domain*** Ω***, so*** $0 \leq \Theta \leq \pi$ ***and*** $0 \leq \varphi \leq 2\pi$.

Consequently, the integral form obtained can be restated as an improper integral where ϵ tends to zero, and so the result of the term (3.19) is:

$$\lim_{\epsilon\to 0}\iint_{\boldsymbol{\xi}\in\Gamma_{B(\boldsymbol{x},\epsilon)}} \nabla\Big(\frac{1}{4\pi\, r(\boldsymbol{x},\boldsymbol{\xi})}\Big)\cdot\boldsymbol{n}(\boldsymbol{\xi})\,\mathrm{d}\Gamma_{B(\boldsymbol{x},\epsilon)} = \lim_{\epsilon\to 0}\int_0^{2\pi}\int_0^{\pi} -\frac{1}{4\pi(\epsilon)^2}\epsilon^2\sin(\Theta)\,\mathrm{d}\Theta\,\mathrm{d}\varphi$$
$$= -1 \tag{3.23}$$

Likewise, the above procedure will be used to analyse the first integral on the right-hand side of equation (3.20), where $V(\boldsymbol{x})$ is assumed as continuous. After that, the following can be stated:

$$\lim_{\epsilon\to 0}\iint_{\boldsymbol{\xi}\in\Gamma_{B(\boldsymbol{x},\epsilon)}} [V(\boldsymbol{\xi})-V(\boldsymbol{x})]\,\nabla\Big(\frac{1}{4\pi\, r(\boldsymbol{x},\boldsymbol{\xi})}\Big)\cdot\boldsymbol{n}(\boldsymbol{\xi})\,\mathrm{d}\Gamma_{B(\boldsymbol{x},\epsilon)} = 0 \tag{3.24}$$

Therefore, the results of equation (3.20) is

$$\lim_{\epsilon\to 0}\iint_{\boldsymbol{\xi}\in\Gamma_{B(\boldsymbol{x},\epsilon)}} V(\boldsymbol{\xi})\,\nabla\Big(\frac{1}{4\pi\, r(\boldsymbol{x},\boldsymbol{\xi})}\Big)\cdot\boldsymbol{n}(\boldsymbol{\xi})\,\mathrm{d}\Gamma_{B(\boldsymbol{x},\epsilon)} = -V(\boldsymbol{x}) \tag{3.25}$$

The same approach will be applied to evaluate the second term of equation (3.18), for which it is obtained after writing it in spherical coordinates and as an improper integral:

$$\begin{aligned}&\lim_{\epsilon\to 0}\iint_{\boldsymbol{\xi}\in\Gamma_{B(\boldsymbol{x},\epsilon)}} \Big(\frac{1}{4\pi\, r(\boldsymbol{x},\boldsymbol{\xi})}\Big)\nabla V(\boldsymbol{\xi})\cdot\boldsymbol{n}(\boldsymbol{\xi})\,\mathrm{d}\Gamma_{B(\boldsymbol{x},\epsilon)}\\ =&\lim_{\epsilon\to 0}\int_0^{2\pi}\int_0^{\pi}\Big(\frac{1}{4\pi\epsilon}\Big)\nabla V(\boldsymbol{\xi})\cdot\boldsymbol{n}(\boldsymbol{\xi})\;\epsilon^2\sin(\Theta)\,\mathrm{d}\Theta\,\mathrm{d}\varphi = 0\end{aligned} \tag{3.26}$$

Finally, adding the results obtained in equations (3.25) and (3.26), the boundary integral $\Gamma_{B(\boldsymbol{x},\epsilon)}$ is reduced to

$$\lim_{\epsilon\to 0} I(\boldsymbol{x},\epsilon) = -V(\boldsymbol{x}) \tag{3.27}$$

Boundary integrals Γ_G and $\Gamma_G^{'}$

The boundary integrals Γ_G and $\Gamma_G^{'}$ can be analysed at the same time, since domain $\Omega_G^{'}$ is symmetric to Ω_G due to apply the method of images, and so, they are directly related. The integral expressions are

$$I(\boldsymbol{x},\boldsymbol{\xi}_G) = \iint_{\boldsymbol{\xi}_G\,\in\,\Gamma_G}\Big(V(\boldsymbol{\xi}_G)\;\nabla\phi^*(\boldsymbol{x},\boldsymbol{\xi}_G)\cdot\boldsymbol{n}(\boldsymbol{\xi}_G) - \phi^*(\boldsymbol{x},\boldsymbol{\xi}_G)\;\nabla V(\boldsymbol{\xi}_G)\cdot\boldsymbol{n}(\boldsymbol{\xi}_G)\Big)\,\mathrm{d}\Gamma_G \tag{3.28}$$

$$I(\boldsymbol{x},\boldsymbol{\xi}_G^{'}) = \iint_{\boldsymbol{\xi}_G^{'}\,\in\,\Gamma_G^{'}}\Big(V(\boldsymbol{\xi}_G^{'})\;\nabla\phi^*(\boldsymbol{x},\boldsymbol{\xi}_G^{'})\cdot\boldsymbol{n}(\boldsymbol{\xi}_G^{'}) - \phi^*(\boldsymbol{x},\boldsymbol{\xi}_G^{'})\;\nabla V(\boldsymbol{\xi}_G^{'})\cdot\boldsymbol{n}(\boldsymbol{\xi}_G^{'})\Big)\,\mathrm{d}\Gamma_G^{'} \tag{3.29}$$

where $\boldsymbol{x}$ is a source point located in the domain Ω, and $\boldsymbol{\xi}_G$ and $\boldsymbol{\xi}_G^{'}$ are field points located on Γ_G and $\Gamma_G^{'}$ surfaces, respectively. A schematic representation of this analysis is depicted in Figure 3.5.

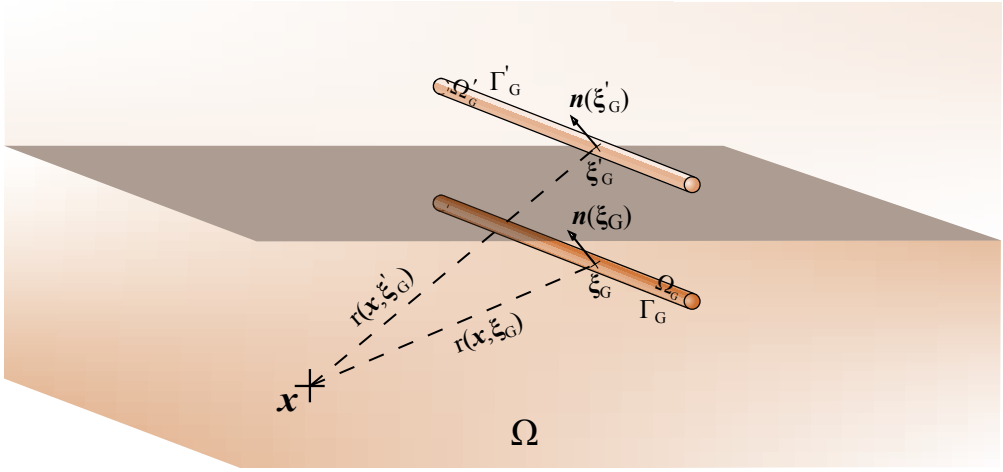

Figure 3.5. Domains of the boundary integrals Γ_G and $\Gamma_G^{'}$.

As it was previously presented, the boundary conditions of the exterior Dirichlet problem are defined as

$$\begin{aligned} V(\boldsymbol{\xi}_G) &= V_G\,, \quad \boldsymbol{\xi}_G \in \Gamma_G \\ V(\boldsymbol{\xi}_G^{'}) &= V_G\,, \quad \boldsymbol{\xi}_G^{'} \in \Gamma_G \end{aligned} \tag{3.30}$$

where V_G is a constant value that represents the Ground Potential Rise. Thus, the above expressions can be rewritten in terms of these boundary conditions as

$$\begin{aligned} I(\boldsymbol{x}, \boldsymbol{\xi}_G) = V_G \iint_{\boldsymbol{\xi}_G \in \Gamma_G} & \nabla \phi^*(\boldsymbol{x}, \boldsymbol{\xi}_G) \cdot \boldsymbol{n}(\boldsymbol{\xi}_G)\, \mathrm{d}\Gamma_G \\ - \iint_{\boldsymbol{\xi}_G \in \Gamma_G} & \phi^*(\boldsymbol{x}, \boldsymbol{\xi}_G)\ \nabla V(\boldsymbol{\xi}_G) \cdot \boldsymbol{n}(\boldsymbol{\xi}_G)\, \mathrm{d}\Gamma_G \end{aligned} \tag{3.31}$$

$$\begin{aligned} I(\boldsymbol{x}, \boldsymbol{\xi}_G^{'}) = V_G \iint_{\boldsymbol{\xi}_G^{'} \in \Gamma_G^{'}} & \nabla \phi^*(\boldsymbol{x}, \boldsymbol{\xi}_G^{'}) \cdot \boldsymbol{n}(\boldsymbol{\xi}_G^{'})\, \mathrm{d}\Gamma_G^{'} \\ - \iint_{\boldsymbol{\xi}_G^{'} \in \Gamma_G^{'}} & \phi^*(\boldsymbol{x}, \boldsymbol{\xi}_G^{'})\ \nabla V(\boldsymbol{\xi}_G^{'}) \cdot \boldsymbol{n}(\boldsymbol{\xi}_G^{'})\, \mathrm{d}\Gamma_G^{'} \end{aligned} \tag{3.32}$$

Next, the first integral on the right-hand side of equations (3.31) and (3.32) will be analysed. In these expressions ϕ^* is the fundamental solution of the Laplace equation, which is a harmonic function that satisfies the Laplace equation and is at least a C^2 function. Moreover, Γ_G and $\Gamma_G^{'}$ are the closed surfaces of the bounded domains Ω_G

and $\Omega_G^{'}$. These conditions allow to apply the property of flux conservation for potential flows (equation (3.5)), and so the integral equations are reduced to

$$\begin{aligned} I(\boldsymbol{x}, \boldsymbol{\xi}_G) &= -\iint_{\boldsymbol{\xi}_G \in \Gamma_G} \phi^*(\boldsymbol{x}, \boldsymbol{\xi}_G)\ \nabla V(\boldsymbol{\xi}_G) \cdot \boldsymbol{n}(\boldsymbol{\xi}_G)\, \mathrm{d}\Gamma_G \\ &= -\iint_{\boldsymbol{\xi}_G \in \Gamma_G} \frac{1}{4\pi\, r(\boldsymbol{x}, \boldsymbol{\xi}_G)}\ \nabla V(\boldsymbol{\xi}_G) \cdot \boldsymbol{n}(\boldsymbol{\xi}_G)\, \mathrm{d}\Gamma_G \end{aligned} \tag{3.33}$$

$$\begin{aligned} I(\boldsymbol{x}, \boldsymbol{\xi}_G^{'}) &= -\iint_{\boldsymbol{\xi}_G^{'} \in \Gamma_G^{'}} \phi^*(\boldsymbol{x}, \boldsymbol{\xi}_G^{'})\ \nabla V(\boldsymbol{\xi}_G^{'}) \cdot \boldsymbol{n}(\boldsymbol{\xi}_G^{'})\, \mathrm{d}\Gamma_G^{'} \\ &= -\iint_{\boldsymbol{\xi}_G^{'} \in \Gamma_G^{'}} \frac{1}{4\pi\, r(\boldsymbol{x}, \boldsymbol{\xi}_G^{'})}\ \nabla V(\boldsymbol{\xi}_G^{'}) \cdot \boldsymbol{n}(\boldsymbol{\xi}_G^{'})\, \mathrm{d}\Gamma_G^{'} \end{aligned} \tag{3.34}$$

As Ω_G and $\Omega_G^{'}$ are symmetric domains due to the hypothesis of horizontal ground surface (Section 2.5), it can be stated that

$$\frac{1}{r(\boldsymbol{x}, \boldsymbol{\xi}_G^{'})} = \frac{1}{r(\boldsymbol{x}^{'}, \boldsymbol{\xi}_G)} \tag{3.35}$$

Introducing this relation into equations (3.33) and (3.34), the boundary integrals Γ_G and $\Gamma_G^{'}$ can be formulated as a unique boundary integral equation defined in Γ_G, which is given by

$$I(\boldsymbol{x}, \boldsymbol{x}^{'}, \boldsymbol{\xi}_G) = -\frac{1}{4\pi} \iint_{\boldsymbol{\xi}_G \in \Gamma_G} \left(\frac{1}{r(\boldsymbol{x}, \boldsymbol{\xi}_G)} + \frac{1}{r(\boldsymbol{x}^{'}, \boldsymbol{\xi}_G)} \right) \nabla V(\boldsymbol{\xi}_G) \cdot \boldsymbol{n}(\boldsymbol{\xi}_G)\, \mathrm{d}\Gamma_G \tag{3.36}$$

In the above equation, the term $\nabla V(\boldsymbol{\xi}_G) \cdot \boldsymbol{n}(\boldsymbol{\xi}_G)$ can be formulated as the normal component of the current density $\sigma_G(\boldsymbol{\xi}_G)$. In the mathematical model of the exterior Dirichlet problem, formulated in Chapter 2, was stated that electric field $\boldsymbol{E}$ admits a potential scalar V like $\boldsymbol{E} = -\nabla V$, and the constitutive equation of electric conduction (equation (2.23)) was written as

$$\boldsymbol{\sigma} = -\gamma\ \nabla V \tag{3.37}$$

where $\boldsymbol{\sigma}$ is the current density vector, and γ is the apparent conductivity of the ground that results from considering Ω as an isotropic and homogenous medium.

If this current density vector is multiplied by an outward normal vector $\boldsymbol{n}$ to boundary Γ_G and applied at any point located on it, the normal component of the current density is obtained as:

$$\sigma_G(\boldsymbol{\xi}_G) = -\gamma\ \nabla V(\boldsymbol{\xi}_G) \cdot \boldsymbol{n}(\boldsymbol{\xi}_G) \tag{3.38}$$

where $\sigma_G(\boldsymbol{\xi}_G)$ is the leakage current density on the surface Γ_G, as Figure 3.6 shows.

Finally, after introducing the above relation into equation (3.36), the boundary integrals Γ_G and $\Gamma_G^{'}$ are reduced to the following equation

$$I(\boldsymbol{x}, \boldsymbol{x}^{'}, \boldsymbol{\xi}_G) = \frac{1}{4\pi\gamma} \iint_{\boldsymbol{\xi}_G \in \Gamma_G} \left(\frac{1}{r(\boldsymbol{x}, \boldsymbol{\xi}_G)} + \frac{1}{r(\boldsymbol{x}^{'}, \boldsymbol{\xi}_G)} \right) \sigma_G(\boldsymbol{\xi}_G)\ \mathrm{d}\Gamma_G \tag{3.39}$$

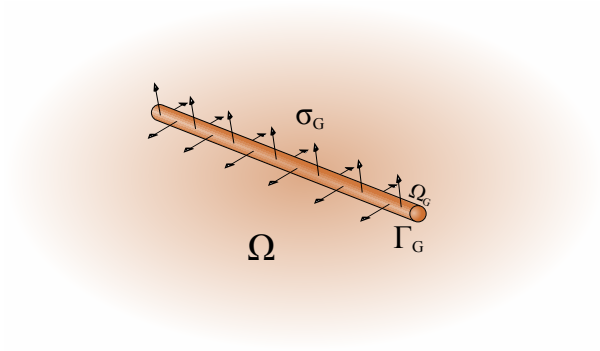

Figure 3.6. Leakage current density σ_G derivated to the ground. ***Criterion:*** *σ_G will be positive if it goes into domain Ω, and it will have the same direction of the normal vector chosen to analyse the problem.*

Boundary integrals Γ_I and $\Gamma_I^{'}$

As it was done in the previous boundary integrals, the boundary integrals Γ_I and $\Gamma_I^{'}$ will be analysed at the same time. In this case, the integral equations are given by

$$I(\boldsymbol{x},\boldsymbol{\xi}_I) = \iint_{\boldsymbol{\xi}_I \in \Gamma_I} \Big(V(\boldsymbol{\xi}_I)\ \nabla\phi^*(\boldsymbol{x},\boldsymbol{\xi}_I)\cdot\boldsymbol{n}(\boldsymbol{\xi}_I) - \phi^*(\boldsymbol{x},\boldsymbol{\xi}_I)\ \nabla V(\boldsymbol{\xi}_I)\cdot\boldsymbol{n}(\boldsymbol{\xi}_I)\Big)\,\mathrm{d}\Gamma_I \quad (3.40)$$

$$I(\boldsymbol{x},\boldsymbol{\xi}_I^{'}) = \iint_{\boldsymbol{\xi}_I^{'} \in \Gamma_I^{'}} \Big(V(\boldsymbol{\xi}_I^{'})\ \nabla\phi^*(\boldsymbol{x},\boldsymbol{\xi}_I^{'})\cdot\boldsymbol{n}(\boldsymbol{\xi}_I^{'}) - \phi^*(\boldsymbol{x},\boldsymbol{\xi}_I^{'})\ \nabla V(\boldsymbol{\xi}_I^{'})\cdot\boldsymbol{n}(\boldsymbol{\xi}_I^{'})\Big)\,\mathrm{d}\Gamma_I^{'} \quad (3.41)$$

where $\boldsymbol{x}$ is a source point located in the domain Ω, and $\boldsymbol{\xi}_I$ and $\boldsymbol{\xi}_I^{'}$ are field points located on Γ_I and $\Gamma_I^{'}$ surfaces, respectively (Figure 3.7).

Replacing the expression of the fundamental solution of the Laplace equation ϕ^* (equation (3.2)), the above integral equations are rewritten as

$$I(\boldsymbol{x},\boldsymbol{\xi}_I) = \iint_{\boldsymbol{\xi}_I \in \Gamma_I} \Big(V(\boldsymbol{\xi}_I)\ \nabla\Big(\frac{1}{4\pi\, r(\boldsymbol{x},\boldsymbol{\xi}_I)}\Big)\cdot\boldsymbol{n}(\boldsymbol{\xi}_I) - \frac{1}{4\pi\, r(\boldsymbol{x},\boldsymbol{\xi}_I)}\ \nabla V(\boldsymbol{\xi}_I)\cdot\boldsymbol{n}(\boldsymbol{\xi}_I)\Big)\,\mathrm{d}\Gamma_I \quad (3.42)$$

$$I(\boldsymbol{x},\boldsymbol{\xi}_I^{'}) = \iint_{\boldsymbol{\xi}_I^{'} \in \Gamma_I^{'}} \Big(V(\boldsymbol{\xi}_I^{'})\ \nabla\Big(\frac{1}{4\pi\, r(\boldsymbol{x},\boldsymbol{\xi}_I^{'})}\Big)\cdot\boldsymbol{n}(\boldsymbol{\xi}_I^{'}) - \frac{1}{4\pi\, r(\boldsymbol{x},\boldsymbol{\xi}_I^{'})}\ \nabla V(\boldsymbol{\xi}_I^{'})\cdot\boldsymbol{n}(\boldsymbol{\xi}_I^{'})\Big)\,\mathrm{d}\Gamma_I^{'} \quad (3.43)$$

These expressions can be reduced into a unique boundary equation on Γ_I by means of the hypothesis of horizontal ground surface, which states that Ω_I and $\Omega_I^{'}$ are symmetric (Section 2.5), and allows to assume that:

$$\begin{aligned} \frac{1}{r(\boldsymbol{x},\boldsymbol{\xi}_I^{'})} &= \frac{1}{r(\boldsymbol{x}^{'},\boldsymbol{\xi}_I)} \\ \nabla\Big(\frac{1}{r(\boldsymbol{x},\boldsymbol{\xi}_I^{'})}\Big)\cdot\boldsymbol{n}(\boldsymbol{\xi}_I^{'}) &= \nabla\Big(\frac{1}{r(\boldsymbol{x}^{'},\boldsymbol{\xi}_I)}\Big)\cdot\boldsymbol{n}(\boldsymbol{\xi}_I) \end{aligned} \quad (3.44)$$

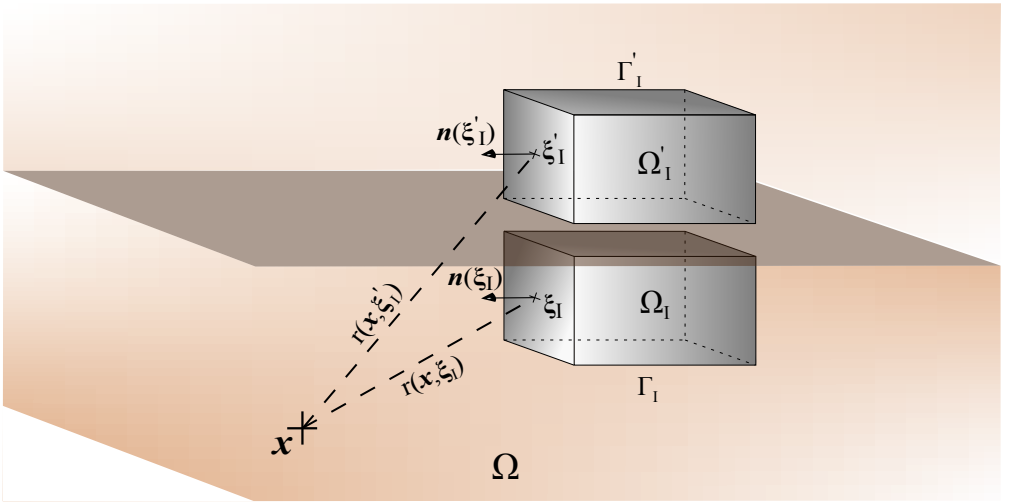

Figure 3.7. Domains of the boundary integrals Γ_I and $\Gamma_I^{'}$.

It should be noted that the first relation is easily verifiable, since domains Ω_I and $\Omega_I^{'}$ are symmetric. However, the second relation is proven in Appendix A.

Therefore, if the above relations are introduced in equation (3.43), the boundary equations in $\Gamma_I^{'}$ are rewritten as

$$I(\boldsymbol{x}^{'},\boldsymbol{\xi}_I)=\iint_{\boldsymbol{\xi}_I\in\Gamma_I}\Big(V(\boldsymbol{\xi}_I)\,\nabla\Big(\frac{1}{4\pi\,r(\boldsymbol{x}',\boldsymbol{\xi}_I)}\Big)\cdot\boldsymbol{n}(\boldsymbol{\xi}_I)-\frac{1}{4\pi\,r(\boldsymbol{x}',\boldsymbol{\xi}_I)}\,\nabla V(\boldsymbol{\xi}_I)\cdot\boldsymbol{n}(\boldsymbol{\xi}_I)\Big)\,\mathrm{d}\Gamma_I \tag{3.45}$$

and the boundary integrals (3.42) and (3.45) can be formulated in a unique boundary equation as

$$\begin{aligned}I(\boldsymbol{x},\boldsymbol{x}^{'},\boldsymbol{\xi}_I)=&-\frac{1}{4\pi}\iint_{\boldsymbol{\xi}_I\in\Gamma_I}\Big(\frac{1}{r(\boldsymbol{x},\boldsymbol{\xi}_I)}+\frac{1}{r(\boldsymbol{x}',\boldsymbol{\xi}_I)}\Big)\,\nabla V(\boldsymbol{\xi}_I)\cdot\boldsymbol{n}(\boldsymbol{\xi}_I)\,\mathrm{d}\Gamma_I\\&+\frac{1}{4\pi}\iint_{\boldsymbol{\xi}_I\in\Gamma_I}V(\boldsymbol{\xi}_I)\,\Big(\nabla\Big(\frac{1}{r(\boldsymbol{x},\boldsymbol{\xi}_I)}\Big)+\nabla\Big(\frac{1}{r(\boldsymbol{x}',\boldsymbol{\xi}_I)}\Big)\Big)\cdot\boldsymbol{n}(\boldsymbol{\xi}_I)\,\mathrm{d}\Gamma_I\end{aligned} \tag{3.46}$$

Again, the term $\nabla V(\boldsymbol{\xi}_I)\cdot\boldsymbol{n}(\boldsymbol{\xi}_I)$ will be defined as the normal component of the current density $\sigma_I(\boldsymbol{\xi}_I)$. As it was explained in the boundary integrals Γ_G and $\Gamma_G^{'}$, the current density vector $\boldsymbol{\sigma}$ can be expressed as

$$\boldsymbol{\sigma}=-\gamma\,\nabla V \tag{3.47}$$

and so, the normal component of this current density at any point located on the boundary Γ_I is given by

$$\sigma_I(\boldsymbol{\xi}_I)=-\gamma\,\nabla V(\boldsymbol{\xi}_I)\cdot\boldsymbol{n}(\boldsymbol{\xi}_I) \tag{3.48}$$

where $\sigma_I(\boldsymbol{\xi}_I)$ is the leakage current density on the surface Γ_I, as Figure 3.8 depicts.

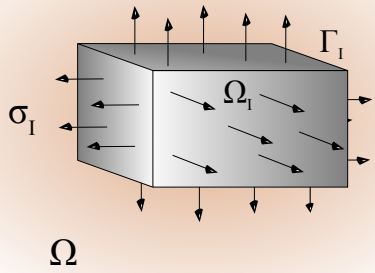

Figure 3.8. Leakage current density σ_I derivated into the ground. ***Criterion:*** *σ_I will be positive if it goes into domain Ω, and it will have the same direction of the normal vector chosen to analyse the problem.*

As a result, if equation (3.48) is introduced into the boundary integral (3.46), the boundary integrals Γ_I and $\Gamma_I^{'}$ are reduced to the following equation

$$\begin{aligned} I(\boldsymbol{x},\boldsymbol{x}^{'},\boldsymbol{\xi}_I) = & \frac{1}{4\pi\gamma}\iint_{\boldsymbol{\xi}_I\in\Gamma_I}\left(\frac{1}{r(\boldsymbol{x},\boldsymbol{\xi}_I)}+\frac{1}{r(\boldsymbol{x}^{'},\boldsymbol{\xi}_I)}\right)\sigma_I(\boldsymbol{\xi}_I)\,\mathrm{d}\Gamma_I \\ & + \frac{1}{4\pi}\iint_{\boldsymbol{\xi}_I\in\Gamma_I} V_I(\boldsymbol{\xi}_I)\left(\nabla\left(\frac{1}{r(\boldsymbol{x},\boldsymbol{\xi}_I)}\right)+\nabla\left(\frac{1}{r(\boldsymbol{x}^{'},\boldsymbol{\xi}_I)}\right)\right)\cdot\boldsymbol{n}(\boldsymbol{\xi}_I)\,\mathrm{d}\Gamma_I \end{aligned} \tag{3.49}$$

where $V(\boldsymbol{\xi}_I)$ is renamed as $V_I(\boldsymbol{\xi}_I)$ to indicate that the value of potential belongs to any point located on surface Γ_I.

Boundary integral equation of the exterior Dirichlet problem

At this point, all terms of equation (3.12) have been analysed. Replacing the results obtained for each integral into that expression, the boundary integral equation of the exterior Dirichlet problem is defined as

$$\lim_{\epsilon\to 0} I(\boldsymbol{x},\epsilon) = \lim_{R\to\infty} I(\boldsymbol{x},R) + \lim_{\epsilon\to 0} I(\boldsymbol{x},\epsilon) + I(\boldsymbol{x},\boldsymbol{x}^{'},\boldsymbol{\xi}_G) + I(\boldsymbol{x},\boldsymbol{x}^{'},\boldsymbol{\xi}_I) \tag{3.50}$$

That is:

$$\begin{aligned} 0 = 0 - V(\boldsymbol{x}) & + \frac{1}{4\pi\gamma}\iint_{\boldsymbol{\xi}_G\in\Gamma_G}\left(\frac{1}{r(\boldsymbol{x},\boldsymbol{\xi}_G)}+\frac{1}{r(\boldsymbol{x}^{'},\boldsymbol{\xi}_G)}\right)\sigma_G(\boldsymbol{\xi}_G)\,\mathrm{d}\Gamma_G \\ & + \frac{1}{4\pi\gamma}\iint_{\boldsymbol{\xi}_I\in\Gamma_I}\left(\frac{1}{r(\boldsymbol{x},\boldsymbol{\xi}_I)}+\frac{1}{r(\boldsymbol{x}^{'},\boldsymbol{\xi}_I)}\right)\sigma_I(\boldsymbol{\xi}_I)\,\mathrm{d}\Gamma_I \\ & + \frac{1}{4\pi}\iint_{\boldsymbol{\xi}_I\in\Gamma_I} V_I(\boldsymbol{\xi}_I)\left(\nabla\left(\frac{1}{r(\boldsymbol{x},\boldsymbol{\xi}_I)}\right)+\nabla\left(\frac{1}{r(\boldsymbol{x}^{'},\boldsymbol{\xi}_I)}\right)\right)\cdot\boldsymbol{n}(\boldsymbol{\xi}_I)\,\mathrm{d}\Gamma_I \end{aligned} \tag{3.51}$$

The above equation can be rewritten as

$$\begin{aligned} V(\boldsymbol{x}) \;=\; & \frac{1}{4\pi\gamma} \iint_{\boldsymbol{\xi}_G \in \Gamma_G} \Big(\frac{1}{r(\boldsymbol{x}, \boldsymbol{\xi}_G)} + \frac{1}{r(\boldsymbol{x}', \boldsymbol{\xi}_G)} \Big) \, \sigma_G(\boldsymbol{\xi}_G) \, \mathrm{d}\Gamma_G \\ & + \frac{1}{4\pi\gamma} \iint_{\boldsymbol{\xi}_I \in \Gamma_I} \Big(\frac{1}{r(\boldsymbol{x}, \boldsymbol{\xi}_I)} + \frac{1}{r(\boldsymbol{x}', \boldsymbol{\xi}_I)} \Big) \, \sigma_I(\boldsymbol{\xi}_I) \, \mathrm{d}\Gamma_I \\ & + \frac{1}{4\pi} \iint_{\boldsymbol{\xi}_I \in \Gamma_I} \Big[\Big(\nabla \Big(\frac{1}{r(\boldsymbol{x}, \boldsymbol{\xi}_I)} \Big) + \nabla \Big(\frac{1}{r(\boldsymbol{x}', \boldsymbol{\xi}_I)} \Big) \Big) \cdot \boldsymbol{n}(\boldsymbol{\xi}_I) \Big] \, V_I(\boldsymbol{\xi}_I) \, \mathrm{d}\Gamma_I \end{aligned} \tag{3.52}$$

where $V(\boldsymbol{x})$ is the value of the potential function in a source point $\boldsymbol{x}$ located in the domain Ω (the ground).

If the boundary condition defined in equation (3.9) is applied to the boundary integral equation (3.52), the following expression is obtained

$$\begin{aligned} V_G \;=\; & \frac{1}{4\pi\gamma} \iint_{\boldsymbol{\xi}_G \in \Gamma_G} \Big(\frac{1}{r(\boldsymbol{\chi}_G, \boldsymbol{\xi}_G)} + \frac{1}{r(\boldsymbol{\chi}_G^{'}, \boldsymbol{\xi}_G)} \Big) \, \sigma_G(\boldsymbol{\xi}_G) \, \mathrm{d}\Gamma_G \\ & + \frac{1}{4\pi\gamma} \iint_{\boldsymbol{\xi}_I \in \Gamma_I} \Big(\frac{1}{r(\boldsymbol{\chi}_G, \boldsymbol{\xi}_I)} + \frac{1}{r(\boldsymbol{\chi}_G^{'}, \boldsymbol{\xi}_I)} \Big) \, \sigma_I(\boldsymbol{\xi}_I) \, \mathrm{d}\Gamma_I \\ & + \frac{1}{4\pi} \iint_{\boldsymbol{\xi}_I \in \Gamma_I} \Big[\Big(\nabla \Big(\frac{1}{r(\boldsymbol{\chi}_G, \boldsymbol{\xi}_I)} \Big) + \nabla \Big(\frac{1}{r(\boldsymbol{\chi}_G^{'}, \boldsymbol{\xi}_I)} \Big) \Big) \cdot \boldsymbol{n}(\boldsymbol{\xi}_I) \Big] \, V_I(\boldsymbol{\xi}_I) \, \mathrm{d}\Gamma_I \end{aligned} \tag{3.53}$$

where the source points $\boldsymbol{\chi}_G$ and $\boldsymbol{\chi}_G^{'}$ are located in Γ_G and $\Gamma_G^{'}$ where the boundary condition is defined.

3.3.2 Boundary integral equations of the interior problems

Differential form of the interior problem

The second part of the problem analysed on Chapter 2 was mathematically modelled as an interior problem, which is given by

$$\Delta V_I = 0 \quad \text{in} \quad \Omega_I \tag{3.54}$$

These equations define the phenomenon of how the current densities emanating from the grounding grid (Ω_G) to the ground (Ω) affect the underground electrical substation (Ω_I), which is buried in Ω.

As in the exterior Dirichlet problem, the aim of the interior problem is to obtain the value of the potential field V_I, which is a harmonic function in Ω_I, since it satisfies the Laplace equation and it is a C^2 function.

An equivalent interior problem is formulated for the symmetric domain $\Omega_I^{'}$.

Boundary integral equation: Formulation

Again, the basic concepts about the fundamental solution of the Laplace equation in three dimensions, the harmonic functions and the equation of Green's second identity

have to be reminded so as to recast the interior problem into an integral boundary equation.

In this case, the potential problem is defined over a region Ω_I, the underground electrical substation, which is closed by boundary Γ_I, as shown in Figure 3.9.

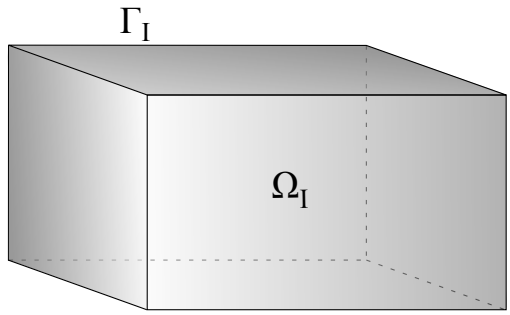

Figure 3.9. Finite domain Ω_I.

As in the exterior problem, the transformation of the interior problem into a boundary integral equation starts from the Green's second identity (3.7), where the functions ϕ and ψ will be substituted for the potential field V_I and the fundamental solution of the Laplace equation ϕ^*, respectively. Consequently, the interior problem is given by

$$\iiint_{\Omega_I} (V_I \Delta\phi^* - \phi^* \Delta V_I)\, \mathrm{d}\Omega_I = \iint_{\Gamma_I} (V_I\, \nabla\phi^* \cdot \boldsymbol{n} - \phi^*\, \nabla V_I \cdot \boldsymbol{n})\, \mathrm{d}\Gamma_I \tag{3.55}$$

where Ω_I is a domain in $\mathbb{R}^3$ bounded by a closed surface Γ_I, and $\boldsymbol{n}$ is the inward unit vector normal to the boundary Γ_I.

The fundamental solution of the Laplace equation ϕ^* is singular at the source point $\boldsymbol{x}_I$, so it is necessary to remove this point from the domain Ω_I isolating it by a sphere $B(\boldsymbol{x}_I, \epsilon)$ centred at $\boldsymbol{x}_I$ with a radius ϵ and a boundary $\Gamma_{B(\boldsymbol{x}_I,\epsilon)}$. This way, the integral equation (3.55) is rewritten as

$$\iiint_{\Omega_I - B(\boldsymbol{x}_I,\epsilon)} (V_I \Delta\phi^* - \phi^* \Delta V_I)\, \mathrm{d}\Omega_I = \iint_{\Gamma_I - \Gamma_{B(\boldsymbol{x}_I,\epsilon)}} (V_I\, \nabla\phi^* \cdot \boldsymbol{n} - \phi^*\, \nabla V_I \cdot \boldsymbol{n})\, \mathrm{d}\Gamma_I \tag{3.56}$$

As a result, a new region is obtained as Figure 3.10 indicates, where domain $\Omega_I - B(\boldsymbol{x}_I, \epsilon)$ is defined by the surfaces $\Gamma_{B(\boldsymbol{x}_I,\epsilon)} \cup \Gamma_I$.

Thus, after removing the source point $\boldsymbol{x}_I$, the boundary integral (3.56) can be divided into

$$\begin{aligned} \iiint_{\Omega_I - B(\boldsymbol{x}_I,\epsilon)} (V_I \Delta\phi^* - \phi^* \Delta V_I)\, \mathrm{d}\Omega_I = & \iint_{\Gamma_{B(\boldsymbol{x}_I,\epsilon)}} (V_I\, \nabla\phi^* \cdot \boldsymbol{n} - \phi^*\, \nabla V_I \cdot \boldsymbol{n})\, \mathrm{d}\Gamma_{B(\boldsymbol{x}_I,\epsilon)} \\ & + \iint_{\Gamma_I} (V_I\, \nabla\phi^* \cdot \boldsymbol{n} - \phi^*\, \nabla V_I \cdot \boldsymbol{n})\, \mathrm{d}\Gamma_I \end{aligned} \tag{3.57}$$

Next, all terms of equation (3.57) will be analysed.

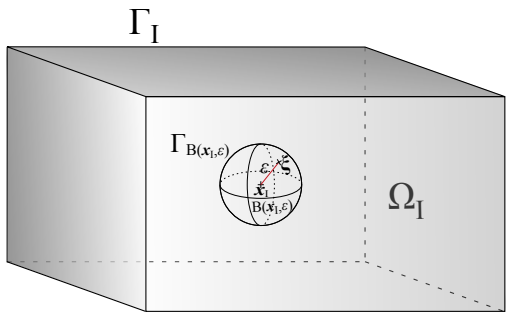

Figure 3.10. Domain $\Omega_I - B(\boldsymbol{x}_I, \epsilon)$.

Volume integral $\Omega_I - B(\boldsymbol{x}_I, \epsilon)$

This volume integral is defined as

$$I(\boldsymbol{x}_I, \epsilon) = \iiint_{\Omega_I - B(\boldsymbol{x}_I, \epsilon)} (V_I \Delta\phi^* - \phi^* \Delta V_I)\, \mathrm{d}\Omega_I \tag{3.58}$$

This integral is similarly to the volume integral (3.13), so the procedure to analyse it will be the same. As V_I and ϕ^* are harmonic functions defined in $\Omega_I - B(\boldsymbol{x}_I, \epsilon)$, the volume integral will be zero. Thus, the domain Ω_I is recovered by taking the improper integral of equation (3.58):

$$\lim_{\epsilon \to 0} I(\boldsymbol{x}_I, \epsilon) = 0 \tag{3.59}$$

Boundary integral $\Gamma_{B(\boldsymbol{x}_I, \epsilon)}$

The analysis of this kind of integral was explained in detail on the boundary integral equation of the exterior Dirichlet problem (Subsection 3.3.1). However, for the interior problem, more cases where the source point $\boldsymbol{x}_I$ can be located will be studied, and so, the resolution of some integral terms will be done again.

As it was presented, this boundary integral appears from the necessity to remove the source point $\boldsymbol{x}_I$ of the Laplace equation when it is singular. The solution proposed is to isolate the source point by a sphere $B(\boldsymbol{x}_I, \epsilon)$ centred at $\boldsymbol{x}_I$ with a redius ϵ and a boundary $\Gamma_B(\boldsymbol{x}_I, \epsilon)$ (Figure 3.11).

In this interior problem, three locations of the source point can be differentiated (Figure 3.12). This is an important point for this analysis because the value of the boundary integral $\Gamma_{B(\boldsymbol{x}_I, \epsilon)}$ depends on where the source point is located.

The boundary integral $\Gamma_B(\boldsymbol{x}_I, \epsilon)$ is

$$\begin{aligned} I(\boldsymbol{x}_I, \epsilon) &= \iint_{\boldsymbol{\xi} \in \Gamma_{B(\boldsymbol{x}_I, \epsilon)}} \Big(V_I(\boldsymbol{\xi})\ \nabla\phi^*(\boldsymbol{x}_I, \boldsymbol{\xi}) \cdot \boldsymbol{n}(\boldsymbol{\xi}) - \phi^*(\boldsymbol{x}_I, \boldsymbol{\xi})\ \nabla V_I(\boldsymbol{\xi}) \cdot \boldsymbol{n}(\boldsymbol{\xi}) \Big)\, \mathrm{d}\Gamma_{B(\boldsymbol{x}_I, \epsilon)} \\ &= \iint_{\boldsymbol{\xi} \in \Gamma_{B(\boldsymbol{x}_I, \epsilon)}} \Big(V_I(\boldsymbol{\xi})\, \nabla \Big(\frac{1}{4\pi\, r(\boldsymbol{x}_I, \boldsymbol{\xi})} \Big) \cdot \boldsymbol{n}(\boldsymbol{\xi}) - \Big(\frac{1}{4\pi\, r(\boldsymbol{x}_I, \boldsymbol{\xi})} \Big) \nabla V_I(\boldsymbol{\xi}) \cdot \boldsymbol{n}(\boldsymbol{\xi}) \Big) \mathrm{d}\Gamma_{B(\boldsymbol{x}_I, \epsilon)} \end{aligned} \tag{3.60}$$

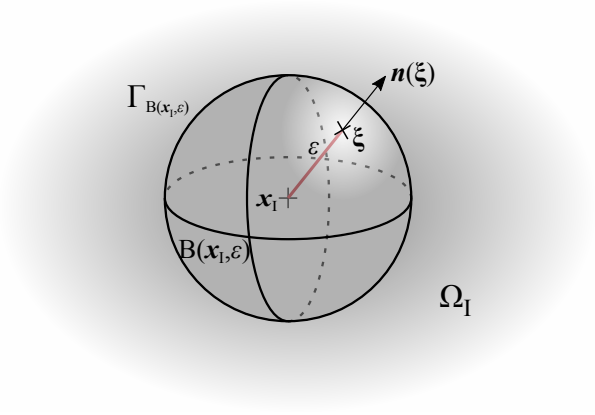

Figure 3.11. Sphere $B(\boldsymbol{x}_I, \epsilon)$ centred at $\boldsymbol{x}_I$ in the domain Ω_I.

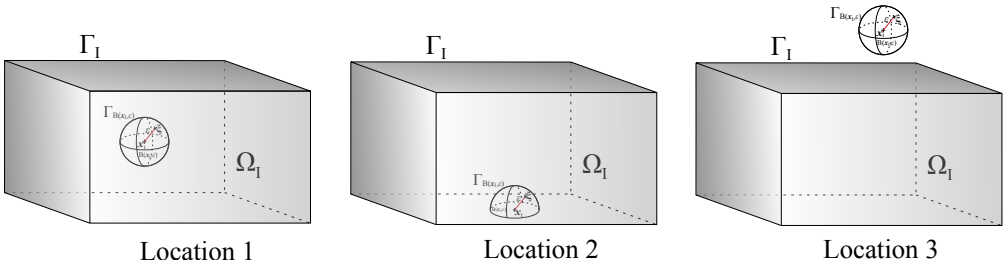

Figure 3.12. Locations of the sphere $B(\boldsymbol{x}_I, \epsilon)$ depend on the situation of the source point $\boldsymbol{x}_I$. *Location 1: $\boldsymbol{x}_I$ is located inside Ω_I; Location 2: $\boldsymbol{x}_I$ is located on the boundary Γ_I; Location 3: $\boldsymbol{x}_I$ is located outside Ω_I.*

First, the first integral of the right-hand side of equation (3.60) will be analysed, in which the value $V_I(\boldsymbol{x}_I)$ is subtracted and added to the value of $V_I(\boldsymbol{\xi})$ to obtain

$$\begin{aligned}
&\iint_{\boldsymbol{\xi}\in\Gamma_{B(\boldsymbol{x}_I,\epsilon)}} V_I(\boldsymbol{\xi})\ \nabla\Big(\frac{1}{4\pi\, r(\boldsymbol{x}_I,\boldsymbol{\xi})}\Big)\cdot \boldsymbol{n}(\boldsymbol{\xi})\,\mathrm{d}\Gamma_{B(\boldsymbol{x}_I,\epsilon)} \\
&= \iint_{\boldsymbol{\xi}\in\Gamma_{B(\boldsymbol{x}_I,\epsilon)}} [V_I(\boldsymbol{\xi}) - V_I(\boldsymbol{x}_I)]\ \nabla\Big(\frac{1}{4\pi\, r(\boldsymbol{x}_I,\boldsymbol{\xi})}\Big)\cdot \boldsymbol{n}(\boldsymbol{\xi})\,\mathrm{d}\Gamma_{B(\boldsymbol{x}_I,\epsilon)} \\
&+ V_I(\boldsymbol{x}_I) \iint_{\boldsymbol{\xi}\in\Gamma_{B(\boldsymbol{x}_I,\epsilon)}} \nabla\Big(\frac{1}{4\pi\, r(\boldsymbol{x}_I,\boldsymbol{\xi})}\Big)\cdot \boldsymbol{n}(\boldsymbol{\xi})\,\mathrm{d}\Gamma_{B(\boldsymbol{x}_I,\epsilon)}
\end{aligned} \tag{3.61}$$

Now, the second integral on the right-hand side of equation (3.61) will be calculated, where after doing the same procedure as in Subsection 3.3.1, the value of the directional derivative is equal to

$$\nabla\Big(\frac{1}{4\pi\, r(\boldsymbol{x}_I,\boldsymbol{\xi})}\Big)\cdot \boldsymbol{n}(\boldsymbol{\xi}) = -\frac{1}{4\pi(r(\boldsymbol{x}_I,\boldsymbol{\xi}))^2} \tag{3.62}$$

The analysed integral can be written in spherical coordinates according to Fig-

ure 3.13. Thus,

$$\mathrm{d}\Gamma_{B(\boldsymbol{x}_I,\epsilon)} = \epsilon^2 \sin(\Theta)\,\mathrm{d}\Theta\,\mathrm{d}\varphi$$

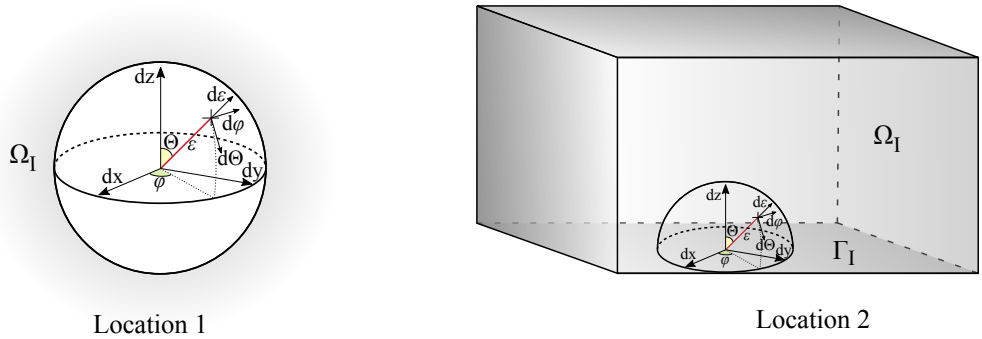

Figure 3.13. Spherical coordinates employed in the boundary integral $\Gamma_{B(\boldsymbol{x}_I,\epsilon)}$. *Location 1: In this case the sphere is totally included in the domain Ω_I, so $0 \leq \Theta \leq \pi$ and $0 \leq \varphi \leq 2\pi$. Location 2: In this case only a hemisphere is included in the domain Ω_I, so $0 \leq \Theta \leq \pi/2$ and $0 \leq \varphi \leq 2\pi$. Location 3: In this case the sphere is not included in the domain Ω_I, so the boundary integral $\Gamma_{B(\boldsymbol{x}_I,\epsilon)}$ does not exist.*

As a result, the analysed integral term can be restated as an improper integral where ϵ tends to zero, and the result for each location of the source point is:

- The source point $\boldsymbol{x}_I$ is located inside Ω_I:

$$\lim_{\epsilon\to 0}\iint_{\boldsymbol{\xi}\in\Gamma_{B(\boldsymbol{x}_I,\epsilon)}} \nabla\Big(\frac{1}{4\pi\, r(\boldsymbol{x}_I,\boldsymbol{\xi})}\Big)\cdot\boldsymbol{n}(\boldsymbol{\xi})\,\mathrm{d}\Gamma_{B(\boldsymbol{x}_I,\epsilon)} = \lim_{\epsilon\to 0}\int_0^{2\pi}\int_0^{\pi} -\frac{1}{4\pi\epsilon^2}\epsilon^2\sin(\Theta)\,\mathrm{d}\Theta\,\mathrm{d}\varphi = -1 \tag{3.63}$$

- The source point $\boldsymbol{x}_I$ is located on boundary Γ_I:

$$\lim_{\epsilon\to 0}\iint_{\boldsymbol{\xi}\in\Gamma_{B(\boldsymbol{x}_I,\epsilon)}} \nabla\Big(\frac{1}{4\pi\, r(\boldsymbol{x}_I,\boldsymbol{\xi})}\Big)\cdot\boldsymbol{n}(\boldsymbol{\xi})\,\mathrm{d}\Gamma_{B(\boldsymbol{x}_I,\epsilon)} = \lim_{\epsilon\to 0}\int_0^{2\pi}\int_0^{\frac{\pi}{2}} -\frac{1}{4\pi\epsilon^2}\epsilon^2\sin(\Theta)\,\mathrm{d}\Theta\,\mathrm{d}\varphi = -\frac{1}{2} \tag{3.64}$$

- The source point $\boldsymbol{x}_I$ is located outside Ω_I:

$$\lim_{\epsilon\to 0}\iint_{\boldsymbol{\xi}\in\Gamma_{B(\boldsymbol{x}_I,\epsilon)}} \nabla\Big(\frac{1}{4\pi\, r(\boldsymbol{x}_I,\boldsymbol{\xi})}\Big)\cdot\boldsymbol{n}(\boldsymbol{\xi})\,\mathrm{d}\Gamma_{B(\boldsymbol{x}_I,\epsilon)} = 0 \tag{3.65}$$

The same procedure will be used to calculate the first integral on the right-hand side of equation (3.61), where $V_I(\boldsymbol{x}_I)$ is assumed as continuous. Therefore, this integral

term will be equal to

$$\lim_{\epsilon\to 0}\iint_{\boldsymbol{\xi}\in\Gamma_{B(\boldsymbol{x}_I,\epsilon)}}\left[V_I(\boldsymbol{\xi})-V_I(\boldsymbol{x}_I)\right]\,\nabla\Big(\frac{1}{4\pi\,r(\boldsymbol{x}_I,\boldsymbol{\xi})}\Big)\cdot\boldsymbol{n}(\boldsymbol{\xi})\,\mathrm{d}\Gamma_{B(\boldsymbol{x}_I,\epsilon)}=0 \tag{3.66}$$

and the general result of the first term of the right-hand side of equation (3.60) is

$$\lim_{\epsilon\to 0}\iint_{\boldsymbol{\xi}\in\Gamma_{B(\boldsymbol{x}_I,\epsilon)}}V_I(\boldsymbol{\xi})\,\nabla\Big(\frac{1}{4\pi\,r(\boldsymbol{x}_I,\boldsymbol{\xi})}\Big)\cdot\boldsymbol{n}(\boldsymbol{\xi})\,\mathrm{d}\Gamma_{B(\boldsymbol{x}_I,\epsilon)}=-c(\boldsymbol{x}_I)V_I(\boldsymbol{x}_I) \tag{3.67}$$

The same approach will be applied to evaluate the term

$$\iint_{\boldsymbol{\xi}\in\Gamma_{B(\boldsymbol{x}_I,\epsilon)}}\Big(\frac{1}{4\pi\,r(\boldsymbol{x}_I,\boldsymbol{\xi})}\Big)\,\nabla V_I(\boldsymbol{\xi})\cdot\boldsymbol{n}(\boldsymbol{\xi})\,\mathrm{d}\Gamma_{B(\boldsymbol{x}_I,\epsilon)} \tag{3.68}$$

This integral can be stated in spherical coordinates as an improper integral where ϵ tends to zero. Thus,

$$\begin{aligned}&\lim_{\epsilon\to 0}\iint_{\boldsymbol{\xi}\in\Gamma_{B(\boldsymbol{x}_I,\epsilon)}}\Big(\frac{1}{4\pi\,r(\boldsymbol{x}_I,\boldsymbol{\xi})}\Big)\,\nabla V_I(\boldsymbol{\xi})\cdot\boldsymbol{n}(\boldsymbol{\xi})\,\mathrm{d}\Gamma_{B(\boldsymbol{x}_I,\epsilon)}\\ =&\lim_{\epsilon\to 0}\int_0^{2\pi}\int_0^{\varphi}\Big(\frac{1}{4\pi\epsilon}\Big)\,\nabla V_I(\boldsymbol{\xi})\cdot\boldsymbol{n}(\boldsymbol{\xi})\epsilon^2\sin(\Theta)\,\mathrm{d}\Theta\,\mathrm{d}\varphi=0\end{aligned} \tag{3.69}$$

where φ depends on the location of $\boldsymbol{x}_I$.

Finally, the boundary integral $\Gamma_{B(\boldsymbol{x}_I,\epsilon)}$ is obtained adding equations (3.67) and (3.69) and its value is

$$\lim_{\epsilon\to 0}I(\boldsymbol{x}_I,\epsilon)=-c(\boldsymbol{x}_I)V_I(\boldsymbol{x}_I) \tag{3.70}$$

where $c(\boldsymbol{x}_I)$ is a free coefficient that depends on the location of $\boldsymbol{x}_I$.

Boundary integral Γ_I

The last boundary integral that is necessary to analyse the interior problem is

$$I(\boldsymbol{x}_I,\boldsymbol{\xi}_I)=\iint_{\boldsymbol{\xi}_I\,\in\,\Gamma_I}\Big(V_I(\boldsymbol{\xi}_I)\,\nabla\phi^*(\boldsymbol{x}_I,\boldsymbol{\xi}_I)\cdot\boldsymbol{n}(\boldsymbol{\xi}_I)-\phi^*(\boldsymbol{x}_I,\boldsymbol{\xi}_I)\,\nabla V_I(\boldsymbol{\xi}_I)\cdot\boldsymbol{n}(\boldsymbol{\xi}_I)\Big)\,\mathrm{d}\Gamma_I \tag{3.71}$$

where $\boldsymbol{x}_I$ is a source point located in the domain Ω_I, and $\boldsymbol{\xi}_I$ is the field point located on Γ_I surface (Figure 3.14).

The above integral can be rewritten in terms of the fundamental solution of the Laplace equation ϕ^* as

$$\begin{aligned}&I(\boldsymbol{x}_I,\boldsymbol{\xi}_I)=\\ &=\iint_{\boldsymbol{\xi}_I\,\in\,\Gamma_I}\Big(V_I(\boldsymbol{\xi}_I)\,\nabla\Big(\frac{1}{4\pi\,r(\boldsymbol{x}_I,\boldsymbol{\xi}_I)}\Big)\cdot\boldsymbol{n}(\boldsymbol{\xi}_I)-\frac{1}{4\pi\,r(\boldsymbol{x}_I,\boldsymbol{\xi}_I)}\,\nabla V_I(\boldsymbol{\xi}_I)\cdot\boldsymbol{n}(\boldsymbol{\xi}_I)\Big)\,\mathrm{d}\Gamma_I\\ &=\frac{1}{4\pi}\iint_{\boldsymbol{\xi}_I\,\in\,\Gamma_I}V_I(\boldsymbol{\xi}_I)\,\nabla\Big(\frac{1}{r(\boldsymbol{x}_I,\boldsymbol{\xi}_I)}\Big)\cdot\boldsymbol{n}(\boldsymbol{\xi}_I)\,\mathrm{d}\Gamma_I\\ &-\frac{1}{4\pi}\iint_{\boldsymbol{\xi}_I\,\in\,\Gamma_I}\frac{1}{r(\boldsymbol{x}_I,\boldsymbol{\xi}_I)}\,\nabla V_I(\boldsymbol{\xi}_I)\cdot\boldsymbol{n}(\boldsymbol{\xi}_I)\,\mathrm{d}\Gamma_I\end{aligned} \tag{3.72}$$

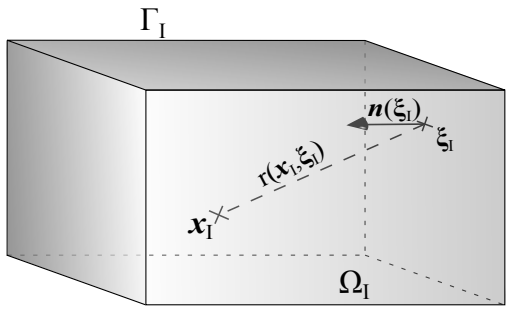

Figure 3.14. Domain of the boundary integral Γ_I.

As it was done in the exterior Dirichlet problem, the term $\nabla V_I(\boldsymbol{\xi}_I) \cdot \boldsymbol{n}(\boldsymbol{\xi}_I)$ can be formulated as the normal component of the current density $\sigma_I(\boldsymbol{\xi}_I)$. In Chapter 2 it was deduced that the electric field $\boldsymbol{E}_I$ admits a potential scalar V_I like $\boldsymbol{E}_I = -\nabla V_I$, and so the constitutive equation (2.23) can be written as

$$\boldsymbol{\sigma}_I = -\gamma_I \, \nabla V_I \tag{3.73}$$

where $\boldsymbol{\sigma}_I$ is the current density vector and γ_I is the apparent conductivity of the finite volume Ω_I buried inside the ground, which represents the substation enclosure.

If this current density vector is multiplied by an inward normal vector $\boldsymbol{n}$ to boundary Γ_I and applied at any point located on it, the normal component of this current density is obtained as:

$$\sigma_I(\boldsymbol{\xi}_I) = -\gamma_I \, \nabla V_I(\boldsymbol{\xi}_I) \cdot \boldsymbol{n}(\boldsymbol{\xi}_I) \tag{3.74}$$

where $\sigma_I(\boldsymbol{\xi}_I)$ is the leakage current density on the surface Γ_I, as Figure 3.15 represents.

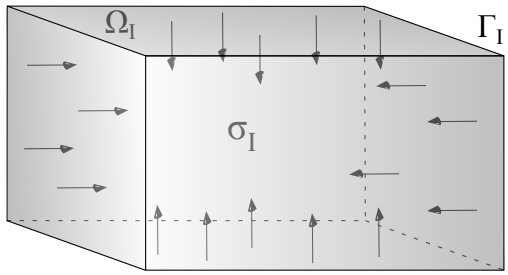

Figure 3.15. Leakage current density σ_I derived into Ω_I. ***Criterion:** σ_I **will be positive if it goes into domain** Ω_I **and it will have the same direction of the normal vector chosen to analise the problem.***

Therefore, introducing the relation (3.74) into equation (3.72), the boundary integral Γ_I is given by

$$\begin{aligned} I(\boldsymbol{x}_I, \boldsymbol{\xi}_I) = & \frac{1}{4\pi\gamma_I} \iint_{\boldsymbol{\xi}_I \in \Gamma_I} \frac{1}{r(\boldsymbol{x}_I, \boldsymbol{\xi}_I)} \, \sigma_I(\boldsymbol{\xi}_I) \, \mathrm{d}\Gamma_I \\ & + \frac{1}{4\pi} \iint_{\boldsymbol{\xi}_I \in \Gamma_I} \left[\nabla \left(\frac{1}{r(\boldsymbol{x}_I, \boldsymbol{\xi}_I)} \right) \cdot \boldsymbol{n}(\boldsymbol{\xi}_I) \right] V_I(\boldsymbol{\xi}_I) \, \mathrm{d}\Gamma_I \end{aligned} \tag{3.75}$$

Boundary integral equations of the interior problems

Finally, after all terms of equation (3.57) have been analysed, the boundary integral equation of the interior problem is obtained as

$$\lim_{\epsilon \to 0} I(\boldsymbol{x}_I, \epsilon) = \lim_{\epsilon \to 0} I(\boldsymbol{x}_I, \epsilon) + I(\boldsymbol{x}_I, \boldsymbol{\xi}_I) \tag{3.76}$$

That is:

$$\begin{aligned} 0 = -c(\boldsymbol{x}_I) V_I(\boldsymbol{x}_I) + \frac{1}{4\pi\gamma_I} \iint_{\boldsymbol{\xi}_I \in \Gamma_I} \frac{1}{r(\boldsymbol{x}_I, \boldsymbol{\xi}_I)} \, \sigma_I(\boldsymbol{\xi}_I) \, \mathrm{d}\Gamma_I \\ + \frac{1}{4\pi} \iint_{\boldsymbol{\xi}_I \in \Gamma_I} \Big[\nabla \Big(\frac{1}{r(\boldsymbol{x}_I, \boldsymbol{\xi}_I)} \Big) \cdot \boldsymbol{n}(\boldsymbol{\xi}_I) \Big] V_I(\boldsymbol{\xi}_I) \, \mathrm{d}\Gamma_I \end{aligned} \tag{3.77}$$

The above equation can be rewritten as

$$\begin{aligned} c(\boldsymbol{x}_I) V_I(\boldsymbol{x}_I) = \frac{1}{4\pi\gamma_I} \iint_{\boldsymbol{\xi}_I \in \Gamma_I} \frac{1}{r(\boldsymbol{x}_I, \boldsymbol{\xi}_I)} \, \sigma_I(\boldsymbol{\xi}_I) \, \mathrm{d}\Gamma_I \\ + \frac{1}{4\pi} \iint_{\boldsymbol{\xi}_I \in \Gamma_I} \Big[\nabla \Big(\frac{1}{r(\boldsymbol{x}_I, \boldsymbol{\xi}_I)} \Big) \cdot \boldsymbol{n}(\boldsymbol{\xi}_I) \Big] V_I(\boldsymbol{\xi}_I) \, \mathrm{d}\Gamma_I \end{aligned} \tag{3.78}$$

where $V_I(\boldsymbol{x}_I)$ is the value of the potential function in a source point $\boldsymbol{x}_I$, which is multiplied by a free coefficient $c(\boldsymbol{x}_I)$ that depends on the location of $\boldsymbol{x}_I$. The main values of $c(\boldsymbol{x}_I)$ for this problem are

$$c(\boldsymbol{x}_I) = 1 \quad \text{if} \quad \boldsymbol{x}_I \in \Omega_I$$

$$c(\boldsymbol{x}_I) = \frac{1}{2} \quad \text{if} \quad \boldsymbol{x}_I \in \Gamma_I$$

$$c(\boldsymbol{x}_I) = 0 \quad \text{if} \quad \boldsymbol{x}_I \notin \Omega_I \text{ and } \boldsymbol{x}_I \notin \Gamma_I$$

A similar boundary integral equation is defined for the symmetric domain $\Omega_I^{'}$

$$\begin{aligned} c(\boldsymbol{x}_I^{'}) V_I(\boldsymbol{x}_I^{'}) = \frac{1}{4\pi\gamma_I} \iint_{\boldsymbol{\xi}_I^{'} \in \Gamma_I^{'}} \frac{1}{r(\boldsymbol{x}_I^{'}, \boldsymbol{\xi}_I^{'})} \, \sigma_I(\boldsymbol{\xi}_I^{'}) \, \mathrm{d}\Gamma_I^{'} \\ + \frac{1}{4\pi} \iint_{\boldsymbol{\xi}_I^{'} \in \Gamma_I^{'}} \Big[\nabla \Big(\frac{1}{r(\boldsymbol{x}_I^{'}, \boldsymbol{\xi}_I^{'})} \Big) \cdot \boldsymbol{n}(\boldsymbol{\xi}_I^{'}) \Big] V_I(\boldsymbol{\xi}_I^{'}) \, \mathrm{d}\Gamma_I^{'} \end{aligned} \tag{3.79}$$

where $V_I(\boldsymbol{x}_I^{'})$ is the value of the potential function in a source point $\boldsymbol{x}_I^{'}$, which is multiplied by a free coefficient $c(\boldsymbol{x}_I^{'})$ that depends on the location of $\boldsymbol{x}_I^{'}$. Again, the main values of $c(\boldsymbol{x}_I^{'})$ for this problem are

$$c(\boldsymbol{x}_I^{'}) = 1 \quad \text{if} \quad \boldsymbol{x}_I^{'} \in \Omega_I^{'}$$

$$c(\boldsymbol{x}_I^{'}) = \frac{1}{2} \quad \text{if} \quad \boldsymbol{x}_I^{'} \in \Gamma_I^{'}$$

$$c(\boldsymbol{x}_I^{'}) = 0 \quad \text{if} \quad \boldsymbol{x}_I^{'} \notin \Omega_I^{'} \text{ and } \boldsymbol{x}_I^{'} \notin \Gamma_I^{'}$$

3.3.3 Compatibility conditions

Once the exterior and the interior problems have been transformed into their integral forms, the compatibility conditions between them will be applied to obtain the equations that allow to solve the problem.

These compatibility conditions, which have been already defined in Chapter 2, are

$$\begin{aligned} V_I &= V && \text{in } \Gamma_I \text{ and } \Gamma_I^{'} \\ \boldsymbol{n}\cdot\boldsymbol{\sigma}_I &= \boldsymbol{n}\cdot\boldsymbol{\sigma} && \text{in } \Gamma_I \text{ and } \Gamma_I^{'} \end{aligned} \tag{3.80}$$

where V_I and $\boldsymbol{\sigma}_I$ are respectively the potential function and the current density vector that belong to the interior problem, and V and $\boldsymbol{\sigma}$ are the potential function and the current density vector belonging to the exterior Dirichlet problem.

It should be noted that in order to obtain the boundary integral equations and solve the problem, only the conditions applied to Γ_I will be necessary (Subsection 2.3.3).

Before the application of these conditions, the formulated boundary integrals will be rewritten as:

- Boundary integral equation of the exterior Dirichlet problem:

$$\begin{aligned} V^e(\boldsymbol{x}) \;=\; & \frac{1}{4\pi\gamma}\iint_{\boldsymbol{\xi}_G\in\Gamma_G}\Big(\frac{1}{r(\boldsymbol{x},\boldsymbol{\xi}_G)}+\frac{1}{r(\boldsymbol{x}',\boldsymbol{\xi}_G)}\Big)\,\sigma_G(\boldsymbol{\xi}_G)\,\mathrm{d}\Gamma_G \\ & + \frac{1}{4\pi\gamma}\iint_{\boldsymbol{\xi}_I\in\Gamma_I}\Big(\frac{1}{r(\boldsymbol{x},\boldsymbol{\xi}_I)}+\frac{1}{r(\boldsymbol{x}',\boldsymbol{\xi}_I)}\Big)\,\sigma_I^e(\boldsymbol{\xi}_I)\,\mathrm{d}\Gamma_I \\ & + \frac{1}{4\pi}\iint_{\boldsymbol{\xi}_I\in\Gamma_I}\Big[\Big(\nabla\Big(\frac{1}{r(\boldsymbol{x},\boldsymbol{\xi}_I)}\Big)+\nabla\Big(\frac{1}{r(\boldsymbol{x}',\boldsymbol{\xi}_I)}\Big)\Big)\cdot\boldsymbol{n}^e(\boldsymbol{\xi}_I)\Big]\,V_I^e(\boldsymbol{\xi}_I)\,\mathrm{d}\Gamma_I \end{aligned} \tag{3.81}$$

  where $V(\boldsymbol{x}), \sigma_I(\boldsymbol{\xi}_I), V_I(\boldsymbol{\xi}_I)$ and $\boldsymbol{n}(\boldsymbol{\xi}_I)$ are renamed as $V^e(\boldsymbol{x}), \sigma_I^e(\boldsymbol{\xi}_I), V_I^e(\boldsymbol{\xi}_I)$, and $\boldsymbol{n}^e(\boldsymbol{\xi}_I)$ to indicate that the values belong to the exterior problem (Subsection 3.3.1).

- Boundary integral equation of the interior problem

$$\begin{aligned} c(\boldsymbol{x}_I)V_I^i(\boldsymbol{x}_I) = & \frac{1}{4\pi\gamma_I}\iint_{\boldsymbol{\xi}_I\in\Gamma_I}\frac{1}{r(\boldsymbol{x}_I,\boldsymbol{\xi}_I)}\;\sigma_I^i(\boldsymbol{\xi}_I)\;\mathrm{d}\Gamma_I \\ & + \frac{1}{4\pi}\iint_{\boldsymbol{\xi}_I\in\Gamma_I}\Big[\nabla\Big(\frac{1}{r(\boldsymbol{x}_I,\boldsymbol{\xi}_I)}\Big)\cdot\boldsymbol{n}^i(\boldsymbol{\xi}_I)\Big]V_I^i(\boldsymbol{\xi}_I)\;\mathrm{d}\Gamma_I \end{aligned} \tag{3.82}$$

  where $V_I(\boldsymbol{x}_I), \sigma_I(\boldsymbol{\xi}_I), V_I(\boldsymbol{\xi}_I)$ and $\boldsymbol{n}(\boldsymbol{\xi}_I)$ are renamed as $V_I^i(\boldsymbol{x}_I), \sigma_I^i(\boldsymbol{\xi}_I), V_I^i(\boldsymbol{\xi}_I)$, and $\boldsymbol{n}^i(\boldsymbol{\xi}_I)$ to indicate that the values belong to the interior problem (Subsection 3.3.2).

The boundary conditions (3.80) can be defined in a form that they can be applied to the boundary integral equations (3.81) and (3.82). Thus, they can be written as:

$$\begin{aligned} V_I^i(\boldsymbol{\chi}_I) &= V^e(\boldsymbol{\chi}_I) \\ V_I^i(\boldsymbol{\xi}_I) &= V_I^e(\boldsymbol{\xi}_I) \end{aligned} \tag{3.83}$$

where $\boldsymbol{\chi}_I$ is a source point located on the surface Γ_I, and $\boldsymbol{\xi}_I$ is a field point located on the surface Γ_I.

And

$$\boldsymbol{\sigma}_I^i(\boldsymbol{\xi}_I) \cdot \boldsymbol{n}^i(\boldsymbol{\xi}_I) = \boldsymbol{\sigma}_I^e(\boldsymbol{\xi}_I) \cdot \boldsymbol{n}^e(\boldsymbol{\xi}_I) \tag{3.84}$$

where $\boldsymbol{\xi}_I$ is a field point located on the surface Γ_I, $\boldsymbol{n}^i$ is the inward normal vector to Γ_I that belongs to the interior problem, and $\boldsymbol{n}^e$ is the outward normal vector to Γ_I belonging to the exterior Dirichlet problem.

The relation between the normal vectors $\boldsymbol{n}^i$ and $\boldsymbol{n}^e$ is

$$\boldsymbol{n}^i(\boldsymbol{\xi}_I) = -\boldsymbol{n}^e(\boldsymbol{\xi}_I) \tag{3.85}$$

Therefore, the compatibility condition between the current densities can be reduced to the following expression that relates the leakage current density on the surface Γ_I:

$$\sigma_I^i(\boldsymbol{\xi}_I) = -\sigma_I^e(\boldsymbol{\xi}_I) \tag{3.86}$$

Next, the above boundary conditions will be applied to the boundary integral equations of the exterior and interior problems.

Compatibility condition $V_I^i(\boldsymbol{\chi}_I) = V^e(\boldsymbol{\chi}_I)$ and $V_I^i(\boldsymbol{\xi}_I) = V_I^e(\boldsymbol{\xi}_I)$

This boundary condition states that at any point located on surface Γ_I, the potential field V_I should have the same value for the exterior and the interior problem. This condition can be introduced into the boundary integrals of the problem as follows:

First, the boundary integral equation of the exterior Dirichlet problem will be formulated on the surface Γ_I. In order to do it, the resolution of the boundary integral $\Gamma_{B(\boldsymbol{x},\epsilon)}$, which was explained in Subsection 3.3.1, needs to be modified. Now, the source point $\boldsymbol{\chi}_I$ is located in the surface of the region Ω_I, so $\boldsymbol{\chi}_I$ will be isolated by a sphere $B(\boldsymbol{\chi}_I, \epsilon)$ centre at $\boldsymbol{\chi}_I$ with a radius ϵ and a boundary $\Gamma_{B(\boldsymbol{\chi}_I,\epsilon)}$, as shown in Figure 3.16.

Therefore, the limits of the improper integral (3.23) has to be changed by

$$\begin{aligned}\lim_{\epsilon\to 0} \iint_{\boldsymbol{\xi}\in\Gamma_{B(\boldsymbol{x},\epsilon)}} \nabla\Big(\frac{1}{4\pi\, r(\boldsymbol{x},\boldsymbol{\xi})}\Big) \cdot \boldsymbol{n}(\boldsymbol{\xi})\, \mathrm{d}\Gamma_{B(\boldsymbol{x},\epsilon)} &= \lim_{\epsilon\to 0} \int_0^{2\pi} \int_0^{\frac{\pi}{2}} -\frac{1}{4\pi(\epsilon)^2}\epsilon^2 \sin(\Theta)\, \mathrm{d}\Theta\, \mathrm{d}\varphi \\ &= -\frac{1}{2}\end{aligned} \tag{3.87}$$

The rest of the terms remain equal, and thus, the boundary integral $\Gamma_{B(\boldsymbol{\chi}_I,\epsilon)}$ is obtained as

$$\lim_{\epsilon\to 0} I(\boldsymbol{\chi}_I, \epsilon) = -\frac{1}{2}\, V^e(\boldsymbol{\chi}_I) \tag{3.88}$$

Introducing the above result in equation (3.50), the boundary integral equation of the exterior Dirichlet problem applied on a source point $\boldsymbol{\chi}_I$ located on the surface Γ_I

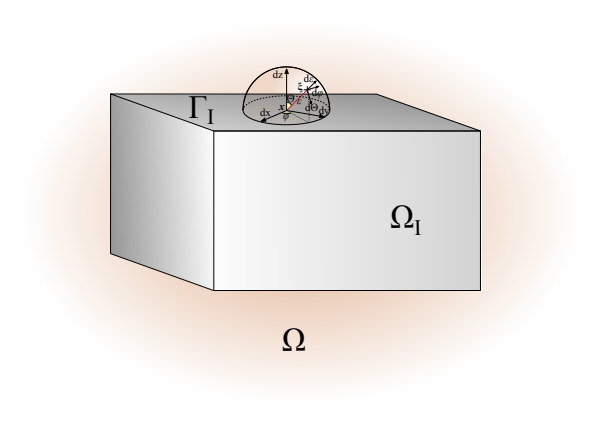

Figure 3.16. Schematic representation of the sphere $B(\boldsymbol{\chi}_I, \epsilon)$ when $\boldsymbol{\chi}_I$ is located on the surface Γ_I.

is given by

$$\begin{aligned}\frac{1}{2}V^e(\boldsymbol{\chi}_I) = &\frac{1}{4\pi\gamma}\iint_{\boldsymbol{\xi}_G\in\Gamma_G}\Big(\frac{1}{r(\boldsymbol{\chi}_I,\boldsymbol{\xi}_G)}+\frac{1}{r(\boldsymbol{\chi}_I',\boldsymbol{\xi}_G)}\Big)\,\sigma_G(\boldsymbol{\xi}_G)\,\mathrm{d}\Gamma_G\\ &+\frac{1}{4\pi\gamma}\iint_{\boldsymbol{\xi}_I\in\Gamma_I}\Big(\frac{1}{r(\boldsymbol{\chi}_I,\boldsymbol{\xi}_I)}+\frac{1}{r(\boldsymbol{\chi}_I',\boldsymbol{\xi}_I)}\Big)\,\sigma_I^e(\boldsymbol{\xi}_I)\,\mathrm{d}\Gamma_I\\ &+\frac{1}{4\pi}\iint_{\boldsymbol{\xi}_I\in\Gamma_I}\Big[\Big(\nabla\Big(\frac{1}{r(\boldsymbol{\chi}_I,\boldsymbol{\xi}_I)}\Big)+\nabla\Big(\frac{1}{r(\boldsymbol{\chi}_I',\boldsymbol{\xi}_I)}\Big)\Big)\cdot\boldsymbol{n}^e(\boldsymbol{\xi}_I)\Big]\,V_I^e(\boldsymbol{\xi}_I)\,\mathrm{d}\Gamma_I\end{aligned} \tag{3.89}$$

For the interior problem, the expression developed in equation (3.78) can be used directly. Thus, if the source point $\boldsymbol{\chi}_I$ is located on the boundary Γ_I, the boundary integral equation of the interior problem is

$$\begin{aligned}\frac{1}{2}V_I^i(\boldsymbol{\chi}_I) = &\frac{1}{4\pi\gamma_I}\iint_{\boldsymbol{\xi}_I\in\Gamma_I}\frac{1}{r(\boldsymbol{\chi}_I,\boldsymbol{\xi}_I)}\,\sigma_I^i(\boldsymbol{\xi}_I)\,\mathrm{d}\Gamma_I\\ &+\frac{1}{4\pi}\iint_{\boldsymbol{\xi}_I\in\Gamma_I}\Big[\nabla\Big(\frac{1}{r(\boldsymbol{\chi}_I,\boldsymbol{\xi}_I)}\Big)\cdot\boldsymbol{n}^i(\boldsymbol{\xi}_I)\Big]\,V_I^i(\boldsymbol{\xi}_I)\,\mathrm{d}\Gamma_I\end{aligned} \tag{3.90}$$

Finally, renaming the compatibility conditions as

$$\begin{aligned}V_I^i(\boldsymbol{\chi}_I) = V^e(\boldsymbol{\chi}_I) &= V_I(\boldsymbol{\chi}_I)\\ V_I^i(\boldsymbol{\xi}_I) = V_I^e(\boldsymbol{\xi}_I) &= V_I(\boldsymbol{\xi}_I)\end{aligned} \tag{3.91}$$

The boundary integral equations of the problem can be rewritten as:

Boundary integral equation of the exterior Dirichlet problem

$$\begin{aligned}\frac{1}{2}V_I(\boldsymbol{\chi}_I) = &\frac{1}{4\pi\gamma}\iint_{\boldsymbol{\xi}_G\in\Gamma_G}\Big(\frac{1}{r(\boldsymbol{\chi}_I,\boldsymbol{\xi}_G)}+\frac{1}{r(\boldsymbol{\chi}_I',\boldsymbol{\xi}_G)}\Big)\,\sigma_G(\boldsymbol{\xi}_G)\,\mathrm{d}\Gamma_G\\ &+\frac{1}{4\pi\gamma}\iint_{\boldsymbol{\xi}_I\in\Gamma_I}\Big(\frac{1}{r(\boldsymbol{\chi}_I,\boldsymbol{\xi}_I)}+\frac{1}{r(\boldsymbol{\chi}_I',\boldsymbol{\xi}_I)}\Big)\,\sigma_I^e(\boldsymbol{\xi}_I)\,\mathrm{d}\Gamma_I\\ &+\frac{1}{4\pi}\iint_{\boldsymbol{\xi}_I\in\Gamma_I}\Big[\Big(\nabla\Big(\frac{1}{r(\boldsymbol{\chi}_I,\boldsymbol{\xi}_I)}\Big)+\nabla\Big(\frac{1}{r(\boldsymbol{\chi}_I',\boldsymbol{\xi}_I)}\Big)\Big)\cdot\boldsymbol{n}^e(\boldsymbol{\xi}_I)\Big]\,V_I(\boldsymbol{\xi}_I)\,\mathrm{d}\Gamma_I\end{aligned} \tag{3.92}$$

Boundary integral equation of the interior problem

$$\begin{aligned}\frac{1}{2}V_I(\boldsymbol{\chi}_I) = &\frac{1}{4\pi\gamma_I}\iint_{\boldsymbol{\xi}_I\in\Gamma_I}\frac{1}{r(\boldsymbol{\chi}_I,\boldsymbol{\xi}_I)}\,\sigma_I^i(\boldsymbol{\xi}_I)\,\mathrm{d}\Gamma_I\\ &+\frac{1}{4\pi}\iint_{\boldsymbol{\xi}_I\in\Gamma_I}\Big[\nabla\Big(\frac{1}{r(\boldsymbol{\chi}_I,\boldsymbol{\xi}_I)}\Big)\cdot\boldsymbol{n}^i(\boldsymbol{\xi}_I)\Big]V_I(\boldsymbol{\xi}_I)\,\mathrm{d}\Gamma_I\end{aligned} \tag{3.93}$$

Compatibility condition $\sigma_I^i(\boldsymbol{\chi}_I) = -\sigma_I^e(\boldsymbol{\chi}_I)$

The second compatibility condition states that at any point located on surface Γ_I, the current density σ_I should have the same value but with different sign for the exterior and the interior problem. This is due to the normal vector chosen to analyse the problems has the same direction but different sense.

Therefore, if this compatibility condition is renamed as

$$\begin{aligned}\sigma_I^e(\boldsymbol{\xi}_I) &= \sigma_I(\boldsymbol{\xi}_I)\\ \sigma_I^i(\boldsymbol{\xi}_I) &= -\sigma_I^e(\boldsymbol{\xi}_I) = -\sigma_I(\boldsymbol{\xi}_I)\end{aligned} \tag{3.94}$$

The boundary integral equations (3.92) and (3.93) can be expressed with the same unknown functions as:
Boundary integral equation of the exterior Dirichlet problem

$$\begin{aligned}\frac{1}{2}V_I(\boldsymbol{\chi}_I) = &\frac{1}{4\pi\gamma}\iint_{\boldsymbol{\xi}_G\in\Gamma_G}\Big(\frac{1}{r(\boldsymbol{\chi}_I,\boldsymbol{\xi}_G)}+\frac{1}{r(\boldsymbol{\chi}_I',\boldsymbol{\xi}_G)}\Big)\,\sigma_G(\boldsymbol{\xi}_G)\,\mathrm{d}\Gamma_G\\ &+\frac{1}{4\pi\gamma}\iint_{\boldsymbol{\xi}_I\in\Gamma_I}\Big(\frac{1}{r(\boldsymbol{\chi}_I,\boldsymbol{\xi}_I)}+\frac{1}{r(\boldsymbol{\chi}_I',\boldsymbol{\xi}_I)}\Big)\,\sigma_I(\boldsymbol{\xi}_I)\,\mathrm{d}\Gamma_I\\ &+\frac{1}{4\pi}\iint_{\boldsymbol{\xi}_I\in\Gamma_I}\Big[\Big(\nabla\Big(\frac{1}{r(\boldsymbol{\chi}_I,\boldsymbol{\xi}_I)}\Big)+\nabla\Big(\frac{1}{r(\boldsymbol{\chi}_I',\boldsymbol{\xi}_I)}\Big)\Big)\cdot\boldsymbol{n}(\boldsymbol{\xi}_I)\Big]\,V_I(\boldsymbol{\xi}_I)\,\mathrm{d}\Gamma_I\end{aligned} \tag{3.95}$$

Boundary integral equation of the interior problem

$$\begin{aligned}\frac{1}{2}V_I(\boldsymbol{\chi}_I) = &-\frac{1}{4\pi\gamma_I}\iint_{\boldsymbol{\xi}_I\in\Gamma_I}\frac{1}{r(\boldsymbol{\chi}_I,\boldsymbol{\xi}_I)}\,\sigma_I(\boldsymbol{\xi}_I)\,\mathrm{d}\Gamma_I\\ &-\frac{1}{4\pi}\iint_{\boldsymbol{\xi}_I\in\Gamma_I}\Big[\nabla\Big(\frac{1}{r(\boldsymbol{\chi}_I,\boldsymbol{\xi}_I)}\Big)\cdot\boldsymbol{n}(\boldsymbol{\xi}_I)\Big]V_I(\boldsymbol{\xi}_I)\,\mathrm{d}\Gamma_I\end{aligned} \tag{3.96}$$

3.4 Boundary integral equations of the model

As it was presented in Chapter 2, the developed approach allows to calculate the leakage current densities emanating from the surface of the grounding grid to the ground ($\sigma_G(\boldsymbol{\xi}_G)$), and the current densities ($\sigma_I(\boldsymbol{\xi}_I)$) and the potential field ($V_I(\boldsymbol{\xi}_I)$) over the enclosure surface (Γ_I). These will be the basic magnitudes in order to calculate the main parameters that characterise a grounding system.

Therefore, three equations are necessary to calculate these unknowns. These will be formed by the boundary integral equations carried out in Section 3.3, which are the result of recasting the potential problems deduced in the previous chapter. The boundary integral equations chosen to solve this problem are:

1. Equation from the boundary condition of the exterior Dirichlet problem $V(\boldsymbol{\chi}_G) = V_G$

$$\begin{aligned} V_G = & \frac{1}{4\pi\gamma} \iint_{\boldsymbol{\xi}_G \in \Gamma_G} \left(\frac{1}{r(\boldsymbol{\chi}_G, \boldsymbol{\xi}_G)} + \frac{1}{r(\boldsymbol{\chi}_G', \boldsymbol{\xi}_G)} \right) \sigma_G(\boldsymbol{\xi}_G)\, \mathrm{d}\Gamma_G \\ & + \frac{1}{4\pi\gamma} \iint_{\boldsymbol{\xi}_I \in \Gamma_I} \left(\frac{1}{r(\boldsymbol{\chi}_G, \boldsymbol{\xi}_I)} + \frac{1}{r(\boldsymbol{\chi}_G', \boldsymbol{\xi}_I)} \right) \sigma_I(\boldsymbol{\xi}_I)\, \mathrm{d}\Gamma_I \\ & + \frac{1}{4\pi} \iint_{\boldsymbol{\xi}_I \in \Gamma_I} \left[\left(\nabla \left(\frac{1}{r(\boldsymbol{\chi}_G, \boldsymbol{\xi}_I)} \right) + \nabla \left(\frac{1}{r(\boldsymbol{\chi}_G', \boldsymbol{\xi}_I)} \right) \right) \cdot \boldsymbol{n}(\boldsymbol{\xi}_I) \right] V_I(\boldsymbol{\xi}_I)\, \mathrm{d}\Gamma_I \end{aligned} \tag{3.97}$$

2. Equation from the compatibility conditions applied on the exterior Dirichlet problem

$$\begin{aligned} \frac{1}{2} V_I(\boldsymbol{\chi}_I) = & \frac{1}{4\pi\gamma} \iint_{\boldsymbol{\xi}_G \in \Gamma_G} \left(\frac{1}{r(\boldsymbol{\chi}_I, \boldsymbol{\xi}_G)} + \frac{1}{r(\boldsymbol{\chi}_I', \boldsymbol{\xi}_G)} \right) \sigma_G(\boldsymbol{\xi}_G)\, \mathrm{d}\Gamma_G \\ & + \frac{1}{4\pi\gamma} \iint_{\boldsymbol{\xi}_I \in \Gamma_I} \left(\frac{1}{r(\boldsymbol{\chi}_I, \boldsymbol{\xi}_I)} + \frac{1}{r(\boldsymbol{\chi}_I', \boldsymbol{\xi}_I)} \right) \sigma_I(\boldsymbol{\xi}_I)\, \mathrm{d}\Gamma_I \\ & + \frac{1}{4\pi} \iint_{\boldsymbol{\xi}_I \in \Gamma_I} \left[\left(\nabla \left(\frac{1}{r(\boldsymbol{\chi}_I, \boldsymbol{\xi}_I)} \right) + \nabla \left(\frac{1}{r(\boldsymbol{\chi}_I', \boldsymbol{\xi}_I)} \right) \right) \cdot \boldsymbol{n}(\boldsymbol{\xi}_I) \right] V_I(\boldsymbol{\xi}_I)\, \mathrm{d}\Gamma_I \end{aligned} \tag{3.98}$$

3. Equation from the compatibility conditions applied on the interior problem

$$\begin{aligned} \frac{1}{2} V_I(\boldsymbol{\chi}_I) = & -\frac{1}{4\pi\gamma_I} \iint_{\boldsymbol{\xi}_I \in \Gamma_I} \frac{1}{r(\boldsymbol{\chi}_I, \boldsymbol{\xi}_I)}\, \sigma_I(\boldsymbol{\xi}_I)\, \mathrm{d}\Gamma_I \\ & - \frac{1}{4\pi} \iint_{\boldsymbol{\xi}_I \in \Gamma_I} \left[\nabla \left(\frac{1}{r(\boldsymbol{\chi}_I, \boldsymbol{\xi}_I)} \right) \cdot \boldsymbol{n}(\boldsymbol{\xi}_I) \right] V_I(\boldsymbol{\xi}_I)\, \mathrm{d}\Gamma_I \end{aligned} \tag{3.99}$$

Once the values of σ_G, σ_I and V_I are obtained from the above system of equations, the electric potential at any point in the ground can be calculated, as well as the ground resistance, and the step and touch voltages, which are the main parameters of grounding systems.

3.5 Equation to calculate the electric potential in the ground

An important point in grounding grid analysis is to be able to calculate the earth surface potentials, since these values are necessary to determine the touch and step voltage distributions and analyse the safety of electrical substations (Section 2.6). In the mathematical model carried out in this thesis to analyse the grounding system of an underground electrical substation, the electric potential at any point in the ground is obtained by means of the following boundary integral equation:

$$\begin{aligned} V(\boldsymbol{x}) = & \frac{1}{4\pi\gamma} \iint_{\boldsymbol{\xi}_G \in \Gamma_G} \left(\frac{1}{r(\boldsymbol{x}, \boldsymbol{\xi}_G)} + \frac{1}{r(\boldsymbol{x}', \boldsymbol{\xi}_G)} \right) \sigma_G(\boldsymbol{\xi}_G) \, \mathrm{d}\Gamma_G \\ & + \frac{1}{4\pi\gamma} \iint_{\boldsymbol{\xi}_I \in \Gamma_I} \left(\frac{1}{r(\boldsymbol{x}, \boldsymbol{\xi}_I)} + \frac{1}{r(\boldsymbol{x}', \boldsymbol{\xi}_I)} \right) \sigma_I(\boldsymbol{\xi}_I) \, \mathrm{d}\Gamma_I \\ & + \frac{1}{4\pi} \iint_{\boldsymbol{\xi}_I \in \Gamma_I} \left[\left(\nabla \left(\frac{1}{r(\boldsymbol{x}, \boldsymbol{\xi}_I)} \right) + \nabla \left(\frac{1}{r(\boldsymbol{x}', \boldsymbol{\xi}_I)} \right) \right) \cdot \boldsymbol{n}(\boldsymbol{\xi}_I) \right] V_I(\boldsymbol{\xi}_I) \, \mathrm{d}\Gamma_I \end{aligned} \tag{3.100}$$

where $V(\boldsymbol{x})$ is the value of the potential function in a source point $\boldsymbol{x}$ located in the domain Ω (the ground).

The above equation can be simplified using the boundary integral equation obtained from the interior problem. The general expression of this equation formulated with the unknowns that belong to the exterior problem is

$$\begin{aligned} c(\boldsymbol{x}_I) V_I(\boldsymbol{x}_I) = & -\frac{1}{4\pi\gamma_I} \iint_{\boldsymbol{\xi}_I \in \Gamma_I} \frac{1}{r(\boldsymbol{x}_I, \boldsymbol{\xi}_I)} \, \sigma_I(\boldsymbol{\xi}_I) \, \mathrm{d}\Gamma_I \\ & - \frac{1}{4\pi} \iint_{\boldsymbol{\xi}_I \in \Gamma_I} \left[\nabla \left(\frac{1}{r(\boldsymbol{x}_I, \boldsymbol{\xi}_I)} \right) \cdot \boldsymbol{n}(\boldsymbol{\xi}_I) \right] V_I(\boldsymbol{\xi}_I) \, \mathrm{d}\Gamma_I \end{aligned} \tag{3.101}$$

where $V_I(\boldsymbol{x}_I)$ is the value of the potential function in a source point $\boldsymbol{x}_I$ located in the domain Ω_I, and $c(\boldsymbol{x}_I)$ is a free coefficient that depends on the location of $\boldsymbol{x}_I$. The principal values of $c(\boldsymbol{x}_I)$ are

$$c(\boldsymbol{x}_I) = 1 \quad \text{if} \quad \boldsymbol{x}_I \in \Omega_I$$

$$c(\boldsymbol{x}_I) = \frac{1}{2} \quad \text{if} \quad \boldsymbol{x}_I \in \Gamma_I$$

$$c(\boldsymbol{x}_I) = 0 \quad \text{if} \quad \boldsymbol{x}_I \notin \Omega_I \text{ and } \boldsymbol{x}_I \notin \Gamma_I$$

Therefore, in order to simplify the boundary integral equation (3.100), the following is taken into account:

Let $\boldsymbol{x}_I$ be a point $\boldsymbol{x}$ located outside the closed domain Ω_I, so the value of the free coefficient is zero and equation (3.101) is equal to

$$\begin{aligned} 0 = &-\frac{1}{4\pi\gamma_I}\iint_{\boldsymbol{\xi}_I\in\Gamma_I}\frac{1}{r(\boldsymbol{x},\boldsymbol{\xi}_I)}\,\sigma_I(\boldsymbol{\xi}_I)\,\mathrm{d}\Gamma_I \\ &-\frac{1}{4\pi}\iint_{\boldsymbol{\xi}_I\in\Gamma_I}\Big[\nabla\Big(\frac{1}{r(\boldsymbol{x},\boldsymbol{\xi}_I)}\Big)\cdot\boldsymbol{n}(\boldsymbol{\xi}_I)\Big]V_I(\boldsymbol{\xi}_I)\,\mathrm{d}\Gamma_I \end{aligned} \tag{3.102}$$

Let $\boldsymbol{x}_I$ be a point $\boldsymbol{x}^{'}$ located outside the closed domain Ω_I and symmetric to the previous $\boldsymbol{x}$. Thus, the value of the free coefficient is zero again and equation (3.101) is equal to

$$\begin{aligned} 0 = &-\frac{1}{4\pi\gamma_I}\iint_{\boldsymbol{\xi}_I\in\Gamma_I}\frac{1}{r(\boldsymbol{x}',\boldsymbol{\xi}_I)}\,\sigma_I(\boldsymbol{\xi}_I)\,\mathrm{d}\Gamma_I \\ &-\frac{1}{4\pi}\iint_{\boldsymbol{\xi}_I\in\Gamma_I}\Big[\nabla\Big(\frac{1}{r(\boldsymbol{x}',\boldsymbol{\xi}_I)}\Big)\cdot\boldsymbol{n}(\boldsymbol{\xi}_I)\Big]V_I(\boldsymbol{\xi}_I)\,\mathrm{d}\Gamma_I \end{aligned} \tag{3.103}$$

Adding equations (3.102) and (3.103) is obtained

$$\begin{aligned} 0 = &-\frac{1}{4\pi\gamma_I}\iint_{\boldsymbol{\xi}_I\in\Gamma_I}\Big(\frac{1}{r(\boldsymbol{x},\boldsymbol{\xi}_I)}+\frac{1}{r(\boldsymbol{x}',\boldsymbol{\xi}_I)}\Big)\,\sigma_I(\boldsymbol{\xi}_I)\,\mathrm{d}\Gamma_I \\ &-\frac{1}{4\pi}\iint_{\boldsymbol{\xi}_I\in\Gamma_I}\Big[\Big(\nabla\Big(\frac{1}{r(\boldsymbol{x},\boldsymbol{\xi}_I)}\Big)+\nabla\Big(\frac{1}{r(\boldsymbol{x}',\boldsymbol{\xi}_I)}\Big)\Big)\cdot\boldsymbol{n}(\boldsymbol{\xi}_I)\Big]V_I(\boldsymbol{\xi}_I)\,\mathrm{d}\Gamma_I \end{aligned} \tag{3.104}$$

The above integral equation can be rewritten as

$$\begin{aligned} &\frac{1}{4\pi}\iint_{\boldsymbol{\xi}_I\in\Gamma_I}\Big[\Big(\nabla\Big(\frac{1}{r(\boldsymbol{x},\boldsymbol{\xi}_I)}\Big)+\nabla\Big(\frac{1}{r(\boldsymbol{x}',\boldsymbol{\xi}_I)}\Big)\Big)\cdot\boldsymbol{n}(\boldsymbol{\xi}_I)\Big]V_I(\boldsymbol{\xi}_I)\,\mathrm{d}\Gamma_I = \\ &-\frac{1}{4\pi\gamma_I}\iint_{\boldsymbol{\xi}_I\in\Gamma_I}\Big(\frac{1}{r(\boldsymbol{x},\boldsymbol{\xi}_I)}+\frac{1}{r(\boldsymbol{x}',\boldsymbol{\xi}_I)}\Big)\,\sigma_I(\boldsymbol{\xi}_I)\,\mathrm{d}\Gamma_I \end{aligned} \tag{3.105}$$

Consequently, if the third integral on the right-hand side on equation (3.100) is replaced by the right-hand side of equation (3.105), the equation to calculate the electric potential at any point in the ground is formulated as

$$\begin{aligned} V(\boldsymbol{x}) = &\frac{1}{4\pi\gamma}\iint_{\boldsymbol{\xi}_G\in\Gamma_G}\Big(\frac{1}{r(\boldsymbol{x},\boldsymbol{\xi}_G)}+\frac{1}{r(\boldsymbol{x}',\boldsymbol{\xi}_G)}\Big)\,\sigma_G(\boldsymbol{\xi}_G)\,\mathrm{d}\Gamma_G \\ &+\frac{1}{4\pi\gamma}\iint_{\boldsymbol{\xi}_I\in\Gamma_I}\Big(\frac{1}{r(\boldsymbol{x},\boldsymbol{\xi}_I)}+\frac{1}{r(\boldsymbol{x}',\boldsymbol{\xi}_I)}\Big)\,\sigma_I(\boldsymbol{\xi}_I)\,\mathrm{d}\Gamma_I \\ &-\frac{1}{4\pi\gamma_I}\iint_{\boldsymbol{\xi}_I\in\Gamma_I}\Big(\frac{1}{r(\boldsymbol{x},\boldsymbol{\xi}_I)}+\frac{1}{r(\boldsymbol{x}',\boldsymbol{\xi}_I)}\Big)\,\sigma_I(\boldsymbol{\xi}_I)\,\mathrm{d}\Gamma_I \end{aligned} \tag{3.106}$$

where the terms involving $\sigma_I(\boldsymbol{\xi}_I)$ can be gathered, and thus equation (3.106) can be rewritten as

$$\begin{aligned} V(\boldsymbol{x}) = & \frac{1}{4\pi\gamma} \iint_{\boldsymbol{\xi}_G \in \Gamma_G} \left(\frac{1}{r(\boldsymbol{x}, \boldsymbol{\xi}_G)} + \frac{1}{r(\boldsymbol{x}', \boldsymbol{\xi}_G)} \right) \sigma_G(\boldsymbol{\xi}_G) \, \mathrm{d}\Gamma_G \\ & + \frac{1}{4\pi\gamma} \left(1 - \frac{\gamma}{\gamma_I}\right) \iint_{\boldsymbol{\xi}_I \in \Gamma_I} \left(\frac{1}{r(\boldsymbol{x}, \boldsymbol{\xi}_I)} + \frac{1}{r(\boldsymbol{x}', \boldsymbol{\xi}_I)} \right) \sigma_I(\boldsymbol{\xi}_I) \, \mathrm{d}\Gamma_I \end{aligned} \tag{3.107}$$

The above equation is the simplified equation to calculate the value of the electric potential at any point in the ground. This is the general equation for a medium with a finite heterogeneity inside it. In that expression, if it is stated that the apparent conductivity of domain Ω_I is equal to the apparent conductivity of domain Ω ($\gamma_I = \gamma$), the simplified boundary integral equation (3.107) is reduced to

$$V(\boldsymbol{x}) = \frac{1}{4\pi\gamma} \iint_{\boldsymbol{\xi}_G \in \Gamma_G} \left(\frac{1}{r(\boldsymbol{x}, \boldsymbol{\xi}_G)} + \frac{1}{r(\boldsymbol{x}', \boldsymbol{\xi}_G)} \right) \sigma_G(\boldsymbol{\xi}_G) \, \mathrm{d}\Gamma_G \tag{3.108}$$

which refers to a homogeneous domain.

It is important to note that the boundary integral equation (3.108) is the same formula that [Colominas, 1995] deduced to calculate the value of potential at any point in a homogenous ground for the grounding system of aboveground electrical substations.

3.6 Conclusions

In this chapter the potential problems that govern the physical phenomenon of fault current derivation into the ground through the grounding grid of an underground electrical substation has been stated and transformed into the integral form, which provides a more practical approach for numerical analysis.

In order to formulate these boundary integral equations, some basics concepts have been presented such as the definition of a harmonic function or the fundamental solution of the Laplace equation. Also, the divergence theorem and its corollaries, the Green's Identities, are introduced, since they are the foundation of the mathematical model to obtain the boundary integral equations.

Based on those concepts, the exterior Dirichlet problem first, and then, the interior problems are formulated as boundary integral equations. As a result, the boundary integral equations of the model are obtained after applying the boundary and compatibility conditions to the integral equations of each problem. The resolution of these coupled equations gives the unknowns functions σ_G, σ_I and V_I, from which the main parameters that characterise a grounding system can be calculated.

In addition, the equation to calculate the electric potential at any point in the ground has been simplified using the boundary integrals of both problems. In this simplified equation has been proven that if the scalar apparent conductivities are equal,

the resulting equation has the same expression that the formula obtained by [Colominas, 1995] to calculate the grounding systems of aboveground electrical substations in uniform soil.

Next chapter is devoted to present the numerical approach used to solve the boundary integral equations of the model.

Chapter 4

Numerical Model

4.1 Introduction

Generally, the boundary integral equations are solved numerically and they can be only solved analytically for some simple problems. So, to calculate the unknown functions that allow to obtain the main parameters that define the grounding systems of electrical substations will be necessary to develop a numerical approach.

The adequate numerical method to solve this problem, where the equations are set in the boundaries of the domains, is the Boundary Element Method (BEM). This method is used to solve general problems, with arbitrary geometry and boundary conditions. It is special useful in problems with unbounded domains, as the ground in this problem, since it is not necessary to use infinite elements to mesh the domain or truncate it. Another advantage of the BEM is that problems are reduced in one dimension since the integral equations are formulated on the boundaries, so 3D problems like this are reduced to 2D problems.

The most important point in the BEM is the integration of kernels. A good resolution of these integrals provides accurate results. At the same time, it is the most crucial aspect because the integrated functions can present singularities at certain points. For the problems where the discretisation procedure is done with constant elements with a straight geometry, the integrals can be calculated analytically, but in most cases linear or high-order elements are used to approximate the geometry and functions. Consequently, the integrals are calculated with numerical techniques.

In this chapter, a numerical model to solve the system of boundary integral equations obtained in Chapter 3 is developed. This model is based on the Boundary Element Method, which has been applied with two different weighted residual techniques: the Point Collocation Method and the Bubnov-Galerkin Method. In order to achieve this objective, a weak formulation is introduced first in Section 4.2 together with a hypothesis in order to simplify the integral equations. The Weighted Residual Methods

and the Boundary Element Method are presented in Sections 4.3 and 4.4. The numerical approaches are developed in Sections 4.5 and 4.6. And finally, the expression to calculate the value of potential function at any point in the ground is obtained in Section 4.7.

4.2 Weak form of the Boundary Integral Equations

In the previous chapter the governing equations for the phenomenon of electric current derivation to ground through a protection system were stated. The system of equations obtained is formed by the following boundary integral equations:

- The equation from the boundary condition of the exterior Dirichlet problem:

$$\begin{aligned} V_G = & \frac{1}{4\pi\gamma} \iint_{\boldsymbol{\xi}_G \in \Gamma_G} \Big(\frac{1}{r(\boldsymbol{\chi}_G, \boldsymbol{\xi}_G)} + \frac{1}{r(\boldsymbol{\chi}_G', \boldsymbol{\xi}_G)} \Big) \, \sigma_G(\boldsymbol{\xi}_G) \, \mathrm{d}\Gamma_G \\ & + \frac{1}{4\pi\gamma} \iint_{\boldsymbol{\xi}_I \in \Gamma_I} \Big(\frac{1}{r(\boldsymbol{\chi}_G, \boldsymbol{\xi}_I)} + \frac{1}{r(\boldsymbol{\chi}_G', \boldsymbol{\xi}_I)} \Big) \, \sigma_I(\boldsymbol{\xi}_I) \, \mathrm{d}\Gamma_I \\ & + \frac{1}{4\pi} \iint_{\boldsymbol{\xi}_I \in \Gamma_I} \Big[\Big(\nabla \Big(\frac{1}{r(\boldsymbol{\chi}_G, \boldsymbol{\xi}_I)} \Big) + \nabla \Big(\frac{1}{r(\boldsymbol{\chi}_G', \boldsymbol{\xi}_I)} \Big) \Big) \cdot \boldsymbol{n}(\boldsymbol{\xi}_I) \Big] \, V_I(\boldsymbol{\xi}_I) \, \mathrm{d}\Gamma_I \end{aligned} \tag{4.1}$$

- The equation from the compatibility conditions applied on the exterior Dirichlet problem:

$$\begin{aligned} \frac{1}{2} V_I(\boldsymbol{\chi}_I) = & \frac{1}{4\pi\gamma} \iint_{\boldsymbol{\xi}_G \in \Gamma_G} \Big(\frac{1}{r(\boldsymbol{\chi}_I, \boldsymbol{\xi}_G)} + \frac{1}{r(\boldsymbol{\chi}_I', \boldsymbol{\xi}_G)} \Big) \, \sigma_G(\boldsymbol{\xi}_G) \, \mathrm{d}\Gamma_G \\ & + \frac{1}{4\pi\gamma} \iint_{\boldsymbol{\xi}_I \in \Gamma_I} \Big(\frac{1}{r(\boldsymbol{\chi}_I, \boldsymbol{\xi}_I)} + \frac{1}{r(\boldsymbol{\chi}_I', \boldsymbol{\xi}_I)} \Big) \, \sigma_I(\boldsymbol{\xi}_I) \, \mathrm{d}\Gamma_I \\ & + \frac{1}{4\pi} \iint_{\boldsymbol{\xi}_I \in \Gamma_I} \Big[\Big(\nabla \Big(\frac{1}{r(\boldsymbol{\chi}_I, \boldsymbol{\xi}_I)} \Big) + \nabla \Big(\frac{1}{r(\boldsymbol{\chi}_I', \boldsymbol{\xi}_I)} \Big) \Big) \cdot \boldsymbol{n}(\boldsymbol{\xi}_I) \Big] \, V_I(\boldsymbol{\xi}_I) \, \mathrm{d}\Gamma_I \end{aligned} \tag{4.2}$$

- The equation from the compatibility conditions applied on the interior problem:

$$\begin{aligned} \frac{1}{2} V_I(\boldsymbol{\chi}_I) = & -\frac{1}{4\pi\gamma_I} \iint_{\boldsymbol{\xi}_I \in \Gamma_I} \frac{1}{r(\boldsymbol{\chi}_I, \boldsymbol{\xi}_I)} \, \sigma_I(\boldsymbol{\xi}_I) \, \mathrm{d}\Gamma_I \\ & - \frac{1}{4\pi} \iint_{\boldsymbol{\xi}_I \in \Gamma_I} \Big[\nabla \Big(\frac{1}{r(\boldsymbol{\chi}_I, \boldsymbol{\xi}_I)} \Big) \cdot \boldsymbol{n}(\boldsymbol{\xi}_I) \Big] V_I(\boldsymbol{\xi}_I) \, \mathrm{d}\Gamma_I \end{aligned} \tag{4.3}$$

These equations are the strong form of the problem. One approach to obtain the solution of this problem is to recast it in an alternative form from which accurate approximate solutions can be calculated. In this case the alternative approach considered is to reformulate the boundary integral equations into a weak form. In order to establish a weak form, equations (4.1) to (4.3) are multiplied by an appropriate arbitrary function and the result expression will be integrated over its space domain [Zienkiewicz

et al., 2013]. The arbitrary functions are called as weighting functions. The definition and properties of these functions are described in [Hughes, 1987].

Let $\omega_G(\boldsymbol{\chi}_G)$ and $\omega_I(\boldsymbol{\chi}_I)$ be weighting functions defined in Γ_G and Γ_I, respectively. The weak form of the governing equations is given by:

- Weak form of the equation from the boundary condition of the exterior Dirichlet problem:

$$\begin{aligned}
&\iint_{\boldsymbol{\chi}_G \in \Gamma_G} \omega_G(\boldsymbol{\chi}_G) \Bigg[V_G - \frac{1}{4\pi\gamma} \iint_{\boldsymbol{\xi}_G \in \Gamma_G} \Big(\frac{1}{r(\boldsymbol{\chi}_G, \boldsymbol{\xi}_G)} + \frac{1}{r(\boldsymbol{\chi}_G^{'}, \boldsymbol{\xi}_G)} \Big) \, \sigma_G(\boldsymbol{\xi}_G) \, \mathrm{d}\Gamma_G \\
&- \frac{1}{4\pi\gamma} \iint_{\boldsymbol{\xi}_I \in \Gamma_I} \Big(\frac{1}{r(\boldsymbol{\chi}_G, \boldsymbol{\xi}_I)} + \frac{1}{r(\boldsymbol{\chi}_G^{'}, \boldsymbol{\xi}_I)} \Big) \, \sigma_I(\boldsymbol{\xi}_I) \, \mathrm{d}\Gamma_I \\
&- \frac{1}{4\pi} \iint_{\boldsymbol{\xi}_I \in \Gamma_I} \Big[\Big(\nabla \Big(\frac{1}{r(\boldsymbol{\chi}_G, \boldsymbol{\xi}_I)} \Big) + \nabla \Big(\frac{1}{r(\boldsymbol{\chi}_G^{'}, \boldsymbol{\xi}_I)} \Big) \Big) \cdot \boldsymbol{n}(\boldsymbol{\xi}_I) \Big] \, V_I(\boldsymbol{\xi}_I) \, \mathrm{d}\Gamma_I \Bigg] \, \mathrm{d}\Gamma_G = 0
\end{aligned} \tag{4.4}$$

- Weak form of the equation from the compatibility conditions applied on the exterior Dirichlet problem:

$$\begin{aligned}
&\iint_{\boldsymbol{\chi}_I \in \Gamma_I} \omega_I(\boldsymbol{\chi}_I) \Bigg[\frac{1}{4\pi\gamma} \iint_{\boldsymbol{\xi}_G \in \Gamma_G} \Big(\frac{1}{r(\boldsymbol{\chi}_I, \boldsymbol{\xi}_G)} + \frac{1}{r(\boldsymbol{\chi}_I^{'}, \boldsymbol{\xi}_G)} \Big) \, \sigma_G(\boldsymbol{\xi}_G) \, \mathrm{d}\Gamma_G \\
&+ \frac{1}{4\pi\gamma} \iint_{\boldsymbol{\xi}_I \in \Gamma_I} \Big(\frac{1}{r(\boldsymbol{\chi}_I, \boldsymbol{\xi}_I)} + \frac{1}{r(\boldsymbol{\chi}_I^{'}, \boldsymbol{\xi}_I)} \Big) \, \sigma_I(\boldsymbol{\xi}_I) \, \mathrm{d}\Gamma_I \\
&+ \frac{1}{4\pi} \iint_{\boldsymbol{\xi}_I \in \Gamma_I} \Big[\Big(\nabla \Big(\frac{1}{r(\boldsymbol{\chi}_I, \boldsymbol{\xi}_I)} \Big) + \nabla \Big(\frac{1}{r(\boldsymbol{\chi}_I^{'}, \boldsymbol{\xi}_I)} \Big) \Big) \cdot \boldsymbol{n}(\boldsymbol{\xi}_I) \Big] \, V_I(\boldsymbol{\xi}_I) \, \mathrm{d}\Gamma_I \\
&- \frac{1}{2} \, V_I(\boldsymbol{\chi}_I) \Bigg] \, \mathrm{d}\Gamma_I = 0
\end{aligned} \tag{4.5}$$

- Weak form of the equation from the compatibility conditions applied on the interior problem:

$$\begin{aligned}
&\iint_{\boldsymbol{\chi}_I \in \Gamma_I} \omega_I(\boldsymbol{\chi}_I) \Bigg[\frac{1}{4\pi\gamma_I} \iint_{\boldsymbol{\xi}_I \in \Gamma_I} \frac{1}{r(\boldsymbol{\chi}_I, \boldsymbol{\xi}_I)} \, \sigma_I(\boldsymbol{\xi}_I) \, \mathrm{d}\Gamma_I \\
&+ \frac{1}{4\pi} \iint_{\boldsymbol{\xi}_I \in \Gamma_I} \Big[\nabla \Big(\frac{1}{r(\boldsymbol{\chi}_I, \boldsymbol{\xi}_I)} \Big) \cdot \boldsymbol{n}(\boldsymbol{\xi}_I) \Big] V_I(\boldsymbol{\xi}_I) \, \mathrm{d}\Gamma_I + \frac{1}{2} \, V_I(\boldsymbol{\chi}_I) \Bigg] \, \mathrm{d}\Gamma_I = 0
\end{aligned} \tag{4.6}$$

Obviously, there must be equivalence between the strong and weak form, since the solution of both formulations have to be the same. This equivalence is established assuming that all approximate functions are smooth [Hughes, 1987].

4.2.1 Assumption of circumferential uniformity in the electrodes

An assumption of circumferential uniformity in the electrodes will be done to simplify the previous equations. It consists of supposing that the leakage current is constant around the perimeter of every cross section on the electrodes [Colominas, 1995]. This assumption is adequate and not too restrictive, taking into account the geometry of the electrodes belonging to the grounding grids. That is, the electrodes used to be longer in comparison with their diameters.

Let $\boldsymbol{\xi}_G$ be a generic point on Γ_G, $\widehat{\boldsymbol{\xi}}_G$ its orthogonal projection, $\phi(\widehat{\boldsymbol{\xi}}_G)$ the diameter and $C(\widehat{\boldsymbol{\xi}}_G)$ the circumferential perimeter of the cross section at this point.

With this assumption a new current density function ($\widehat{\sigma}_G$) is defined. It can be expressed as

$$\sigma_G(\boldsymbol{\xi}_G) = \widehat{\sigma}_G(\widehat{\boldsymbol{\xi}}_G), \qquad \forall\ \boldsymbol{\xi}_G \in C(\widehat{\boldsymbol{\xi}}_G)$$

So, $\widehat{\sigma}_G$ is the current density which emanates from the electrodes of a grounding grid assuming that there is a circumferential uniformity.

This new current density will be introduced in equations (4.4) and (4.5). In order to satisfy equation (4.4), the weighting functions are restricted to functions with circumferential uniformity. So,

$$\omega_G(\boldsymbol{\chi}_G) = \widehat{\omega}_G(\widehat{\boldsymbol{\chi}}_G), \qquad \forall\ \boldsymbol{\chi}_G \in C(\widehat{\boldsymbol{\chi}}_G)$$

Thus, equations (4.4) and (4.5) are rewritten as:

$$\begin{aligned}
&\int_{\widehat{\boldsymbol{\chi}}_G \in L_G} \int_{\boldsymbol{\chi}_G \in C_G(\widehat{\boldsymbol{\chi}}_G)} \omega_G(\boldsymbol{\chi}_G) \Bigg[V_G \\
&-\frac{1}{4\pi\gamma} \int_{\widehat{\boldsymbol{\xi}}_G \in L_G} \int_{\boldsymbol{\xi}_G \in C_G(\widehat{\boldsymbol{\chi}}_G)} \left(\frac{1}{r(\boldsymbol{\chi}_G, \boldsymbol{\xi}_G)} + \frac{1}{r(\boldsymbol{\chi}_G^{'}, \boldsymbol{\xi}_G)} \right) \sigma_G(\boldsymbol{\xi}_G)\, \mathrm{d}C_G\, \mathrm{d}L_G \\
&-\frac{1}{4\pi\gamma} \iint_{\boldsymbol{\xi}_I \in \Gamma_I} \left(\frac{1}{r(\boldsymbol{\chi}_G, \boldsymbol{\xi}_I)} + \frac{1}{r(\boldsymbol{\chi}_G^{'}, \boldsymbol{\xi}_I)} \right) \sigma_I(\boldsymbol{\xi}_I)\, \mathrm{d}\Gamma_I \\
&-\frac{1}{4\pi} \iint_{\boldsymbol{\xi}_I \in \Gamma_I} \left[\left(\nabla\left(\frac{1}{r(\boldsymbol{\chi}_G, \boldsymbol{\xi}_I)} \right) + \nabla\left(\frac{1}{r(\boldsymbol{\chi}_G^{'}, \boldsymbol{\xi}_I)} \right) \right) \cdot \boldsymbol{n}(\boldsymbol{\xi}_I) \right] V_I(\boldsymbol{\xi}_I)\, \mathrm{d}\Gamma_I \Bigg] \mathrm{d}C_G\, \mathrm{d}L_G = 0
\end{aligned} \tag{4.7}$$

$$\begin{aligned}
&\iint_{\boldsymbol{\chi}_I \in \Gamma_I} \omega_I(\boldsymbol{\chi}_I) \Bigg[\frac{1}{4\pi\gamma} \int_{\widehat{\boldsymbol{\xi}}_G \in L_G} \int_{\boldsymbol{\xi}_G \in C_G(\widehat{\boldsymbol{\xi}}_G)} \left(\frac{1}{r(\boldsymbol{\chi}_I, \boldsymbol{\xi}_G)} + \frac{1}{r(\boldsymbol{\chi}_I^{'}, \boldsymbol{\xi}_G)} \right) \sigma_G(\boldsymbol{\xi}_G)\, \mathrm{d}L_G\, \mathrm{d}C_G \\
&+\frac{1}{4\pi\gamma} \iint_{\boldsymbol{\xi}_I \in \Gamma_I} \left(\frac{1}{r(\boldsymbol{\chi}_I, \boldsymbol{\xi}_I)} + \frac{1}{r(\boldsymbol{\chi}_I^{'}, \boldsymbol{\xi}_I)} \right) \sigma_I(\boldsymbol{\xi}_I)\, \mathrm{d}\Gamma_I \\
&+\frac{1}{4\pi} \iint_{\boldsymbol{\xi}_I \in \Gamma_I} \left[\left(\nabla\left(\frac{1}{r(\boldsymbol{\chi}_I, \boldsymbol{\xi}_I)} \right) + \nabla\left(\frac{1}{r(\boldsymbol{\chi}_I^{'}, \boldsymbol{\xi}_I)} \right) \right) \cdot \boldsymbol{n}(\boldsymbol{\xi}_I) \right] V_I(\boldsymbol{\xi}_I)\, \mathrm{d}\Gamma_I \\
&-\frac{1}{2} V_I(\boldsymbol{\chi}_I) \Bigg] \mathrm{d}\Gamma_I = 0
\end{aligned} \tag{4.8}$$

where the boundary integrals Γ_G can be decoupled in integrals in the axial line of the electrodes L_G and integrals in the circumferential perimeter C_G.

Every term of the previous equations can be written alone as follows:

- The first integral on the left-hand of equation (4.7):

$$\widehat{\nu}_G = V_G \int_{\widehat{\boldsymbol{\chi}}_G \in L_G} \widehat{\omega}_G(\widehat{\boldsymbol{\chi}}_G) \left[\int_{\boldsymbol{\chi}_G \in C_G(\widehat{\boldsymbol{\chi}}_G)} \mathrm{d}C_G \right] \mathrm{d}L_G \tag{4.9}$$

- The second integral on the left-hand of equation (4.7):

$$\widehat{R}_{GG} = \frac{1}{4\pi\gamma} \int_{\widehat{\boldsymbol{\chi}}_G \in L_G} \widehat{\omega}_G(\widehat{\boldsymbol{\chi}}_G) \left[\int_{\widehat{\boldsymbol{\xi}}_G \in L_G} K(\widehat{\boldsymbol{\chi}}_G, \widehat{\boldsymbol{\xi}}_G)\ \widehat{\sigma}_G(\widehat{\boldsymbol{\xi}}_G)\ \mathrm{d}L_G \right] \mathrm{d}L_G \tag{4.10}$$

  where

$$K(\widehat{\boldsymbol{\chi}}_G, \widehat{\boldsymbol{\xi}}_G) = \int_{\boldsymbol{\chi}_G \in C_G(\widehat{\boldsymbol{\chi}}_G)} \left[\int_{\boldsymbol{\xi}_G \in C_G(\widehat{\boldsymbol{\xi}}_G)} \left(\frac{1}{r(\boldsymbol{\chi}_G, \boldsymbol{\xi}_G)} + \frac{1}{r(\boldsymbol{\chi}_G', \boldsymbol{\xi}_G)} \right) \mathrm{d}C_G \right] \mathrm{d}C_G \tag{4.11}$$

- The third integral on the left-hand of equation (4.7):

$$\widehat{R}_{GI} = \frac{1}{4\pi\gamma} \int_{\widehat{\boldsymbol{\chi}}_G \in L_G} \widehat{\omega}_G(\widehat{\boldsymbol{\chi}}_G) \left[\iint_{\boldsymbol{\xi}_I \in \Gamma_I} K(\widehat{\boldsymbol{\chi}}_G, \boldsymbol{\xi}_I)\ \sigma_I(\boldsymbol{\xi}_I)\ \mathrm{d}\Gamma_I \right] \mathrm{d}L_G \tag{4.12}$$

  where

$$K(\widehat{\boldsymbol{\chi}}_G, \boldsymbol{\xi}_I) = \int_{\boldsymbol{\chi}_G \in C_G(\widehat{\boldsymbol{\chi}}_G)} \left(\frac{1}{r(\boldsymbol{\chi}_G, \boldsymbol{\xi}_I)} + \frac{1}{r(\boldsymbol{\chi}_G', \boldsymbol{\xi}_I)} \right) \mathrm{d}C_G \tag{4.13}$$

- The fourth integral on the left-hand of equation (4.7):

$$\widehat{S}_{GI} = \frac{1}{4\pi} \int_{\widehat{\boldsymbol{\chi}}_G \in L_G} \widehat{\omega}_G(\widehat{\boldsymbol{\chi}}_G) \left[\iint_{\boldsymbol{\xi}_I \in \Gamma_I} K^*(\widehat{\boldsymbol{\chi}}_G, \boldsymbol{\xi}_I)\ V_I(\boldsymbol{\xi}_I)\ \mathrm{d}\Gamma_I \right] \mathrm{d}L_G \tag{4.14}$$

  where

$$K^*(\widehat{\boldsymbol{\chi}}_G, \boldsymbol{\xi}_I) = \int_{\boldsymbol{\chi}_G \in C_G(\widehat{\boldsymbol{\chi}}_G)} \left[\nabla \left(\frac{1}{r(\boldsymbol{\chi}_G, \boldsymbol{\xi}_I)} \right) + \nabla \left(\frac{1}{r(\boldsymbol{\chi}_G', \boldsymbol{\xi}_I)} \right) \right] \cdot \boldsymbol{n}(\boldsymbol{\xi}_I)\ \mathrm{d}C_G \tag{4.15}$$

- The first integral on the left-hand of equation (4.8):

$$\widehat{R}_{IG} = \frac{1}{4\pi\gamma} \iint_{\boldsymbol{\chi}_I \in \Gamma_I} \omega_I(\boldsymbol{\chi}_I) \left[\int_{\widehat{\boldsymbol{\xi}}_G \in L_G} K(\boldsymbol{\chi}_I, \widehat{\boldsymbol{\xi}}_G)\ \widehat{\sigma}_G(\widehat{\boldsymbol{\xi}}_G)\ \mathrm{d}L_G \right] \mathrm{d}\Gamma_I \tag{4.16}$$

  where

$$K(\boldsymbol{\chi}_I, \widehat{\boldsymbol{\xi}}_G) = \int_{\boldsymbol{\xi}_G \in C_G(\widehat{\boldsymbol{\xi}}_G)} \left(\frac{1}{r(\boldsymbol{\chi}_I, \boldsymbol{\xi}_G)} + \frac{1}{r(\boldsymbol{\chi}_I', \boldsymbol{\xi}_G)} \right) \mathrm{d}C_G \tag{4.17}$$

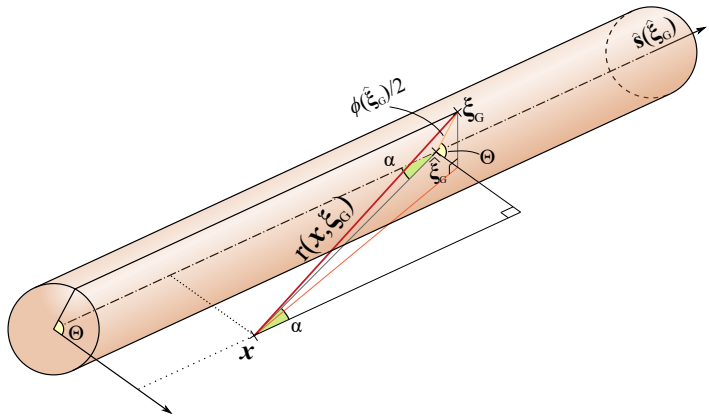

Figure 4.1. Schematic representation of distance between x and ξ_G.

In the previous expressions the circumferential integrals (C_G) will be calculated applying the circumferential uniformity condition. Next, the resolution of them is developed.

The circumferential integral in equation (4.9) will be calculated as:

$$\int_{\boldsymbol{\chi}_G \in C_G(\widehat{\boldsymbol{\chi}}_G)} \mathrm{d}C_G = \frac{\phi(\widehat{\boldsymbol{\chi}}_G)}{2} \int_{-\pi}^{\pi} \mathrm{d}\Theta = \phi(\widehat{\boldsymbol{\chi}}_G)\,\pi \tag{4.18}$$

However, the resolution of the other integrals is not so simple. As a starting point, two types of circumferential integrals can be differentiated: the integrals when $\boldsymbol{\chi}$ and $\boldsymbol{\xi}$ are located in different domains (equations (4.13), (4.15), and (4.17)) and the integrals when $\boldsymbol{\chi}$ and $\boldsymbol{\xi}$ are located on the surface of the electrodes (equation (4.11)).

First, the analysis of the circumferential integrals when the source and the field points are located in different domains will be done.

This type of circumferential integral can be expressed in a general way as:

$$\int_{\boldsymbol{\xi}_G \in C_G(\widehat{\boldsymbol{\xi}}_G)} \frac{1}{r(\boldsymbol{x}, \boldsymbol{\xi}_G)}\, \mathrm{d}C_G \tag{4.19}$$

where $\boldsymbol{x}$ is a point located in a domain different to the electrodes, and $\boldsymbol{\xi}_G$ is a point located on the boundary Γ_G (the electrodes), as shown in Figure 4.1.

The value of $r(\boldsymbol{x}, \boldsymbol{\xi}_G)$ can be defined based on $\widehat{\boldsymbol{\xi}}_G$ as

$$r(\boldsymbol{x}, \boldsymbol{\xi}_G) = \sqrt{|\boldsymbol{x} - \widehat{\boldsymbol{\xi}}_G|^2 + \frac{\phi^2(\widehat{\boldsymbol{\xi}}_G)}{4} - |\boldsymbol{x} - \widehat{\boldsymbol{\xi}}_G|\ \phi(\widehat{\boldsymbol{\xi}}_G) \sin(\alpha) \cos(\Theta)} \tag{4.20}$$

where Θ is the angular position in the perimeter of cross section of the electrode, and α is the angle formed by the vector $(\widehat{\boldsymbol{\xi}}_G - \boldsymbol{x})$ and the unit vector of electrode axis $\widehat{\boldsymbol{s}}(\widehat{\boldsymbol{\xi}}_G)$, that is

$$\sin\alpha = \frac{|(\widehat{\boldsymbol{\xi}}_G - \boldsymbol{x}) \times \widehat{\boldsymbol{s}}(\widehat{\boldsymbol{\xi}}_G)|}{|\widehat{\boldsymbol{\xi}}_G - \boldsymbol{x}|\,|\widehat{\boldsymbol{s}}(\widehat{\boldsymbol{\xi}}_G)|}$$

Introducing the previous expression in equation (4.19) and writing it in polar coordinates, the integral is rewritten as

$$\frac{\phi(\widehat{\boldsymbol{\xi}}_G)}{2}\int_{-\pi}^{\pi}\frac{1}{\sqrt{|\boldsymbol{x}-\widehat{\boldsymbol{\xi}}_G|^2+\frac{\phi^2(\widehat{\boldsymbol{\xi}}_G)}{4}-|\boldsymbol{x}-\widehat{\boldsymbol{\xi}}_G|\ \phi(\widehat{\boldsymbol{\xi}}_G)\sin(\alpha)\cos(\Theta)}}\,\mathrm{d}\Theta \tag{4.21}$$

Integral (4.21) can be approximated with an open Newton-Cotes formula with one point in the interval $-1 \leq \cos(\Theta) \leq 1$, as indicated in [Colominas, 1995]. If the change of variable $t = \cos(\Theta)$ is introduced in the integral, the equivalence

$$\begin{aligned}&\frac{\phi(\widehat{\boldsymbol{\xi}}_G)}{2}\int_{-\pi}^{\pi}\frac{1}{\sqrt{|\boldsymbol{x}-\widehat{\boldsymbol{\xi}}_G|^2+\frac{\phi^2(\widehat{\boldsymbol{\xi}}_G)}{4}-|\boldsymbol{x}-\widehat{\boldsymbol{\xi}}_G|\ \phi(\widehat{\boldsymbol{\xi}}_G)\sin(\alpha)\cos(\Theta)}}\,\mathrm{d}\Theta = \\ &\frac{\phi(\widehat{\boldsymbol{\xi}}_G)}{2}\int_{-1}^{1}\frac{1}{\sqrt{|\boldsymbol{x}-\widehat{\boldsymbol{\xi}}_G|^2+\frac{\phi^2(\widehat{\boldsymbol{\xi}}_G)}{4}-|\boldsymbol{x}-\widehat{\boldsymbol{\xi}}_G|\ \phi(\widehat{\boldsymbol{\xi}}_G)\sin(\alpha)\,t}}\,\frac{\mathrm{d}t}{\sqrt{1-t^2}}\end{aligned}$$

can be done. In this expression the Newton-Cotes formula is applied in $t = 0$ which is equal to $\cos(\Theta) = 0$. So,

$$\int_{-\pi}^{\pi} f(\cos(\Theta))\,\mathrm{d}\Theta \approx 2hf_0 \tag{4.22}$$

where f_0 is the integrand evaluated in $\cos(\Theta)$ equal to 0 and the step size h equal to π.

As a result, the circumferential integral can be approximated as

$$\int_{\boldsymbol{\xi}_G\,\in\,C_G(\widehat{\boldsymbol{\xi}}_G)}\frac{1}{r(\boldsymbol{x},\boldsymbol{\xi}_G)}\,\mathrm{d}C_G \approx \frac{\phi(\widehat{\boldsymbol{\xi}}_G)}{2}\left(2\pi\frac{1}{\sqrt{|\boldsymbol{x}-\widehat{\boldsymbol{\xi}}_G|^2+\frac{\phi^2(\widehat{\boldsymbol{\xi}}_G)}{4}}}\right) \tag{4.23}$$

This approximation can be done in the same way for the symmetric field point $\widehat{\boldsymbol{\xi}}'_G$, and the expression obtained is

$$\int_{\boldsymbol{\xi}'_G\,\in\,C_G(\widehat{\boldsymbol{\xi}}'_G)}\frac{1}{r(\boldsymbol{x},\boldsymbol{\xi}'_G)}\,\mathrm{d}C_G \approx \frac{\phi(\widehat{\boldsymbol{\xi}}'_G)}{2}\left(2\pi\frac{1}{\sqrt{|\boldsymbol{x}-\widehat{\boldsymbol{\xi}}'_G|^2+\frac{\phi^2(\widehat{\boldsymbol{\xi}}'_G)}{4}}}\right) \tag{4.24}$$

Thus, applying this analysis in equations (4.13), (4.14), and (4.17), the circumferential integrals can be approximated by:

- Kernel $K(\widehat{\boldsymbol{\chi}}_G, \boldsymbol{\xi}_I)$ (4.13):

$$\begin{aligned}&\int_{\boldsymbol{\chi}_G\,\in\,C_G(\widehat{\boldsymbol{\chi}}_G)}\left(\frac{1}{r(\boldsymbol{\chi}_G,\boldsymbol{\xi}_I)}+\frac{1}{r(\boldsymbol{\chi}'_G,\boldsymbol{\xi}_I)}\right)\mathrm{d}C_G \approx \\ &\frac{\phi(\widehat{\boldsymbol{\chi}}_G)}{2}\left(2\pi\frac{1}{\sqrt{|\widehat{\boldsymbol{\chi}}_G-\boldsymbol{\xi}_I|^2+\frac{\phi^2(\widehat{\boldsymbol{\chi}}_G)}{4}}}\right)+\frac{\phi(\widehat{\boldsymbol{\chi}}'_G)}{2}\left(2\pi\frac{1}{\sqrt{|\widehat{\boldsymbol{\chi}}'_G-\boldsymbol{\xi}_I|^2+\frac{\phi^2(\widehat{\boldsymbol{\chi}}'_G)}{4}}}\right)\end{aligned} \tag{4.25}$$

- Kernel $K(\boldsymbol{\chi}_I, \widehat{\boldsymbol{\xi}}_G)$ (4.17):

$$\int_{\boldsymbol{\xi}_G \in C_G(\widehat{\boldsymbol{\xi}}_G)} \Big(\frac{1}{r(\boldsymbol{\chi}_I, \boldsymbol{\xi}_G)} + \frac{1}{r(\boldsymbol{\chi}_I', \boldsymbol{\xi}_G)}\Big)\, \mathrm{d}C_G \approx \frac{\phi(\widehat{\boldsymbol{\xi}}_G)}{2}\left(2\pi \frac{1}{\sqrt{|\boldsymbol{\chi}_I - \widehat{\boldsymbol{\xi}}_G|^2 + \frac{\phi^2(\widehat{\boldsymbol{\xi}}_G)}{4}}}\right) + \frac{\phi(\widehat{\boldsymbol{\xi}}_G)}{2}\left(2\pi \frac{1}{\sqrt{|\boldsymbol{\chi}_I' - \widehat{\boldsymbol{\xi}}_G|^2 + \frac{\phi^2(\widehat{\boldsymbol{\xi}}_G)}{4}}}\right) \tag{4.26}$$

- Kernel $K^*(\widehat{\boldsymbol{\chi}}_G, \boldsymbol{\xi}_I)$ (4.15):

$$\int_{\boldsymbol{\chi}_G \in C_G(\widehat{\boldsymbol{\chi}}_G)} \Big[\nabla\Big(\frac{1}{r(\boldsymbol{\chi}_G, \boldsymbol{\xi}_I)}\Big) + \nabla\Big(\frac{1}{r(\boldsymbol{\chi}_G', \boldsymbol{\xi}_I)}\Big)\Big] \cdot \boldsymbol{n}(\boldsymbol{\xi}_I)\, \mathrm{d}C_G \approx \frac{\phi(\widehat{\boldsymbol{\chi}}_G)}{2}\left(2\pi\, \nabla\Big(\frac{1}{r(\widehat{\boldsymbol{\chi}}_G, \boldsymbol{\xi}_I)}\Big) \cdot \boldsymbol{n}(\boldsymbol{\xi}_I)\right) + \frac{\phi(\widehat{\boldsymbol{\chi}}_G')}{2}\left(2\pi\, \nabla\Big(\frac{1}{r(\widehat{\boldsymbol{\chi}}_G', \boldsymbol{\xi}_I)}\Big) \cdot \boldsymbol{n}(\boldsymbol{\xi}_I)\right) \tag{4.27}$$

where

$$\frac{1}{r(\widehat{\boldsymbol{\chi}}_G, \boldsymbol{\xi}_I)} = \frac{1}{\sqrt{|\widehat{\boldsymbol{\chi}}_G - \boldsymbol{\xi}_I|^2 + \frac{\phi^2(\widehat{\boldsymbol{\chi}}_G)}{4}}}\,, \qquad \frac{1}{r(\widehat{\boldsymbol{\chi}}_G', \boldsymbol{\xi}_I)} = \frac{1}{\sqrt{|\widehat{\boldsymbol{\chi}}_G' - \boldsymbol{\xi}_I|^2 + \frac{\phi^2(\widehat{\boldsymbol{\chi}}_G')}{4}}}$$

Now, the analysis of the circumferential integrals when the source and field points are located on the surface of the electrodes (Γ_G) will be done. In this case the integral is given by

$$K(\widehat{\boldsymbol{\chi}}_G, \widehat{\boldsymbol{\xi}}_G) = \int_{\boldsymbol{\chi}_G \in C_G(\widehat{\boldsymbol{\chi}}_G)} \Big[\int_{\boldsymbol{\xi}_G \in C_G(\widehat{\boldsymbol{\xi}}_G)} \Big(\frac{1}{r(\boldsymbol{\chi}_G, \boldsymbol{\xi}_G)} + \frac{1}{r(\boldsymbol{\chi}_G', \boldsymbol{\xi}_G)}\Big)\, \mathrm{d}C_G\Big]\, \mathrm{d}C_G \tag{4.28}$$

Two types of situations have to be considered: the points are located in the same electrode or the points are located in different electrodes.

When $\boldsymbol{\chi}_G$ and $\boldsymbol{\xi}_G$ belong to the same electrode, the circumferential integral will be approximated as follows:

The first integral on the right hand-side of equation (4.28) is the integral that will be analysed:

$$\int_{\boldsymbol{\chi}_G \in C_G(\widehat{\boldsymbol{\chi}}_G)} \Big[\int_{\boldsymbol{\xi}_G \in C_G(\widehat{\boldsymbol{\xi}}_G)} \frac{1}{r(\boldsymbol{\chi}_G, \boldsymbol{\xi}_G)}\, \mathrm{d}C_G\Big]\, \mathrm{d}C_G \tag{4.29}$$

where $\boldsymbol{\chi}_G$ and $\boldsymbol{\xi}_G$ are located on the boundary Γ_G, as shown in Figure 4.2.

The value of $r(\boldsymbol{\chi}_G, \boldsymbol{\xi}_G)$ can be defined based on $\widehat{\boldsymbol{\chi}}_G$ and $\widehat{\boldsymbol{\xi}}_G$ as

$$r(\boldsymbol{\chi}_G, \boldsymbol{\xi}_G) = \sqrt{|\widehat{\boldsymbol{\chi}}_G - \widehat{\boldsymbol{\xi}}_G|^2 + \frac{\phi^2(\widehat{\boldsymbol{\chi}}_G)}{4} + \frac{\phi^2(\widehat{\boldsymbol{\xi}}_G)}{4} - \frac{\phi(\widehat{\boldsymbol{\chi}}_G)\phi(\widehat{\boldsymbol{\xi}}_G)}{2}\cos(\Theta_\xi)} \tag{4.30}$$

where $\widehat{\boldsymbol{\chi}}_G$ is the orthogonal projection of $\boldsymbol{\chi}_G$, $\phi(\widehat{\boldsymbol{\chi}}_G)$ is the diameter of the electrode at this point, and Θ_ξ is the angular position in the perimeter of cross section of the electrode as regards $\boldsymbol{\chi}_G$.

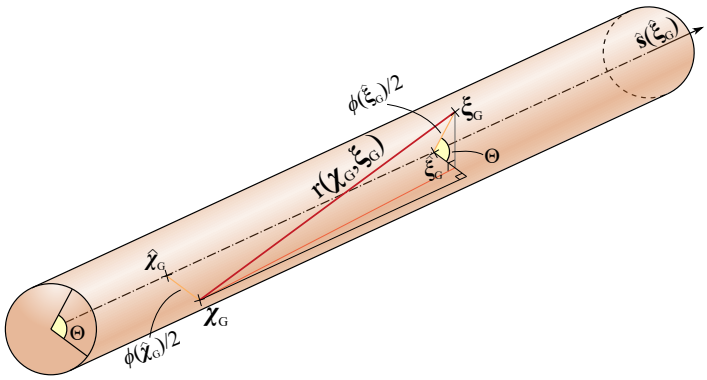

Figure 4.2. Schematic representation of distance between $\boldsymbol{\chi}_G$ and $\boldsymbol{\xi}_G$ when they are located on the same boundary Γ_G.

Introducing the previous expression in equation (4.29) and writing it in polar coordinates, the integral is rewritten as:

$$\frac{\phi(\widehat{\boldsymbol{\chi}}_G)}{2}\frac{\phi(\widehat{\boldsymbol{\xi}}_G)}{2}\int_{-\pi}^{\pi}\left[\int_{-\pi}^{\pi}\frac{1}{\sqrt{|\widehat{\boldsymbol{\chi}}_G-\widehat{\boldsymbol{\xi}}_G|^2+\frac{\phi^2(\widehat{\boldsymbol{\chi}}_G)}{4}+\frac{\phi^2(\widehat{\boldsymbol{\xi}}_G)}{4}-\frac{\phi(\widehat{\boldsymbol{\chi}}_G)\phi(\widehat{\boldsymbol{\xi}}_G)}{2}\cos(\Theta_\xi)}}\,\mathrm{d}\Theta_\xi\right]\mathrm{d}\Theta_\chi \tag{4.31}$$

The Θ_ξ integral will be approximated with a Newton-Cotes formula, as it was done with equation (4.21). In this case, an open Newton-Cotes formula with two points will be used. Thus,

$$\int_{-\pi}^{\pi} f(\Theta_\xi)\,\mathrm{d}\Theta_\xi \approx \frac{3h}{2}(f_0+f_1) \tag{4.32}$$

where f_0 is the integrand evaluated in Θ_ξ equal to $-\pi/3$, f_1 is the integrand evaluated in Θ_ξ equal to $\pi/3$, and the step size h is equal to $2\pi/3$.

As a result, the circumferential integral Θ_ξ can be approximate as

$$\begin{aligned}&\int_{\boldsymbol{\xi}_G\in C_G(\widehat{\boldsymbol{\xi}}_G)}\frac{1}{r(\boldsymbol{\chi}_G,\boldsymbol{\xi}_G)}\,\mathrm{d}C_G\approx\\&\frac{\phi(\widehat{\boldsymbol{\xi}}_G)}{2}\left(2\pi\frac{1}{\sqrt{|\widehat{\boldsymbol{\chi}}_G-\widehat{\boldsymbol{\xi}}_G|^2+\frac{\phi^2(\widehat{\boldsymbol{\chi}}_G)}{4}+\frac{\phi^2(\widehat{\boldsymbol{\xi}}_G)}{4}-\frac{\phi(\widehat{\boldsymbol{\chi}}_G)\phi(\widehat{\boldsymbol{\xi}}_G)}{4}}}\right)\end{aligned} \tag{4.33}$$

Since $\boldsymbol{\xi}_G$ and $\boldsymbol{\chi}_G$ belong to the same element, the value of $\phi(\widehat{\boldsymbol{\xi}}_G)$ and $\phi(\widehat{\boldsymbol{\chi}}_G)$ are considered equal in practice and the approximated expression can be reduced to

$$\int_{\boldsymbol{\xi}_G\in C_G(\widehat{\boldsymbol{\xi}}_G)}\frac{1}{r(\boldsymbol{\chi}_G,\boldsymbol{\xi}_G)}\,\mathrm{d}C_G\approx\frac{\phi(\widehat{\boldsymbol{\xi}}_G)}{2}\left(2\pi\frac{1}{\sqrt{|\widehat{\boldsymbol{\chi}}_G-\widehat{\boldsymbol{\xi}}_G|^2+\frac{\phi^2(\widehat{\boldsymbol{\xi}}_G)}{4}}}\right) \tag{4.34}$$

Introducing the previous expression in equation (4.29) and evaluating the circumferential integral Θ_χ, the approximation of the double integral is given by

$$\int_{\boldsymbol{\chi}_G \in C_G(\widehat{\boldsymbol{\chi}}_G)} \left[\int_{\boldsymbol{\xi}_G \in C_G(\widehat{\boldsymbol{\xi}}_G)} \frac{1}{r(\boldsymbol{\chi}_G, \boldsymbol{\xi}_G)} \, \mathrm{d}C_G \right] \mathrm{d}C_G \approx \pi\phi(\widehat{\boldsymbol{\xi}}_G)\pi\phi(\widehat{\boldsymbol{\chi}}_G) \frac{1}{\sqrt{|\widehat{\boldsymbol{\chi}}_G - \widehat{\boldsymbol{\xi}}_G|^2 + \frac{\phi^2(\widehat{\boldsymbol{\xi}}_G)}{4}}} \tag{4.35}$$

On the other hand, when $\boldsymbol{\chi}_G$ and $\boldsymbol{\xi}_G$ are located in different electrodes, as happens with the second integral on the right hand-side of equation (4.28), the circumferential integral can be approximated as follows:

The integral that will be analysed is

$$\int_{\boldsymbol{\chi}_G \in C_G(\widehat{\boldsymbol{\chi}}_G)} \left[\int_{\boldsymbol{\xi}_G \in C_G(\widehat{\boldsymbol{\xi}}_G)} \frac{1}{r(\boldsymbol{\chi}_G, \boldsymbol{\xi}_G)} \, \mathrm{d}C_G \right] \mathrm{d}C_G \tag{4.36}$$

where $\boldsymbol{\chi}_G$ and $\boldsymbol{\xi}_G$ are located in different electrodes. The procedure developed to solve this integral is the same as it is indicated in [Colominas, 1995].

Once again there is a double circumferential integral. First,

$$\int_{\boldsymbol{\xi}_G \in C_G(\widehat{\boldsymbol{\xi}}_G)} \frac{1}{r(\boldsymbol{\chi}_G, \boldsymbol{\xi}_G)} \, \mathrm{d}C_G \tag{4.37}$$

will be analysed, where $\boldsymbol{\chi}_G$ is a point located on the surface of one electrode and $\boldsymbol{\xi}_G$ is a point located on the boundary of other electrode.

The value of $r(\boldsymbol{\chi}_G, \boldsymbol{\xi}_G)$ can be defined based on $\widehat{\boldsymbol{\xi}}_G$ (Figure 4.3) as

$$r(\boldsymbol{\chi}_G, \boldsymbol{\xi}_G) = \sqrt{|\boldsymbol{\chi}_G - \widehat{\boldsymbol{\xi}}_G|^2 + \frac{\phi^2(\widehat{\boldsymbol{\xi}}_G)}{4} - |\boldsymbol{\chi}_G - \widehat{\boldsymbol{\xi}}_G| \; \phi(\widehat{\boldsymbol{\xi}}_G) \sin(\alpha_\xi) \cos(\Theta_\xi)} \tag{4.38}$$

where Θ_ξ is the angular position in the perimeter of cross section of the electrode, and α_ξ is the angle formed by the vector $(\widehat{\boldsymbol{\xi}}_G - \boldsymbol{\chi}_G)$ and the unit vector of electrode axis $\widehat{\boldsymbol{s}}(\widehat{\boldsymbol{\xi}}_G)$, that is

$$\sin\alpha_\xi = \frac{|(\widehat{\boldsymbol{\xi}}_G - \boldsymbol{\chi}_G) \times \widehat{\boldsymbol{s}}(\widehat{\boldsymbol{\xi}}_G)|}{|\widehat{\boldsymbol{\xi}}_G - \boldsymbol{\chi}_G| \, |\widehat{\boldsymbol{s}}(\widehat{\boldsymbol{\xi}}_G)|}$$

Introducing the $r(\boldsymbol{\chi}_G, \boldsymbol{\xi}_G)$ expression in (4.37) and writing it in polar coordinates, the integral is rewritten as

$$\frac{\phi(\widehat{\boldsymbol{\xi}}_G)}{2} \int_{-\pi}^{\pi} \frac{1}{\sqrt{|\boldsymbol{\chi}_G - \widehat{\boldsymbol{\xi}}_G|^2 + \frac{\phi^2(\widehat{\boldsymbol{\xi}}_G)}{4} - |\boldsymbol{\chi}_G - \widehat{\boldsymbol{\xi}}_G| \; \phi(\widehat{\boldsymbol{\xi}}_G) \sin(\alpha_\xi) \cos(\Theta_\xi)}} \, \mathrm{d}\Theta \tag{4.39}$$

This integral can be approximated as it was done in equation (4.21). As a result, the first circumferential integral can be obtained as

$$\int_{\boldsymbol{\xi}_G \in C_G(\widehat{\boldsymbol{\xi}}_G)} \frac{1}{r(\boldsymbol{\chi}_G, \boldsymbol{\xi}_G)} \, \mathrm{d}C_G \approx \frac{\phi(\widehat{\boldsymbol{\xi}}_G)}{2} \left(2\pi \frac{1}{\sqrt{|\boldsymbol{\chi}_G - \widehat{\boldsymbol{\xi}}_G|^2 + \frac{\phi^2(\widehat{\boldsymbol{\xi}}_G)}{4}}} \right) \tag{4.40}$$

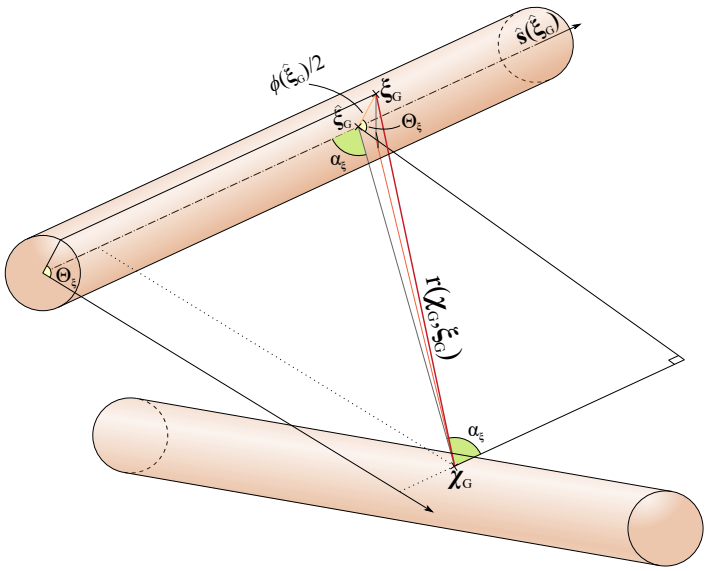

Figure 4.3. Schematic representation of distance between $\boldsymbol{\chi}_G$ and $\boldsymbol{\xi}_G$ based on $\widehat{\boldsymbol{\xi}}_G$ when they are located in different electrodes.

Now, the second circumferential integral will be calculated. The expression of this equation is

$$\int_{\boldsymbol{\chi}_G \in C_G(\widehat{\boldsymbol{\chi}}_G)} \frac{\phi(\widehat{\boldsymbol{\xi}}_G)}{2} \left(2\pi \frac{1}{\sqrt{|\boldsymbol{\chi}_G - \widehat{\boldsymbol{\xi}}_G|^2 + \frac{\phi^2(\widehat{\boldsymbol{\xi}}_G)}{4}}} \right) \mathrm{d}C_G \tag{4.41}$$

In this case it is necessary to know the value of $r(\boldsymbol{\chi}_G, \widehat{\boldsymbol{\xi}}_G)$ based on $\widehat{\boldsymbol{\chi}}_G$ (Figure 4.4). This distance is given by

$$r(\boldsymbol{\chi}_G, \widehat{\boldsymbol{\xi}}_G) = \sqrt{|\widehat{\boldsymbol{\chi}}_G - \widehat{\boldsymbol{\xi}}_G|^2 + \frac{\phi^2(\widehat{\boldsymbol{\chi}}_G)}{4} - |\widehat{\boldsymbol{\chi}}_G - \widehat{\boldsymbol{\xi}}_G|\ \phi(\widehat{\boldsymbol{\chi}}_G) \sin(\alpha_\chi) \cos(\Theta_\chi)} \tag{4.42}$$

where Θ_χ is the angular position in the perimeter of cross section of the electrode, and α_χ is the angle formed by the vector $(\widehat{\boldsymbol{\chi}}_G - \widehat{\boldsymbol{\xi}}_G)$ and the unit vector of electrode axis $\widehat{\boldsymbol{s}}(\widehat{\boldsymbol{\chi}}_G)$, that is

$$\sin \alpha_\chi = \frac{|(\widehat{\boldsymbol{\chi}}_G - \widehat{\boldsymbol{\xi}}_G) \times \widehat{\boldsymbol{s}}(\widehat{\boldsymbol{\chi}}_G)|}{|\widehat{\boldsymbol{\chi}}_G - \widehat{\boldsymbol{\xi}}_G|\, |\widehat{\boldsymbol{s}}(\widehat{\boldsymbol{\chi}}_G)|}$$

Introducing the value of $|\boldsymbol{\chi}_G - \widehat{\boldsymbol{\xi}}_G|$ in equation (4.41) and writing it in polar coordinates, the integral is rewritten as

$$\frac{1}{2} \int_{-\pi}^{\pi} \frac{\pi \phi(\widehat{\boldsymbol{\xi}}_G) \phi(\widehat{\boldsymbol{\chi}}_G)}{\sqrt{|\widehat{\boldsymbol{\chi}}_G - \widehat{\boldsymbol{\xi}}_G|^2 + \frac{\phi^2(\widehat{\boldsymbol{\chi}}_G)}{4} - |\widehat{\boldsymbol{\chi}}_G - \widehat{\boldsymbol{\xi}}_G|\ \phi(\widehat{\boldsymbol{\chi}}_G) \sin(\alpha_\chi) \cos(\Theta_\chi) + \frac{\phi^2(\widehat{\boldsymbol{\xi}}_G)}{4}}} \mathrm{d}\Theta_\chi \tag{4.43}$$

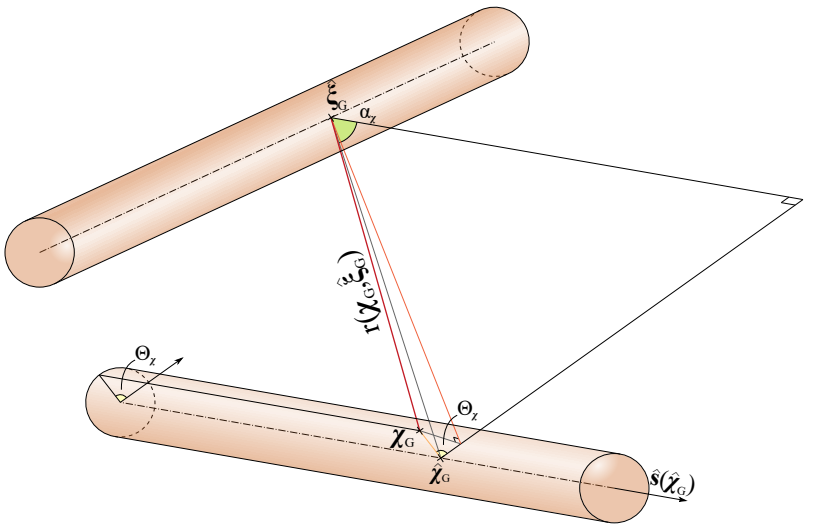

Figure 4.4. Schematic representation of distance between $\boldsymbol{\chi}_G$ and $\widehat{\boldsymbol{\xi}}_G$ based on $\widehat{\boldsymbol{\chi}}_G$ when they are located in different electrodes.

Doing the same approximation that it was done for equation (4.39), the approximation of this integral is

$$\begin{aligned}\int_{\boldsymbol{\chi}_G \in C_G(\widehat{\boldsymbol{\chi}}_G)} \frac{\phi(\widehat{\boldsymbol{\xi}}_G)}{2}\left(2\pi \frac{1}{\sqrt{|\boldsymbol{\chi}_G - \widehat{\boldsymbol{\xi}}_G|^2 + \frac{\phi^2(\widehat{\boldsymbol{\xi}}_G)}{4}}}\right) \mathrm{d}C_G \approx \\ \pi\phi(\widehat{\boldsymbol{\xi}}_G)\frac{\phi(\widehat{\boldsymbol{\chi}}_G)}{2}\left(2\pi \frac{1}{\sqrt{|\widehat{\boldsymbol{\chi}}_G - \widehat{\boldsymbol{\xi}}_G|^2 + \frac{\phi^2(\widehat{\boldsymbol{\xi}}_G)}{4} + \frac{\phi^2(\widehat{\boldsymbol{\chi}}_G)}{4}}}\right)\end{aligned} \tag{4.44}$$

Therefore, the double circumferential integral when $\boldsymbol{\chi}_G$ and $\boldsymbol{\xi}_G$ are located in different electrodes is approximated as

$$\begin{aligned}\int_{\boldsymbol{\chi}_G \in C_G(\widehat{\boldsymbol{\chi}}_G)} \left[\int_{\boldsymbol{\xi}_G \in C_G(\widehat{\boldsymbol{\xi}}_G)} \frac{1}{r(\boldsymbol{\chi}_G, \boldsymbol{\xi}_G)}\, \mathrm{d}C_G\right] \mathrm{d}C_G \approx \\ \pi\phi(\widehat{\boldsymbol{\xi}}_G)\pi\phi(\widehat{\boldsymbol{\chi}}_G)\frac{1}{\sqrt{|\widehat{\boldsymbol{\chi}}_G - \widehat{\boldsymbol{\xi}}_G|^2 + \frac{\phi^2(\widehat{\boldsymbol{\xi}}_G)}{4} + \frac{\phi^2(\widehat{\boldsymbol{\chi}}_G)}{4}}}\end{aligned} \tag{4.45}$$

Thus, the circumferential integrals (4.11) can be approximated by:

- Kernel $K(\widehat{\boldsymbol{\chi}}_G, \widehat{\boldsymbol{\xi}}_G)$ (when $\widehat{\boldsymbol{\chi}}_G$ and $\widehat{\boldsymbol{\xi}}_G$ are located in the same electrode):

$$\begin{aligned}\int_{\boldsymbol{\chi}_G \in C_G(\widehat{\boldsymbol{\chi}}_G)} \left[\int_{\boldsymbol{\xi}_G \in C_G(\widehat{\boldsymbol{\xi}}_G)} \left(\frac{1}{r(\boldsymbol{\chi}_G, \boldsymbol{\xi}_G)} + \frac{1}{r(\boldsymbol{\chi}'_G, \boldsymbol{\xi}_G)}\right) \mathrm{d}C_G\right] \mathrm{d}C_G \approx \\ \pi\phi(\widehat{\boldsymbol{\xi}}_G)\pi\phi(\widehat{\boldsymbol{\chi}}_G)\left(\frac{1}{\sqrt{|\widehat{\boldsymbol{\chi}}_G - \widehat{\boldsymbol{\xi}}_G|^2 + \frac{\phi^2(\widehat{\boldsymbol{\xi}}_G)}{4}}} + \frac{1}{\sqrt{|\widehat{\boldsymbol{\chi}}'_G - \widehat{\boldsymbol{\xi}}_G|^2 + \frac{\phi^2(\widehat{\boldsymbol{\xi}}_G)}{4} + \frac{\phi^2(\widehat{\boldsymbol{\chi}}'_G)}{4}}}\right)\end{aligned} \tag{4.46}$$

- Kernel $K(\widehat{\boldsymbol{\chi}}_G, \widehat{\boldsymbol{\xi}}_G)$ (when $\widehat{\boldsymbol{\chi}}_G$ and $\widehat{\boldsymbol{\xi}}_G$ are located in different electrodes):

$$\int_{\boldsymbol{\chi}_G \in C_G(\widehat{\boldsymbol{\chi}}_G)} \Big[\int_{\boldsymbol{\xi}_G \in C_G(\widehat{\boldsymbol{\xi}}_G)} \Big(\frac{1}{r(\boldsymbol{\chi}_G, \boldsymbol{\xi}_G)} + \frac{1}{r(\boldsymbol{\chi}'_G, \boldsymbol{\xi}_G)} \Big) \, \mathrm{d}C_G \Big] \, \mathrm{d}C_G \approx$$
$$\pi\phi(\widehat{\boldsymbol{\xi}}_G)\pi\phi(\widehat{\boldsymbol{\chi}}_G) \Bigg(\frac{1}{\sqrt{|\widehat{\boldsymbol{\chi}}_G - \widehat{\boldsymbol{\xi}}_G|^2 + \frac{\phi^2(\widehat{\boldsymbol{\xi}}_G)}{4} + \frac{\phi^2(\widehat{\boldsymbol{\chi}}_G)}{4}}} + \frac{1}{\sqrt{|\widehat{\boldsymbol{\chi}}'_G - \widehat{\boldsymbol{\xi}}_G|^2 + \frac{\phi^2(\widehat{\boldsymbol{\xi}}_G)}{4} + \frac{\phi^2(\widehat{\boldsymbol{\chi}}'_G)}{4}}} \Bigg) \tag{4.47}$$

As noted above, the assumption of circumferential uniformity can be adopted in this problem. Therefore, the approximated expressions obtained will be introduced in equations (4.7) and (4.8).

4.3 Weighted Residual Methods

Weighted residual methods are a numerical class of approximate solution methods which are based on reducing the errors of the global problem to a minimum. This reduction is obtained by a distribution of these errors over the global problem through the use of the weak forms of the original equations. The idea is to force the weak form to vanish over the solution domain. Mathematically, that is

$$\int_{\Omega} R\,\omega \, \mathrm{d}\Omega = 0 \tag{4.48}$$

where ω is the weighting functions and R is the residual or error function in Ω. The residual can be defined as the error due to assume an approximate solution that does not satisfy the original equations.

There are different weighted residual methods depending on the nature of the weighting functions selected [Brebbia & Dominguez, 1992; Zienkiewicz et al., 2013]. A brief description of the most common methods is presented below:

Subdomain Collocation

In this method, a generic domain Ω is divided into M non-overlapping subdomains. The weighting functions are chosen as unity over a specific subdomain and set equal to zero over the others, that is:

$$\omega_j = \begin{cases} 1 & \text{for } x \in \Omega_j \\ 0 & \text{for } x \notin \Omega_j \end{cases} \quad , \qquad j = 1, \ldots, M$$

Thus, equation (4.48) can be written as

$$\int_{\Omega_j} R \, \mathrm{d}x = 0 \, , \qquad j = 1, \ldots, M$$

which means that the integral of the residual over each subdomain is forced to be zero.

The subdomain collocation method provides the basis for the Finite Volume Method [Hansen et al., 2005].

Point Collocation

In the point collocation method, the weighting functions are defined in such a way that the residual is set equal to zero at k points located in a generic domain Ω, which are called as collocation points. This can be achieved by choosing these functions in terms of Dirac delta function. That is:

$$\omega_j = \delta(x - x_j)\,, \qquad j = 1, \ldots, k$$

Introducing these weighting functions in equation (4.48) is obtained

$$\int_\Omega R\,\delta(x - x_j)\,\mathrm{d}\Omega = 0\,, \qquad j = 1, \ldots, k$$

The previous expression can be rewritten by means of the sifting property of Dirac delta function as

$$R|_{x=x_j}\,, \qquad j = 1, \ldots, k$$

which means that the residual R is forced to be zero at collocation points.

This method is the typical weighted residual method used in the Boundary Element Method.

Galerkin Method (Bubnov-Galerkin)

In the Galerkin method, the weighting functions will be the same as the functions used to approximate the solution of the problem:

$$\omega_j = N_j\,, \qquad j = 1, \ldots, n$$

where n are the number of terms used to approximate the solution and N_j are the shape functions.

Thus, equation (4.48) is written as

$$\int_{\Omega_j} R\,N_j\,\mathrm{d}\Omega = 0\,, \qquad j = 1, \ldots, n$$

This method is the base for the Finite Element formulations [Hughes, 1987].

In this thesis the approximate methods of Point Collocation and Bubnov-Galerkin are used to calculate the problem studied. The starting point to apply these weighted residual methods is the weak forms presented in Section 4.2. Afterwards, these weak forms will be solved by means of the Boundary Element Method.

4.4 The Boundary Element Method

The Boundary Element Method (BEM) is a numerical technique for solving boundary-value problems formulated as boundary integral equations. The BEM can be classified as a *boundary* method since the numerical discretisations are restricted only to the bounding surfaces, unlike other methods as the Finite Element Method (FEM) or the Finite Difference Method (FDM) which are classified as *domain* methods. This characteristic makes the BEM the suitable technique to analyse external problems where domains extend to infinity, since only the internal boundaries have to be discretised and there is no need to truncate the domain at a finite distance and impose artificial boundary conditions.

Therefore, the BEM is the appropriate method to solve the governing equations proposed in this thesis to model the electric current derivation to an infinity domain like the ground.

A review of the history of this method is presented in [Cheng & Cheng, 2005].

The BEM is a method based on a discretisation procedure which requires two types of approximation: the geometrical and the functional. The geometrical discretisation consists of a subdivision of a boundary Γ into n_{el} elements. In this problem the boundary integral equations are defined in Γ_G and Γ_I, so the geometrical approximation will be

$$\Gamma_G = \bigcup_{\alpha=1}^{n_{el_G}} \Gamma_G^\alpha$$

$$\Gamma_I = \bigcup_{\alpha=1}^{n_{el_I}} \Gamma_I^\alpha$$

where n_{el_G} is the total number of elements to approximate Γ_G and n_{el_I} is the total number of elements to approximate Γ_I.

In order to improve the geometrical representation of domains, the number of elements or the order of their approximation must be increased.

The functional approximation consists of approximating the variation of the unknown functions at each element (n_{el}) by writing them in terms of their values at some fixed points in the element, called as nodal points, using interpolation functions. In this problem there are three unknown functions: $\widehat{\sigma}_G$, σ_I and V_I. Their functional approximations are:

$$\widehat{\sigma}_G(\widehat{\boldsymbol{\xi}}_G) = \sum_{i=1}^{n_{np_G}} \widehat{\sigma}_{Gi}^\alpha \, N_{Gi}(\widehat{\boldsymbol{\xi}}_G)$$

$$\sigma_I(\boldsymbol{\xi}_I) = \sum_{i=1}^{n_{np_I}} \sigma_{Ii}^\alpha \, N_{Ii}(\boldsymbol{\xi}_I)$$

$$V_I(\boldsymbol{\xi}_I) = \sum_{i=1}^{n_{np_I}} V_{Ii}^\alpha \, N_{Ii}(\boldsymbol{\xi}_I)$$

where n_{np_G} is the number of nodes per element in Γ_G, n_{np_I} is the number of nodes per element in Γ_I, $\widehat{\sigma}^{\alpha}_{Gi}$, σ^{α}_{Ii} and V^{α}_{Ii} are the values of the functions at nodal point i that belongs to element α, and N_{Gi} and N_{Ii} are the interpolation functions.

As in the geometrical approximation, the accuracy to represent the variation of the functions can be improved increasing the order of the interpolation functions.

This discretisation procedure also has to be done for the integral of the weak form. Therefore, another geometrical discretisation for Γ_G and Γ_I and a functional approximation for the weighting functions will be done. That is,

$$\Gamma_G = \bigcup_{\beta=1}^{n_{el_G}} \Gamma_G^{\beta}, \qquad \widehat{\omega}_G(\widehat{\boldsymbol{\chi}}_G) = \sum_{j=1}^{n_{np_G}} \widehat{\omega}_{Gj}(\widehat{\boldsymbol{\chi}}_G)$$

$$\Gamma_I = \bigcup_{\beta=1}^{n_{el_I}} \Gamma_I^{\beta}, \qquad \omega_I(\boldsymbol{\chi}_I) = \sum_{j=1}^{n_{np_I}} \omega_{Ij}(\boldsymbol{\chi}_I)$$

where $\widehat{\omega}_{Gj}$ and ω_{Ij} are the values of the weighting functions at nodal point j.

In order to simplify the formulation of the problem, the approximations of the weak form and the boundary integral equations will be the same.

After applying the BEM, the original system of equations can be expressed in matrix form as

$$\boldsymbol{A}\boldsymbol{x} = \boldsymbol{f}$$

where $\boldsymbol{A}$ is a full and non-symmetric matrix, $\boldsymbol{x}$ is the unknown vector and $\boldsymbol{f}$ is the load vector.

This system can be calculated using direct solvers as Gauss elimination or Crout matrix decomposition, or iterative solvers as GMRES.

The BEM will be the method used to solve the studied problem together with the weighted residual methods of point collocation and Bubnov-Galerkin. The numerical approaches carried out in this thesis are presented on the next sections.

4.5 Point Collocation Method

4.5.1 Introduction

As it was explained in Section 4.3, the point collocation method is one of the most common weighted residual methods, where the weighting functions are Dirac delta functions. The Dirac delta function can be defined as

$$\delta(\boldsymbol{\chi}, \boldsymbol{\xi}) = \begin{cases} \infty & \text{if } \boldsymbol{\chi} = \boldsymbol{\xi} \\ 0 & \text{if } \boldsymbol{\chi} \neq \boldsymbol{\xi} \end{cases} \tag{4.49}$$

The main characteristic of this function is that it takes the value of zero at all points, except at $\boldsymbol{\chi} = \boldsymbol{\xi}$, where it becomes infinity.

An important property of the Dirac delta function is the sifting property, which is expressed as

$$\int_a^b f(\boldsymbol{\xi})\,\delta(\boldsymbol{\chi},\boldsymbol{\xi})\,\mathrm{d}\boldsymbol{\xi} = f(\boldsymbol{\chi}) \tag{4.50}$$

where $-\infty \leq a, b \leq \infty$, and $f(\boldsymbol{\xi})$ is a continuous function.

Thus, the weighting functions defined in the weak form of the governing equations will be replaced by the Dirac delta function. That is,

$$\begin{aligned} \widehat{\omega}(\widehat{\boldsymbol{\chi}}_G) &= \delta(\widehat{\boldsymbol{\chi}}_G - \widehat{\boldsymbol{\chi}}_{Gj}) \qquad j = 1,\ldots,n_{cp_G} \\ \omega(\boldsymbol{\chi}_I) &= \delta(\boldsymbol{\chi}_I - \boldsymbol{\chi}_{Ij}) \qquad j = 1,\ldots,n_{cp_I} \end{aligned} \tag{4.51}$$

where n_{cp_G} is the number of collocation points in Γ_G, and n_{cp_I} is the number of collocation points in Γ_I.

4.5.2 System of equations

After formulating the boundary integral equations into weak forms and introducing the assumption of circumferential uniformity in the electrodes, the system of equations is formed by

$$\begin{aligned} &\int_{\widehat{\boldsymbol{\chi}}_G \in L_G} \widehat{\omega}_G(\widehat{\boldsymbol{\chi}}_G)\Bigg[\pi\phi(\widehat{\boldsymbol{\chi}}_G)V_G - \frac{1}{4\pi\gamma}\int_{\widehat{\boldsymbol{\xi}}_G \in L_G} K(\widehat{\boldsymbol{\chi}}_G,\widehat{\boldsymbol{\xi}}_G)\;\widehat{\sigma}_G(\widehat{\boldsymbol{\xi}}_G)\,\mathrm{d}L_G \\ &- \frac{1}{4\pi\gamma}\iint_{\boldsymbol{\xi}_I \in \Gamma_I} K(\widehat{\boldsymbol{\chi}}_G,\boldsymbol{\xi}_I)\;\sigma_I(\boldsymbol{\xi}_I)\;\mathrm{d}\Gamma_I - \frac{1}{4\pi}\iint_{\boldsymbol{\xi}_I \in \Gamma_I} K^*(\widehat{\boldsymbol{\chi}}_G,\boldsymbol{\xi}_I)\;V_I(\boldsymbol{\xi}_I)\;\mathrm{d}\Gamma_I\Bigg]\,\mathrm{d}L_G \\ &= 0 \end{aligned} \tag{4.52}$$

$$\begin{aligned} &\iint_{\boldsymbol{\chi}_I \in \Gamma_I} \omega_I(\boldsymbol{\chi}_I)\Bigg[\frac{1}{4\pi\gamma}\int_{\widehat{\boldsymbol{\xi}}_G \in L_G} K(\boldsymbol{\chi}_I,\widehat{\boldsymbol{\xi}}_G)\;\widehat{\sigma}_G(\widehat{\boldsymbol{\xi}}_G)\;\mathrm{d}L_G \\ &+ \frac{1}{4\pi\gamma}\iint_{\boldsymbol{\xi}_I \in \Gamma_I}\Big(\frac{1}{r(\boldsymbol{\chi}_I,\boldsymbol{\xi}_I)} + \frac{1}{r(\boldsymbol{\chi}_I',\boldsymbol{\xi}_I)}\Big)\;\sigma_I(\boldsymbol{\xi}_I)\;\mathrm{d}\Gamma_I \\ &+ \frac{1}{4\pi}\iint_{\boldsymbol{\xi}_I \in \Gamma_I}\Big[\Big(\nabla\Big(\frac{1}{r(\boldsymbol{\chi}_I,\boldsymbol{\xi}_I)}\Big) + \nabla\Big(\frac{1}{r(\boldsymbol{\chi}_I',\boldsymbol{\xi}_I)}\Big)\Big)\cdot\boldsymbol{n}(\boldsymbol{\xi}_I)\Big]\;V_I(\boldsymbol{\xi}_I)\;\mathrm{d}\Gamma_I \\ &- \frac{1}{2}V_I(\boldsymbol{\chi}_I)\Bigg]\,\mathrm{d}\Gamma_I = 0 \end{aligned} \tag{4.53}$$

$$\begin{aligned} &\iint_{\boldsymbol{\chi}_I \in \Gamma_I} \omega_I(\boldsymbol{\chi}_I)\Bigg[\frac{1}{4\pi\gamma_I}\iint_{\boldsymbol{\xi}_I \in \Gamma_I}\frac{1}{r(\boldsymbol{\chi}_I,\boldsymbol{\xi}_I)}\;\sigma_I(\boldsymbol{\xi}_I)\;\mathrm{d}\Gamma_I \\ &+ \frac{1}{4\pi}\iint_{\boldsymbol{\xi}_I \in \Gamma_I}\Big[\nabla\Big(\frac{1}{r(\boldsymbol{\chi}_I,\boldsymbol{\xi}_I)}\Big)\cdot\boldsymbol{n}(\boldsymbol{\xi}_I)\Big]V_I(\boldsymbol{\xi}_I)\;\mathrm{d}\Gamma_I + \frac{1}{2}V_I(\boldsymbol{\chi}_I)\Bigg]\,\mathrm{d}\Gamma_I = 0 \end{aligned} \tag{4.54}$$

For the point collocation method the governing equations are obtained replacing the weighting functions by the Dirac delta function (4.51) and applying the sifting property. Therefore, the previous equations take the form

$$\begin{aligned}
&\pi\phi(\widehat{\boldsymbol{\chi}}_{Gj})V_G - \frac{1}{4\pi\gamma}\int_{\widehat{\boldsymbol{\xi}}_G \in L_G} K(\widehat{\boldsymbol{\chi}}_{Gj},\widehat{\boldsymbol{\xi}}_G)\ \widehat{\sigma}_G(\widehat{\boldsymbol{\xi}}_G)\,\mathrm{d}L_G \\
&- \frac{1}{4\pi\gamma}\iint_{\boldsymbol{\xi}_I \in \Gamma_I} K(\widehat{\boldsymbol{\chi}}_{Gj},\boldsymbol{\xi}_I)\ \sigma_I(\boldsymbol{\xi}_I)\,\mathrm{d}\Gamma_I - \frac{1}{4\pi}\iint_{\boldsymbol{\xi}_I \in \Gamma_I} K^*(\widehat{\boldsymbol{\chi}}_{Gj},\boldsymbol{\xi}_I)\ V_I(\boldsymbol{\xi}_I)\,\mathrm{d}\Gamma_I \\
&= 0\,, \qquad j = 1,\dots,n_{cp_G}
\end{aligned} \tag{4.55}$$

$$\begin{aligned}
&\frac{1}{4\pi\gamma}\int_{\widehat{\boldsymbol{\xi}}_G \in L_G} K(\boldsymbol{\chi}_{Ij},\widehat{\boldsymbol{\xi}}_G)\ \widehat{\sigma}_G(\widehat{\boldsymbol{\xi}}_G)\,\mathrm{d}L_G \\
&+ \frac{1}{4\pi\gamma}\iint_{\boldsymbol{\xi}_I \in \Gamma_I}\Big(\frac{1}{r(\boldsymbol{\chi}_{Ij},\boldsymbol{\xi}_I)} + \frac{1}{r(\boldsymbol{\chi}'_{Ij},\boldsymbol{\xi}_I)}\Big)\ \sigma_I(\boldsymbol{\xi}_I)\,\mathrm{d}\Gamma_I \\
&+ \frac{1}{4\pi}\iint_{\boldsymbol{\xi}_I \in \Gamma_I}\Big[\Big(\nabla\Big(\frac{1}{r(\boldsymbol{\chi}_{Ij},\boldsymbol{\xi}_I)}\Big) + \nabla\Big(\frac{1}{r(\boldsymbol{\chi}'_{Ij},\boldsymbol{\xi}_I)}\Big)\Big)\cdot\boldsymbol{n}(\boldsymbol{\xi}_I)\Big]\ V_I(\boldsymbol{\xi}_I)\,\mathrm{d}\Gamma_I \\
&- \frac{1}{2}V_I(\boldsymbol{\chi}_{Ij}) = 0\,, \qquad j = 1,\dots,n_{cp_I}
\end{aligned} \tag{4.56}$$

$$\begin{aligned}
&\frac{1}{4\pi\gamma_I}\iint_{\boldsymbol{\xi}_I \in \Gamma_I}\frac{1}{r(\boldsymbol{\chi}_{Ij},\boldsymbol{\xi}_I)}\sigma_I(\boldsymbol{\xi}_I)\,\mathrm{d}\Gamma_I + \frac{1}{4\pi}\iint_{\boldsymbol{\xi}_I \in \Gamma_I}\Big[\nabla\Big(\frac{1}{r(\boldsymbol{\chi}_{Ij},\boldsymbol{\xi}_I)}\Big)\cdot\boldsymbol{n}(\boldsymbol{\xi}_I)\Big]V_I(\boldsymbol{\xi}_I)\,\mathrm{d}\Gamma_I \\
&+ \frac{1}{2}V_I(\boldsymbol{\chi}_{Ij}) = 0\,, \qquad j = 1,\dots,n_{cp_I}
\end{aligned} \tag{4.57}$$

Once the weighted residual method chosen to approximate the solution has been applied, the numerical technique to solve the problem will be the BEM. In order to apply it, the discretisations explained in Section 4.4 for the geometries and unknown functions have to be introduced in equations (4.55) to (4.57).

Consequently, the boundary integral equations are split into a sum of n_{cp_G} or n_{cp_I} integrals over each element defined in Γ_G (n_{el_G}) or Γ_I (n_{el_I}). Thus, the equations can be rewritten as:

- Equation (4.55)

$$\begin{aligned}
&\frac{1}{4\pi\gamma}\sum_{\alpha=1}^{n_{el_G}}\int_{\widehat{\boldsymbol{\xi}}_G \in L_G^\alpha} K(\widehat{\boldsymbol{\chi}}_{Gj},\widehat{\boldsymbol{\xi}}_G)\ \sum_{i=1}^{n_{np_G}}\widehat{\sigma}_{Gi}^{\alpha}\,N_{Gi}(\widehat{\boldsymbol{\xi}}_G)\,\mathrm{d}L_G^\alpha \\
&+ \frac{1}{4\pi\gamma}\sum_{\alpha=1}^{n_{el_I}}\iint_{\boldsymbol{\xi}_I \in \Gamma_I^\alpha} K(\widehat{\boldsymbol{\chi}}_{Gj},\boldsymbol{\xi}_I)\ \sum_{i=1}^{n_{np_I}}\sigma_{Ii}^{\alpha}\,N_{Ii}(\boldsymbol{\xi}_I)\,\mathrm{d}\Gamma_I^\alpha \\
&+ \frac{1}{4\pi}\sum_{\alpha=1}^{n_{el_I}}\iint_{\boldsymbol{\xi}_I \in \Gamma_I^\alpha} K^*(\widehat{\boldsymbol{\chi}}_{Gj},\boldsymbol{\xi}_I)\ \sum_{i=1}^{n_{np_I}}V_{Ii}^{\alpha}\,N_{Ii}(\boldsymbol{\xi}_I)\,\mathrm{d}\Gamma_I^\alpha = \ \pi\phi(\widehat{\boldsymbol{\chi}}_{Gj})V_G\,, \quad j = 1,\dots,n_{cp_G}
\end{aligned} \tag{4.58}$$

This equation can be written in discretised form as:

$$\sum_{j=1}^{n_{cpG}} \left[\sum_{\alpha=1}^{n_{elG}} \sum_{i=1}^{n_{npG}} R^{\alpha}_{GG_{ji}} \widehat{\sigma}^{\alpha}_{Gi} + \sum_{\alpha=1}^{n_{elI}} \sum_{i=1}^{n_{npI}} R^{\alpha}_{GI_{ji}} \sigma^{\alpha}_{Ii} + \sum_{\alpha=1}^{n_{elI}} \sum_{i=1}^{n_{npI}} S^{\alpha}_{GI_{ji}} V^{\alpha}_{Ii} \right] = \sum_{j=1}^{n_{cpG}} \nu_{G_j} \tag{4.59}$$

where

$$\nu_{G_j} = \pi \phi(\widehat{\boldsymbol{\chi}}_{Gj}) V_G \tag{4.60}$$

$$R^{\alpha}_{GG_{ji}} = \frac{1}{4\pi\gamma} \int_{\widehat{\boldsymbol{\xi}}_G \in L^{\alpha}_G} K(\widehat{\boldsymbol{\chi}}_{Gj}, \widehat{\boldsymbol{\xi}}_G)\ N_{Gi}(\widehat{\boldsymbol{\xi}}_G)\, \mathrm{d}L^{\alpha}_G \tag{4.61}$$

$$R^{\alpha}_{GI_{ji}} = \frac{1}{4\pi\gamma} \iint_{\boldsymbol{\xi}_I \in \Gamma^{\alpha}_I} K(\widehat{\boldsymbol{\chi}}_{Gj}, \boldsymbol{\xi}_I)\ N_{Ii}(\boldsymbol{\xi}_I)\, \mathrm{d}\Gamma^{\alpha}_I \tag{4.62}$$

$$S^{\alpha}_{GI_{ji}} = \frac{1}{4\pi} \iint_{\boldsymbol{\xi}_I \in \Gamma^{\alpha}_I} K^*(\widehat{\boldsymbol{\chi}}_{Gj}, \boldsymbol{\xi}_I)\ N_{Ii}(\boldsymbol{\xi}_I)\, \mathrm{d}\Gamma^{\alpha}_I \tag{4.63}$$

and $\widehat{\sigma}^{\alpha}_{Gi}$, σ^{α}_{Ii} and V^{α}_{Ii} are the values of the unknown functions at nodal point i that belongs to element α.

- Equation (4.56)

$$\begin{aligned}
&\frac{1}{4\pi\gamma} \sum_{\alpha=1}^{n_{elG}} \int_{\widehat{\boldsymbol{\xi}}_G \in L^{\alpha}_G} K(\boldsymbol{\chi}_{Ij}, \widehat{\boldsymbol{\xi}}_G) \sum_{i=1}^{n_{npG}} \widehat{\sigma}^{\alpha}_{Gi}\, N_{Gi}(\widehat{\boldsymbol{\xi}}_G)\, \mathrm{d}L^{\alpha}_G \\
&+ \frac{1}{4\pi\gamma} \sum_{\alpha=1}^{n_{elI}} \iint_{\boldsymbol{\xi}_I \in \Gamma^{\alpha}_I} \Big(\frac{1}{r(\boldsymbol{\chi}_{Ij}, \boldsymbol{\xi}_I)} + \frac{1}{r(\boldsymbol{\chi}'_{Ij}, \boldsymbol{\xi}_I)} \Big) \sum_{i=1}^{n_{npI}} \sigma^{\alpha}_{Ii}\, N_{Ii}(\boldsymbol{\xi}_I)\, \mathrm{d}\Gamma^{\alpha}_I \\
&+ \frac{1}{4\pi} \sum_{\alpha=1}^{n_{elI}} \iint_{\boldsymbol{\xi}_I \in \Gamma^{\alpha}_I} \Big[\Big(\nabla \Big(\frac{1}{r(\boldsymbol{\chi}_{Ij}, \boldsymbol{\xi}_I)} \Big) + \nabla \Big(\frac{1}{r(\boldsymbol{\chi}'_{Ij}, \boldsymbol{\xi}_I)} \Big) \Big) \cdot \boldsymbol{n}(\boldsymbol{\xi}_I) \Big] \sum_{i=1}^{n_{npI}} V^{\alpha}_{Ii}\, N_{Ii}(\boldsymbol{\xi}_I)\, \mathrm{d}\Gamma^{\alpha}_I \\
&- \frac{1}{2} \sum_{i=1}^{n_{npI}} V^{\alpha}_{Ii}\, N_{Ii}(\boldsymbol{\chi}_{Ij}) = 0\,, \qquad j = 1, \ldots, n_{cpI}
\end{aligned} \tag{4.64}$$

This equation can be written in discretised form as:

$$\sum_{j=1}^{n_{cpI}} \left[\sum_{\alpha=1}^{n_{elG}} \sum_{i=1}^{n_{npG}} R^{\alpha}_{IG_{ji}} \widehat{\sigma}^{\alpha}_{Gi} + \sum_{\alpha=1}^{n_{elI}} \sum_{i=1}^{n_{npI}} R^{\alpha}_{II_{ji}} \sigma^{\alpha}_{Ii} + \sum_{\alpha=1}^{n_{elI}} \sum_{i=1}^{n_{npI}} S^{\alpha}_{II_{ji}} V^{\alpha}_{Ii} \right] = 0 \tag{4.65}$$

where

$$R^{\alpha}_{IG_{ji}} = \frac{1}{4\pi\gamma} \int_{\widehat{\boldsymbol{\xi}}_G \in L^{\alpha}_G} K(\boldsymbol{\chi}_{Ij}, \widehat{\boldsymbol{\xi}}_G)\ N_{Gi}(\widehat{\boldsymbol{\xi}}_G)\, \mathrm{d}L^{\alpha}_G \tag{4.66}$$

$$R^{\alpha}_{II_{ji}} = \frac{1}{4\pi\gamma} \iint_{\boldsymbol{\xi}_I \in \Gamma^{\alpha}_I} \Big(\frac{1}{r(\boldsymbol{\chi}_{Ij}, \boldsymbol{\xi}_I)} + \frac{1}{r(\boldsymbol{\chi}'_{Ij}, \boldsymbol{\xi}_I)} \Big)\ N_{Ii}(\boldsymbol{\xi}_I)\, \mathrm{d}\Gamma^{\alpha}_I \tag{4.67}$$

$$S^{\alpha}_{II_{ji}} = \frac{1}{4\pi} \iint_{\boldsymbol{\xi}_I \in \Gamma^{\alpha}_I} \left[\left(\nabla\Big(\frac{1}{r(\boldsymbol{\chi}_I, \boldsymbol{\xi}_I)}\Big) + \nabla\Big(\frac{1}{r(\boldsymbol{\chi}'_I, \boldsymbol{\xi}_I)}\Big) \right) \cdot \boldsymbol{n}(\boldsymbol{\xi}_I) \right] N_{Ii}(\boldsymbol{\xi}_I)\, \mathrm{d}\Gamma^{\alpha}_I - \frac{1}{2}\, N_{Ii}(\boldsymbol{\chi}_{Ij}) \tag{4.68}$$

- Equation (4.57)

$$\begin{aligned} &\frac{1}{4\pi\gamma_I} \sum_{\alpha=1}^{n_{el_I}} \iint_{\boldsymbol{\xi}_I \in \Gamma^{\alpha}_I} \frac{1}{r(\boldsymbol{\chi}_{Ij}, \boldsymbol{\xi}_I)} \sum_{i=1}^{n_{np_I}} \sigma^{\alpha}_{Ii}\, N_{Ii}(\boldsymbol{\xi}_I)\, \mathrm{d}\Gamma^{\alpha}_I \\ &+ \frac{1}{4\pi} \sum_{\alpha=1}^{n_{el_I}} \iint_{\boldsymbol{\xi}_I \in \Gamma^{\alpha}_I} \left[\nabla\Big(\frac{1}{r(\boldsymbol{\chi}_{Ij}, \boldsymbol{\xi}_I)}\Big) \cdot \boldsymbol{n}(\boldsymbol{\xi}_I) \right] \sum_{i=1}^{n_{np_I}} V^{\alpha}_{Ii}\, N_{Ii}(\boldsymbol{\xi}_I)\, \mathrm{d}\Gamma^{\alpha}_I \\ &+ \frac{1}{2} \sum_{i=1}^{n_{np_I}} V^{\alpha}_{Ii}\, N_{Ii}(\boldsymbol{\chi}_{Ij}) = 0\,, \qquad j = 1, \ldots, n_{cp_I} \end{aligned} \tag{4.69}$$

This equation can be written in discretised form as:

$$\sum_{j=1}^{n_{cp_I}} \left[\sum_{\alpha=1}^{n_{el_I}} \sum_{i=1}^{n_{np_I}} T^{\alpha}_{I_{ji}} \sigma^{\alpha}_{Ii} + \sum_{\alpha=1}^{n_{el_I}} \sum_{i=1}^{n_{np_I}} S^{\alpha}_{I_{ji}} V^{\alpha}_{Ii} \right] = 0 \tag{4.70}$$

where

$$T^{\alpha}_{I_{ji}} = \frac{1}{4\pi\gamma_I} \iint_{\boldsymbol{\xi}_I \in \Gamma^{\alpha}_I} \frac{1}{r(\boldsymbol{\chi}_{Ij}, \boldsymbol{\xi}_I)}\, N_{Ii}(\boldsymbol{\xi}_I)\, \mathrm{d}\Gamma^{\alpha}_I \tag{4.71}$$

$$S^{\alpha}_{I_{ji}} = \frac{1}{4\pi} \iint_{\boldsymbol{\xi}_I \in \Gamma^{\alpha}_I} \left[\nabla\Big(\frac{1}{r(\boldsymbol{\chi}_{Ij}, \boldsymbol{\xi}_I)}\Big) \cdot \boldsymbol{n}(\boldsymbol{\xi}_I) \right] N_{Ii}(\boldsymbol{\xi}_I)\, \mathrm{d}\Gamma^{\alpha}_I + \frac{1}{2}\, N_{Ii}(\boldsymbol{\chi}_{Ij}) \tag{4.72}$$

As a result, the application of the BEM generates a system of discretised equations which can be expressed in matrix form as

$$\left(\begin{array}{c|c|c} \boldsymbol{R}_{GG} & \boldsymbol{R}_{GI} & \boldsymbol{S}_{GI} \\ \hline \boldsymbol{R}_{IG} & \boldsymbol{R}_{II} & \boldsymbol{S}_{II} \\ \hline \boldsymbol{0} & \boldsymbol{T}_I & \boldsymbol{S}_I \end{array} \right) \left(\begin{array}{c} \widehat{\boldsymbol{\sigma}}_G \\ \hline \boldsymbol{\sigma}_I \\ \hline \boldsymbol{V}_I \end{array} \right) = \left(\begin{array}{c} \boldsymbol{\nu}_G \\ \hline \boldsymbol{0} \\ \hline \boldsymbol{0} \end{array} \right) \tag{4.73}$$

where:

- $\boldsymbol{R}_{GG}$ is a square $(n_{cp_G} \times n_{cp_G})$ matrix, $\boldsymbol{R}_{GI}$ and $\boldsymbol{S}_{GI}$ are $(n_{cp_G} \times n_{cp_I})$ matrices, $\boldsymbol{R}_{IG}$ is a $(n_{cp_I} \times n_{cp_G})$ matrix, and $\boldsymbol{R}_{II}$, $\boldsymbol{S}_{II}$, $\boldsymbol{T}_I$ and $\boldsymbol{S}_I$ are square $(n_{cp_I} \times n_{cp_I})$ matrices.
- $\widehat{\boldsymbol{\sigma}}_G$, $\boldsymbol{\sigma}_I$ and $\boldsymbol{V}_I$ are the vectors which contain the nodal values of the current density of the electrodes, the current density of the electrical substation and the potential of the electrical substation, respectively.

- $\boldsymbol{\nu}_G$ is the vector which contains the boundary condition of the problem.

Thus, the system of equations is formed by a full and non-symmetric matrix with a dimension $(n_{cp_G} + 2n_{cp_I}) \times (n_{cp_G} + 2n_{cp_I})$, an unknown vector with a dimension $(n_{cp_G} + 2n_{cp_I})$, and a load vector with a dimension $(n_{cp_G} + 2n_{cp_I})$. This system will be solved using the technique of Crout matrix decomposition.

4.5.3 Discretisation Procedure

As it was stated in Section 4.4, the BEM is a method based on discretisation procedure, where the unknown functions are calculated on the boundary of domains. It will be necessary to define the approximations done to obtain the solution of the problem indicated in (4.73). In this problem a parametric representation for the approximation of L_G and Γ_I and the unknown functions is done. This parametric representation is similar to the isoparametric formulation in the Finite Element Method.

In general, three types of nodes can be defined in the discretisation procedure with different purposes. First, the geometric nodes which define the shape of boundary elements; second, the nodal points which are used to approximate the unknowns using interpolation functions; and third, the collocation points which are the points where the residual function is set equal to zero in the point collocation method. Although it is possible to define these three sets of nodes, it is usually considered the same points to approximate the geometry and functions. However, there are some situations where having more than one set of nodes contributes to have more flexibility and it has an important role in the treatment of corners and edges.

To deal with the problem studied an isoparametric formulation will be defined, so the same shape functions will be used to approximate the geometry and unknowns. In this case, a linear parametric representation will be chosen and two different kinds of functions will be defined. On one hand, for Γ_G and $\widehat{\sigma}_G$ discretisation one-dimensional elements will be used, since the integrals on the surface of electrodes were reduced to 1D with the assumption of circumferential uniformity of current densities. On the other hand, to approximate the geometry and unknowns of the underground electrical substation (3D region), two-dimensional elements formed by quadrilateral elements will be used.

One-dimensional elements

One-dimensional elements are used for approximating the axial line of the electrodes (L_G). These elements will be linear elements which connect two nodes, as shown in Figure 4.5.

Each element will be transformed to an intrinsic coordinate ξ which follows the direction of the element. This local system is defined as shown in Figure 4.5 and the relation between the local system (ξ) and the global Cartesian system $(\widehat{\boldsymbol{\xi}}_G)$ is given by

$$\widehat{\boldsymbol{\xi}}_G(\xi) = \widehat{\boldsymbol{\xi}}_{G_0} + \frac{L^\alpha}{2}\widehat{\boldsymbol{s}}^\alpha(\widehat{\boldsymbol{\xi}}_G)\xi \tag{4.74}$$

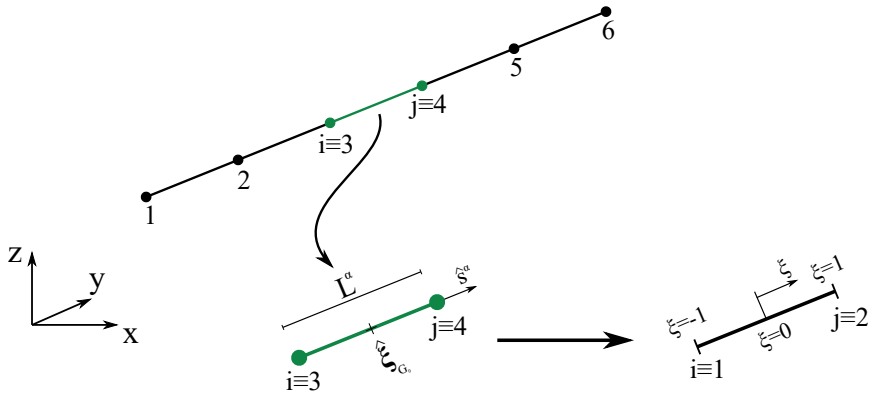

Figure 4.5. Axial line of electrodes approximated by linear elements in the global Cartesian system and in the local system.

where $\widehat{\boldsymbol{\xi}}_{G_0}$ is the midpoint of the element α, L^α is its length, and $\widehat{\boldsymbol{s}}^\alpha$ is its unit vector. The Jacobian of this transformation is

$$J = \frac{L^\alpha}{2}$$

Thus, the approximation of the geometry L_G and function $\widehat{\sigma}_G$ can be written based on the intrinsic coordinate. That is,

$$\widehat{\boldsymbol{\xi}}_G = \sum_{i=1}^{n_{np_G}} N_{Gi}(\xi)\, \widehat{\boldsymbol{\xi}}_{Gi} \tag{4.75}$$

$$\widehat{\sigma}_G = \sum_{i=1}^{n_{np_G}} N_{Gi}(\xi)\, \widehat{\sigma}_{Gi} \tag{4.76}$$

where N_G are the shape function.

In general, the shape functions can be obtained from the Lagrangian polynomials which are defined as

$$N_i(\xi) = \prod_{j=1, j\neq i}^{m} \frac{(\xi - \xi_j)}{(\xi_i - \xi_j)} \tag{4.77}$$

For this problem the shape functions will be

$$N_1(\xi) = \frac{1}{2}(1-\xi) \tag{4.78a}$$

$$N_2(\xi) = \frac{1}{2}(1+\xi) \tag{4.78b}$$

Two-dimensional elements

Similarly, two-dimensional elements are used for approximating the surface of the underground electrical substation (Γ_I). These elements will be quadrilateral elements with four nodes.

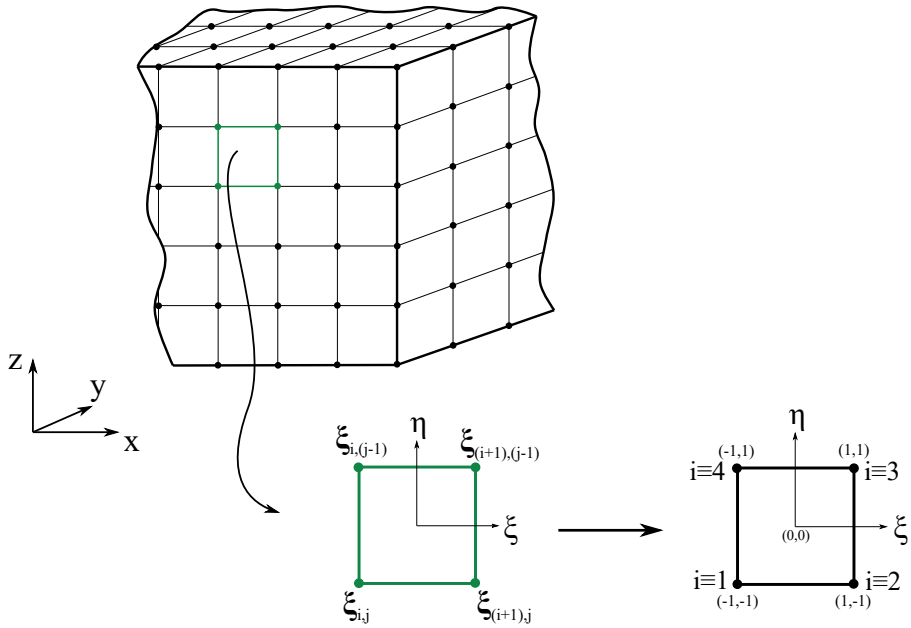

Figure 4.6. Underground electrical substation surface approximated by linear elements in the global Cartesian system and in the local system.

As in one-dimensional elements, each quadrilateral will be transformed to two intrinsic coordinates (ξ, η) (Figure 4.6).

Thus, the Cartesian coordinates ($\boldsymbol{\xi}_I$) and the unknown functions (σ_I, V_I) can be written with these intrinsic coordinates as:

$$\boldsymbol{\xi}_I = \sum_{i=1}^{n_{np_I}} N_{Ii}(\xi,\eta)\,\boldsymbol{\xi}_{Ii} \tag{4.79}$$

$$\sigma_I = \sum_{i=1}^{n_{np_I}} N_{Ii}(\xi,\eta)\,\sigma_{Ii} \tag{4.80}$$

$$V_I = \sum_{i=1}^{n_{np_I}} N_{Ii}(\xi,\eta)\,V_{Ii} \tag{4.81}$$

where N_I are the shape functions.

This change from the global Cartesian system to a local system (ξ, η) is equivalent to transform a boundary element into a unit local square (Figure 4.6).

For three-dimensional elements, the Jacobian of this transformation is given by

$$|J| = \sqrt{J_1^2 + J_2^2 + J_3^2} \tag{4.82}$$

where

$$J_1 = \frac{\partial y}{\partial \xi}\frac{\partial z}{\partial \eta} - \frac{\partial y}{\partial \eta}\frac{\partial z}{\partial \xi}$$

$$J_2 = \frac{\partial x}{\partial \eta}\frac{\partial z}{\partial \xi} - \frac{\partial x}{\partial \xi}\frac{\partial z}{\partial \eta}$$

$$J_3 = \frac{\partial x}{\partial \xi}\frac{\partial y}{\partial \eta} - \frac{\partial x}{\partial \eta}\frac{\partial y}{\partial \xi}$$

Again, the shape functions are obtained from the Lagrangian polynomials. For this problem they will be

$$N_1(\xi,\eta) = \frac{1}{4}(1-\xi)(1-\eta) \tag{4.83a}$$

$$N_2(\xi,\eta) = \frac{1}{4}(1+\xi)(1-\eta) \tag{4.83b}$$

$$N_3(\xi,\eta) = \frac{1}{4}(1+\xi)(1+\eta) \tag{4.83c}$$

$$N_4(\xi,\eta) = \frac{1}{4}(1-\xi)(1+\eta) \tag{4.83d}$$

Treatment of corners and edges

The point collocation method is a proper method when the boundary surfaces of domains are smooth. However, when the geometry of domains presents corners and/or edges, serious numerical problems appear with the collocation approach. The problem is caused by the ambiguity in the normal vector along an edge or at a corner where a not uniquely normal vector is defined.

In this problem, domain Ω_G is approximated by one-dimensional elements, which can be considered smooth. However, domain Ω_I has the geometry of an underground electrical substation, that is similar to a parallelepiped in which each side is planar with a normal vector associated at it. So, boundary Γ_I presents edges and corners (Figure 4.7), and the collocation approach does not give accurate results at these singularities.

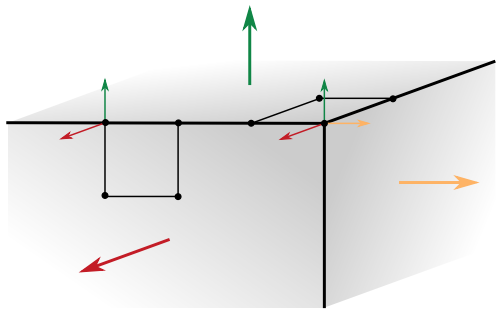

Figure 4.7. Ambiguity in normal vector along edges and/or corners.

Numerous schemes for dealing with corners and edges have been proposed and studied [Patterson & Sheikh, 1984; Subia & Ingber, 1995; Shen & Sterz, 1998; Aliabadi,

2002; Ong & Lim, 2005; Guzina et al., 2006; Beer et al., 2008]. In this thesis, the method chosen to deal with them is the semidiscontinuous element approach.

The semidiscontinuous element approach consists on moving the nodal and the collocation points from the edges and corners to the interior of element. Thus, the geometric points and the nodal and collocation points are no coincident for some boundary elements. That is, if the geometric points do not lie on an element that contains a corner or an edge, a continuous element is used in the discretisation procedure. In this case, the shape boundaries expounded in equation (4.83) are used for approximating the geometry (Γ_I) and the unknown functions (σ_I, V_I). However, if one or more sides of an element lie along an edge, a semidiscontinuous element is used in the discretisation procedure.

Four cases of this kind of discontinuities can be presented depends on the discretisation done in the boundary surface Γ_I [Patterson & Sheikh, 1984]:

- Class 1: Single edge discontinuity

  In this case, only one edge of the element coincides with a geometric edge of the domain, as shown in Figure 4.8.

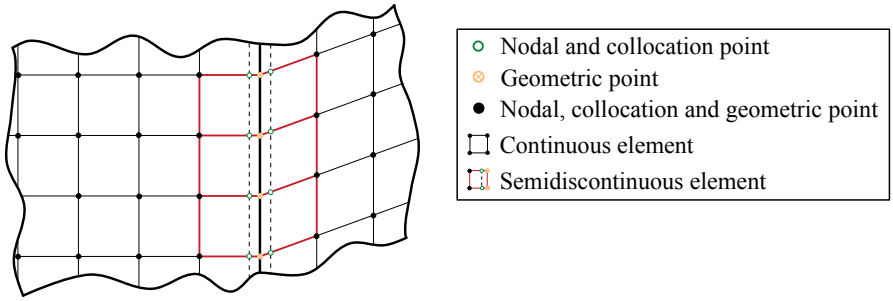

Figure 4.8. Class 1: Single edge discontinuity.

- Class 2: Two adjacent edge discontinuities

  In this case, two edges of the element coincide with the geometric edges of the domain, which represents a corner element, as shown in Figure 4.9.

- Class 3: Two non-adjacent edge discontinuities

  This case is more unusual, since it only could be present when the discretisation procedure has few elements, for example a side is divided in three elements (Figure 4.10).

- Class 4: Three edge discontinuities

  As Class 3, three edge discontinuities are unusual and it could be present in discretisations with few elements (Figure 4.11).

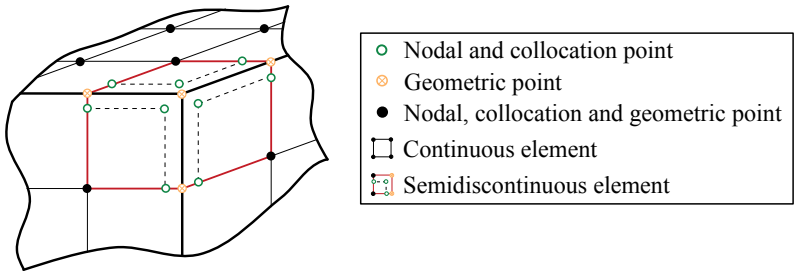

Figure 4.9. Class 2: Two adjacent edge discontinuities.

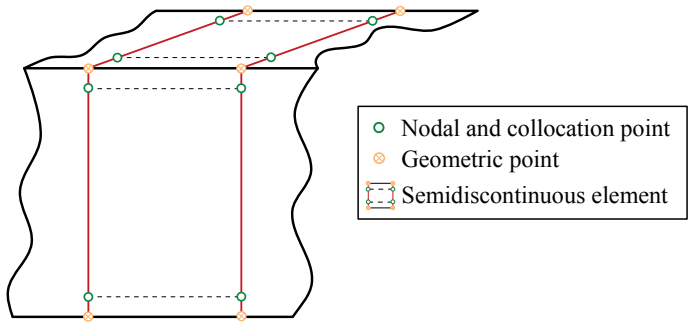

Figure 4.10. Class 3: Two non-adjacent edge discontinuities.

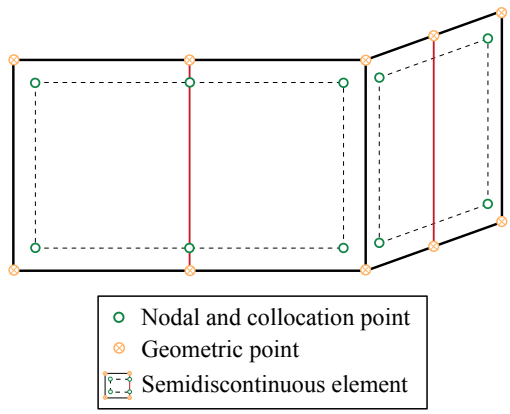

Figure 4.11. Class 4: Three edge discontinuities.

For the elements approximated with the semidiscontinuos approach, the geometry will be approximated with continuous elements and the shape functions are given by (4.83). But, to approximate the unknown functions, the nodal and collocation points will be displaced into the interior of the element and modified shape functions will be

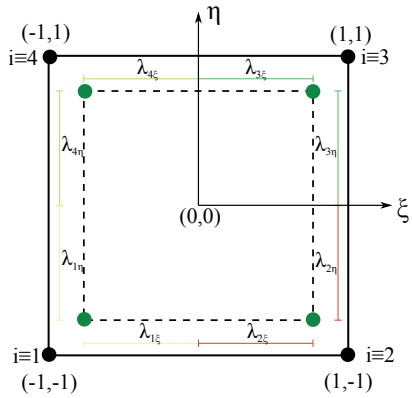

Figure 4.12. General discontinuous element.

necessary. The general expressions of the modified linear shape functions are given by

$$N_1(\xi,\eta) = \frac{1}{-\lambda_{1\xi}+\lambda_{2\xi}}(\lambda_{2\xi}-\xi)\frac{1}{-\lambda_{1\eta}+\lambda_{4\eta}}(\lambda_{4\eta}-\eta) \tag{4.84a}$$

$$N_2(\xi,\eta) = \frac{1}{-\lambda_{2\xi}+\lambda_{1\xi}}(\lambda_{1\xi}-\xi)\frac{1}{-\lambda_{2\eta}+\lambda_{3\eta}}(\lambda_{3\eta}-\eta) \tag{4.84b}$$

$$N_3(\xi,\eta) = \frac{1}{-\lambda_{3\xi}+\lambda_{4\xi}}(\lambda_{4\xi}-\xi)\frac{1}{-\lambda_{3\eta}+\lambda_{2\eta}}(\lambda_{2\eta}-\eta) \tag{4.84c}$$

$$N_4(\xi,\eta) = \frac{1}{-\lambda_{4\xi}+\lambda_{3\xi}}(\lambda_{3\xi}-\xi)\frac{1}{-\lambda_{4\eta}+\lambda_{1\eta}}(\lambda_{1\eta}-\eta) \tag{4.84d}$$

where λ parameters are the distances indicated in Figure 4.12.

In general, the value of λ is a pre-defined parameter which specifies the position of internal nodes, $0 < \lambda \leq 1$. Optimal values for λ can be found in the literature, as the range $0.75 < \lambda < 0.95$ proposed by [Guzina et al., 2006] which gives a good numerical accuracy.

In this thesis, surface Γ_I will be discretised with medium-size meshes, so the treatment of edges and corners will be done with the semidiscontinuous elements of Class 1 and Class 2, respectively.

4.5.4 Integration of kernels

The integration is the most important step in the BEM to obtain accurate and stable results. That is, no matter how refined the boundary discretisations are if the integrations are not sufficiently accurate.

In order to solve the integrals of equations (4.58), (4.64), and (4.69), numerical techniques are used.

Depending on the position of the collocation point with respect to the element on which the integration is being carried out, two types of integrals can be identified: regular integrals and weakly singular integrals.

Regular Integrals

This type of integral applies to all kernels where $\boldsymbol{\xi}$ and $\boldsymbol{\chi}$ do not belong to the same element. That is, the collocation point is not in the element in which the integration is being carried out. So, the integral is not singular and the integrand does not vary sharply in the region of integration.

The numerical method chosen to evaluate these integrals is the Gauss-Legendre quadrature.

Weakly Singular Integrals

The weakly singular integrals apply to all kernels where $\boldsymbol{\xi}$ and $\boldsymbol{\chi}$ belong to the same element. In the point collocation method these integrals appear when the collocation point is located on the element analysed or on an adjacent element to the analysed one. In this problem the singularity of the kernel is of order $O(1/r)$. In order to solve these integrals, different approaches are selected to calculate them in one-dimensional and in two-dimensional elements.

Weakly singular integrals over one-dimensional elements

In one-dimensional elements, the integrals are not properly weakly singular. The reason is that after doing the assumption of circumferential uniformity in the electrodes, the kernel expressions are formed by the Euclidean distance between $\widehat{\boldsymbol{\chi}}_G$ and $\widehat{\boldsymbol{\xi}}_G$ and an extra coefficient. This coefficient depends on the electrode diameter.

So, when $\widehat{\boldsymbol{\chi}}_G$ and $\widehat{\boldsymbol{\xi}}_G$ belong to the same element, the integral

$$\pi\phi(\widehat{\boldsymbol{\chi}}_G)\pi\phi(\widehat{\boldsymbol{\xi}}_G)\int_{\widehat{\boldsymbol{\xi}}_G \in L_G} \frac{1}{\sqrt{|\widehat{\boldsymbol{\chi}}_G - \widehat{\boldsymbol{\xi}}_G|^2 + \frac{\phi^2(\widehat{\boldsymbol{\xi}}_G)}{4}}}\, N_G(\widehat{\boldsymbol{\xi}}_G)\, \mathrm{d}L_G \tag{4.85}$$

is not weakly singular. But the function

$$\frac{1}{\sqrt{|\widehat{\boldsymbol{\chi}}_G - \widehat{\boldsymbol{\xi}}_G|^2 + \frac{\phi^2(\widehat{\boldsymbol{\xi}}_G)}{4}}}$$

varies sharply as $\widehat{\boldsymbol{\xi}}_G$ approaches the collocation point ($\widehat{\boldsymbol{\chi}}_G$), as shown in Figure 4.13.

Thus, in order to calculate these integrals with a numerical approach a special treatment is required, since the directly application of Gauss-Legendre formula does not provide results with enough accuracy. An alternative to calculate these integrals is to obtain the analytical expressions as it was developed in [Colominas, 1995]. But getting these expressions is not obvious and it will be complex for generic spatial arrangements of electrodes. Therefore, in this thesis, a numerical technique is chosen to calculate them. The numerical approach chosen is the Element Subdivision Technique.

The Element Subdivision Technique consists of dividing the element of the integration into K intervals [Aliabadi, 2002]. The length of these intervals can be equal or different and the order of quadrature can be varied in each one. As a result, the accuracy of an integral can be improved dividing the element into small intervals where

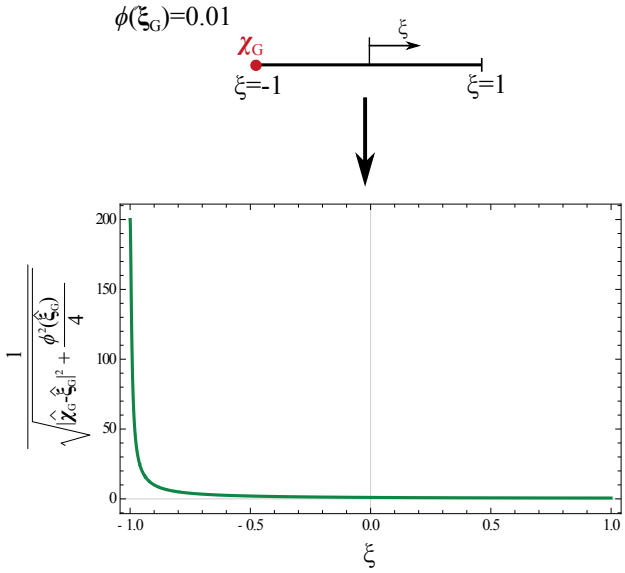

Figure 4.13. Variation of function $\frac{1}{\sqrt{|\widehat{\boldsymbol{x}}_G-\widehat{\boldsymbol{\xi}}_G|^2+\frac{\phi^2(\widehat{\boldsymbol{\xi}}_G)}{4}}}$ when $\widehat{\boldsymbol{x}}_G$ and $\widehat{\boldsymbol{\xi}}_G$ belong to the same element.

the function varies sharply and calculating the integral with a numerical quadrature, as Gauss-Legendre, with high-order in these intervals.

In this case, so as to calculate the integrals (4.85), the idea is to divide into three intervals the integrated element. This division will be done in the local system (ξ). The length of each interval will be different and its location will be depending where the collocation point is, as shown in Figure 4.14.

Then, each interval is transformed to a new intrinsic coordinate $\bar{\xi}$ which follows the direction of the element (Figure 4.14). The relation between the intrinsic coordinate ξ and $\bar{\xi}$ is

$$\xi = \xi_0 + \frac{\bar{L}}{2}\,\bar{\xi} \tag{4.86}$$

where ξ_0 is the midpoint of the interval, and $\bar{L}$ is its length. The Jacobian of this transformation is

$$\bar{J} = \frac{\bar{L}}{2}$$

Thus, the approximation of L_G geometry and $\widehat{\sigma}_G$ function can be rewritten as:

$$\widehat{\boldsymbol{\xi}}_G = \sum_{i=1}^{n_{np_G}} N_{Gi}(\xi(\bar{\xi}))\,\widehat{\boldsymbol{\xi}}_{Gi} \tag{4.87}$$

$$\widehat{\sigma}_G = \sum_{i=1}^{n_{np_G}} N_{Gi}(\xi(\bar{\xi}))\,\widehat{\sigma}_{Gi} \tag{4.88}$$

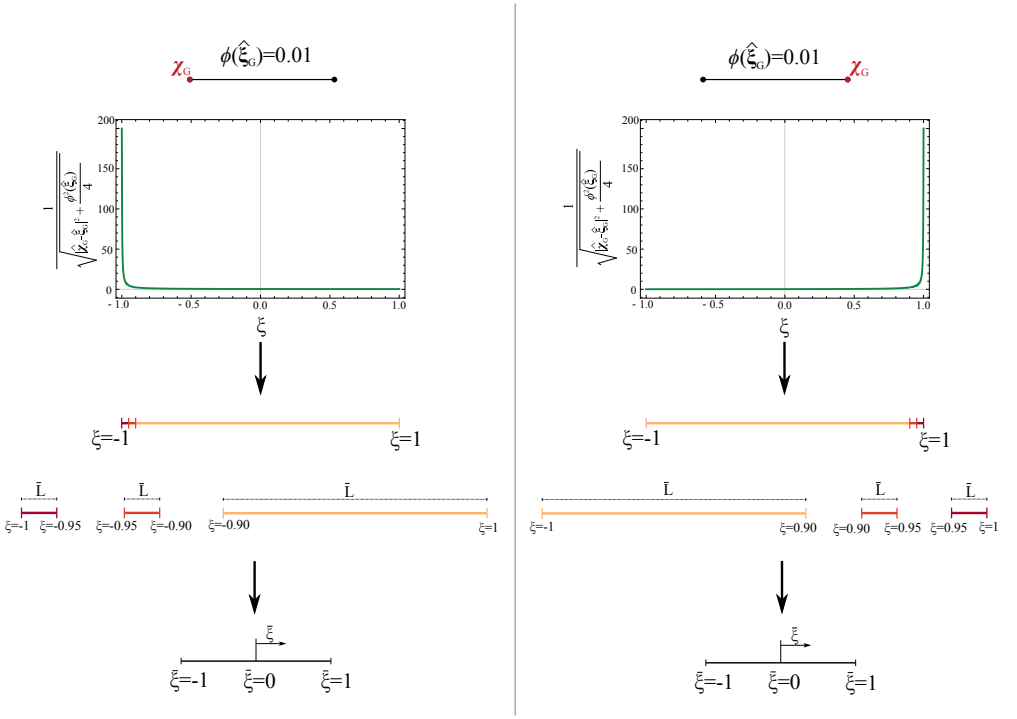

Figure 4.14. Element Subdivision Technique in one-dimensional elements.

Finally, integral (4.85) can be calculated with a good accuracy by means of applying the Gauss-Legendre formula with different order of quadrature in each interval. The order of quadrature will be higher in the intervals where the function varies sharply.

The general Gauss-Legendre formula to calculate this kind of integrals with the Element Subdivision Technique is

$$\begin{aligned} &\pi\phi(\widehat{\boldsymbol{\xi}}_G)\pi\phi(\widehat{\boldsymbol{\chi}}_G)\int_{\widehat{\boldsymbol{\xi}}_G\in L_G}\frac{1}{\sqrt{|\widehat{\boldsymbol{\chi}}_G-\widehat{\boldsymbol{\xi}}_G|^2+\frac{\phi^2(\widehat{\boldsymbol{\xi}}_G)}{4}}}\,N_G(\widehat{\boldsymbol{\xi}}_G)\,\mathrm{d}L_G \\ &\approx \pi\phi(\widehat{\boldsymbol{\xi}}_G)\pi\phi(\widehat{\boldsymbol{\chi}}_G)\sum_{k=1}^{K}\sum_{l=0}^{n_k}\omega_l\,f(\xi(\bar{\xi}_l))\,|\bar{J}_k|\,|J| \end{aligned} \tag{4.89}$$

where n_k is the number of Gauss points for each interval k, ω_l are the weights, and $f(\xi(\bar{\xi}_l))$ is the following function:

$$\frac{1}{\sqrt{|\widehat{\boldsymbol{\chi}}_G-\widehat{\boldsymbol{\xi}}_G(\xi(\bar{\xi}_l))|^2+\frac{\phi^2(\widehat{\boldsymbol{\xi}}_G)}{4}}}\,N_G(\widehat{\boldsymbol{\xi}}_G(\xi(\bar{\xi}_l)))$$

Weakly singular integrals over two-dimensional elements

Two types of weakly singular integrals over two-dimensional elements can be differentiated in this problem:

$$\iint_{\boldsymbol{\xi}_I \in \Gamma_I} \frac{1}{r(\boldsymbol{\chi}_I, \boldsymbol{\xi}_I)} \, N_I(\boldsymbol{\xi}_I) \, \mathrm{d}\Gamma_I \tag{4.90}$$

$$\iint_{\boldsymbol{\xi}_I \in \Gamma_I} \left[\nabla \Big(\frac{1}{r(\boldsymbol{\chi}_I, \boldsymbol{\xi}_I)} \Big) \cdot \boldsymbol{n}(\boldsymbol{\xi}_I) \right] N_I(\boldsymbol{\xi}_I) \, \mathrm{d}\Gamma_I \tag{4.91}$$

First, integral (4.90) will be analysed in which the singularity of the kernel is of order $O(1/r)$. The singularity of this integral depends on the position of the collocation point $(\boldsymbol{\chi}_I)$ in the quadrilateral elements with four nodes in which boundary Γ_I is discretised, as it was explained in Subsection 4.5.3. Thus, two cases can be studied:

When $\boldsymbol{\chi}_I$ is a node of the element but is not node $\boldsymbol{\xi}_I$, the function

$$\frac{1}{r(\boldsymbol{\chi}_I, \boldsymbol{\xi}_I)}$$

approaches infinity $(O(1/r))$ but the shape function N_I approaches zero, so the integral can be determined using Gauss-Legendre formula as it was a regular integral. As shown in Figure 4.15, the integrand does not vary sharply in these situations.

However, when $\boldsymbol{\chi}_I$ and $\boldsymbol{\xi}_I$ are the same node, the function

$$\frac{1}{r(\boldsymbol{\chi}_I, \boldsymbol{\xi}_I)}$$

approaches infinity $(O(1/r))$ and the shape function N_I approaches one. Due to this, the integrand is not determined and Gauss-Legendre formula cannot calculate properly the integral. Therefore, a special treatment is required to calculate these integrals with a good accuracy. In this thesis, the Lachat-Watson Transformation is used [Lachat & Watson, 1976]. This is a transformation of variable technique which is based on a triangle to square transformation that allows to exactly cancel out the singularity by means of the Jacobian of this transformation.

Thus, the Lachat-Watson Transformation consists in splitting up the integrated parent element into triangular subelements and for each subelement a local coordinate system is defined (Figure 4.16). This transformation is chosen in such a way that the Jacobian of the transformation is equal to zero in the point of singularity. That is, the transformation cancels out the singularity. The general expressions of the Lachat-Watson Transformation used in this thesis are carried out in [Fischnaller, 2009].

After introducing this transformation, the integral becomes regular and can be calculated with a good accuracy by means of the Gauss-Legendre quadrature.

The general Gauss-Legendre formula to calculate this kind of integrals with the Lachat-Watson Transformation is

$$\iint_{\boldsymbol{\xi}_I \in \Gamma_I} \frac{1}{r(\boldsymbol{\chi}_I, \boldsymbol{\xi}_I)} \, N_I(\boldsymbol{\xi}_I) \, \mathrm{d}\Gamma_I \approx \sum_{s=1}^{S} \sum_{l=0}^{n_l} \sum_{m=0}^{n_m} \omega_l \, \omega_m \, f(\xi(\bar{\xi}_l, \bar{\eta}_m), \eta(\bar{\xi}_l, \bar{\eta}_m)) \, |\bar{J}_s| \, |J| \tag{4.92}$$

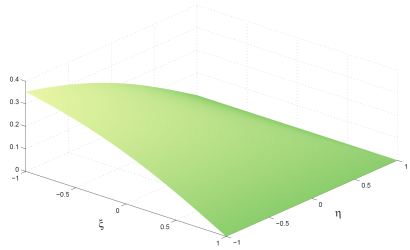

(a) Variation of the integrand when $\boldsymbol{\chi}_I$ is node 1 in a parent element and $\boldsymbol{\xi}_I$ is node 3 of this element.

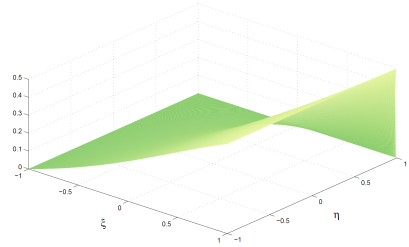

(b) Variation of the integrand when $\boldsymbol{\chi}_I$ is node 2 in a parent element and $\boldsymbol{\xi}_I$ is node 3 of this element.

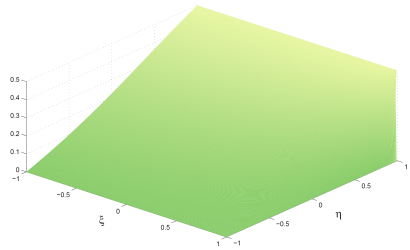

(c) Variation of the integrand when $\boldsymbol{\chi}_I$ is node 4 in a parent element and $\boldsymbol{\xi}_I$ is node 3 of this element.

Figure 4.15. Variation of the integrand when $\boldsymbol{\chi}_I$ is a node of the element but not $\boldsymbol{\xi}_I$.

where S is the number of triangular subelements, n_l is the number of Gauss points in $\bar{\xi}$ direction, n_m is the number of Gauss points in $\bar{\eta}$ direction, ω_l and ω_m are the weights, and $f(\xi(\bar{\xi}_l, \bar{\eta}_m), \eta(\bar{\xi}_l, \bar{\eta}_m))$ is the following function:

$$\frac{1}{r(\boldsymbol{\chi}_I, \boldsymbol{\xi}_I(\xi(\bar{\xi}_l, \bar{\eta}_m), \eta(\bar{\xi}_l, \bar{\eta}_m)))} \; N_I(\boldsymbol{\xi}_I(\xi(\bar{\xi}_l, \bar{\eta}_m), \eta(\bar{\xi}_l, \bar{\eta}_m)))$$

The other weakly integral to be analysed is integral (4.91) in which the singularity of the kernel is of order $O(1/r^2)$. In this integral, the kernel is formed by the shape function N_I and the directional derivative

$$\nabla\Big(\frac{1}{r(\boldsymbol{\chi}_I, \boldsymbol{\xi}_I)}\Big) \cdot \boldsymbol{n}(\boldsymbol{\xi}_I)$$

When $\boldsymbol{\chi}_I$ and $\boldsymbol{\xi}_I$ belong to the same element or to the same side of the parallelepiped

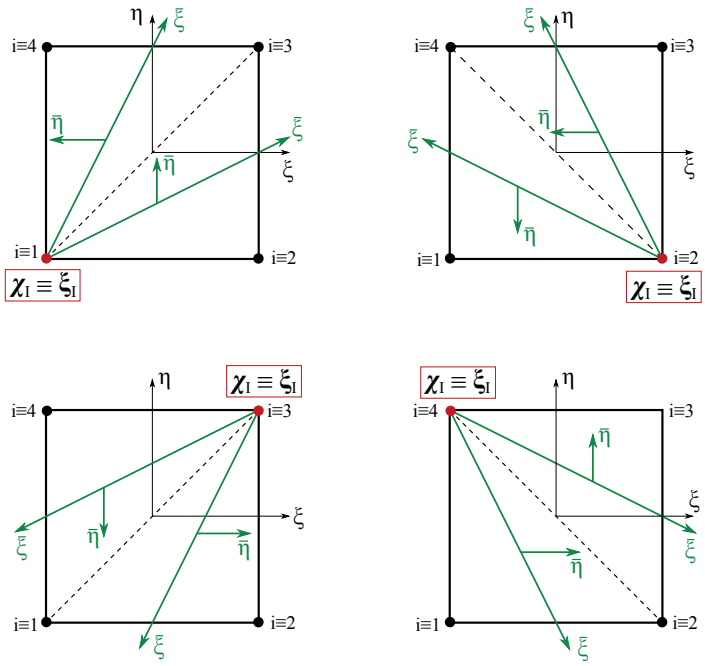

Figure 4.16. Lachat-Watson Transformation when the singular point is a coner node of element.

that define the geometry of the underground electrical substation, the gradient function

$$\nabla\Big(\frac{1}{r(\boldsymbol{\chi}_I, \boldsymbol{\xi}_I)}\Big)$$

and the normal vector $\boldsymbol{n}(\boldsymbol{\xi}_I)$ are perpendicular. As a consequence, the directional derivative is zero and there are not weakly singular integrals in this case.

4.6 Bubnov-Galerkin Method

4.6.1 Introduction

The Bubnov-Galerkin method is other of the most common weighted residual methods, as it was explained in Section 4.3. In this method the weighting functions are the same as the functions used to approximate the unknowns of the problem.

Thus, the weighting functions defined in the weak form of the governing equations will be replaced by

$$\begin{aligned} \widehat{\omega}_{Gj}(\widehat{\boldsymbol{\chi}}_G) &= N_{Gj}(\widehat{\boldsymbol{\chi}}_G) \qquad j = 1, \ldots, n_{npG} \\ \omega_{Ij}(\boldsymbol{\chi}_I) &= N_{Ij}(\boldsymbol{\chi}_I) \qquad j = 1, \ldots, n_{npI} \end{aligned} \tag{4.93}$$

where n_{npG} is the number of nodes per element in Γ_G, and n_{npI} is the number of nodes per element in Γ_I.

4.6.2 System of equations

Such as it was done in the point collocation method, the first step is to remember the system of equations obtained after formulating the boundary integral equations into weak forms and introducing the assumption of circumferential uniformity in the electrodes. That is,

$$\int_{\widehat{\boldsymbol{\chi}}_G \in L_G} \widehat{\omega}_G(\widehat{\boldsymbol{\chi}}_G) \left[\pi\phi(\boldsymbol{\chi}_G) V_G - \frac{1}{4\pi\gamma} \int_{\widehat{\boldsymbol{\xi}}_G \in L_G} K(\widehat{\boldsymbol{\chi}}_G, \widehat{\boldsymbol{\xi}}_G)\ \widehat{\sigma}_G(\widehat{\boldsymbol{\xi}}_G)\, \mathrm{d}L_G \right.$$
$$\left. - \frac{1}{4\pi\gamma} \iint_{\boldsymbol{\xi}_I \in \Gamma_I} K(\widehat{\boldsymbol{\chi}}_G, \boldsymbol{\xi}_I)\ \sigma_I(\boldsymbol{\xi}_I)\, \mathrm{d}\Gamma_I - \frac{1}{4\pi} \iint_{\boldsymbol{\xi}_I \in \Gamma_I} K^*(\widehat{\boldsymbol{\chi}}_G, \boldsymbol{\xi}_I)\ V_I(\boldsymbol{\xi}_I)\, \mathrm{d}\Gamma_I \right] \mathrm{d}L_G$$
$$= 0 \tag{4.94}$$

$$\begin{aligned} &\iint_{\boldsymbol{\chi}_I \in \Gamma_I} \omega_I(\boldsymbol{\chi}_I) \left[\frac{1}{4\pi\gamma} \int_{\widehat{\boldsymbol{\xi}}_G \in L_G} K(\boldsymbol{\chi}_I, \widehat{\boldsymbol{\xi}}_G)\ \widehat{\sigma}_G(\widehat{\boldsymbol{\xi}}_G)\ \mathrm{d}L_G \right. \\ &+ \frac{1}{4\pi\gamma} \iint_{\boldsymbol{\xi}_I \in \Gamma_I} \left(\frac{1}{r(\boldsymbol{\chi}_I, \boldsymbol{\xi}_I)} + \frac{1}{r(\boldsymbol{\chi}_I', \boldsymbol{\xi}_I)} \right) \sigma_I(\boldsymbol{\xi}_I)\ \mathrm{d}\Gamma_I \\ &+ \frac{1}{4\pi} \iint_{\boldsymbol{\xi}_I \in \Gamma_I} \left[\left(\nabla \left(\frac{1}{r(\boldsymbol{\chi}_I, \boldsymbol{\xi}_I)} \right) + \nabla \left(\frac{1}{r(\boldsymbol{\chi}_I', \boldsymbol{\xi}_I)} \right) \right) \cdot \boldsymbol{n}(\boldsymbol{\xi}_I) \right] V_I(\boldsymbol{\xi}_I)\ \mathrm{d}\Gamma_I \\ &\left. - \frac{1}{2} V_I(\boldsymbol{\chi}_I) \right] \mathrm{d}\Gamma_I = 0 \end{aligned} \tag{4.95}$$

$$\begin{aligned} &\iint_{\boldsymbol{\chi}_I \in \Gamma_I} \omega_I(\boldsymbol{\chi}_I) \left[\frac{1}{4\pi\gamma_I} \iint_{\boldsymbol{\xi}_I \in \Gamma_I} \frac{1}{r(\boldsymbol{\chi}_I, \boldsymbol{\xi}_I)}\ \sigma_I(\boldsymbol{\xi}_I)\ \mathrm{d}\Gamma_I \right. \\ &\left. + \frac{1}{4\pi} \iint_{\boldsymbol{\xi}_I \in \Gamma_I} \left[\nabla \left(\frac{1}{r(\boldsymbol{\chi}_I, \boldsymbol{\xi}_I)} \right) \cdot \boldsymbol{n}(\boldsymbol{\xi}_I) \right] V_I(\boldsymbol{\xi}_I)\ \mathrm{d}\Gamma_I + \frac{1}{2} V_I(\boldsymbol{\chi}_I) \right] \mathrm{d}\Gamma_I = 0 \end{aligned} \tag{4.96}$$

For the Bubnov-Galerkin method the governing equations are obtained replacing the weighting functions by the functions defined in (4.93). Again, the numerical technique to solve the problem will be the BEM, so the discretisations defined in Section 4.4 have to be introduced in equations (4.94) to (4.96).

As a result, the boundary integral equations are split into a sum of integrals which are rewritten as:

- Equation (4.94)

$$\begin{aligned}
&\sum_{\beta=1}^{n_{el_G}} \int_{\widehat{\boldsymbol{\chi}}_G \in L_G^\beta} \sum_{j=1}^{n_{np_G}} N_{Gj}(\widehat{\boldsymbol{\chi}}_G) \Bigg[\pi\phi(\widehat{\boldsymbol{\chi}}_G) V_G \\
&- \frac{1}{4\pi\gamma} \sum_{\alpha=1}^{n_{el_G}} \int_{\widehat{\boldsymbol{\xi}}_G \in L_G^\alpha} K(\widehat{\boldsymbol{\chi}}_G, \widehat{\boldsymbol{\xi}}_G) \sum_{i=1}^{n_{np_G}} \widehat{\sigma}_{Gi}^\alpha \, N_{Gi}(\widehat{\boldsymbol{\xi}}_G) \, \mathrm{d}L_G^\alpha \\
&- \frac{1}{4\pi\gamma} \sum_{\alpha=1}^{n_{el_I}} \iint_{\boldsymbol{\xi}_I \in \Gamma_I^\alpha} K(\widehat{\boldsymbol{\chi}}_G, \boldsymbol{\xi}_I) \sum_{i=1}^{n_{np_I}} \sigma_{Ii}^\alpha \, N_{Ii}(\boldsymbol{\xi}_I) \, \mathrm{d}\Gamma_I^\alpha \\
&- \frac{1}{4\pi} \sum_{\alpha=1}^{n_{el_I}} \iint_{\boldsymbol{\xi}_I \in \Gamma_I^\alpha} K^*(\widehat{\boldsymbol{\chi}}_G, \boldsymbol{\xi}_I) \sum_{i=1}^{n_{np_I}} V_{Ii}^\alpha \, N_{Ii}(\boldsymbol{\xi}_I) \, \mathrm{d}\Gamma_I^\alpha \Bigg] \mathrm{d}L_G^\beta = 0
\end{aligned} \tag{4.97}$$

This equation can be written in discretised form as:

$$\sum_{\beta=1}^{n_{el_G}} \sum_{j=1}^{n_{np_G}} \left[\sum_{\alpha=1}^{n_{el_G}} \sum_{i=1}^{n_{np_G}} R_{GG_{ji}}^{\beta\alpha} \widehat{\sigma}_{Gi}^\alpha + \sum_{\alpha=1}^{n_{el_I}} \sum_{i=1}^{n_{np_I}} R_{GI_{ji}}^{\beta\alpha} \sigma_{Ii}^\alpha + \sum_{\alpha=1}^{n_{el_I}} \sum_{i=1}^{n_{np_I}} S_{GI_{ji}}^{\beta\alpha} V_{Ii}^\alpha \right] = \sum_{\beta=1}^{n_{el_G}} \sum_{j=1}^{n_{np_G}} \nu_{G_j}^\beta \tag{4.98}$$

where

$$\nu_{G_j}^\beta = \pi\phi(\widehat{\boldsymbol{\chi}}_G) V_G \int_{\widehat{\boldsymbol{\chi}}_G \in L_G^\beta} N_{Gj}(\widehat{\boldsymbol{\chi}}_G) \, \mathrm{d}L_G^\beta \tag{4.99}$$

$$R_{GG_{ji}}^{\beta\alpha} = \frac{1}{4\pi\gamma} \int_{\widehat{\boldsymbol{\chi}}_G \in L_G^\beta} N_{Gj}(\widehat{\boldsymbol{\chi}}_G) \left[\int_{\widehat{\boldsymbol{\xi}}_G \in L_G^\alpha} K(\widehat{\boldsymbol{\chi}}_G, \widehat{\boldsymbol{\xi}}_G) \, N_{Gi}(\widehat{\boldsymbol{\xi}}_G) \, \mathrm{d}L_G^\alpha \right] \mathrm{d}L_G^\beta \tag{4.100}$$

$$R_{GI_{ji}}^{\beta\alpha} = \frac{1}{4\pi\gamma} \int_{\widehat{\boldsymbol{\chi}}_G \in L_G^\beta} N_{Gj}(\widehat{\boldsymbol{\chi}}_G) \left[\iint_{\boldsymbol{\xi}_I \in \Gamma_I^\alpha} K(\widehat{\boldsymbol{\chi}}_G, \boldsymbol{\xi}_I) \, N_{Ii}(\boldsymbol{\xi}_I) \, \mathrm{d}\Gamma_I^\alpha \right] \mathrm{d}L_G^\beta \tag{4.101}$$

$$S_{GI_{ji}}^{\beta\alpha} = \frac{1}{4\pi} \int_{\widehat{\boldsymbol{\chi}}_G \in L_G^\beta} N_{Gj}(\widehat{\boldsymbol{\chi}}_G) \left[\iint_{\boldsymbol{\xi}_I \in \Gamma_I^\alpha} K^*(\widehat{\boldsymbol{\chi}}_G, \boldsymbol{\xi}_I) \, N_{Ii}(\boldsymbol{\xi}_I) \, \mathrm{d}\Gamma_I^\alpha \right] \mathrm{d}L_G^\beta \tag{4.102}$$

and $\widehat{\sigma}_G^\alpha$, σ_I^α an V_I^α are the values of the unknown functions at nodal point i that belongs to element α.

- Equation (4.95)

$$\sum_{\beta=1}^{n_{el_I}} \iint_{\boldsymbol{\chi}_I \in \Gamma_I^\beta} \sum_{j=1}^{n_{np_I}} N_{Ij}(\boldsymbol{\chi}_I) \Bigg[\frac{1}{4\pi\gamma} \sum_{\alpha=1}^{n_{el_G}} \int_{\widehat{\boldsymbol{\xi}}_G \in L_G^\alpha} K(\boldsymbol{\chi}_I, \widehat{\boldsymbol{\xi}}_G) \sum_{i=1}^{n_{np_G}} \widehat{\sigma}_{Gi}^\alpha \, N_{Gi}(\widehat{\boldsymbol{\xi}}_G) \, \mathrm{d}L_G^\alpha$$
$$+ \frac{1}{4\pi\gamma} \sum_{\alpha=1}^{n_{el_I}} \iint_{\boldsymbol{\xi}_I \in \Gamma_I^\alpha} \Big(\frac{1}{r(\boldsymbol{\chi}_I, \boldsymbol{\xi}_I)} + \frac{1}{r(\boldsymbol{\chi}_I', \boldsymbol{\xi}_I)} \Big) \sum_{i=1}^{n_{np_I}} \sigma_{Ii}^\alpha \, N_{Ii}(\boldsymbol{\xi}_I) \, \mathrm{d}\Gamma_I^\alpha$$
$$+ \frac{1}{4\pi} \sum_{\alpha=1}^{n_{el_I}} \iint_{\boldsymbol{\xi}_I \in \Gamma_I^\alpha} \Big[\Big(\nabla \Big(\frac{1}{r(\boldsymbol{\chi}_I, \boldsymbol{\xi}_I)} \Big) + \nabla \Big(\frac{1}{r(\boldsymbol{\chi}_I', \boldsymbol{\xi}_I)} \Big) \Big) \cdot \boldsymbol{n}(\boldsymbol{\xi}_I) \Big] \sum_{i=1}^{n_{np_I}} V_{Ii}^\alpha \, N_{Ii}(\boldsymbol{\xi}_I) \, \mathrm{d}\Gamma_I^\alpha$$
$$- \frac{1}{2} \sum_{i=1}^{n_{np_I}} V_{Ii}^\alpha \, N_{Ii}(\boldsymbol{\chi}_I) \Bigg] \mathrm{d}\Gamma_I^\beta = 0 \tag{4.103}$$

This equation can be written in discretised form as:

$$\sum_{\beta=1}^{n_{el_I}} \sum_{j=1}^{n_{np_I}} \Bigg[\sum_{\alpha=1}^{n_{el_G}} \sum_{i=1}^{n_{np_G}} R_{IG_{ji}}^{\beta\alpha} \widehat{\sigma}_{Gi}^\alpha + \sum_{\alpha=1}^{n_{el_I}} \sum_{i=1}^{n_{np_I}} R_{II_{ji}}^{\beta\alpha} \sigma_{Ii}^\alpha + \sum_{\alpha=1}^{n_{el_I}} \sum_{i=1}^{n_{np_I}} S_{II_{ji}}^{\beta\alpha} V_{Ii}^\alpha \Bigg] = 0 \tag{4.104}$$

where

$$R_{IG_{ji}}^{\beta\alpha} = \frac{1}{4\pi\gamma} \iint_{\boldsymbol{\chi}_I \in \Gamma_I^\beta} N_{Ij}(\boldsymbol{\chi}_I) \Bigg[\int_{\widehat{\boldsymbol{\xi}}_G \in L_G^\alpha} K(\boldsymbol{\chi}_I, \widehat{\boldsymbol{\xi}}_G) \, N_{Gi}(\widehat{\boldsymbol{\xi}}_G) \, \mathrm{d}L_G^\alpha \Bigg] \mathrm{d}\Gamma_I^\beta \tag{4.105}$$

$$R_{II_{ji}}^{\beta\alpha} = \frac{1}{4\pi\gamma} \iint_{\boldsymbol{\chi}_I \in \Gamma_I^\beta} N_{Ij}(\boldsymbol{\chi}_I) \Bigg[\iint_{\boldsymbol{\xi}_I \in \Gamma_I^\alpha} \Big(\frac{1}{r(\boldsymbol{\chi}_I, \boldsymbol{\xi}_I)} + \frac{1}{r(\boldsymbol{\chi}_I', \boldsymbol{\xi}_I)} \Big) N_{Ii}(\boldsymbol{\xi}_I) \, \mathrm{d}\Gamma_I^\alpha \Bigg] \mathrm{d}\Gamma_I^\beta \tag{4.106}$$

$$\begin{aligned} S_{II_{ji}}^{\beta\alpha} = \frac{1}{4\pi} & \iint_{\boldsymbol{\chi}_I \in \Gamma_I^\beta} N_{Ij}(\boldsymbol{\chi}_I) \\ & \Bigg[\iint_{\boldsymbol{\xi}_I \in \Gamma_I^\alpha} \Big[\Big(\nabla \Big(\frac{1}{r(\boldsymbol{\chi}_I, \boldsymbol{\xi}_I)} \Big) + \nabla \Big(\frac{1}{r(\boldsymbol{\chi}_I', \boldsymbol{\xi}_I)} \Big) \Big) \cdot \boldsymbol{n}(\boldsymbol{\xi}_I) \Big] N_{Ii}(\boldsymbol{\xi}_I) \, \mathrm{d}\Gamma_I^\alpha \Bigg] \mathrm{d}\Gamma_I^\beta \\ & - \frac{1}{2} \iint_{\boldsymbol{\chi}_I \in \Gamma_I^\beta} N_{Ij}(\boldsymbol{\chi}_I) \, N_{Ii}(\boldsymbol{\chi}_I) \, \mathrm{d}\Gamma_I^\beta \end{aligned} \tag{4.107}$$

- Equation (4.96)

$$\sum_{\beta=1}^{n_{el_I}} \iint_{\boldsymbol{\chi}_I \in \Gamma_I^\beta} \sum_{j=1}^{n_{np_I}} N_{Ij}(\boldsymbol{\chi}_I) \left[\frac{1}{4\pi\gamma_I} \sum_{\alpha=1}^{n_{el_I}} \iint_{\boldsymbol{\xi}_I \in \Gamma_I^\alpha} \frac{1}{r(\boldsymbol{\chi}_I, \boldsymbol{\xi}_I)} \sum_{i=1}^{n_{np_I}} \sigma_{Ii}^\alpha \, N_{Ii}(\boldsymbol{\xi}_I) \, \mathrm{d}\Gamma_I^\alpha \right.$$
$$+ \frac{1}{4\pi} \sum_{\alpha=1}^{n_{el_I}} \iint_{\boldsymbol{\xi}_I \in \Gamma_I^\alpha} \left[\nabla\Big(\frac{1}{r(\boldsymbol{\chi}_I, \boldsymbol{\xi}_I)} \Big) \cdot \boldsymbol{n}(\boldsymbol{\xi}_I) \right] \sum_{i=1}^{n_{np_I}} V_{Ii}^\alpha \, N_{Ii}(\boldsymbol{\xi}_I) \, \mathrm{d}\Gamma_I^\alpha \tag{4.108}$$
$$\left. + \frac{1}{2} \sum_{i=1}^{n_{np_I}} V_{Ii}^\alpha \, N_{Ii}(\boldsymbol{\chi}_I) \right] \mathrm{d}\Gamma_I^\beta = 0$$

This equation can be written in discretised form as:

$$\sum_{\beta=1}^{n_{el_I}} \sum_{j=1}^{n_{np_I}} \left[\sum_{\alpha=1}^{n_{el_I}} \sum_{i=1}^{n_{np_I}} T_{Iji}^{\beta\alpha} \, \sigma_{Ii}^\alpha + \sum_{\alpha=1}^{n_{el_I}} \sum_{i=1}^{n_{np_I}} S_{I_{ji}}^{\beta\alpha} \, V_{Ii}^\alpha \right] = 0 \tag{4.109}$$

where

$$T_{Iji}^{\beta\alpha} = \frac{1}{4\pi\gamma_I} \iint_{\boldsymbol{\chi}_I \in \Gamma_I^\beta} N_{Ij}(\boldsymbol{\chi}_I) \left[\iint_{\boldsymbol{\xi}_I \in \Gamma_I^\alpha} \frac{1}{r(\boldsymbol{\chi}_I, \boldsymbol{\xi}_I)} \, N_{Ii}(\boldsymbol{\xi}_I) \, \mathrm{d}\Gamma_I^\alpha \right] \mathrm{d}\Gamma_I^\beta \tag{4.110}$$

$$S_{I_{ji}}^{\beta\alpha} = \frac{1}{4\pi} \iint_{\boldsymbol{\chi}_I \in \Gamma_I^\beta} N_{Ij}(\boldsymbol{\chi}_I) \left[\iint_{\boldsymbol{\xi}_I \in \Gamma_I^\alpha} \left[\nabla\Big(\frac{1}{r(\boldsymbol{\chi}_I, \boldsymbol{\xi}_I)} \Big) \cdot \boldsymbol{n}(\boldsymbol{\xi}_I) \right] N_{Ii}(\boldsymbol{\xi}_I) \, \mathrm{d}\Gamma_I^\alpha \right] \mathrm{d}\Gamma_I^\beta$$
$$+ \frac{1}{2} \iint_{\boldsymbol{\chi}_I \in \Gamma_I^\beta} N_{Ij}(\boldsymbol{\chi}_I) \, N_{Ii}(\boldsymbol{\chi}_I) \, \mathrm{d}\Gamma_I^\beta \tag{4.111}$$

As a result, the application of the BEM generates a system of discretised equations which can be expressed in matrix form as

$$\left(\begin{array}{c|c|c} \boldsymbol{R}_{GG} & \boldsymbol{R}_{GI} & \boldsymbol{S}_{GI} \\ \hline \boldsymbol{R}_{IG} & \boldsymbol{R}_{II} & \boldsymbol{S}_{II} \\ \hline \boldsymbol{0} & \boldsymbol{T}_I & \boldsymbol{S}_I \end{array} \right) \left(\begin{array}{c} \widehat{\boldsymbol{\sigma}}_G \\ \hline \boldsymbol{\sigma}_I \\ \hline \boldsymbol{V}_I \end{array} \right) = \left(\begin{array}{c} \boldsymbol{\nu}_G \\ \hline \boldsymbol{0} \\ \hline \boldsymbol{0} \end{array} \right) \tag{4.112}$$

where:

- $\boldsymbol{R}_{GG}$ is a square $(n_G \times n_G)$ matrix, $\boldsymbol{R}_{GI}$ and $\boldsymbol{S}_{GI}$ are $(n_G \times n_I)$ matrices, $\boldsymbol{R}_{IG}$ is a $(n_I \times n_G)$ matrix, and $\boldsymbol{R}_{II}$, $\boldsymbol{S}_{II}$, $\boldsymbol{T}_I$ and $\boldsymbol{S}_I$ are square $(n_I \times n_I)$ matrices.

  Note that: n_G is the number of points of Γ_G discretisation and n_I is the number of point of Γ_I discretisation. n_G and n_I are the same as the collocation points n_{cpG} and n_{cpI}, respectively.

- $\widehat{\boldsymbol{\sigma}}_G$, $\boldsymbol{\sigma}_I$ and $\boldsymbol{V}_I$ are the vectors which contain the nodal values of the current density of the electrodes, the current density of the electrical substation and the potential of the electrical substation, respectively.

- $\boldsymbol{\nu}_G$ is the vector which contains the boundary condition of the problem.

Thus, the system of equations is formed by a full and non-symmetric matrix with a dimension $(n_G + 2n_I) \times (n_G + 2n_I)$, an unknown vector with a dimension $(n_G + 2n_I)$, and a load vector with a dimension $(n_G + 2n_I)$. This system will be calculated using the technique of Crout matrix decomposition, as in the Point Collocation method.

4.6.3 Discretisation Procedure

The discretisation procedure to solve the problem formulated will be the same as the approximation explained in Subsection 4.5.3 for the Point Collocation method.

Only an additional aspect has to be added. As it was shown, in the Bubnov-Galerkin method a double integral over the boundaries has to be done. So, a double discretisation procedure is necessary, one for each line or surface integral. In order to facilitate the resolution of the system of equations the same approximation will be done for the weak integral and for the boundary integral equation. That is, boundary elements α will be equal to elements β, and nodal points j will be the same as nodal points i.

Treatment of corners and edges

The Bubnov-Galerkin method does not present numerical problems with corner and/or edges. The reason is that in this weighted residual method, the boundary integral

$$\int_{\Omega_j} R\,\omega_j \,\mathrm{d}\Omega = 0$$

is forced to be equal zero in the boundary element, not in a point. Therefore, there is not ambiguity in the normal vector along an edge or at a corner, since the normal used for every integral is the normal belong to the element, which is well defined.

4.6.4 Integration of kernels

As stated in the Point Collocation method, the integration is the most important step to obtain accurate and stable results.

In order to solve the integrals of equations (4.97), (4.103), and (4.108), numerical techniques are used.

Depending on the relative location between α and β elements, three types of integrals can be identified: regular integrals, near singular integrals and weakly singular integrals.

Regular Integrals

This type of integral applies to all kernels where α and β elements are not the same or they do not share an edge and/or a corner. Thus, the integral is not singular and the integrand does not vary sharply in the region of integration.

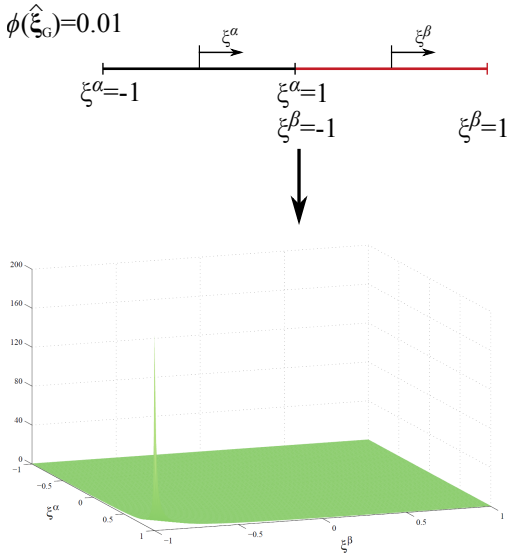

Figure 4.17. Variation of function $\frac{1}{\sqrt{|\widehat{\boldsymbol{\chi}}_G-\widehat{\boldsymbol{\xi}}_G|^2+\frac{\phi^2(\widehat{\boldsymbol{\xi}}_G)}{4}}}$ when $\widehat{\boldsymbol{\chi}}_G$ and $\widehat{\boldsymbol{\xi}}_G$ belong to adjacent elements.

The numerical method chosen to evaluate these integrals is the Gauss-Legendre quadrature.

Near Singular Integrals

The near singular integrals apply to all kernels where α and β elements are adjacent. That is, the elements share an edge or a corner between them. In these cases, a special treatment is required as the integrand varies sharply as point $\boldsymbol{\chi}$ that belongs to element β approaches point $\boldsymbol{\xi}$ that belongs to element α.

Near singular integrals over one-dimensional elements

In one-dimensional elements, the integrals

$$\pi\phi(\widehat{\boldsymbol{\xi}}_G)\pi\phi(\widehat{\boldsymbol{\chi}}_G)\int_{\widehat{\boldsymbol{\chi}}_G\in L_G^\beta} N_G(\widehat{\boldsymbol{\chi}}_G)\left[\int_{\widehat{\boldsymbol{\xi}}_G\in L_G^\alpha}\frac{1}{\sqrt{|\widehat{\boldsymbol{\chi}}_G-\widehat{\boldsymbol{\xi}}_G|^2+\frac{\phi^2(\widehat{\boldsymbol{\xi}}_G)}{4}}}N_G(\widehat{\boldsymbol{\xi}}_G)\,\mathrm{d}L_G^\alpha\right]\mathrm{d}L_G^\beta \tag{4.113}$$

are near singular when $\widehat{\boldsymbol{\chi}}_G$ and $\widehat{\boldsymbol{\xi}}_G$ belong to different elements which are adjacent. In this case, the function

$$\frac{1}{\sqrt{|\widehat{\boldsymbol{\chi}}_G-\widehat{\boldsymbol{\xi}}_G|^2+\frac{\phi^2(\widehat{\boldsymbol{\xi}}_G)}{4}}} \tag{4.114}$$

tends to vary sharply when $\widehat{\boldsymbol{\chi}}_G$ and $\widehat{\boldsymbol{\xi}}_G$ are closer, as shown in Figure 4.17.

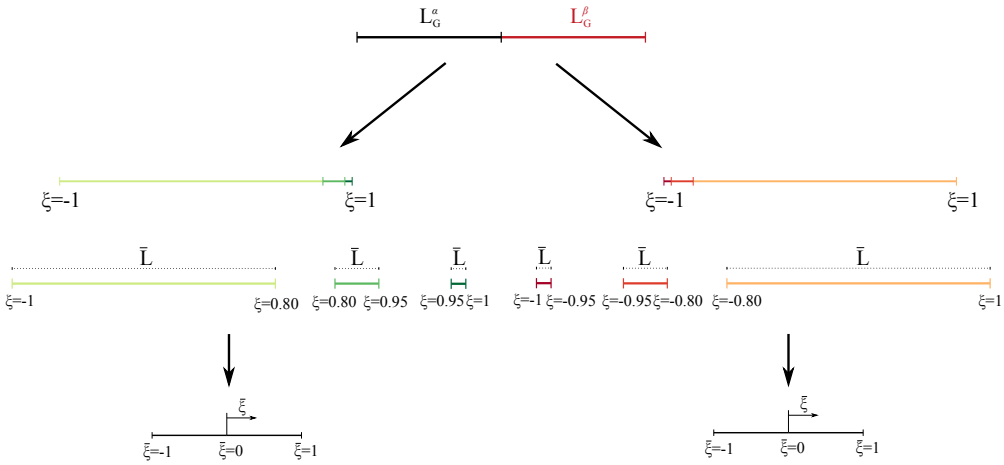

(a) Element subdivision when the adjacent element β is on the right-hand side of element α.

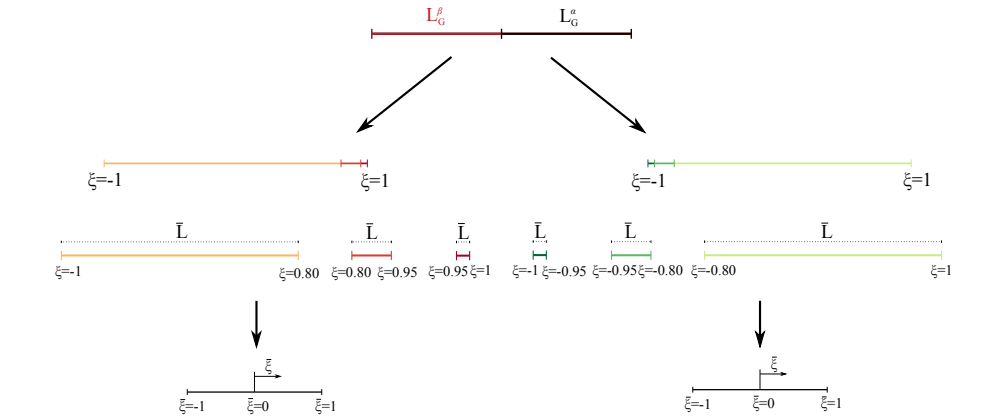

(b) Element subdivision when the adjacent element β is on the left-hand side of element α.

Figure 4.18. Element Subdivision Technique in one-dimensional element.

In order to calculate these integrals with a numerical technique that provides enough accuracy a special treatment is required. The numerical technique chosen to obtain these results is the Element Subdivision Technique. The application of this technique was explained in Subsection 4.5.4.

In this case, so as to calculate integral (4.113), the idea is to divide into three intervals both integrated elements (α and β). This division will be done in the local system (ξ). The length of each interval will be different and its location will depend on the location of the adjacent element, as shown in Figure 4.18.

Then, each interval is transformed to a new intrinsic coordinate $\bar{\xi}$ which follows the direction of the element (Figure 4.18). The relation between the intrinsic coordinate ξ

and $\bar{\xi}$ is

$$\xi = \xi_0 + \frac{\bar{L}}{2}\,\bar{\xi} \tag{4.115}$$

where ξ_0 is the midpoint of the interval, and $\bar{L}$ is its length. The Jacobian of this transformation is

$$\bar{J} = \frac{\bar{L}}{2} \tag{4.116}$$

Thus, the approximation of L_G^α and L_G^β geometries and $\widehat{\sigma}_G$ function can be rewritten as:

$$\widehat{\boldsymbol{\xi}}_G = \sum_{i=1}^{n_{npG}} N_{Gi}(\xi(\bar{\xi}))\,\widehat{\boldsymbol{\xi}}_{Gi} \tag{4.117}$$

$$\widehat{\boldsymbol{\chi}}_G = \sum_{i=1}^{n_{npG}} N_{Gi}(\xi(\bar{\xi}))\,\widehat{\boldsymbol{\chi}}_{Gi} \tag{4.118}$$

$$\widehat{\sigma}_G = \sum_{i=1}^{n_{npG}} N_{Gi}(\xi(\bar{\xi}))\,\widehat{\sigma}_{Gi} \tag{4.119}$$

Finally, integral (4.113) can be calculated with a good accuracy by means of applying the Gauss-Legendre formula with different order of quadrature in each interval. The order of quadrature will be higher in the intervals where the function varies sharply.

The general Gauss-Legendre formula to calculate this kind of integrals with the Element Subdivision Technique is

$$\begin{aligned}
&\pi\phi(\widehat{\boldsymbol{\xi}}_G)\pi\phi(\widehat{\boldsymbol{\chi}}_G)\int_{\widehat{\boldsymbol{\chi}}_G\,\in\,L_G^\beta} N_G(\widehat{\boldsymbol{\chi}}_G)\left[\int_{\widehat{\boldsymbol{\xi}}_G\,\in\,L_G^\alpha} \frac{1}{\sqrt{|\widehat{\boldsymbol{\chi}}_G - \widehat{\boldsymbol{\xi}}_G|^2 + \frac{\phi^2(\widehat{\boldsymbol{\xi}}_G)}{4}}}\, N_G(\widehat{\boldsymbol{\xi}}_G)\,\mathrm{d}L_G^\alpha\right]\mathrm{d}L_G^\beta \\
\approx&\pi\phi(\widehat{\boldsymbol{\xi}}_G)\pi\phi(\widehat{\boldsymbol{\chi}}_G)\sum_{k=1}^{K^\beta}\sum_{m=0}^{n_k} N_G(\widehat{\boldsymbol{\chi}}_G(\xi(\bar{\xi}_m)))\,\omega_m\,|\bar{J}_k^\beta|\,|J^\beta| \\
&\sum_{k=1}^{K^\alpha}\sum_{l=0}^{n_k} f(\widehat{\boldsymbol{\chi}}_G(\xi(\bar{\xi}_m)),\widehat{\boldsymbol{\xi}}_G(\xi(\bar{\xi}_l)))\,\omega_l\,|\bar{J}_k^\alpha|\,|J^\alpha|
\end{aligned} \tag{4.120}$$

where n_k is the number of Gauss points for each interval k, ω_l and ω_m are the weights, and $f(\widehat{\boldsymbol{\chi}}_G(\xi(\bar{\xi}_m)),\widehat{\boldsymbol{\xi}}_G(\xi(\bar{\xi}_l)))$ is the function:

$$\frac{1}{\sqrt{|\widehat{\boldsymbol{\chi}}_G(\xi(\bar{\xi}_m)) - \widehat{\boldsymbol{\xi}}_G(\xi(\bar{\xi}_l))|^2 + \frac{\phi^2(\widehat{\boldsymbol{\xi}}_G)}{4}}}\, N_G(\widehat{\boldsymbol{\xi}}_G(\xi(\bar{\xi}_l)))$$

Near singular integrals over two-dimensional elements

In two-dimensional elements, the integrals

$$\iint_{\boldsymbol{\chi}_I\,\in\,\Gamma_I^\beta} N_I(\boldsymbol{\chi}_I)\left[\iint_{\boldsymbol{\xi}_I\,\in\,\Gamma_I^\alpha} \frac{1}{r(\boldsymbol{\chi}_I,\boldsymbol{\xi}_I)}\, N_I(\boldsymbol{\xi}_I)\,\mathrm{d}\Gamma_I^\alpha\right]\mathrm{d}\Gamma_I^\beta \tag{4.121}$$

$$\iint_{\boldsymbol{\chi}_I \in \Gamma_I^\beta} N_I(\boldsymbol{\chi}_I) \left[\iint_{\boldsymbol{\xi}_I \in \Gamma_I^\alpha} \left[\nabla\Big(\frac{1}{r(\boldsymbol{\chi}_I, \boldsymbol{\xi}_I)} \Big) \cdot \boldsymbol{n}(\boldsymbol{\xi}_I) \right] N_I(\boldsymbol{\xi}_I) \, \mathrm{d}\Gamma_I^\alpha \right] \mathrm{d}\Gamma_I^\beta \tag{4.122}$$

are near singular when $\boldsymbol{\chi}_I$ and $\boldsymbol{\xi}_I$ belong to different elements which share an edge or a corner. In these cases, the functions

$$\frac{1}{r(\boldsymbol{\chi}_I, \boldsymbol{\xi}_I)} \tag{4.123}$$

$$\nabla\Big(\frac{1}{r(\boldsymbol{\chi}_I, \boldsymbol{\xi}_I)} \Big) \cdot \boldsymbol{n}(\boldsymbol{\xi}_I) \tag{4.124}$$

tend to vary sharply when $\boldsymbol{\chi}_I$ and $\boldsymbol{\xi}_I$ are closer.

In the same way as it was done for the integrals over one-dimensional elements, the Element Subdivision Technique is used to calculate integrals (4.121) and (4.122). However, depending on whether the elements share an edge or a corner, the subdivision is different.

First, the application of this technique will be explained for elements that share a corner. The variation of (4.123) and (4.124) functions in this case is showed in Figures 4.19 and 4.20.

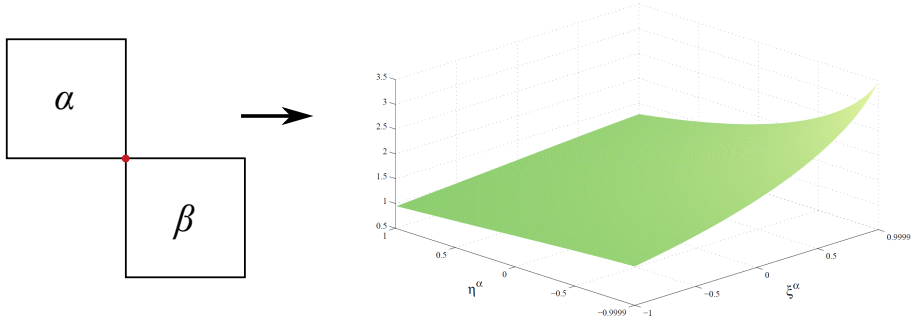

Figure 4.19. Variation of function $\frac{1}{r(\boldsymbol{\chi}_I, \boldsymbol{\xi}_I)}$ when element α and element β share a corner. Representation over element α.

The proposed approach consists of dividing into 4×4 interval both integrated elements (α and β). This division will be done in the local system (ξ, η). The length of each interval will be different and its location will depend on where the share corner is located in the parent element, as shown in Figure 4.21 .

Then, each interval is transformed to a new intrinsic coordinate system $(\bar{\xi}, \bar{\eta})$ (Figure 4.22). The relation between the coordinate systems (ξ, η) and $(\bar{\xi}, \bar{\eta})$ is

$$\xi = \sum_{i=1}^{n_{np_I}} N_{Ii}(\bar{\xi}, \bar{\eta}) \, \xi_i \tag{4.125}$$

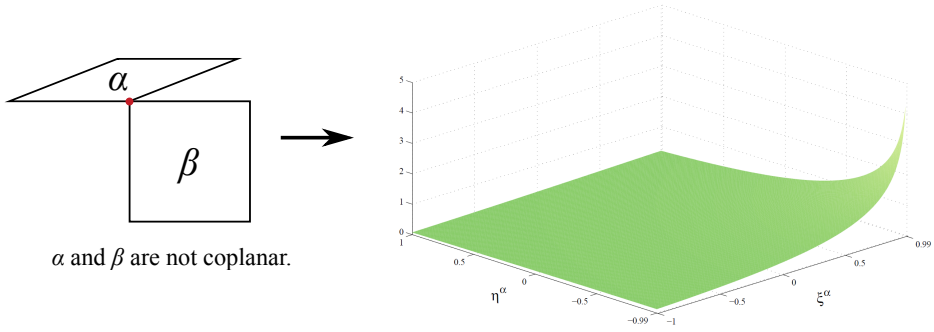

Figure 4.20. Variation of function $\nabla\left(\frac{1}{r(\boldsymbol{x}_I,\boldsymbol{\xi}_I)}\right)\cdot\boldsymbol{n}(\boldsymbol{\xi}_I)$ when element α and element β share a corner. Representation over element α.

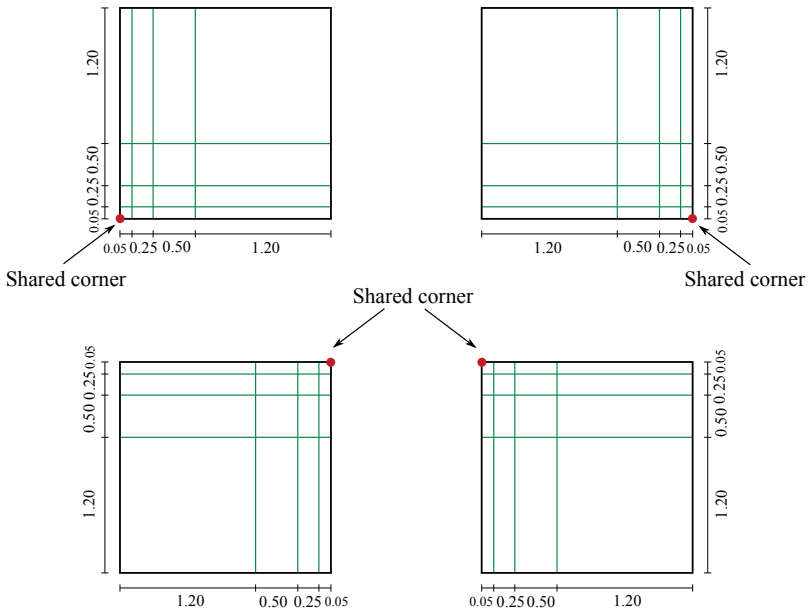

Figure 4.21. Element Subdivision Technique in two-dimensional elements when they share a corner.

$$\eta = \sum_{i=1}^{n_{npI}} N_{Ii}(\bar{\xi},\bar{\eta})\,\eta_i \tag{4.126}$$

where the shape functions are given by

$$N_{I1}(\bar{\xi},\bar{\eta}) = \frac{1}{4}(1-\bar{\xi})(1-\bar{\eta}) \tag{4.127a}$$

$$N_{I2}(\bar{\xi},\bar{\eta}) = \frac{1}{4}(1+\bar{\xi})(1-\bar{\eta}) \tag{4.127b}$$

$$N_{I3}(\bar{\xi},\bar{\eta}) = \frac{1}{4}(1+\bar{\xi})(1+\bar{\eta}) \tag{4.127c}$$

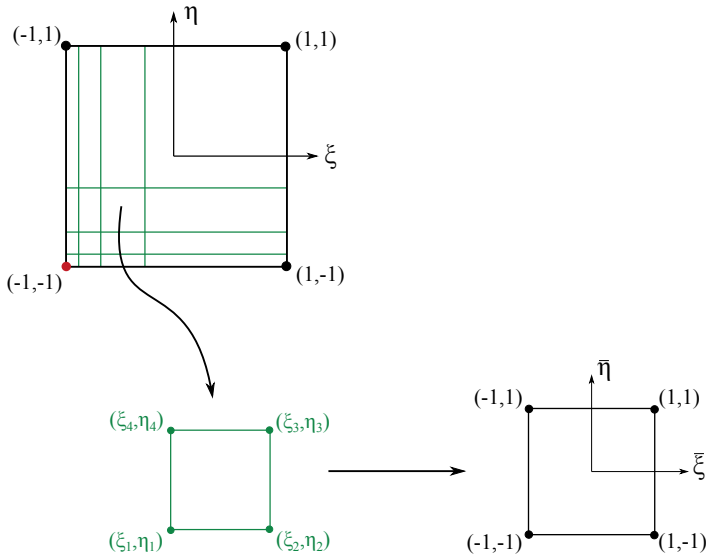

Figure 4.22. Schematic representation of subelement transformation into the coordinate system $(\bar{\xi}, \bar{\eta})$.

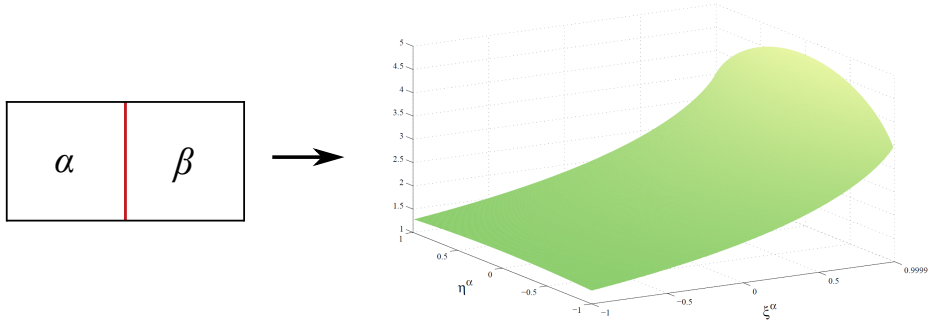

Figure 4.23. Variation of function $\frac{1}{r(\boldsymbol{x}_I, \boldsymbol{\xi}_I)}$ when element α and element β share an edge. Representation over element α.

$$N_{I4}(\bar{\xi}, \bar{\eta}) = \frac{1}{4}(1 - \bar{\xi})(1 + \bar{\eta}) \tag{4.127d}$$

and the Jacobian of this transformation is obtained with the following expression:

$$\bar{J} = \frac{\partial \xi}{\partial \bar{\xi}} \frac{\partial \eta}{\partial \bar{\eta}} - \frac{\partial \xi}{\partial \bar{\eta}} \frac{\partial \eta}{\partial \bar{\xi}} \tag{4.128}$$

Likewise, this technique is used to calculate (4.121) and (4.122) when the elements share an edge. (4.123) and (4.124) functions vary sharply along the all edge, as shown in Figures 4.23 and 4.24.

In order to calculate the integrals, a similar approach was developed, but the subdivision procedure is more complex. This approach consists of dividing element β into

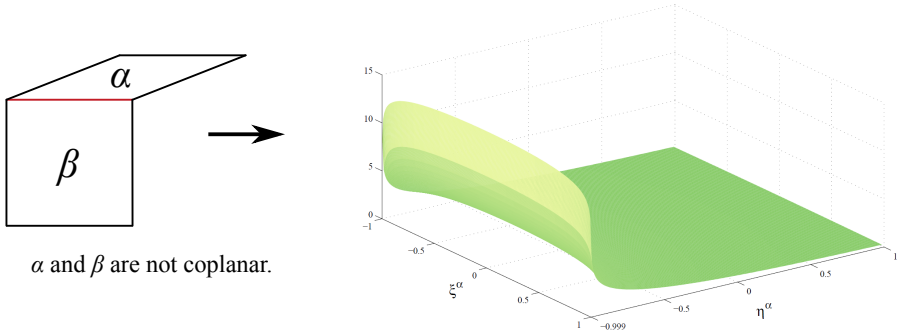

Figure 4.24. Variation of function $\nabla\left(\frac{1}{r(\boldsymbol{\chi}_I,\boldsymbol{\xi}_I)}\right)\cdot\boldsymbol{n}(\boldsymbol{\xi}_I)$ when element α and element β share an edge. Representation over element α.

3×3 fixed intervals and element α into 7×5 not fixed intervals to solve integral (4.121), and element β into 2×2 fixed intervals and elements α into 7×5 not fixed intervals to solve integral (4.122). This division will be done in the local system (ξ,η). The length of each interval will be different and its location will be depends on where the share edge is located and the shape functions.

Finally, the near singular integrals over two-dimensional elements can be calculated with a good accuracy by means of applying the Gauss-Legendre formula with different order of quadrature in each interval. The order of quadrature will be higher in the intervals where the function varies sharply.

The general Gauss-Legendre formula to calculate this kind of integrals with the Element Subdivision Technique is

$$\begin{aligned}
&\iint_{\boldsymbol{\chi}_I\in\Gamma_I^\beta} N_I(\boldsymbol{\chi}_I)\left[\iint_{\boldsymbol{\xi}_I\in\Gamma_I^\alpha} F(\boldsymbol{\chi}_I,\boldsymbol{\xi}_I)\,N_I(\boldsymbol{\xi}_I)\,\mathrm{d}\Gamma_I^\alpha\right]\mathrm{d}\Gamma_I^\beta\\
&\approx\sum_{k=1}^{K^\beta}\sum_{l_1=0}^{n_{l_1}}\sum_{m_1=0}^{n_{m_1}} N_I(\boldsymbol{\chi}_I(\xi(\bar\xi_{l_1},\bar\eta_{m_1}),\eta(\bar\xi_{l_1},\bar\eta_{m_1})))\,\omega_{l_1}\,\omega_{m_1}\,|\bar J_k^\beta|\,|J^\beta|\\
&\sum_{k=1}^{K^\alpha}\sum_{l_2=0}^{n_{l_2}}\sum_{m_2=0}^{n_{m_2}} f(\boldsymbol{\chi}_I(\xi(\bar\xi_{l_1},\bar\eta_{m_1}),\eta(\bar\xi_{l_1},\bar\eta_{m_1})),\boldsymbol{\xi}_I(\xi(\bar\xi_{l_2},\bar\eta_{m_2}),\eta(\bar\xi_{l_2},\bar\eta_{m_2})))\\
&\omega_{l_2}\,\omega_{m_2}\,|\bar J_k^\alpha|\,|J^\alpha|
\end{aligned}\tag{4.129}$$

where for element β: K^β is the number of subdivisions, n_{l_1} is the number of Gauss points in $\bar\xi$ direction, n_{m_1} is the number of Gauss points in $\bar\eta$ direction, ω_{l_1} and ω_{m_1} are the weights, and for element α: K^α is the number of subdivisions, n_{l_2} is the number of Gauss points in $\bar\xi$ direction, n_{m_2} is the number of Gauss points in $\bar\eta$ direction, ω_{l_2} and ω_{m_2} are the weights, and $f(\boldsymbol{\chi}_I(\xi(\bar\xi_{l_1},\bar\eta_{m_1}),\eta(\bar\xi_{l_1},\bar\eta_{m_1})),\boldsymbol{\xi}_I(\xi(\bar\xi_{l_2},\bar\eta_{m_2}),\eta(\bar\xi_{l_2},\bar\eta_{m_2})))$ is

$$\frac{1}{r(\boldsymbol{\chi}_I(\xi(\bar\xi_{l_1},\bar\eta_{m_1}),\eta(\bar\xi_{l_1},\bar\eta_{m_1})),\boldsymbol{\xi}_I(\xi(\bar\xi_{l_2},\bar\eta_{m_2}),\eta(\bar\xi_{l_2},\bar\eta_{m_2})))}\,N_I(\boldsymbol{\xi}_I)$$

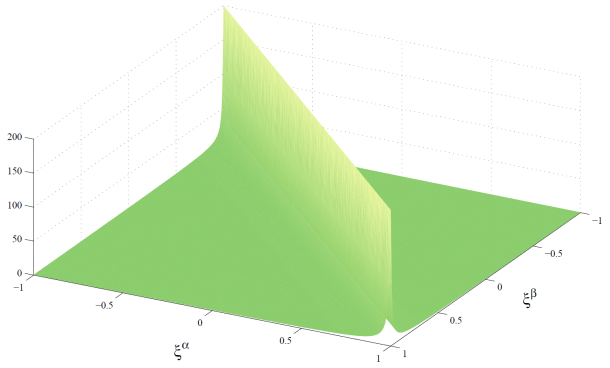

Figure 4.25. Variation of function $\frac{1}{\sqrt{|\widehat{\boldsymbol{\chi}}_G-\widehat{\boldsymbol{\xi}}_G|^2+\frac{\phi^2(\widehat{\boldsymbol{\xi}}_G)}{4}}}$ when $\widehat{\boldsymbol{\chi}}_G$ and $\widehat{\boldsymbol{\xi}}_G$ belong to the same element.

or

$$\left[\nabla\Big(\frac{1}{r(\boldsymbol{\chi}_I(\xi(\bar{\xi}_{l_1},\bar{\eta}_{m_1}),\eta(\bar{\xi}_{l_1},\bar{\eta}_{m_1})),\boldsymbol{\xi}_I(\xi(\bar{\xi}_{l_2},\bar{\eta}_{m_2}),\eta(\bar{\xi}_{l_2},\bar{\eta}_{m_2})))}\Big)\cdot\boldsymbol{n}(\boldsymbol{\xi}_I)\right]N_I(\boldsymbol{\xi}_I)$$

Weakly Singular Integrals

The weakly singular integrals apply to all kernels where α and β elements are the same. In these cases the singularity of the kernel is of order $O(1/r)$. In order to solve these integrals, different approaches are selected to calculate them in one and two-dimensional elements.

Weakly singular integrals over one-dimensional elements

As it was explained in the Point Collocation method, the integrals are not properly weakly singular in one-dimensional elements, since the kernel expressions are formed by the sum of the Euclidean distance between $\widehat{\boldsymbol{\chi}}_G$ and $\widehat{\boldsymbol{\xi}}_G$ and the electrode diameter.

So, when $\widehat{\boldsymbol{\chi}}_G$ and $\widehat{\boldsymbol{\xi}}_G$ belong to the same element, that is element β is the same as element α, the integral

$$\pi\phi(\widehat{\boldsymbol{\xi}}_G)\pi\phi(\widehat{\boldsymbol{\chi}}_G)\int_{\widehat{\boldsymbol{\chi}}_G\in L_G^\beta}N_G(\widehat{\boldsymbol{\chi}}_G)\left[\int_{\widehat{\boldsymbol{\xi}}_G\in L_G^\alpha}\frac{1}{\sqrt{|\widehat{\boldsymbol{\chi}}_G-\widehat{\boldsymbol{\xi}}_G|^2+\frac{\phi^2(\widehat{\boldsymbol{\xi}}_G)}{4}}}N_G(\widehat{\boldsymbol{\xi}}_G)\,\mathrm{d}L_G^\alpha\right]\mathrm{d}L_G^\beta \tag{4.130}$$

is not weakly singular. But the function

$$\frac{1}{\sqrt{|\widehat{\boldsymbol{\chi}}_G-\widehat{\boldsymbol{\xi}}_G|^2+\frac{\phi^2(\widehat{\boldsymbol{\xi}}_G)}{4}}} \tag{4.131}$$

varies sharply when $\widehat{\boldsymbol{\xi}}_G$ are closer or equal to $\widehat{\boldsymbol{\chi}}_G$, as shown in Figure 4.25.

Again, the Element Subdivision Technique is the numerical approach chosen to calculate these integrals with enough accuracy.

The proposed technique consists of dividing into five fixed intervals the integrated element β and into six or seven not fixed intervals the integrated element α. This division will be done in the local system (ξ). The length of each interval will be different and its location will be depending where $\widehat{\boldsymbol{\chi}}_G$ is, as shown in Figure 4.26.

Table 4.1. Length of the intervals in which element β is divided.

	Element β
$\bar{L}_1$	0.3
$\bar{L}_2$	0.3
$\bar{L}_3$	0.8
$\bar{L}_4$	0.3
$\bar{L}_5$	0.3

Table 4.2. Length of the intervals in which element α is divided.

	Case a)	Case b)	Case c)
$\bar{L}_1$	$\frac{5}{6}(\xi^\beta + 1)$	$\xi^\beta + 1 - 0.3$	1.4
$\bar{L}_2$	$\frac{1}{6}(\xi^\beta + 1)$	0.28	0.2
$\bar{L}_3$	$\frac{1}{6}(0.3 - (\xi^\beta + 1))$	0.02	0.1
$\bar{L}_4$	$\frac{5}{6}(0.3 - (\xi^\beta + 1))$	0.02	$\frac{5}{6}(0.3 - (\xi^\beta + 1))$
$\bar{L}_5$	0.1	0.28	$\frac{1}{6}(0.3 - (\xi^\beta + 1))$
$\bar{L}_6$	0.2	$1 - \xi^\beta - 0.3$	$\frac{1}{6}(\xi^\beta + 1)$
$\bar{L}_7$	1.4	-	$\frac{5}{6}(\xi^\beta + 1)$

Finally, integral (4.130) can be calculated with a good accuracy by means of applying the Gauss-Legendre formula with different order of quadrature in each interval, being higher when the function varies sharply.

The general Gauss-Legendre formula to calculate this kind of integrals with the Element Subdivision Technique is (4.120).

Weakly singular integrals over two-dimensional elements

Two types of weakly singular integrals over two-dimensional elements can be differ-

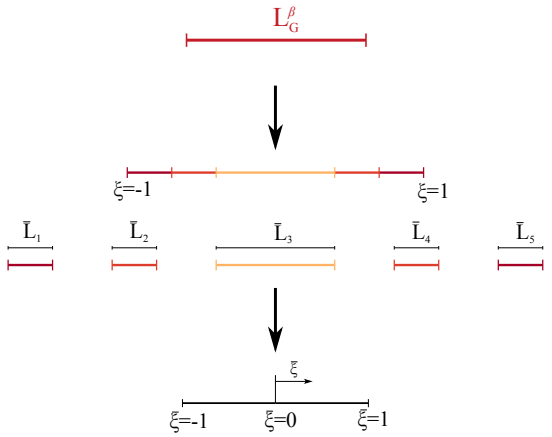

(a) Subdivision of the integrated element β. The length of each interval is indicated on Table 4.1.

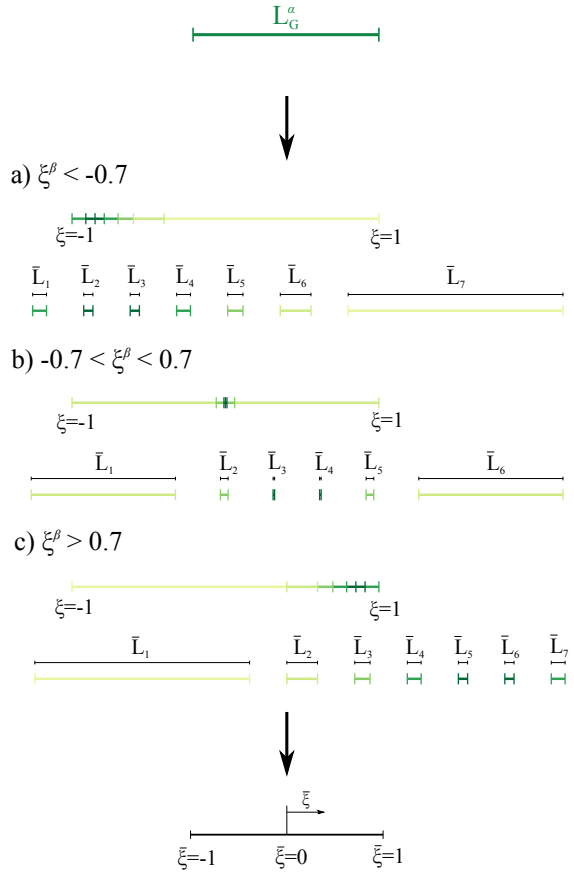

(b) Subdivision of the integrated element α. The length of each interval is indicated on Table 4.2.

Figure 4.26. Element Subdivision Technique for weakly singular integrals over one-dimensional element.

Table 4.3. Number of intervals in which element β is divided.

$N_{Ii}(\boldsymbol{\chi}_I)$	$N_{Ii}(\boldsymbol{\xi}_I)$	Subdivisions	$N_{Ii}(\boldsymbol{\chi}_I)$	$N_{Ii}(\boldsymbol{\xi}_I)$	Subdivisions
1	1	6×6	2	1	7×6
1	2	7×6	2	2	6×6
1	3	6×6	2	3	6×7
1	4	6×7	2	4	6×6

$N_{Ii}(\boldsymbol{\chi}_I)$	$N_{Ii}(\boldsymbol{\xi}_I)$	Subdivisions	$N_{Ii}(\boldsymbol{\chi}_I)$	$N_{Ii}(\boldsymbol{\xi}_I)$	Subdivisions
3	1	6×6	4	1	6×7
3	2	6×7	4	2	6×6
3	3	6×6	4	3	7×6
3	4	7×6	4	4	6×6

entiated:

$$\iint_{\boldsymbol{\chi}_I \in \Gamma_I^\beta} N_I(\boldsymbol{\chi}_I) \left[\iint_{\boldsymbol{\xi}_I \in \Gamma_I^\alpha} \frac{1}{r(\boldsymbol{\chi}_I, \boldsymbol{\xi}_I)} N_I(\boldsymbol{\xi}_I) \, \mathrm{d}\Gamma_I^\alpha \right] \mathrm{d}\Gamma_I^\beta \tag{4.132}$$

$$\iint_{\boldsymbol{\chi}_I \in \Gamma_I^\beta} N_I(\boldsymbol{\chi}_I) \left[\iint_{\boldsymbol{\xi}_I \in \Gamma_I^\alpha} \left[\nabla \left(\frac{1}{r(\boldsymbol{\chi}_I, \boldsymbol{\xi}_I)} \right) \cdot \boldsymbol{n}(\boldsymbol{\xi}_I) \right] N_I(\boldsymbol{\xi}_I) \, \mathrm{d}\Gamma_I^\alpha \right] \mathrm{d}\Gamma_I^\beta \tag{4.133}$$

First, integral (4.132) will be analysed in which the singularity of the kernel is of order $O(1/r)$.

A special treatment is required to calculate these integrals with a good accuracy. The numerical approach developed consists of applying the Element Subdivision Technique and the Lachat-Watson Transformation at the same time.

The idea is to calculate the integral over element β with the Element Subdivision Technique and the integral over element α with the Lachat-Watson Transformation.

That is, element β is divided into the intervals indicated in Table 4.3. This division will be done in the local system (ξ, η), and the length and location of each interval will be different and depends on the shape functions. Some examples of the proposed subdivision are shown in Figure 4.27.

Then, each interval is transformed to a new intrinsic coordinate system $(\bar{\xi}, \bar{\eta})$, as shown in Figure 4.22. The relation between the coordinates systems (ξ, η) and $(\bar{\xi}, \bar{\eta})$ is

$$\xi = \sum_{i=1}^{n_{npI}} N_{Ii}(\bar{\xi}, \bar{\eta}) \, \xi_i \tag{4.134}$$

$$\eta = \sum_{i=1}^{n_{npI}} N_{Ii}(\bar{\xi}, \bar{\eta}) \, \eta_i \tag{4.135}$$

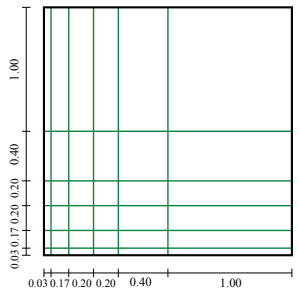

(a) Element subdivision for $N_{I1}(\boldsymbol{\chi}_I)$ and $N_{I1}(\boldsymbol{\xi}_I)$.

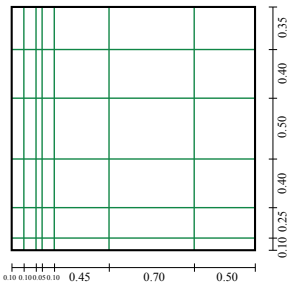

(b) Element subdivision for $N_{I1}(\boldsymbol{\chi}_I)$ and $N_{I2}(\boldsymbol{\xi}_I)$.

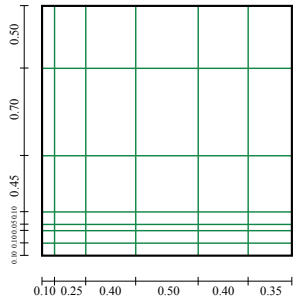

(c) Element subdivision for $N_{I1}(\boldsymbol{\chi}_I)$ and $N_{I4}(\boldsymbol{\xi}_I)$.

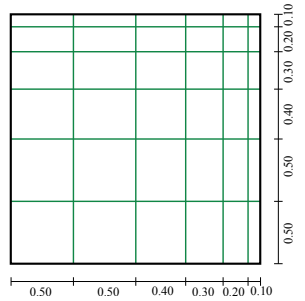

(d) Element subdivision for $N_{I1}(\boldsymbol{\chi}_I)$ and $N_{I3}(\boldsymbol{\xi}_I)$.

Figure 4.27. Some of the proposed subdivisions for element β.

where the shape functions are given by (4.127), and the Jacobian of this transformation is

$$\bar{J} = \frac{\partial \xi}{\partial \bar{\xi}} \frac{\partial \eta}{\partial \bar{\eta}} - \frac{\partial \xi}{\partial \bar{\eta}} \frac{\partial \eta}{\partial \bar{\xi}} \tag{4.136}$$

For each interval the Gauss-Legendre formula will be applied with different order of quadrature. Then, for each Gauss point the Lachat-Watson Transformation will be used to solve the integral over element α, as if each point was a collocation point.

In this case, it will be necessary to modify the Lachat-Watson Transformation in order to increase the accuracy of the results. Thus, instead of splitting up the integrated parent element into four triangular subelements, it will split up into eight [Pérez-Gavilán, 2004].

This transformation is showed in Figure 4.28. It consists of transforming each triangular subelement into a master element. A general transformation formula has been developed for programming this approach:

$$\xi = \bar{N}_1(\bar{\xi}, \bar{\eta})\, v_1^{\xi} + \bar{N}_2(\bar{\xi}, \bar{\eta})\, v_2^{\xi} + \bar{N}_3(\bar{\xi}, \bar{\eta})\, \xi_{\boldsymbol{\chi}_I} \tag{4.137a}$$

$$\eta = \bar{N}_1(\bar{\xi}, \bar{\eta})\, v_1^{\eta} + \bar{N}_2(\bar{\xi}, \bar{\eta})\, v_2^{\eta} + \bar{N}_3(\bar{\xi}, \bar{\eta})\, \eta_{\boldsymbol{\chi}_I} \tag{4.137b}$$

where v_1 and v_2 coefficients are defined in Table 4.4, and the shape functions are given

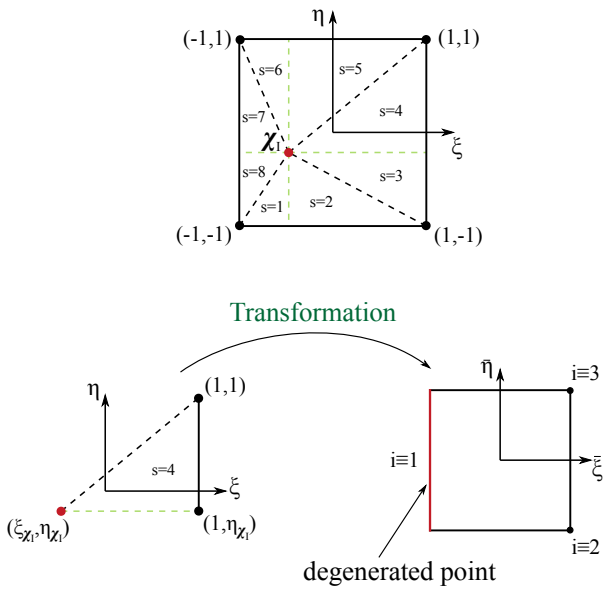

Figure 4.28. Subdivision of a master element into eight triangular subelements and general triangular transformation.

Table 4.4. Coefficients for transformation of triangular subelements.

s	v_1^ξ	v_2^ξ
1	-1	$\xi_{\boldsymbol{\chi}_I}$
2	$\xi_{\boldsymbol{\chi}_I}$	1
3	1	1
4	1	1
5	1	$\xi_{\boldsymbol{\chi}_I}$
6	$\xi_{\boldsymbol{\chi}_I}$	-1
7	-1	-1
8	-1	-1

s	v_1^η	v_2^η
1	-1	-1
2	-1	-1
3	-1	$\eta_{\boldsymbol{\chi}_I}$
4	$\eta_{\boldsymbol{\chi}_I}$	1
5	1	1
6	1	1
7	1	$\eta_{\boldsymbol{\chi}_I}$
8	$\eta_{\boldsymbol{\chi}_I}$	-1

by:

$$\bar{N}_1(\bar{\xi},\bar{\eta}) = \frac{1}{4}(1-\bar{\xi})(1-\bar{\eta}) \tag{4.138a}$$

$$\bar{N}_2(\bar{\xi},\bar{\eta}) = \frac{1}{4}(1+\bar{\xi})(1+\bar{\eta}) \tag{4.138b}$$

$$\bar{N}_3(\bar{\xi},\bar{\eta}) = \frac{1}{2}(1-\bar{\xi}) \tag{4.138c}$$

The Jacobian of this transformation is obtained with the following expression:

$$\bar{J}_s = \frac{\partial \xi}{\partial \bar{\xi}} \frac{\partial \eta}{\partial \bar{\eta}} - \frac{\partial \xi}{\partial \bar{\eta}} \frac{\partial \eta}{\partial \bar{\xi}} \tag{4.139}$$

Finally, integral (4.132) can be calculated with a good accuracy by means of applying the Gauss-Legendre quadrature with the proposed approach. The order of the quadrature will be higher in the intervals where the function varies sharply.

The general Gauss-Legendre formula is

$$\begin{aligned}
&\iint_{\boldsymbol{\chi}_I \in \Gamma_I^\beta} N_I(\boldsymbol{\chi}_I) \left[\iint_{\boldsymbol{\xi}_I \in \Gamma_I^\alpha} F(\boldsymbol{\chi}_I, \boldsymbol{\xi}_I)\, N_I(\boldsymbol{\xi}_I)\, \mathrm{d}\Gamma_I^\alpha \right] \mathrm{d}\Gamma_I^\beta \\
&\approx \sum_{k=1}^{K^\beta} \sum_{l_1=0}^{n_{l_1}} \sum_{m_1=0}^{n_{m_1}} N_I(\boldsymbol{\chi}_I(\xi(\bar{\xi}_{l_1}, \bar{\eta}_{m_1}), \eta(\bar{\xi}_{l_1}, \bar{\eta}_{m_1}))) \, \omega_{l_1}\, \omega_{m_1}\, |\bar{J}_k^\beta|\, |J^\beta| \\
&\sum_{s=1}^{S} \sum_{l_2=0}^{n_{l_2}} \sum_{m_2=0}^{n_{m_2}} f(\boldsymbol{\chi}_I(\xi(\bar{\xi}_{l_1}, \bar{\eta}_{m_1}), \eta(\bar{\xi}_{l_1}, \bar{\eta}_{m_1})), \boldsymbol{\xi}_I(\xi(\bar{\xi}_{l_2}, \bar{\eta}_{m_2}), \eta(\bar{\xi}_{l_2}, \bar{\eta}_{m_2}))) \\
&\omega_{l_2}\, \omega_{m_2}\, |\bar{J}_s|\, |J^\alpha|
\end{aligned} \tag{4.140}$$

where for element β: K^β is the number of subdivisions with the Element Subdivision Technique, n_{l_1} is the number of Gauss points in $\bar{\xi}$ direction, n_{m_1} is the number of Gauss points in $\bar{\eta}$ direction, ω_{l_1} and ω_{m_1} are the weights, and for element α: S is the number of triangular subelements, n_{l_2} is the number of Gauss points in $\bar{\xi}$ direction, n_{m_2} is the number of points in $\bar{\eta}$ direction, ω_{l_2} and ω_{m_2} are the weights, and $f(\boldsymbol{\chi}_I(\xi(\bar{\xi}_{l_1}, \bar{\eta}_{m_1}), \eta(\bar{\xi}_{l_1}, \bar{\eta}_{m_1})), \boldsymbol{\xi}_I(\xi(\bar{\xi}_{l_2}, \bar{\eta}_{m_2}), \eta(\bar{\xi}_{l_2}, \bar{\eta}_{m_2})))$ is

$$\frac{1}{r(\boldsymbol{\chi}_I(\xi(\bar{\xi}_{l_1}, \bar{\eta}_{m_1}), \eta(\bar{\xi}_{l_1}, \bar{\eta}_{m_1})), \boldsymbol{\xi}_I(\xi(\bar{\xi}_{l_2}, \bar{\eta}_{m_2}), \eta(\bar{\xi}_{l_2}, \bar{\eta}_{m_2})))} N_I(\boldsymbol{\xi}_I)$$

The other weakly integral to be analysed is integral (4.133) in which the singularity of the kernel is of order $O(1/r^2)$. In this integral, the kernel is formed by the shape functions N_I and the directional derivative

$$\nabla\Big(\frac{1}{r(\boldsymbol{\chi}_I, \boldsymbol{\xi}_I)}\Big) \cdot \boldsymbol{n}(\boldsymbol{\xi}_I)$$

When $\boldsymbol{\chi}_I$ and $\boldsymbol{\xi}_I$ belong to the same element the gradient functions $\nabla\Big(\frac{1}{r(\boldsymbol{\chi}_I, \boldsymbol{\xi}_I)}\Big)$ and the normal vector $\boldsymbol{n}(\boldsymbol{\xi}_I)$ are perpendicular. As a consequence, the directional derivative is zero and there are not weakly singular integrals in this case.

4.7 Equation to calculate the electric potential in the ground

The boundary integral equation to calculate the electric potential at any point in the ground was obtained in Chapter 3. After introducing the assumption of circumferential

uniformity explained in Subsection 4.2.1, the integral equation is simplified as:

$$\begin{aligned} V(\boldsymbol{x}) \;=\; & \frac{1}{4\pi\gamma}\int_{\widehat{\boldsymbol{\xi}}_G\,\in\,L_G}\Big(\frac{1}{r(\boldsymbol{x},\widehat{\boldsymbol{\xi}}_G)}+\frac{1}{r(\boldsymbol{x}',\widehat{\boldsymbol{\xi}}_G)}\Big)\,\widehat{\sigma}_G(\widehat{\boldsymbol{\xi}}_G)\,\mathrm{d}L_G \\ & + \frac{1}{4\pi\gamma}\iint_{\boldsymbol{\xi}_I\,\in\,\Gamma_I}\Big(\frac{1}{r(\boldsymbol{x},\boldsymbol{\xi}_I)}+\frac{1}{r(\boldsymbol{x}',\boldsymbol{\xi}_I)}\Big)\,\sigma_I(\boldsymbol{\xi}_I)\,\mathrm{d}\Gamma_I \\ & + \frac{1}{4\pi}\iint_{\boldsymbol{\xi}_I\,\in\,\Gamma_I}\Big[\Big(\nabla\Big(\frac{1}{r(\boldsymbol{x},\boldsymbol{\xi}_I)}\Big)+\nabla\Big(\frac{1}{r(\boldsymbol{x}',\boldsymbol{\xi}_I)}\Big)\Big)\cdot\boldsymbol{n}(\boldsymbol{\xi}_I)\Big]\,V_I(\boldsymbol{\xi}_I)\,\mathrm{d}\Gamma_I \end{aligned} \tag{4.141}$$

where $V(\boldsymbol{x})$ is the value of the potential function at any point $\boldsymbol{x}$ located in the ground.

$V(\boldsymbol{x})$ can be calculated solving equation (4.141) with the BEM and discretising the boundary integral equation as it was indicated in Section 4.4. Thus, the value of the potential function at any point can be approximated as

$$\begin{aligned} V(\boldsymbol{x}) \;\approx\; & \frac{1}{4\pi\gamma}\sum_{\alpha=1}^{n_{el_G}}\int_{\widehat{\boldsymbol{\xi}}_G\,\in\,L_G^\alpha}\Big(\frac{1}{r(\boldsymbol{x},\widehat{\boldsymbol{\xi}}_G)}+\frac{1}{r(\boldsymbol{x}',\widehat{\boldsymbol{\xi}}_G)}\Big)\,\sum_{i=1}^{n_{np_G}}\widehat{\sigma}_{Gi}N_{Gi}(\widehat{\boldsymbol{\xi}}_G)\,\mathrm{d}L_G^\alpha \\ & + \frac{1}{4\pi\gamma}\sum_{\alpha=1}^{n_{el_I}}\iint_{\boldsymbol{\xi}_I\,\in\,\Gamma_I^\alpha}\Big(\frac{1}{r(\boldsymbol{x},\boldsymbol{\xi}_I)}+\frac{1}{r(\boldsymbol{x}',\boldsymbol{\xi}_I)}\Big)\,\sum_{i=1}^{n_{np_I}}\sigma_{Ii}N_{Ii}(\boldsymbol{\xi}_I)\,\mathrm{d}\Gamma_I^\alpha \\ & + \frac{1}{4\pi}\sum_{\alpha=1}^{n_{el_I}}\iint_{\boldsymbol{\xi}_I\,\in\,\Gamma_I^\alpha}\Big[\Big(\nabla\Big(\frac{1}{r(\boldsymbol{x},\boldsymbol{\xi}_I)}\Big)+\nabla\Big(\frac{1}{r(\boldsymbol{x}',\boldsymbol{\xi}_I)}\Big)\Big)\cdot\boldsymbol{n}(\boldsymbol{\xi}_I)\Big]\,\sum_{i=1}^{n_{np_I}}V_{Ii}N_{Ii}(\boldsymbol{\xi}_I)\,\mathrm{d}\Gamma_I^\alpha \end{aligned} \tag{4.142}$$

This equation can be written in discretised form as:

$$V(\boldsymbol{x}) \approx \sum_{\alpha=1}^{n_{el_G}}\sum_{i=1}^{n_{np_G}} R_{xGi}^\alpha\,\widehat{\sigma}_{Gi}^\alpha + \sum_{\alpha=1}^{n_{el_I}}\sum_{i=1}^{n_{np_I}} R_{xIi}^\alpha\,\sigma_{Ii}^\alpha + \sum_{\alpha=1}^{n_{el_I}}\sum_{i=1}^{n_{np_I}} S_{xIi}^\alpha\,V_{Ii}^\alpha \tag{4.143}$$

where

$$R_{xGi}^\alpha = \frac{1}{4\pi\gamma}\int_{\widehat{\boldsymbol{\xi}}_G\,\in\,L_G^\alpha}\Big(\frac{1}{r(\boldsymbol{x},\widehat{\boldsymbol{\xi}}_G)}+\frac{1}{r(\boldsymbol{x}',\widehat{\boldsymbol{\xi}}_G)}\Big)\,N_{Gi}(\widehat{\boldsymbol{\xi}}_G)\,\mathrm{d}L_G^\alpha \tag{4.144}$$

$$R_{xIi}^\alpha = \frac{1}{4\pi\gamma}\iint_{\boldsymbol{\xi}_I\,\in\,\Gamma_I^\alpha}\Big(\frac{1}{r(\boldsymbol{x},\boldsymbol{\xi}_I)}+\frac{1}{r(\boldsymbol{x}',\boldsymbol{\xi}_I)}\Big)\,N_{Ii}(\boldsymbol{\xi}_I)\,\mathrm{d}\Gamma_I^\alpha \tag{4.145}$$

$$S_{xIi}^\alpha = \frac{1}{4\pi}\iint_{\boldsymbol{\xi}_I\,\in\,\Gamma_I^\alpha}\Big[\Big(\nabla\Big(\frac{1}{r(\boldsymbol{x},\boldsymbol{\xi}_I)}\Big)+\nabla\Big(\frac{1}{r(\boldsymbol{x}',\boldsymbol{\xi}_I)}\Big)\Big)\cdot\boldsymbol{n}(\boldsymbol{\xi}_I)\Big]\,N_{Ii}(\boldsymbol{\xi}_I)\,\mathrm{d}\Gamma_I^\alpha \tag{4.146}$$

and, $\widehat{\sigma}_{Gi}^\alpha$, σ_{Ii}^α and V_{Ii}^α are the values of the unknown functions which have been calculated after solving the system of equations formulated with Point Collocation method or Bubnov-Galerkin method.

In this case, integrals (4.144), (4.145) and (4.146) are regular integrals and they can be evaluated with a good accuracy applying the Gauss-Legendre formula.

4.8 Conclusions

In this chapter two numerical approaches to solve the system of equations proposed in Chapter 3 have been presented.

First, the boundary integral equations have been reformulated into a weak form so accurate approximate solutions can be calculated. In addition, in order to simplify the integral equations, an assumption of circumferential uniformity in the electrodes has been done. This assumption consists of supposing that the leakage current is constant around the perimeter of every cross section on the electrodes.

Then, the Weighted Residual Method is introduced as the approximate solution method to solve the weak forms formulated, as well as the Boundary Element Method is chosen as the technique that better fits to solve the boundary integral equations.

As a result, two numerical approaches have been completely developed to solve the boundary integral equations: the Point Collocation Method and the Bubnov-Galerkin Method.

Finally, the results obtained from the Point Collocation Method or the Bubnov-Galerkin Method will be used to calculate the value of the potential function at any point in the ground. For the analysis of this problem, it will be interesting to calculate the potential distribution on the surface of the earth by means of the formulation presented.

So, after the implementation of these methods, a protection system formed by grounding grids in the underground electrical substations can be characterized.

In Chapter 5, the results obtained from the application of these methods will be showed. Moreover, these approaches will be compared and they will be validated with the method developed by [Colominas, 1995] for the case of supposing that the ground and the underground electrical substations conductivities are equal.

Chapter 5

Practical Applications

5.1 Introduction

On the previous chapters, the physical, mathematical and numerical approaches proposed in order to analyse grounding systems have been presented. The principal objective of these approaches is to calculate the main parameters that define the protection system of underground electrical substations. To this end, firstly the numerical methods will be validated, and then, grounding system analysis for real underground transformer substations will be done.

In order to validate the proposed methods several test cases and benchmarks will be analysed. These cases will be formed by different grid configurations and various domain models will be analysed. That is, in some analyses the resistivity for the ground and the prefabricated enclosure will be supposed equal, which is a homogenous domain, and in others the resistivity will not be equal, which is a heterogeneous domain. Then, the outcomes obtained will be validated with commercial programs based on different numerical procedures, as well as with the empirical formulas proposed by the standards.

After the validation, an analysis about the differences between the weighted residual methods used in the developed approaches will be done. This analysis will explain why the outcomes obtained with the Point Collocation Method and the Bubnov-Galerkin Method present divergences between them.

Finally, the industrial applications derived from the proposed approaches will be presented. The principal application is the grounding system analysis for underground electrical substations, since the formulation developed allows to design and analyse the grid configurations and to ensure that the grounding system does not exceed the safe voltage limits. As a consequence of these analyses, the voltage and current density distributions over the buried enclosure are obtained. Obtaining of these parameters bring about another application of this formulation due to these distributions may be help to improve the design and properties of the prefabricated concrete enclosures.

5.2 Validation of the proposed numerical models

In this section, the validation of the numerical models proposed in Chapter 4 to design and analyse substation grounding systems is presented. For this validation purpose, first, the numerical models will be compared with the TOTBEM, and then, they will be checked against with the IEEE and Spanish standards and several substation grounding programs.

5.2.1 Validation with TOTBEM

The TOTBEM is a computer tool to design and analyse substation grounding grids which is based on the formulation developed in [Colominas, 1995] for uniform soil model and in [Aneiros Blanco, 1996] for two-layer soil model. This numerical formulation consists of an approximated 1D Boundary Element Method approach with Galerkin type weighting functions. The TOTBEM computes the main parameters of protection systems from the Ground Potential Rise (GPR). These parameters are the substation grid resistance, and the surface, step and mesh voltages at any location inside or outside the grid.

In order to validate the proposed numerical models with the TOTBEM and compare the results obtained, a few analyses with the uniform soil assumption will be done. That is, it will be supposed that the prefabricated enclosure conductivity (γ_I) is equal to the soil conductivity (γ). Therefore, as it was stated in Chapter 3, the equation to calculate the electric potential at any point in the ground is reduced to equation (3.108) which refers to a homogeneous domain. In fact, this equation is equal to the expression obtained in [Colominas, 1995] and implemented in the TOTBEM to calculate the value of potential at any point in a uniform soil.

Consequently, two test cases with basic grid configurations will be calculated with the TOTBEM and with the proposed formulation based on the Point Collocation Method and the Bubnov-Galerkin Method. In these cases, the main parameters obtained with each approach will be used to validate the proposed formulation. These main parameters are the grid resistance and the step and mesh voltages, which can be defined as: the grid resistance is the quotient between the GPR and the maximum grid current; the step voltage is the difference between the surface voltage 1 m apart, with one point over the corner of the grid and the other on a diagonal and 1 m beyond the first point; and, the mesh voltage is the difference between the GPR and the smallest surface voltage on the grid.

Test case 1

The first test case consists of a grounding system formed by a square 8 m $\times$ 8 m grid without ground rods. This case was analysed in [Colominas, 1995] with the purpose of validating the TOTBEM formulation. The main characteristics of this analysis are shown in Table 5.1.

Table 5.1. Design data for Test case 1.

GENERAL DATA	
Ground Potential Rise (GPR)	1 V
Soil resistivity	100 Ω m
Grid burial depth	0.5 m
Conductor diameter	0.014 m
Total surface analysed	16 m × 16 m

For the analysis done with the TOTBEM, the numerical model is based on a Galerkin formulation with linear elements. In this analysis, the grounding grid is not discretised, as shown in Table 5.2.

Table 5.2. Parameters of numerical model for TOTBEM analysis - Test case 1.

NUMERICAL MODEL	
Numerical approach	BEM-Galerkin
BEM elements	Linear
Number of elements	4
Degrees of freedom	4

And for the analysis performed with the proposed approaches, their main characteristics are summarised in Table 5.3. As well as in the TOTBEM model, the grid is not discretised and linear elements are used. In this model, it is define an enclosure with dimensions 4 m × 4 m × 4 m, buried 0.4 m and located in the middle of the grid, which represents the underground substation. As it was stated, the enclosure resistivity will be equal to soil resistivity (100 Ω m) so as to simulate a uniform soil.

Table 5.3. Parameters of numerical model for Point Collocation Method and Bubnov-Galerkin Method analysis - Test case 1.

NUMERICAL MODEL		
Numerical approach	Point Collocation Method	Bubnov-Galerkin Method
BEM elements	Linear ($\lambda = 0.85$)	Linear
No. of elements (electrodes)	4	4
Degrees of freedom (electrodes)	4	4
No. of elements (enclosure)	600	600
Degrees of freedom (enclosure)	726	726

Finally, the main parameters obtained for this grid analysis with the TOTBEM, the Point Collocation Method and the Bubnov-Galerkin Method are given in Table 5.4.

Table 5.4. Comparison of results for grounding system analysis - Test case 1.

	Grid resistance (Ω)	Mesh voltage (V)	Step voltage (V)
TOTBEM	6.42	0.457	0.200
PCM	6.10	0.428	0.211
BGM	6.42	0.457	0.200

As it is shown, the results obtained with the TOTBEM and Bubnov-Galerkin Method are equal as it was expected since the numerical approach is the same after doing the uniform soil assumption. However, the results obtained with the Point Collocation Method differ 5% to 6% from the other approaches. The reason of this divergence will be explained in Section 5.3.

In addition to the previous values, the surface and step voltage distributions are shown in Figures 5.1 and 5.2, respectively. In these figures, it can be seen that the same distributions are obtained and only the values from the Point Collocation Method differ slightly.

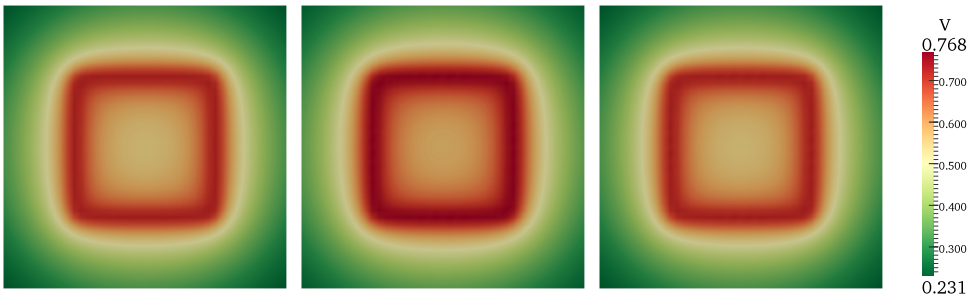

(a) TOTBEM. **(b) PCM.** **(c) BGM.**

Figure 5.1. Surface voltage distribution - Test case 1.

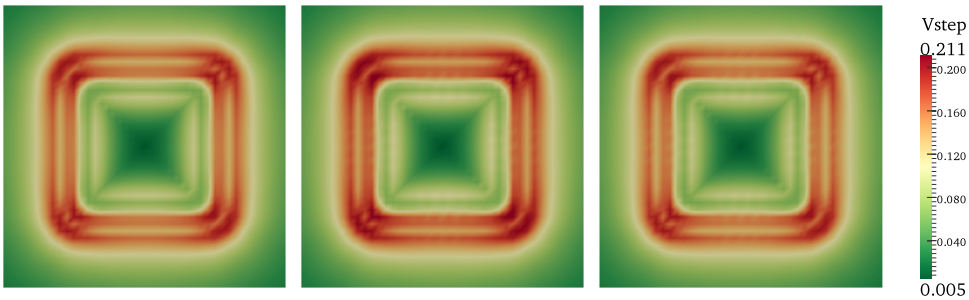

(a) TOTBEM. **(b) PCM.** **(c) BGM.**

Figure 5.2. Step voltage distribution - Test case 1.

Test case 2

In this second test case, the grounding system is formed by a rectangular 6 m × 4 m grid with 4 ground rods, one on each corner of the grid, as shown in Figure 5.3. The main characteristics of this analysis are summarised in Table 5.5.

Figure 5.3. Schematic representation of grid configuration for Test case 2.

Table 5.5. Design data for Test case 2.

GENERAL DATA	
Ground Potential Rise (GPR)	10 V
Soil resistivity	500 Ω m
Grid burial depth	0.5 m
Conductor diameter	0.008 m
Ground rod diameter	0.014 m
Total surface analysed	12 m × 12 m

Similarly as in test case 1, for the analysis with the TOTBEM the grounding grid will not be discretised and the elements used will be linear (Table 5.6).

Table 5.6. Parameters of numerical model for TOTBEM analysis - Test case 2.

NUMERICAL MODEL	
Numerical approach	BEM-Galerkin
BEM elements	Linear
Number of elements	8
Degrees of freedom	8

And for the analysis performed with the Point Collocation Method and the Bubnov-Galerkin Method the number of grounding grid elements will be equal to the TOTBEM model, and linear elements will be used too. Again, an enclosure with dimensions 4 m × 3 m × 2.4 m, buried 0.4 m, located in the middle of the grid and with a resistivity equal to soil resistivity (500 Ω m) is defined.

After doing these analyses, the values calculated for the grid resistance, and for the step and mesh voltages are given in Table 5.8.

Table 5.7. Parameters of numerical model for Point Collocation Method and Bubnov-Galerkin Method analysis - Test case 2.

NUMERICAL MODEL		
Numerical approach	Point Collocation Method	Bubnov-Galerkin Method
BEM elements	Linear ($\lambda = 0.85$)	Linear
No. of elements (electrodes)	8	8
Degrees of freedom (electrodes)	8	8
No. of elements (enclosure)	600	600
Degrees of freedom (enclosure)	726	726

Table 5.8. Comparison of results for grounding system analysis - Test case 2.

	Grid resistance (Ω)	Mesh voltage (V)	Step voltage (V)
TOTBEM	40.20	3.775	2.061
PCM	41.73	4.456	1.567
BGM	40.20	3.775	2.061

As in test case 1, the values of these main parameters coincide between the TOTBEM and Bubnov-Galerkin Method and the results obtained with the Point Collocation Method differ. As it can be seen, in this test case the results differ more, 18% for mesh voltage and 24% for step voltage, due to the ground rods. This divergence will be explained in detail in Section 5.3.

Likewise, the surface and step voltage distributions are equal for the three approaches, but the values obtained with the Point Collocation Method are smaller, as shown in Figures 5.4 and 5.5.

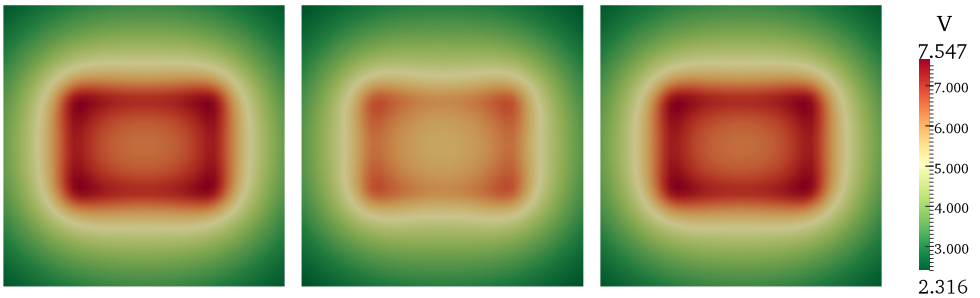

(a) TOTBEM. **(b) PCM.** **(c) BGM.**

Figure 5.4. Surface voltage distribution - Test case 2.

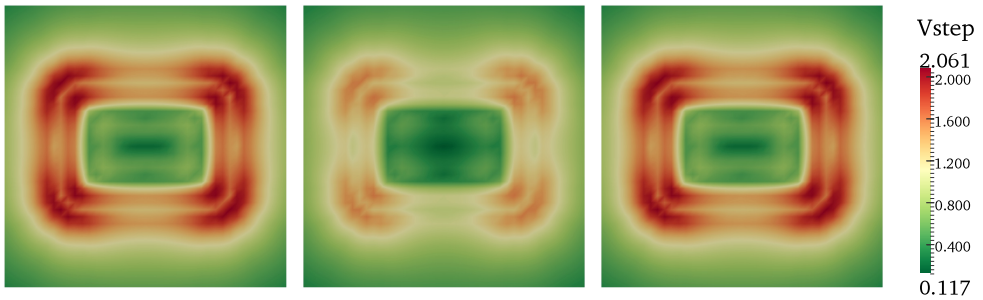

(a) TOTBEM. (b) PCM. (c) BGM.

Figure 5.5. Step voltage distribution - Test case 2.

Conclusions

As noted above, the results obtained in the previous analyses show an excellent agreement with the TOTBEM outcomes for uniform soil assumption, especially the values obtained with the Bubnov-Galerkin Method. Thus, it is demonstrated the equivalence between the equation to calculate the electric potential in the ground (equation (3.107)) with the equation obtained in [Colominas, 1995] for substation grounding analysis with uniform soil model.

5.2.2 Validation with standards and commercial software

In this validation procedure, the next step is to prove the proposed numerical models with the standards and some commercial software. For this purpose, the IEEE Guide for Safety in AC Substation Grounding [IEEE Std 80, 2013] and the Spanish standard: *"Reglamento sobre condiciones técnicas y garantías de seguridad en intalaciones eléctricas de alta tensión"* [RD 337/2014, 2014] have been chosen.

This procedure will consist on validate the formulation carried out in this thesis, first, with the benchmarks proposed in [IEEE Std 80, 2013] for uniform soil model, and, second, with the programme amiKIT, which is based on [RD 337/2014, 2014], for the analysis of a commercial underground electrical substation. It should be noted that the technique that follows these standards to calculate the main parameters of grounding systems differs from the model developed in this thesis. That is, the standards use as a general datum the grid current instead of the Ground Potential Rise. Thus, the cases analysed with the formulation carried out will be calculated with a GPR equal 1 V in order to obtain the grid resistance, and then, the results will be scaled by means of the GPR of the substation which will be obtained as the product between the grid resistance obtained and the datum of grid current.

IEEE Std 80-2013

The IEEE Guide for Safety in AC Substation Grounding is a standard with the objective of providing a guidance to design properly substations grounding systems. Its

specific purposes are to establish safety limits of potential differences under fault conditions in AC substations, develop safety criteria and practical aspects to design grounding systems, and develop procedures and evaluation techniques for the grounding grid assessments. Additionally, it provides benchmark cases to compare the results of the proposed equations to software programs.

As it is well known, an essential aspect to design grounding systems is the soil model. In [IEEE Std 80, 2013], the most commonly used soil models (uniform and multilayer soil) are explained and the equations used to represent these soil conditions are presented. However, this guide does not consider complex soil conditions as the case dicussed in this thesis in which a finite volume with different resistivity appears in a uniform soil. Thus, in order to validate the proposed formulations with the [IEEE Std 80, 2013] formulas, only grid designs with uniform soil assumption can be done.

In this case, so as to compare the proposed models, the benchmarks provide by this standard will be used. These benchmarks are performed using the [IEEE Std 80, 2013] formulas, and some of the most representative commercial computer programs: CDGES, ETAP and WinIGS. The main parameters provide by the [IEEE Std 80, 2013] to check against the results of each formulation/approach are the grid resistance, the GPR, and the step and touch voltages at different points.

Benchmark 1

The ground grid for this comparison is formed by a square 70 m × 70 m grid with equally space conductors, grid burial depth 0.5 m, and no ground rods (Figure 5.6). The design data of this grounding system are given in Table 5.9.

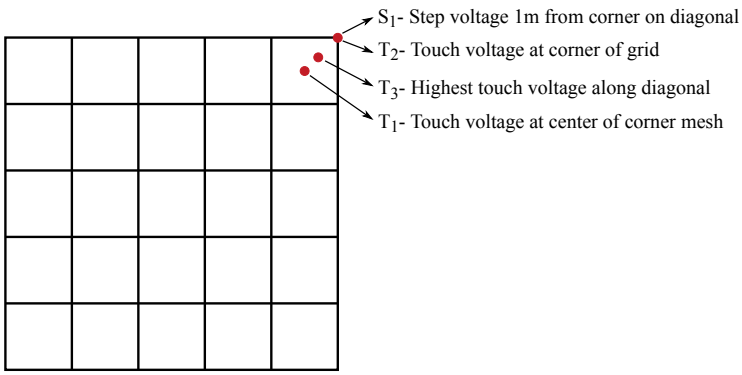

Figure 5.6. Schematic representation of grounding system for Benchmark 1. (Reproduced from [IEEE Std 80, 2013])

In order to analyse this grid configuration with the proposed models, the same grid and an enclosure with dimensions 5 m × 3 m × 2 m, buried 0.6 m and a resistivity equal to soil resistivity (140 Ω m) are considered. The enclosure location does not change the results obtained since uniform soil model is considered, so it will not be represented.

Table 5.9. Design data for Benchmark 1.

GENERAL DATA	
Grid current	744.8 A
Soil resistivity	140 Ω m
Grid burial depth	0.5 m
Conductor spacing	14 m
Conductor diameter (2/0 AWG)	9.265 mm

For this analysis two numerical models have been calculated with the Point Collocation Method, the first, called as Model 1, in which the grid is not discretised, and the second, called Model 2, in which every grid conductor has been discretised into 5 elements. However, for the analysis with the Bubnov-Galerkin Method the grid is not discretised, as in Model 1. These characteristics are summarised in Table 5.10.

Table 5.10. Parameters of numerical model for Point Collocation Method and Bubnov-Galerkin Method analysis - Benchmark 1.

NUMERICAL MODEL			
Numerical approach	Point Collocation Method		Bubnov-Galerkin Method
BEM elements	Linear ($\lambda = 0.85$)		Linear
	Model 1	Model 2	
No. of elements (electrodes)	60	300	60
Degrees of freedom (electrodes)	36	276	36
No. of elements (enclosure)	600	600	600
Degrees of freedom (enclosure)	726	726	726

As it was stated previously, the main parameters that will be compared are the grid resistance, the GPR and the step and touch voltages. In this case, the step and touch voltages will be determined at the specific points showed in Figure 5.6. Thus, the touch voltage will be calculated at T_1, T_2 and T_3; where T_1 is located at the centre of the corner mesh, T_2 is located at the extreme corner of the grid, and T_3 is located on the diagonal near the centre of the corner mesh. And the step voltage will be calculated at S_1, which has the same position as T_2.

As a result, the comparison between the main parameters obtained with the proposed models and the values provided by the [IEEE Std 80, 2013] is shown in Table 5.11.

It can be observed that the values obtained with the Point Collocation Method (Model 2) and the Bubnov-Galerkin Method show an excellent agreement with the grid resistance, the GPR and the touch voltages provided by the [IEEE Std 80, 2013] formulas and commercial software, and the step value differs slightly from the com-

Table 5.11. Comparison of results for grounding system analysis - Benchmark 1.

	R_{Grid} (Ω)	GPR(V)	Touch voltages (V)			Step Voltages (V)
			T_1	T_2	T_3	S_1
Std 80	1.05	780.0	232.0	-	-	96.0
CDEGS	1.00	743.9	194.9	147.4	202.7	89.3
ETAP	1.01	751.7	200.9	164.2	209.0	87.2
WinIGS	1.00	744.9	196.3	151.2	203.4	88.7
PCM (Model 1)	1.11	825.1	270.8	177.4	272.9	112.7
PCM (Model 2)	1.01	752.4	202.7	148.7	209.9	95.5
BGM	1.01	748.9	198.3	141.6	204.7	96.2

mercial software. Only the parameters obtained with Model 1 differ so much from the other approaches. The reason of this divergence will be explained in Section 5.3.

Benchmark 2

The grounding system for this second case is the same as for Benchmark 1, with the addition of twenty ground rods located at each intersection around the perimeter of the grid, as shown in Figure 5.7. The main characteristics of this grounding system are given in Table 5.12.

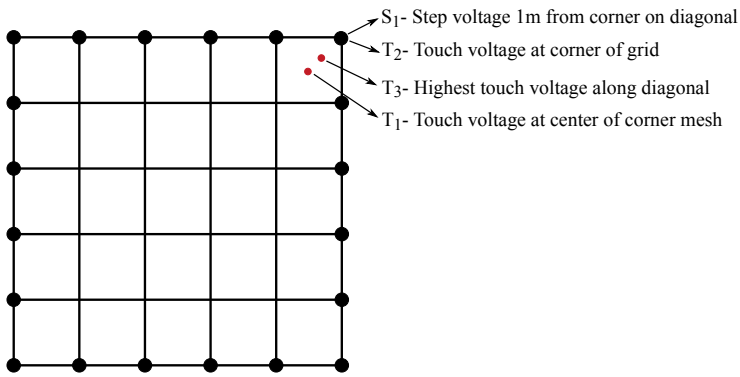

Figure 5.7. Schematic representation of grounding system for Benchmark 2. (Reproduced from [IEEE Std 80, 2013])

Similarly to Benchmark 1, in order to analyse this grid with the numerical models developed, an enclosure with dimensions 9 m × 5 m × 2.4 m, buried 0.8 m and a resistivity equal to soil resistivity (140 Ω m) is considered. As in Benchmark 1, the enclosure location will not be depicted since it does not alter the outcomes. It is worth saying that the ground rods do not pierce the enclosure since it is located inside the square defined by the grid.

In this case, two different numerical models have been calculated with the Point Collocation Method and the Bubnov-Galerkin Method, which are called as Model 1

Table 5.12. Design data for Benchmark 2.

GENERAL DATA	
Grid current	744.8 A
Soil resistivity	140 Ω m
Grid burial depth	0.5 m
Conductor spacing	14 m
Conductor diameter (2/0 AWG)	9.265 mm
Ground rod diameter (5/8 in)	15.8 mm
Ground rod length	7.5 m

and Model 2. For both Model 1, the conductors and ground rods are not discretised; however, in Model 2, every electrode is discretised into 5 elements. The characteristics of these numerical models are summarised in Table 5.13.

Table 5.13. Parameters of numerical model for Point Collocation Method and Bubnov-Galerkin Method analysis - Benchmark 2.

NUMERICAL MODEL				
Numerical approach	Point Collocation Method		Bubnov-Galerkin Method	
BEM elements	Linear ($\lambda = 0.85$)		Linear	
	Model 1	Model 2	Model 1	Model 2
No. of elements (electrodes)	80	400	80	400
Degrees of freedom (electrodes)	56	376	56	376
No. of elements (enclosure)	600	600	600	600
Degrees of freedom (enclosure)	726	726	726	726

Again, the grid resistance, the GPR and the step and touch voltages will be compared between the values obtained by the proposed numerical models and the values provided by the [IEEE Std 80, 2013]. Notice that the step and touch voltages are calculated at the specific points showed in Figure 5.7, which have the same location as the points described in Benchmark 1. These comparisons are shown in Table 5.14.

It can be clearly seen in Table 5.14 that the results of PCM (Model 2) and BGM (Model 2) present a good agreement with the values calculated with the commercial software, especially BGM (Model 2) with the WinIGS. On the contrary, both Model 1 differ enough from the computer programs, due to every conductor and ground rod has a length of 7 m and 7.5 m, respectively, and the analysis without a discretisation does not give sufficient precision.

The reason that PCM (Model 2) does not have the same precision as BGM (Model 2) will be explained in Section 5.3.

Table 5.14. Comparison of results for grounding system analysis - Benchmark 1.

	R_{Grid} (Ω)	GPR(V)	Touch voltages (V)			Step Voltages (V)
			T_1	T_2	T_3	S_1
Std 80	1.022	761.0	163.0	-	-	80.0
CDEGS	0.917	682.8	145.4	85.8	149.6	70.7
ETAP	0.920	687.9	150.2	77.2	154.0	79.3
WinIGS	0.919	684.8	146.9	91.0	151.3	71.5
PCM (Model 1)	0.978	728.6	205.5	143.3	209.3	58.7
PCM (Model 2)	0.917	683.0	147.2	105.8	151.2	60.9
BGM (Model 1)	0.925	688.7	152.5	71.0	157.1	80.7
BGM (Model 2)	0.919	684.5	147.3	89.4	151.4	71.6

RD 337/2014

The RD 337/2014 is a Spanish standard with the purpose to establish the technical conditions and the security guarantees of electrical installations. Among its principal objectives is to ensure the safety conditions for people and the proper functioning of electrical equipment. This standard is composed of a series of *"Normas de obligado cumplimiento"*, called as ITCs (*"Instrucciones Técnicas Complementarias"*), in which are determined the UNE and international standards with mandatory compliance. In this thesis, the interesting ITC will be the ITC-RAT13 *Instalaciones de puesta a tierra* [RD 337/2014, 2014].

The ITC-RAT13 determines the general safety measures to design the grounding systems, as well as the principal procedures to analyse them. Thus, this guide establishes the formulas to calculate the safe step and touch voltage limits.

In order to validate the proposed approaches with this ITC, a commercial programme based on the [RD 337/2014, 2014] will be used. The selected programme is amiKIT, software developed by Ormazabal company, which designs, calculates and assesses transformer substations. Thus, to do this comparison, first the grounding grid of an underground transformer substation will be designed and calculated with amiKIT, and then, the resulting configuration will be analysed with the proposed methods. Finally, the results will be checked against.

For this analysis a commercial underground transformer substation has been chosen. This is the PFS-62 by Ormazabal with vertical ventilation and its main characteristics are set out in [General Instructions for PFS-62, 2008]. The design data introduced into amiKIT to calculate the grounding system are given in Table 5.15.

So as to calculate the safe step voltage limit, amiKIT establishes a fault duration $t = 0.2\,s$ for this analysis. Therefore, using the formula defined in [RD 337/2014, 2014] to calculate this value, the following safe step voltage limit is obtained:

$$V_{step,max} = 31152\,V$$

It should be noted that the formula to calculate this voltage limit is based on the

Table 5.15. Design data for the analysis with [RD 337/2014, 2014].

GENERAL DATA	
Operating voltage	20 kV
Grid current	1000 A
Soil resistivity	150 Ω m
Concrete resistivity	3000 Ω m

soil resistivity and the touch voltage that a body can be subjected, which depends on the fault duration.

In addition, for the purpose of avoiding the appearance of touch voltages that can be dangerous for any person who is around or inside the substation, the amiKIT report suggests these secure measures:

- Exterior metal doors and covers will not have electrical contact with conductive materials that may be subject to voltage due to defects or breakdowns.
- On the floor inside the transformer substation, a mesh covered by a layer of concrete of 10 cm and connected to the grounding system will be installed.
- And, if the ground rods are installed in a row, they will be arranged in line with the front of the substation.

In this case, amiKIT assumes as a grounding grid the configuration 70-40/8/82 from the Anexo 2 of [UNESA, 1989]. Before continuing with the grid description, it is appropriate to introduce briefly what is [UNESA, 1989]. [UNESA, 1989] is a Spanish guide in which is presented a method to design and calculate grounding systems based on standard configurations. This guide allows to apply the [RD 337/2014, 2014] in a simplify manner with the purpose of providing a useful grounding design tool for project engineers.

Following with the analysis, the grounding system 70-40/8/82 is formed by a rectangular 7 m × 4 m grid with eight ground rods around the perimeter of the grid, as shown in Figure 5.8, and the underground transformer substation is located in the middle of it. The main grid characteristics are given in Table 5.16.

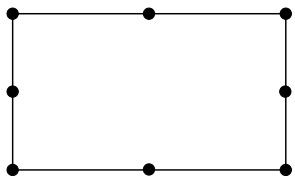

Figure 5.8. Schematic representation of grounding grid 70-40/8/82.

Table 5.16. Parameters for grid configuration 70-40/8/82

GROUNDING GRID DATA	
Grid burial depth	0.8 m
Conductor diameter	8 mm
Ground rod diameter	14 mm
Ground rod length	2 m

In this comparison, the main parameters that will be checked against are the grid resistance, the GPR and the maximum step voltage. The values obtained after doing the analysis with the amiKIT are shown in Table 5.18. Notice that these results are calculated with the formulas proposed in UNESA [1989] which considered a uniform soil model, model that does not reflect the real soil structure.

The same grounding grid is analysed with the proposed numerical models. In these models, an enclosure with dimensions 6.56 m × 2.46 m × 2.84 m, buried 0.1 m and resistivity equal to 3000 Ω m is considered, and every conductor and ground rod will be discretised into 3 and 2 elements, respectively. The characteristics for each numerical model are summarized in Table 5.17.

Table 5.17. Parameters of numerical model to analyse the grid 70-40/8/82 with Point Collocation Method and Bubnov-Galerkin Method.

NUMERICAL MODEL		
Numerical approach	Point Collocation Method	Bubnov-Galerkin Method
BEM elements	Linear ($\lambda = 0.85$)	Linear
No. of elements (electrodes)	36	36
Degrees of freedom (electrodes)	36	36
No. of elements (enclosure)	600	600
Degrees of freedom (enclosure)	726	726

As a result, the grid resistance, the GPR and the maximum step voltage are obtained with the proposed models (Table 5.18).

Table 5.18. Comparison of results for grounding system analysis - grid 70-40/8/82.

	Grid resistance (Ω)	GPR (V)	Step voltage (V)
amiKIT	9.90	9900	1515.000
PCM	9.63	9631	1329.608
BGM	10.05	10050	1483.571

The outcomes given in Table 5.18 show that the results of amiKIT and the values

obtained with the Point Collocation Method and the Bubnov-Galerkin Method have a difference of 2-3% for the grid resistance and that the formulas proposed in UNESA [1989] give a higher value for the step voltage. At the same time, it can be seen that the values obtained with each proposed approach differs in a 4% for the grid resistance and a 12% for the step voltage. The reason of this divergence will be explained in Section 5.3, as it was indicated in the previous comparisons.

Conclusions

In short, after doing the comparisons between the proposed methods and the IEEE and Spanish standard and some commercial software, it can be stated that:

The results obtained with the methods proposed in this thesis have a good agreement with the benchmarks provided by the IEEE for uniform soil assumption, and in addition, it can be seen that the Bubnov-Galerkin Method have minor discrepancies with the standard and commercial programs results.

And the analysis done with amiKIT, which is based on the Spanish standard, shows that the safe step voltage limit is not exceeded by the proposed numerical methods, but there is a divergence between the results obtained with amiKIT and the parameter obtained with the Point Collocation Method and the Bubnov-Galerkin Method. The principal reason of this divergence is the different soil model, since the formulas of the Spanish standard considered a uniform soil.

5.3 A comparative study of Point Collocation Method and Bubnov-Galerkin Method

In the previous section, it has been seen that the results obtained with the proposed approaches based on Point Collocation Method and Bubnov-Galerkin Method present a difference. The principal reason of this difference is the nature of the weighted residual methods chosen to develop each approach. As it was explained in Section 4.3, the weighted residual methods are approximate methods based on making the residual function as small as possible. There are different types of methods depending on the nature of the weighting functions and the way to set the error equal to zero, as for example the Point Collocation Method or the Bubnov-Galerkin Method. In consequence of the differences in the weighted residual methods, a discrepancy between the values obtained with both proposed approaches appears as shown in Section 5.2 and it will be shown on the Industrial Applications section.

As explained previously, in the Point Collocation Method the residual or error function is forced to be zero at a series of points, which means that the solution is exact at these collocation points, but it is not at all domain. It is evident that as many points are defined, the residual vanishes at more points, and if infinite points are defined, the error function will be zero at the domain. On the other hand, in the Bubnov-Galerkin Method the error function is forced to be zero by making it orthogonal to the weighting

functions. Unlike the Point Collocation Method, this method gives a function that is defined in the domain, which means that the residual does not necessary vanish at any point in the domain, it vanishes in the average sense. Therefore, the approximate solutions are overall more accurate for the Bubnov-Galerkin Method than for the Point Collocation, although it requires to carry out more integrations.

Thus, after explaining briefly the principal reason why divergences appear between the results obtained in the grounding system analyses with the proposed methods, now some specific grounding system will be calculated to know how affect this divergence. In order to do this analysis, three cases with basic grid configurations will be analysed, and the grid resistance and current density distribution over the electrodes will be presented. For each case, every conductor and ground rod will be discretised into 5, 10 and 20 one-dimensional linear elements to study if with more points the results obtained with the Point Collocation Method approaches to Bubnov-Galerkin results, and if the outcomes got with the Bubnov-Galerkin method remain without significant variations.

The same design data, which are summarised in Table 5.19, and the same enclosure with dimensions 3.46 m × 2.46 m × 2.35 m and buried 0.1 m will be used in these analyses. The enclosure will be discretised into 600 two-dimensional linear elements, which means that every side is formed by 10 × 10 elements and for the analyses with the Point Collocation Method λ will be 0.85.

Table 5.19. Design data for comparative analyses between Point Collocation Method and Bubnov-Galerkin Method.

GENERAL DATA	
Ground Potential Rise (GPR)	1 V
Soil resistivity	80 Ω m
Concrete resistivity	3000 Ω m
Conductor diameter	0.008 m
Ground rod diameter	0.014 m

Case 1

For this first case, the grounding grid is formed just by one conductor with length 3.54 m.

After the grid analysis, the grid resistance obtained for each approach and each discretisation is given in Table 5.20. As it was expected, the grid resistance obtained with the Bubnov-Galerkin Method remains without significant variations, and the divergence between the model with 5 elements and 20 elements is about 0.14%. On the contrary, as it was stated at the beginning of the section, the grid resistance obtained with the approach based on the Point Collocation Method presents variations about 8.8%. It can be seen that the value tends to be similar to the Bubnov-Galerkin results

if the number of elements are increased, and it is proved that increasing the number of collocation points reduces the error.

Table 5.20. Comparison of grid resistance - Case 1.

Grid resistance (Ω)		
	Point Collocation Method	Bubnov-Galerkin Method
5 elements	23.542	26.393
10 elements	24.891	26.371
20 elements	25.618	26.355

A variable directly related with the grid resistance is the current density of conductors, so next the current density of the grounding grid analysed will be presented. The current density distributions over the conductor for both approaches are depicted in Figure 5.9. These distributions belong to the results obtained for the analyses in which the conductor is discretised into 20 elements. In this figure, it can be observed that the current density distribution is smooth in the centre of the conductor and the values of both approaches present an excellent agreement. However, the distribution varies sharply at the last element of each free end and the results of the proposed methods present an evident discrepancy. This divergence between the Point Collocation Method and the Bubnov-Galerkin Method is due to the different way to vanish the residual function, as it was explained at the beginning of this section, and it is the principal reason for what the grid resistance has not a good agreement for both proposed methods.

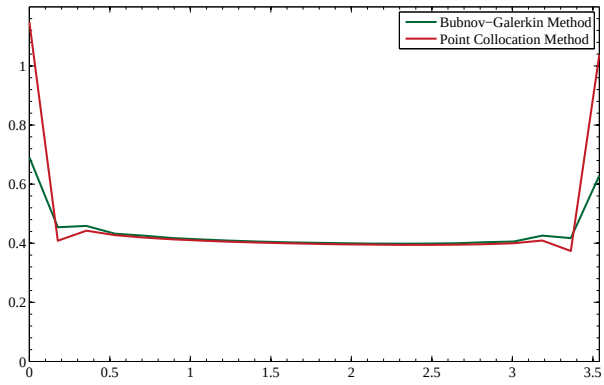

Figure 5.9. Current density distribution over conductor (Conductor discretised into 20 elements) - Case 1.

This divergence does not only affect the value of the grid resistance, but also the mesh and step voltages, as it can be seen in the examples presented along this chapter.

Case 2

The same analysis as in Case 1 about the grid resistance and the current density distribution will be done here, but in this case the grounding grid is formed by a rectangular 5 m × 3.5 m grid without ground rods and buried 1.3 m. In this configuration the underground substation is located in the middle of the perimeter ring and buried 0.1 m.

Again, the grid resistance obtained with each numerical method and for each discretisation is given in Table 5.21. These values show that in the analyses done with the Bubnov-Galerkin Method the grid resistance remains constant and the increased number of elements do not affect the results. In the same manner, the values obtained with the Point Collocation Method present small variances with a difference between the 5 elements and 20 elements model about 0.6%. Simultaneously, it is observed that the grid resistance calculated with both proposed methods present a good agreement, and that the divergence between them are less if the number of elements are increased, as it happens in Case 1.

Table 5.21. Comparison of grid resistance - Case 2.

	Grid resistance (Ω)	
	Point Collocation Method	Bubnov-Galerkin Method
5 elements	8.391	8.455
10 elements	8.423	8.455
20 elements	8.438	8.455

As it was done before, the current density distribution over the conductors will be depicted. In this case two different distributions will be shown since the grid conductors have different length. Because of the grid configuration, the results obtained are symmetric and it is not necessary to study the four conductors. The results presented in Figure 5.10 belong to the analysis in which every conductor is discretised into 20 elements. Figure 5.10a shows the current density distribution over the longest grid conductor, which is 5 m long, and Figure 5.10b shows the distribution over the conductor with length 3.5 m. As seen in Case 1, these distributions are smooth at the centre of the conductor and vary at the last element of each end. Note that in this case the ends of conductors are not free, and so that this variation is not so sharply.

Therefore, it can be stated that for grid configurations in which the conductors have not free ends, the divergence between the weighted residual methods used in the proposed models is not so significant and the results have a good agreement if a few elements are used in the Point Collocation Method.

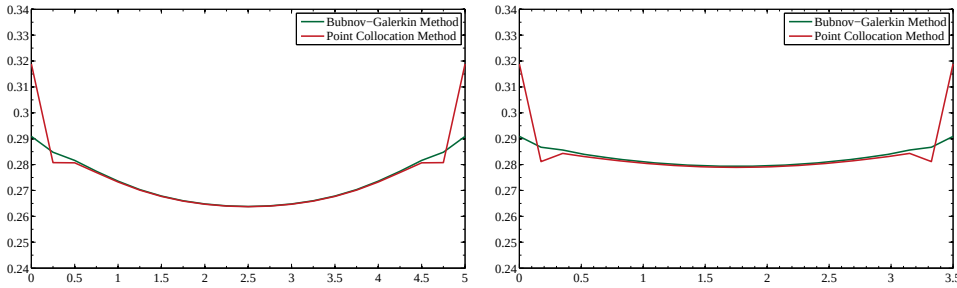

(a) Current density distribution over conductor with length 5 m.

(b) Current density distribution over conductor with length 3.5 m.

Figure 5.10. Current density distributions over conductors (Conductor discretised into 20 elements) - Case 2.

Case 3

Finally, in this third case, a grounding system formed by a combination of both grids presented before will be analysed. That is, the grid configuration is formed by a rectangular 5 m × 4 m grid with 4 ground rods, one on each corner of the grid and a length of 2 m. In addition, this grid is buried 0.8 m and the underground substation is located in the middle of it and buried 0.1 m.

Table 5.22 presents the values of grid resistance obtained for each analysis. These values show that the grid resistance varies with the increased number of elements, and there are divergences between the values obtained with each method. As in Case 1, the grid resistance obtained with the Bubnov-Galerkin Method remains without significant variations with a divergence about 0.11%, but it does not remain constant as in Case 2. For the values obtained with the Point Collocation Method the variations are about 0.52%, which are less than in Case 1 and similar to Case 2. Although it may seem that the results for this grid configuration are as good as for the grounding system analysed in Case 2 without free ends, the divergence between the grid resistances for the model with 20 elements per conductor and ground rod is about 0.4%, while in Case 2 is about 0.2%.

Table 5.22. Comparison of grid resistance - Case 3.

Grid resistance (Ω)		
	Point Collocation Method	Bubnov-Galerkin Method
5 elements	6.549	6.614
10 elements	6.568	6.609
20 elements	6.583	6.607

Figure 5.11 shows the current density distributions over one of the conductors with length 5 m (Figure 5.11a), one of the conductors with length 4 m (Figure 5.11b) and one

of the ground rods (Figure 5.11c) for the analysis in which every conductor and ground rod is discretised into 20 elements. It is not necessary to depict all distributions due to the grid configuration is symmetric and therefore the results. The current density distributions over the conductors are similar to the other analyses. They are smooth at the centre of conductors and vary sharply at the last element of each ends. It can be seen that the variation is bigger than in Case 2, and on account of the ground rods at each corner this variation is negative instead of being positive as in Case 1 and Case 2. On the other hand, the current density distribution over the ground rod presents a different behaviour. In this case, the current distribution increases slowly with depth until the last element which belongs to the free end and in which the current density varies sharply.

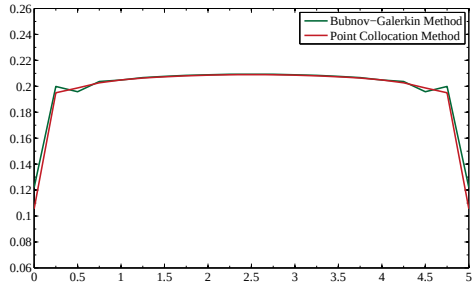

(a) Current density distribution over conductor with length 5 m.

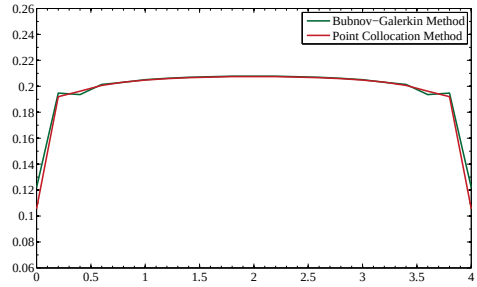

(b) Current density distribution over conductor with length 4 m.

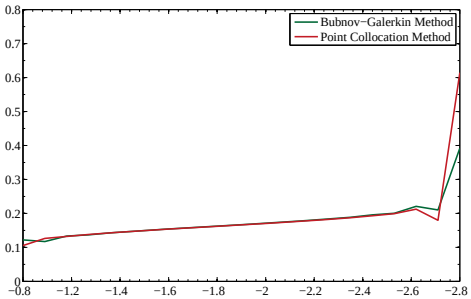

(c) Current density distribution over ground rod.

Figure 5.11. Current density distributions over conductors and ground rods (Conductor and ground rod discretised into 20 elements) - Case 3.

Note that in the depicted distributions over the conductors the results obtained with the Point Collocation Method and the Bubnov-Galerkin Method have excellent agreements, even better than in the previous cases. Likewise, the distributions over the ground rods have a good agreement, except at the last element since it belong to the free end.

Conclusions

In summary, it can be stated that the differences between the results obtained with the Point Collocation Method and the Bubnov-Galerkin Method are because of the different way to vanish the residual function in the weighted residual methods. In this section, it has been presented that for grounding systems with no free ends, that is, configurations formed by perimeter rings, the proposed approaches in this thesis have a good agreement which can be improved increasing the discretisations. Additionally, it has been seen that the main parameters of grid configurations with ground rods have also a good agreement, although no so good as for perimeter ring configurations, since the ground rods have a free end. However, increasing the discretisation also improves the accuracy.

5.4 Industrial Applications

After validating the numerical models proposed in Chapter 4, the industrial applications of this work will be presented. This section will be divided in two parts. First, two examples of grounding system analysis will be done for real underground transformer substations. In these analyses the main parameters of the grounding systems will be calculated as well as the surface and step voltage distributions, and then, the values obtained will be compared with the safe limits established by the Spanish standard. In the second part, it will be presented the voltage and current density distributions over the surface of underground electrical substations, and it will be shown if the results obtained in these analyses can be affected by changes in the concrete resistivity.

5.4.1 Grounding system analysis

The principal application of the numerical models developed in thesis is the grounding system analysis for underground electrical substations. In order to present this application, two real examples will be performed, in which their main parameters (the grid resistance, the GPR and the step and mesh voltages) will be calculated. Each example will be analysed for two different grid configurations. One of them, it is the configuration proposed in the general instructions for the underground transformer substations, and the other will be chosen from the Anexo 2 of [UNESA, 1989]. Finally, the results obtained for each grounding system will be checked against and they will be compared with the safe voltage limits.

Note that these grounding analyses will be done as in Subsection 5.2.2, so the operating voltage and the grid current will be the general data of the problem.

Example 1

For this first example a commercial underground electrical substation is chosen. The main characteristics necessary for this analysis are the enclosure dimensions, which are 5.40 m $\times$ 2.46 m $\times$ 2.84 m.

In order to carry out the grounding analysis of this substation, a soil resistivity of 50 Ω m and a total grid current of 1000 A with a fault duration of 0.2 s are supposed. These fault values are the normal operating values for a medium electrical substation. In addition, a concrete resistivity of 3000 Ω m is supposed for the enclosure. These design data are summarised in Table 5.23.

Table 5.23. Design data for Example 1.

GENERAL DATA	
Operating voltage	20 kV
Grid current	1000 A
Fault duration	0.2 s
Soil resistivity	50 Ω m
Concrete resistivity	3000 Ω m

Before presenting the grid configurations and the results obtained in these analyses, the safe voltage limits will be calculated. As it was explained in Subsection 5.2.2, the appearance of touch voltages can be avoided assuming the secure measures described previously. Thus, only the safe step voltage limit has to be calculated using the formula defined in [RD 337/2014, 2014], and the soil resistivity and the fault duration set in the design data. In this case, the limit obtained is:

$$V_{step,max} = 27984\,V$$

Following with the example, the first grounding grid analysed is formed by two perimeter rings, one located in the base of the excavation at a distance of 0.4 m from the substation, and another at a depth of 0.8 m under the ground surface at a distance of 1 m from the substation. Both rings are connected with each other with two bare copper conductors. In Figure 5.12 a schematic representation of this configuration is shown.

Therefore, the grounding system is formed by 10 bare copper conductors with a cross-sectional area of 50 mm^2, which means that the conductor diameter is approximately 8 mm.

The numerical model used to calculate this configuration with the Point Collocation Method and the Bubnov-Galerkin Method is formed by 14 one-dimensional linear elements to model the conductors, which are not discretised, and 600 two-dimensional linear elements to model the enclosure, in which every side is discretised into 10 × 10 elements. This model considers that the electrical substation is buried 0.1 m. All these characteristics are summarised in Table 5.24.

As a result, the grid resistance, the GPR, the mesh voltage and the maximum step voltage are obtained with the proposed methods (Table 5.25).

It can be seen in Table 5.25 that the grid resistance shows an excellent agreement between the values obtained with the Point Collocation Method and the Bubnov-

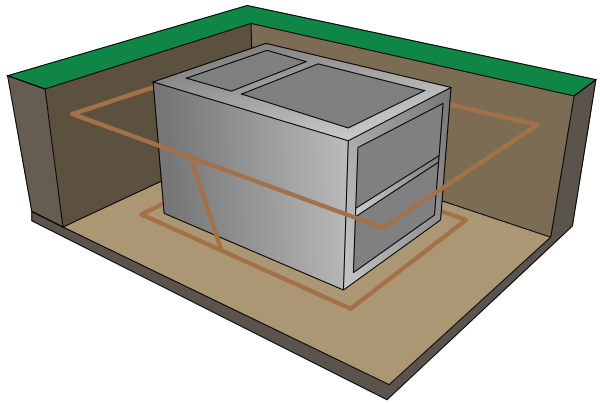

Figure 5.12. Schematic representation of the grounding system with two perimeter rings.

Table 5.24. Parameters of numerical model - Example 1: two perimeter rings grid configuration.

NUMERICAL MODEL		
Numerical approach	Point Collocation Method	Bubnov-Galerkin Method
BEM elements	Linear ($\lambda = 0.85$)	Linear
No. of elements (electrodes)	14	14
Degrees of freedom (electrodes)	12	12
No. of elements (enclosure)	600	600
Degrees of freedom (enclosure)	726	726

Table 5.25. Comparison of results for grounding system analysis - Example 1: two perimeter rings grid configuration.

	Grid resistance (Ω)	GPR (V)	Mesh voltage (V)	Step voltage (V)
PCM	3.005	3005.0	937.897	443.222
BGM	3.003	3003.0	1035.489	424.504

Galerkin Method, and as a consequence the GPR also has this excellent agreement. For the step voltage, it can be observed a good agreement between the values with only a divergence about 4%; however, the mesh voltage differs about 11%. This divergence is due to the difference between the weighted residual methods and the nature of their weighting functions, as it was explained in Section 5.3.

Even so, it can be observed that the maximum step voltage obtained does not overtake the safe step limit; on the contrary it is about 1.6% of the safe value.

In addition to the main parameters, the surface and step voltage distributions have been calculated. Figure 5.13 shows a general 3D view of the potential distributions for this grounding system. The total area studied is a rectangle of 14 m by 12 m, which

implies a surface of 168 m^2 and in which 1600 points are defined so as to compute the voltage distributions.

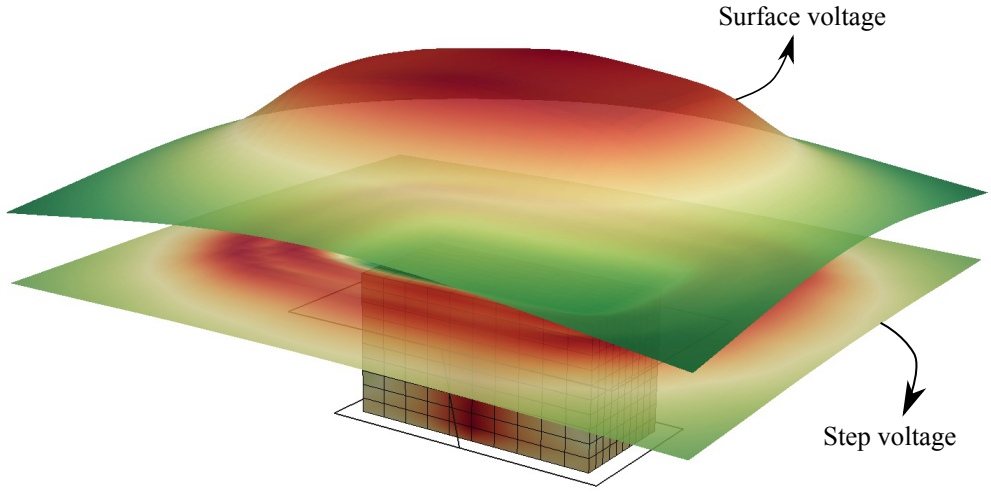

Figure 5.13. General 3D view of potential distributions - Example 1: two perimeter rings grid configuration.

Figures 5.14 and 5.15 present the surface and step voltage distributions over the total area studied. It can be observed that the distributions obtained with both methods present a good agreement.

Figure 5.14 shows that the largest voltages appear just above the substation with an important homogenisation and the largest gradients appear at the perimeter areas. Consequently, the largest step voltages appear at the perimeter areas due to these gradients, and the safest area is located above the underground substation, as shown in Figure 5.15. It can be seen that the presented distributions have a symmetrical solution, as it was expected due to the symmetry of the grounding system.

Although the distributions obtained with the Point Collocation Method and the Bubnov-Galerkin Method have a good agreement, Figure 5.15 shows that the potential contour lines for each method present some divergence between the step voltage distributions, especially at the area above the substation and at the largest side of the enclosure where the conductors which connect both rings are located.

Now, another grounding system will be analysed for the same underground electrical substation. This second grid configuration will be designed according to the method described on [UNESA, 1989] and [RD 337/2014, 2014]. In order to choose a grid defined in the Anexo 2 of [UNESA, 1989], it is required a coefficient expressed in this guide as K_r (Ω / Ω m), which its maximum is calculated as:

$$K_r = \frac{R_t}{\rho_s}$$

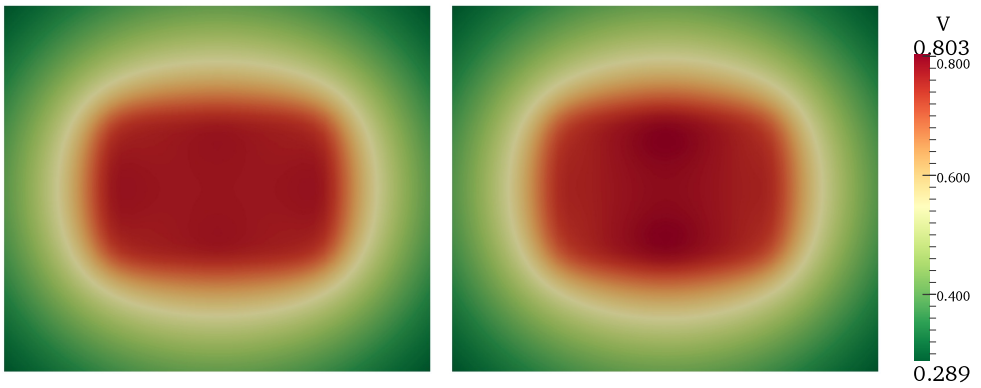

(a) Point Collocation Method. **(b) Bubnov-Galerkin Method.**

Figure 5.14. Surface voltage distributions (× GPR) - Example 1: two perimeter rings grid configuration.

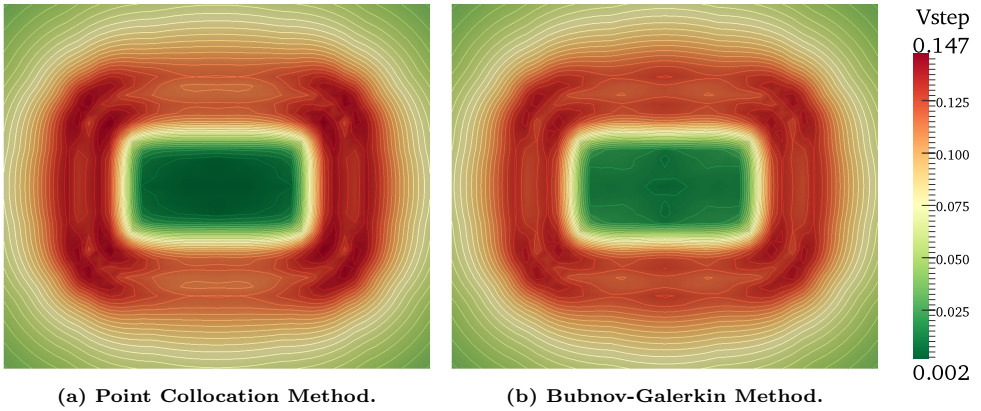

(a) Point Collocation Method. **(b) Bubnov-Galerkin Method.**

Figure 5.15. Step voltage distributions (× GPR) - Example 1: two perimeter rings grid configuration.

where R_t is the maximum grid resistance (Ω) and ρ_s is the soil resistivity (Ω m). In turn, the maximum grid resistance (R_t) is defined as the quotient between the isolation voltage, which for a low-voltage installation is supposed equal to 10 kV, and the grid current.

Thus, in this example the maximum value of K_r is 0.2 Ω / Ω m and the grid configuration selected in the Anexo 2 has to have a K_r less than 0.2 but close to this value. In addition, it has to keep in mind the dimensions of the underground substation. As a result, the configuration 30-35/8/42 is assumed as the grounding grid.

This configuration is formed by a rectangular 6 m × 3.5 m grid with 4 ground rods, one on each corner of the grid and a length of 2 m, as shown in Figure 5.16. Just as in the first configuration, the conductor diameter is approximately 8 mm, and for the ground rods the diameter will be 14 mm.

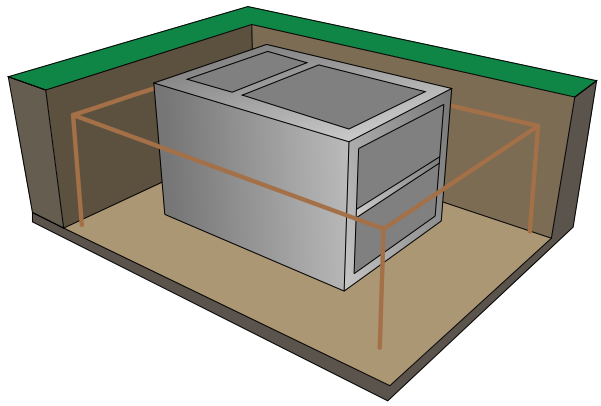

Figure 5.16. Schematic representation of grounding system 30-35/8/42.

Different numerical models are defined to analyse this grounding grid with the proposed methods. For the Point Collocation Method, the grid model is formed by 18 one-dimensional linear elements, which means that the electrodes are discretised. In this case, the conductors located on the long side of the substation are discretised into 3 elements, the others into 2 elements, and the ground rods are also discretised into 2 elements. On the other hand, for the Bubnov-Galerkin Method the conductors and ground rods are not discretised, so the grid model is formed by 8 one-dimensional linear elements. For both methods, the enclosure will be discretised into 600 two-dimensional elements, as in the first configuration. Again, it is considered that the electrical substation is buried 0.1 m. These numerical models are summarised in Table 5.26.

Table 5.26. Parameters of numerical model - Example 1: grid configuration 30-35/8/42.

NUMERICAL MODEL		
Numerical approach	Point Collocation Method	Bubnov-Galerkin Method
BEM elements	Linear ($\lambda = 0.85$)	Linear
No. of elements (electrodes)	18	8
Degrees of freedom (electrodes)	18	8
No. of elements (enclosure)	600	600
Degrees of freedom (enclosure)	726	726

The results obtained for this grounding grid analysis can be found in Table 5.27.

Table 5.27 shows that the grid resistance and the mesh voltage obtained with the proposed methods have a good agreement with only a difference about 3% and 2%, respectively. In the case of the step voltage the divergence is about 14% between the results obtained.

Even though, the step voltage for this grounding system is higher than in the first grid, but it does not overtake the safe step limit. It is just about 2.3% of this safe

Table 5.27. Comparison of results for grounding system analysis - Example 1: grid configuration 30-35/8/42.

	Grid resistance (Ω)	GPR (V)	Mesh voltage (V)	Step voltage (V)
PCM	3.993	3993	1433.048	558.353
BGM	4.118	4118	1398.304	636.050

value.

As it was done for the first grid configuration, the surface and step voltage distributions have been calculated. A general 3D view of these potential distributions is presented in Figure 5.17. In this case, the total area studied is a rectangle of 12 m by 10 m, which implies a surface of 120 m^2 with 1600 points set to compute the voltage distributions.

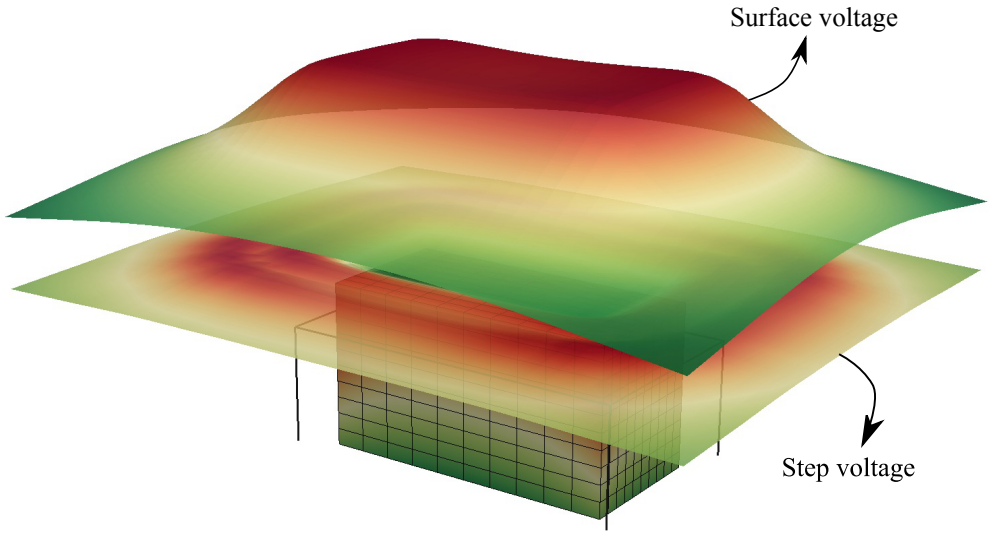

Figure 5.17. General 3D view of potential distributions - Example 1: grid configuration 30-35/8/42.

In Figures 5.18 and 5.19 the surface and step voltage distributions are compared for the different approaches, and again similar distributions are obtained.

Figure 5.18 shows the surface voltage distribution for this grounding grid. It can be observed that the largest voltages appear just above the substation and the largest gradients appear at the perimeter area where the grid configuration is located, just as it happens in the first grid. But, in this case the maximum surface voltage is lower.

Similarly, the largest step voltages appear at the grid location due to the gradients of the surface potential, and the safest area is located above the substation, as depicted in Figure 5.19. At first sight the distributions obtained with the Point Collocation

Method and the Bubnov-Galerkin Method present a good agreement, but analysing the potential contour lines plotted on the step voltage distribution, it can be observed disagreements between them, especially at the areas where the ground rods are located and above the substation. This divergence will be motivated by the differences between the weighted residual techniques used.

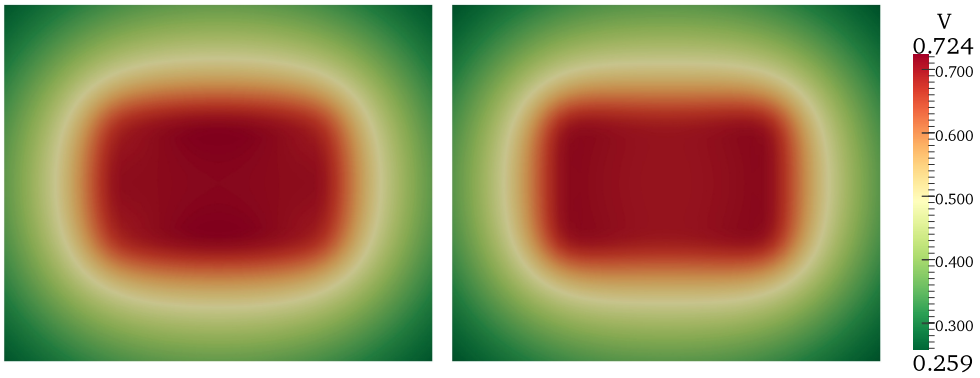

(a) Point Collocation Method. (b) Bubnov-Galerkin Method.

Figure 5.18. Surface voltage distribution (× GPR) - Example 1: grid configuration 30-35/8/42.

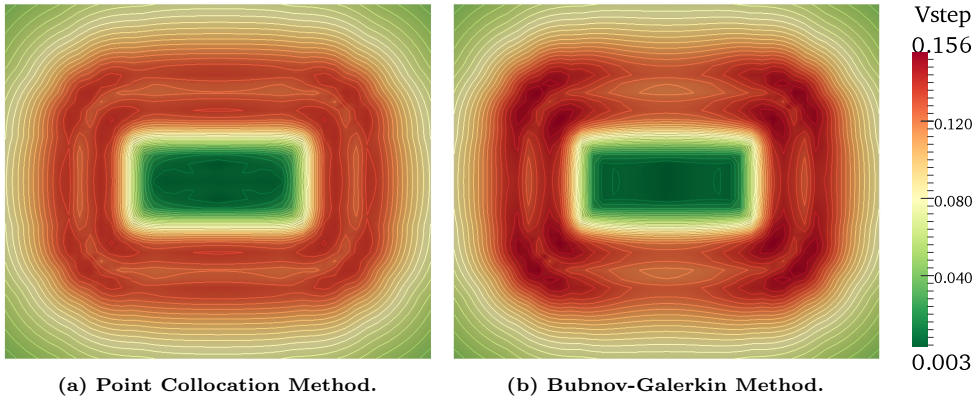

(a) Point Collocation Method. (b) Bubnov-Galerkin Method.

Figure 5.19. Step voltage distribution (× GPR) - Example 1: grid configuration 30-35/8/42.

In short, the main parameters and potential distributions obtained for both grounding systems present similar results, although the mesh voltage and the maximum step voltage are lower in the configuration formed by two perimeter rings, which means that for this example the first grounding grid is safer.

Example 2

For this second example a similar analysis as it was done in Example 1 will be performed.

In this example, the grounding system for another commercial power transformer will be analysed. Again, for this grounding analysis only the enclosure dimensions are necessary, which are 3.46 m × 2.46 m × 2.35 m.

The same design data as in Example 1 are defined for these analyses with the only difference that now a soil resistivity of 120 Ω m is supposed. These data are summarised in Table 5.28.

Table 5.28. Design data for Example 2.

GENERAL DATA	
Operating voltage	20 kV
Grid current	1000 A
Fault duration	0.2 s
Soil resistivity	120 Ω m
Concrete resistivity	3000 Ω m

As noted in Example 1, the safe voltage limits will be calculated first of all. Only the safe step voltage limit has to be calculated, since the appearance of dangerous touch voltage can be avoided assuming the secure measures described in Subsection 5.2.2. The formula defined in [RD 337/2014, 2014], and the soil resistivity and the fault duration of the design data will be used to calculate the safe step limit, which for these analyses is:

$$V_{step,max} = 30201.6\,V$$

The first grounding system analysed has the same configuration as the first grid proposed in Example 1, which is formed by 10 bare copper conductors with a diameter of 8 mm. Thus, in Figure 5.12 a schematic representation is shown.

The numerical model used to calculate this grounding grid with the proposed methods is the same as for Example 1. This is formed by 14 one-dimensional linear elements to model the conductors and 600 two-dimensional linear elements to model the enclosure, as it is presented in Table 5.24. For this analysis it is considered that the electrical substation is buried 0.1 m.

The main parameters obtained after doing the grounding analysis are given in Table 5.29. These are the grid resistance, the GPR, the mesh voltage and the maximum step voltage.

Table 5.29 shows that the main parameters obtained with the Point Collocation Method and the Bubnov-Galerkin Method have a good agreement, with only a difference about 0.8% for the grid resistance and the GPR, and about 5.5% and 4% for the mesh and the step voltage, respectively.

Table 5.29. Comparison of results for grounding system analysis - Example 2: two perimeter rings grid configuration.

	Grid resistance (Ω)	GPR (V)	Mesh voltage (V)	Step voltage (V)
PCM	8.370	8370	2700.045	1292.085
BGM	8.433	8433	2849.317	1247.570

It should be noted that the maximum step voltage obtained does not overtake the safe step limit, since it is only a 4.3% of this safe value.

In addition to the main parameters, the surface and step voltage distributions have been calculated, as well as some voltage profiles in order to compare the distributions obtained with the proposed methods. The total area studied is a rectangle of 12 m by 10 m, which implies a surface of 120 m^2 with the same number of points as set in Example 1 to compute the voltage distributions.

Figure 5.20 presents the surface voltage distribution over the area studied. As it happens in Example 1, the largest voltages appear just above the electrical substation with a uniform distribution, and the largest gradients appear at the perimeter areas where the grid is located. It can be seen that the distributions calculated with the proposed approaches have a good agreement.

On the other hand, Figure 5.21 plots the step voltage distribution. Again, as it has been shown in Example 1, the largest step voltages are at the perimeter areas due to the largest surface potential gradients appear at this area and the safest area is situated above the substation where the surface potential distribution is homogeneous and there are not voltage gradients. At first sight, these step distributions present an excellent agreement, but analysing the colour lines plotted in Figure 5.21 it can be seen some disagreements between the Point Collocation Method and the Bubnov-Galerkin Method, especially at the areas above the substation and where the conductors that connect both rings are located. These differences are motivated by the nature of the weighting functions used in each weighted residual method (Section 5.3).

Finally, Figure 5.22 shows the voltage profiles along a horizontal line which crosses the middle of the area depicted on the surface and step voltage distributions. The left figure illustrates the surface potential profile for the Point Collocation Method (solid line) and for the Bubnov-Galerkin Method (dash line), and on the right figure the step voltage is presented. As it was stated previously, it can be observed that the largest surface potential appear above the substation with a uniform distribution, and the largest step voltage appear above the grid location. The step voltage profile shows that the lowest values appear on the area above the substation due to in this area there are barely potential gradients, and two peaks which coincide with the perimeter ring locations. These peaks appear where the maximum gradients happen, as it was stated before.

The second grounding system analysed will be designed according to the method

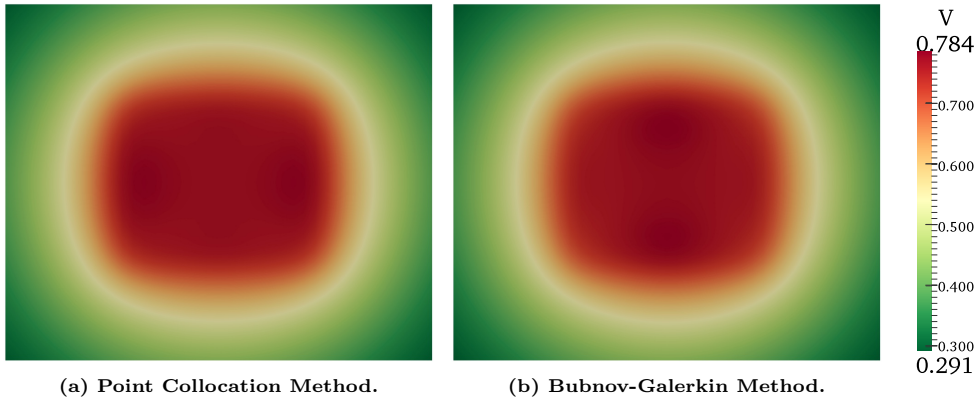

(a) Point Collocation Method. (b) Bubnov-Galerkin Method.

Figure 5.20. Surface voltage distributions (× GPR) - Example 2: two perimeter rings grid configuration.

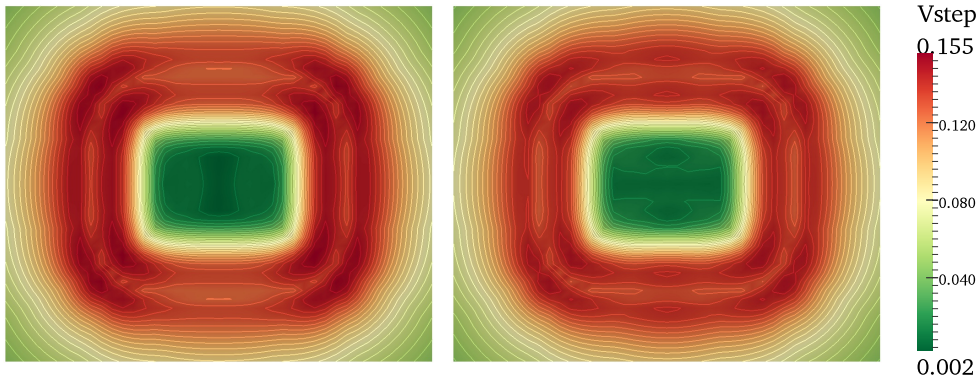

(a) Point Collocation Method. (b) Bubnov-Galerkin Method.

Figure 5.21. Step voltage distributions (× GPR) - Example 2: two perimeter rings grid configuration.

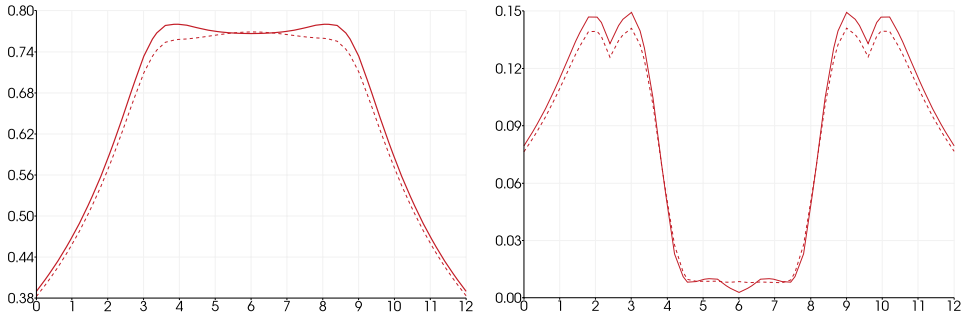

(a) Surface voltage profile (× GPR). (b) Step voltage profile (× GPR).

Figure 5.22. Voltage profiles - Example 2: two perimeter rings grid configuration.

described in [UNESA, 1989] and [RD 337/2014, 2014], as it was done in Example 1. In this case the maximum value of K_r is 0.08333 Ω / Ω m. Thus, keeping in mind the dimensions of the underground substation and the maximum value of K_r, the grid selected in the Anexo 2 of [UNESA, 1989] is the configuration 50-35/8/82.

This configuration is formed by a rectangular 5 m x 3.5 m grid with eight ground rods around the perimeter of the grid and a length of 2 m, as shown in Figure 5.23. Just as in Example 1, the conductor diameter is 8 mm, and for the ground rods the diameter will be 14 mm.

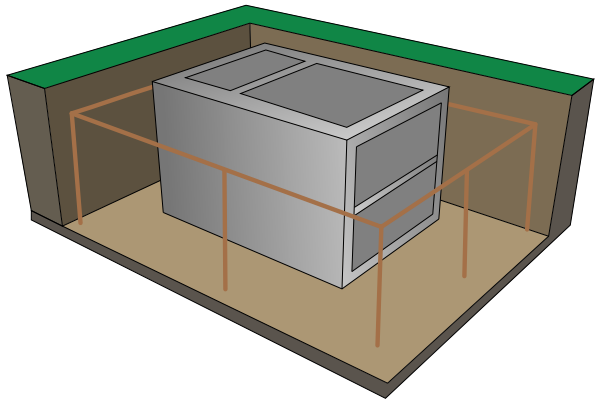

Figure 5.23. Schematic representation of grounding system 50-35/8/82.

Different discretisations are done to model this grounding grid with the proposed methods (Table 5.30). For the Point Collocation Method, the conductors located on the long side of the substation are discretised into 3 elements and the others into 2 elements, and the ground rods are discretised into 2 elements. Thus, the grid model will be formed by 32 one-dimensional linear elements. However, for the Bubnov-Galerkin Method the grounding grid is not discretised, so the grid model will be formed by 16 one-dimensional linear elements. The enclosure will be discretised into 600 two-dimensional linear elements as it was done in the previous examples.

Table 5.30. Parameters of numerical model - Example 2: grid configuration 50-35/8/82.

NUMERICAL MODEL		
Numerical approach	Point Collocation Method	Bubnov-Galerkin Method
BEM elements	Linear ($\lambda = 0.85$)	Linear
No. of elements (electrodes)	32	16
Degrees of freedom (electrodes)	30	16
No. of elements (enclosure)	600	600
Degrees of freedom (enclosure)	726	726

After doing the analysis, the grid resistance, the GPR, the mesh voltage and

the maximum step voltage that characterise this grounding system are obtained (Table 5.31).

Table 5.31. Comparison of results for grounding system analysis - Example 2: grid configuration 50-35/8/82.

	Grid resistance (Ω)	GPR (V)	Mesh voltage (V)	Step voltage (V)
PCM	8.430	8430	2552.756	1212.386
BGM	9.137	9137	2855.459	1355.337

The results shown in Table 5.31 for the proposed methods present a difference of 8.4% for the grid resistance and the GPR, and about 12% for the mesh and step voltages. The divergence between both methods is higher in this analysis due to the existence of more ground rods in the grid, and consequently the difference between the weighted residual methods is emphasised (Section 5.3).

Such as in the grounding grid formed by two perimeter rings, for configuration 50-35/8/82 the maximum step voltage obtained does not overtake the safe step limit, since it is only a 4.5% of this safe value.

Similarly to the other analyses, the surface and step voltage distributions have been calculated. The total area studied is a rectangle of 12 m by 10 m, as it was made for the first grounding grid.

Figures 5.24 and 5.25 show the surface and step voltage distributions, respectively. As it was stated before, the largest surface voltages appear above the substation and the largest step voltages appear at the perimeter area where the grid is located. It can be observed that similar distributions are obtained for both methods, but analysing in detail the colour lines plotted in Figure 5.25 some disagreements between them can be seen, especially in the areas above the substation and where the ground rods are located.

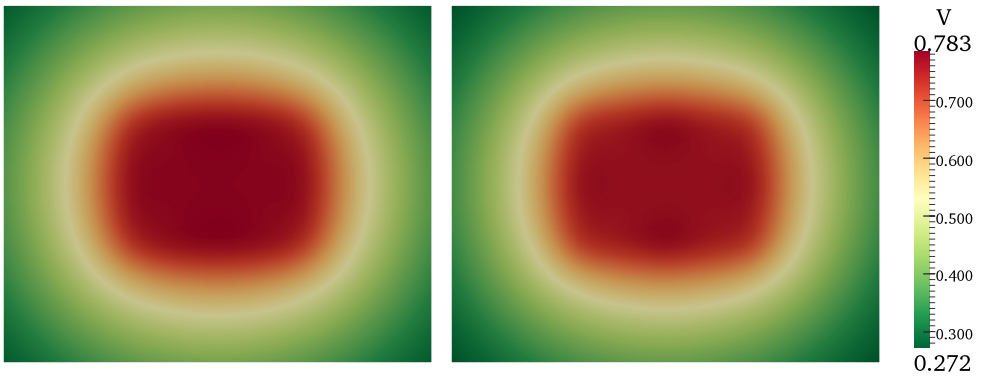

(a) Point Collocation Method. **(b) Bubnov-Galerkin Method.**

Figure 5.24. Surface voltage distributions (× GPR) - Example 2: grid configuration 50-35/8/82.

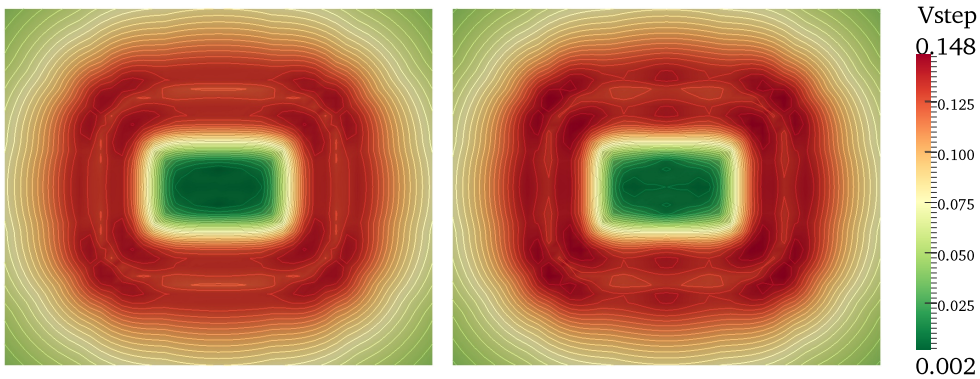

(a) Point Collocation Method. **(b) Bubnov-Galerkin Method.**

Figure 5.25. Step voltage distributions (× GPR) - Example 2: grid configuration 50-35/8/82.

Additionally, Figure 5.26 shows the potential profiles along a horizontal line which crosses the middle of the area depicted on the surface and step voltage distributions, as in the previous analysis performed the first grid configuration. It can be observed that these profiles have the same shape as the profiles obtained with the analysis of the first grounding grid. Again, the left figure shows the surface voltage profile for the Point Collocation Method (solid line) and the Bubnov-Galerkin Method (dash line), and the right figure presents the step voltage profile. The same characteristics as it was commented previously can be seen. That is, the maximum surface voltage appears above the substation with constant value along all length and the highest gradients are just located before this maximum. Due to these gradients, two peaks appear in the step voltage profile, which coincide with the perimeter ring, and a plain can be observed where the potential gradients are minimum.

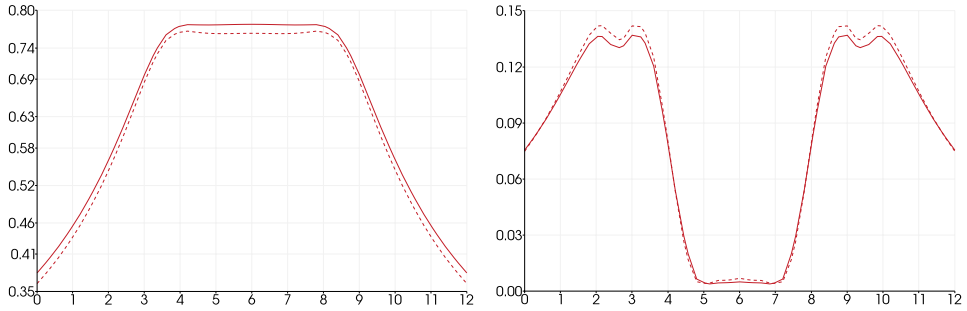

(a) Surface voltage profile (× GPR). **(b) Step voltage profile (× GPR).**

Figure 5.26. Voltage profiles - Example 2: grid configuration 50-35/8/82.

Lastly, the main parameters and potential distributions are obtained for both grid configurations in this second example. As it can be observed the maximum surface potential and step voltage have approximately the same value for each grounding grid,

so for this example both grounding systems are safe, but more electrodes are needed in the second configuration. Thus, the first grounding system is more economic, not only in material, but also in computational time.

5.4.2 Other applications

A secondary application results as a consequence of the grounding system analysis with the numerical approaches proposed in this thesis, which is the study of the voltage and current density distributions over the enclosure of electrical substations.

In Chapter 4, the system of equations obtained for Point Collocation Method and Bubnov-Galerkin Method was stated (equations (4.73) and (4.112)). In these systems, in addition to calculate the current density of the electrodes, the current density and potential on the electrical substation is also obtained. Therefore, the distributions of these parameters can be presented and studied now.

An application related with getting the voltage and current density distributions over the enclosure may be the study of induced corrosion in reinforced concrete due to possible stray currents. Stray currents can be defined as the continuous flow of any current which are deviated from their path since they find an alternative route, as for example pipelines, railways, buried metal structures or even reinforced concrete structures. This deviated current can bring about corrosion of metallic structures by a phenomenon which is known as stray current corrosion. In this case, the stray current that comes from the grounding grid can flow through reinforced concrete enclosure and induce corrosion of steel reinforcement.

The corrosion of steel reinforcement in concrete is a complex and important phenomenon to analyse and there are several studies about it in the concrete literature. The corrosion is usually an electrochemical process caused by carbonation of concrete or chloride contamination, which affects the mechanical and structural properties of components causing serial problems in the durability and the global response of structures. This phenomenon can be also motivated by DC or AC stray currents, as it is studied in [Bertolini et al., 2007, 2013].

Thus, from the distributions obtained with the developed models it can be observed the areas which present high values of current flow and have more possibilities of suffering from stray-current-induced corrosion. This application may help to improve the enclosure designs or the concrete properties with the purpose of guarantee that the original characteristics of prefabricated enclosures do not change by possible stray currents. It is true that the actual proposed methods do not model the steel reinforcements, but it is a first approach to know how the voltage and current density distributions over the enclosure surface are and where are located the weakness areas to suffer corrosion.

Next, some of the distributions obtained in the previous grounding analyses will be shown. In order to depict the complete structure of the enclosures, only the values calculated with the Bubnov-Galerkin Method will be plotted, since as it was presented in Subsection 4.5.3 the Point Collocation Method presents serious numerical problems

at corners and edges and semidiscontinuos elements are used to discretise the enclosures. The distributions that will be presented come from the analysis of the grounding grid formed by two perimeter rings in Example 1, and from the analysis of the grid configuration selected in the Anexo 2 of [UNESA, 1989] in Example 2.

The first distributions shown in Figures 5.27 and 5.28 belong to the first grounding grid analysed in Example 1. This grounding grid is formed by two perimeter rings connected each other with two bare copper conductors, as it was described previously. Figure 5.27 shows the voltage distribution over the surface of the substation. As it might be expected, the highest voltage values are located on the areas closer to the grid. Likewise, the voltages at the top of surface are higher than at the bottom since the top is situated a 0.1 m from the ground surface, and so, the voltages have not space to dissipate. It can be observed that the values at the top are similar as the surface distribution plotted in Figure 5.14. However, the space behind the bottom of the enclosure is supposed semi-infinite, so, there is enough area to dissipate the potentials and this zone presents the lowest voltages.

On the other hand, Figure 5.28 shows the current density distribution for the same grounding system. In this figure the negative values represent the current density that enters the enclosure and the positive ones represent the current density that leaves it. It is observed that the highest values of this parameter appear on the underside of the substation, where the majority of the current enters in the perimeter area closer to the perimeter ring and leaves the enclosure through the bottom. Based on these results, it can be assumed that the enclosure zones with more danger to suffer the phenomenon of stray current corrosion are located on the underside.

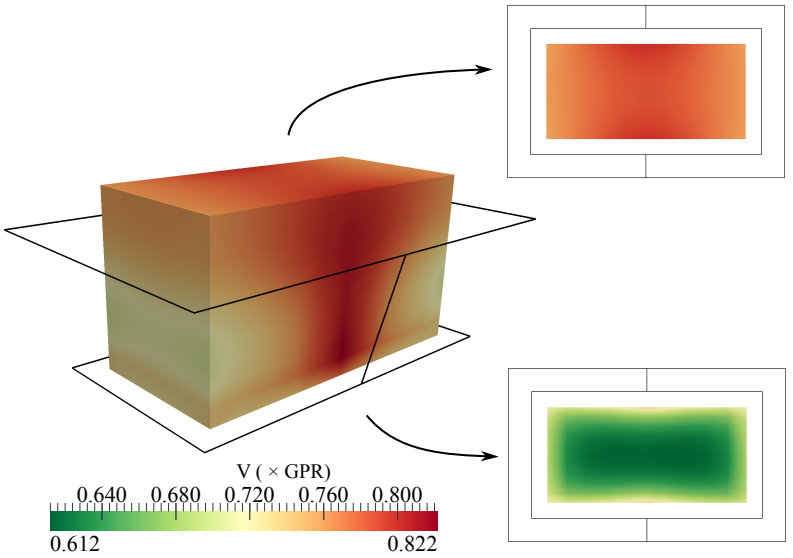

Figure 5.27. Voltage distribution over the enclosure for the first grounding grid analysed in Example 1.

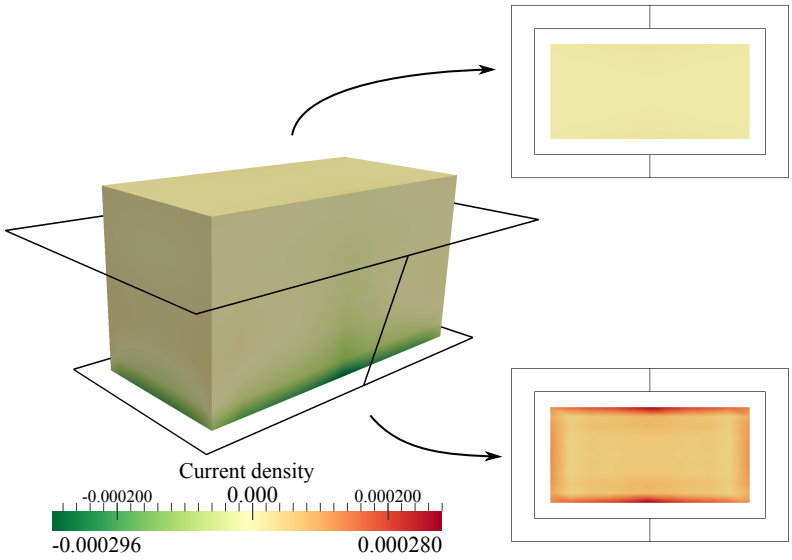

Figure 5.28. Current density distribution over the enclosure for the first grounding grid analysed in Example 1.

Similarly, the voltage and current density distributions for the grounding grid of Example 2 are showed in Figures 5.29 and 5.30. This grid configuration was selected from the Anexo 2 of [UNESA, 1989] and it is formed by a rectangular grid with eight ground rods around the perimeter, as it was presented previously. As in Example 1, Figure 5.29 presents the voltage distribution over the surface of the substation, and it can be observed that the highest voltages follow the ground rods direction and all the enclosure presents high potential values, except the bottom of the enclosure. As it was explained in the previous distributions, the voltages at the top of the substation are similar to the surface distribution showed in Figure 5.24, and the values are higher since it is situated 0.1 m from the ground surface and the voltages do not have space to dissipate. However, the values at the bottom are the lowest since there is enough area to dissipate the potentials.

The current density distribution is depicted in Figure 5.30. Again, the negative values represent the current density which enters the enclosure and the positives represent the current density which leaves it. As it happens in Example 1, the majority of the current enters through the areas where the perimeter ring and the ground rods are located, and it leaves the substation through the bottom. As a result, it might be supposed that the areas with more danger to present the phenomenon of stray current corrosion are located at the perimeter ring, at the bottom and in the areas closer to the middle ground rod.

In the previous examples analysed, the value used for the concrete resistivity was 3000 Ω m. An interesting point to study is what happens when the concrete resistivity is increased. In [Bertolini et al., 2013] it is indicated that high concrete resistivity

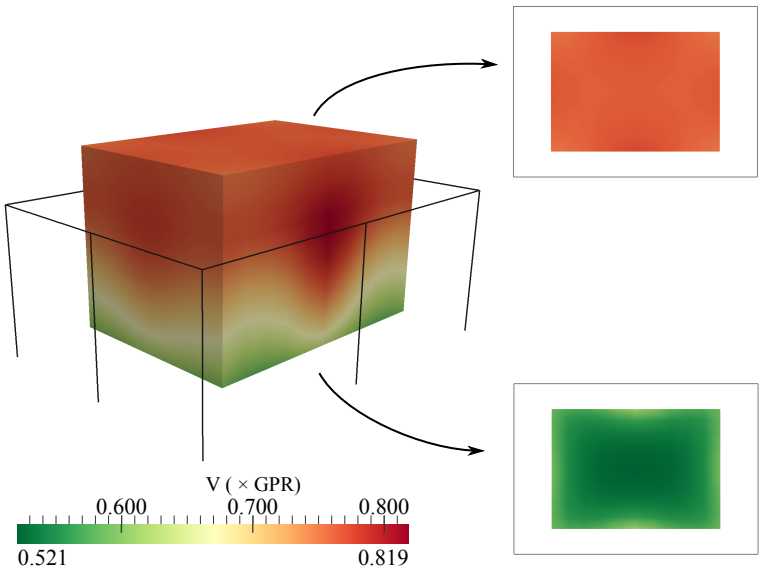

Figure 5.29. Voltage distribution over the enclosure for grid configuration 50-35/8/82 analysed in Example 2.

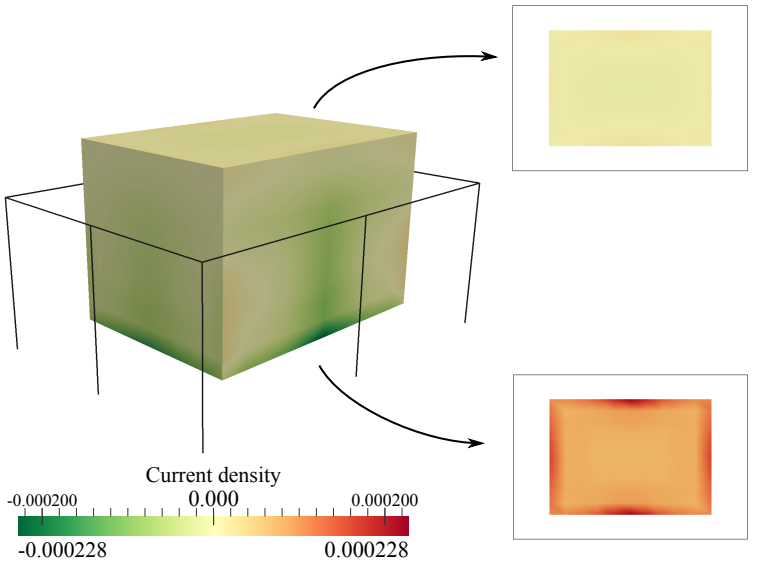

Figure 5.30. Current density distribution over the enclosure for grid configuration 50-35/8/82 analysed in Example 2.

will reduce the current flow and less stray currents appear, and as a consequence, the possibilities of suffering stray current corrosion are less. Next, the grid configuration presented in Example 2 will be analysed again changing the concrete resistivity to 8000

Ω m, and the main parameters and distributions obtained will be presented to study what happens. The approach used to this analysis is the Bubnov-Galerkin Method and the design data will be the same as defined in Table 5.28.

The values of the grid resistance, the GPR, the mesh voltage and the maximum step voltage obtained are given in Table 5.32.

Table 5.32. Results for grounding system analysis - grid configuration 50-35/8/82 and concrete resistivity 8000 Ω m.

	Grid resistance (Ω)	GPR (V)	Mesh voltage (V)	Step voltage (V)
BGM	9.144	9144	2856.686	1357.601

Comparing the results from this analysis with the main parameters given in Table 5.31, it can be stated that changes in the concrete resistivity does not affect the outcomes. In fact, the divergence between both analyses is 0.08% for the grid resistance and the GPR, and 0.043% and 0.17% for the mesh and step voltage, respectively.

In addition to the main parameter comparison, the surface and step voltage distributions for both analyses are also shown (Figures 5.31 and 5.32), and it is observed that the same distributions are obtained. So again, it can be stated that the increase of concrete resistivity does not affect the surface and step voltage distributions.

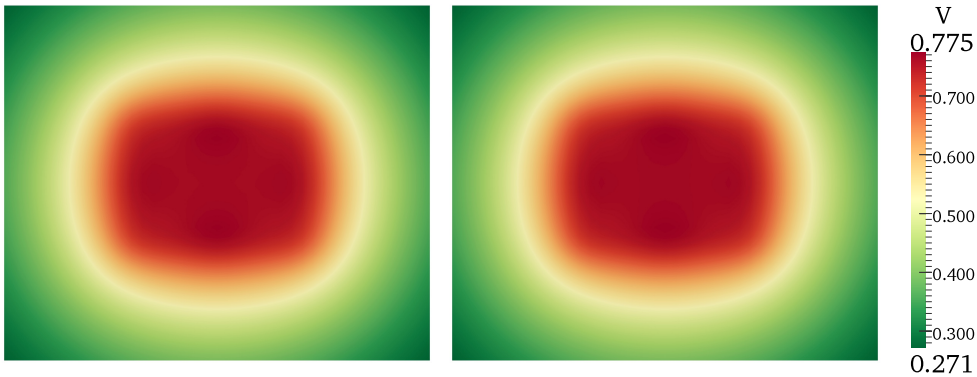

(a) Bubnov-Galerkin Method (3000 Ω m). (b) Bubnov-Galerkin Method (8000 Ω m).

Figure 5.31. Surface voltage distributions (× GPR).

Finally, the voltage and current density distributions over the enclosure are presented (Figures 5.33 and 5.34). Likewise, changes in concrete resistivity does not affect the voltage distribution significantly, as it can be seen comparing the values of Figure 5.33 and Figure 5.30; however, the values of current density have dropped by an order of magnitude, as it is depicted in Figure 5.34. Thus, as noted above, if concrete resistivity is increased, the current density over the prefabricated enclosure is reduced and with this reduction the effects of suffering stray current corrosion.

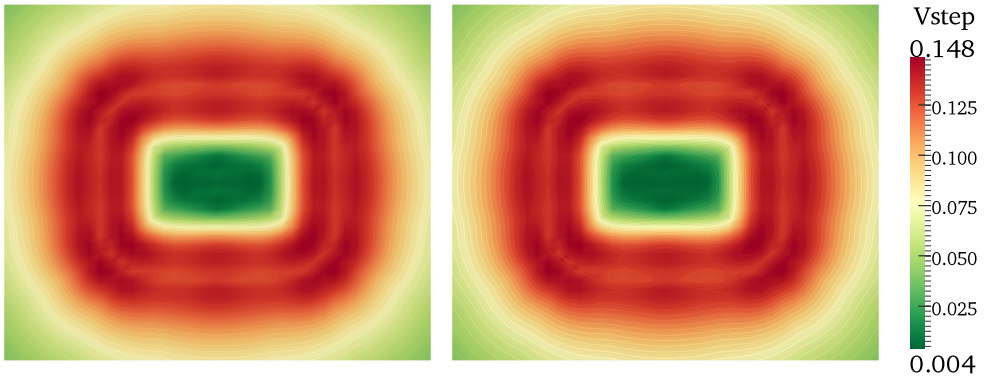

(a) Bubnov-Galerkin Method (3000 Ω m). (b) Bubnov-Galerkin Method (8000 Ω m).

Figure 5.32. Step voltage distributions (× GPR).

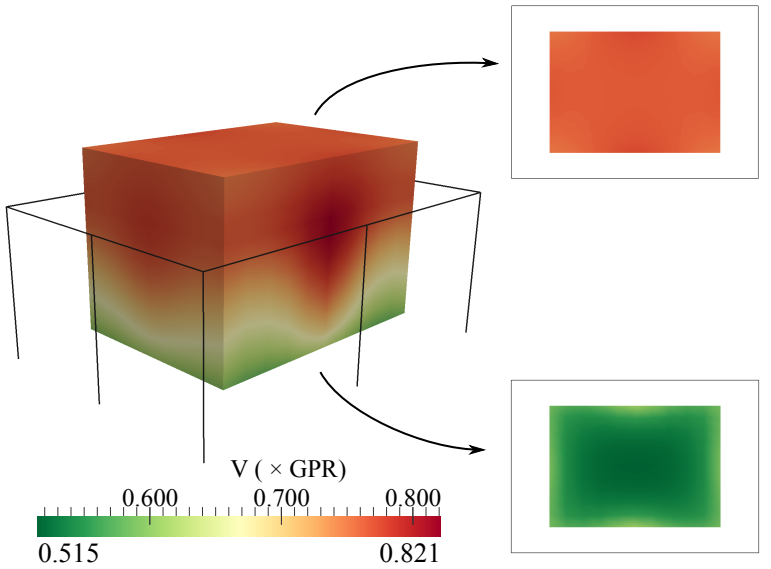

Figure 5.33. Voltage distribution over the enclosure for grid configuration 50-35/8/82 and concrete resistivity 8000 Ω m.

5.5 Conclusions

In conclusion, the numerical methods proposed in this thesis are a new tool to design and analyse the grounding systems of underground electrical substations. As it has been demonstrated, these approaches have a good agreement with the current techniques to calculate these protection systems, and they introduce a soil model which is few studied and developed until now. This soil model consists of a homogeneous domain with a finite heterogeneity inside it. The model allows to calculate properly the grounding grids for underground electrical substations. In addition, these developed methods

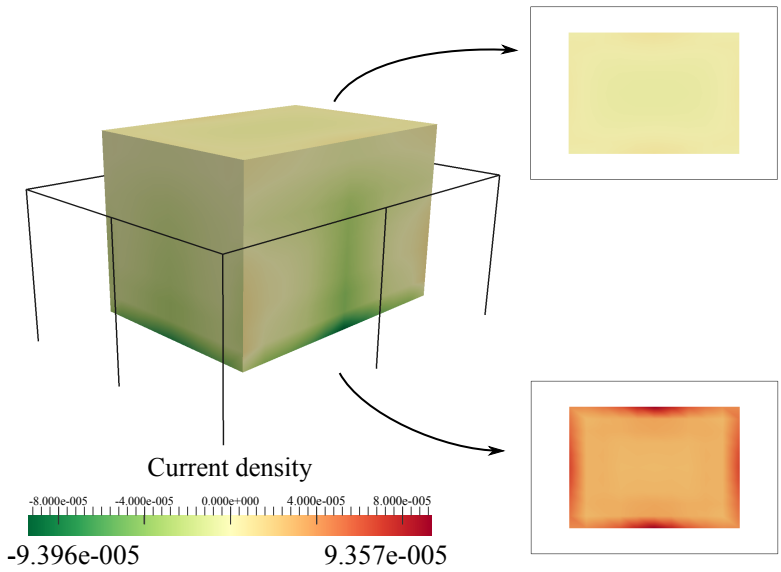

Figure 5.34. Current density distribution over the enclosure for grid configuration 50-35/8/82 and concrete resistivity 8000 Ω m.

allow to obtain the voltage and current density distributions over the enclosure. These distributions allow to do analyses about how affect the concrete resistivity in the main parameters of the grounding grid, as well as to study phenomena as the stray current corrosion in the enclosure reinforcement.

Chapter 6

Conclusions and further research

6.1 Conclusions

This thesis has carried out a mathematical and numerical model that allows to calculate and analyse the main parameters and voltage distributions of grounding systems of underground electrical substations when a fault situation occurs.

The presented work has been divided into the following steps:

Mathematical model

The fault current flowing through a grounding grid has been modelled by means of the steady-state behaviour of the general equations of electromagnetism. Thus, the set of differential equations that govern the physical phenomenon of electric current derivation in a generic conductive medium and in the interface of a non-homogeneous region was obtained. The mathematical formulation was carried out splitting up the problem into the subregions with different electrical properties, which are the ground and the finite volume that represents the underground substation, and applying at each one the set of equations that govern the electric phenomenon. This formulation was developed considering conductive media as isotropic and homogeneous, and the ground surface as horizontal. Then, the model formulated as an exterior and two interior potential problems was recast into three boundary integral equations. These equations provided a way to solve the problem by calculating only the unknowns on the surfaces of the conductors and the underground enclosure. This transformation offers a practical point of view for the numerical analysis. Finally, the equation to calculate the electric potential at any point developed in this thesis provides a boundary integral equation to obtain the surface voltage distributions as well as the touch and step voltages.

From this mathematical model, the following conclusions can be extracted:

- The steady-state behaviour of the general equations of electromagnetism allows to model the fault current flowing through a grounding grid of an underground electrical substation.

- If the conductivities involve in this problem are equal, the boundary integral equation to calculate the electric potential at any point is reduced to a well-known expression for a uniform soil which allows to design and analyse grounding systems of aboveground electrical substations.

Numerical model

The boundary integral equations was solved numerically. To do it, the equations were reformulated into a weak form in order to calculate accurate approximate solutions. In particular, the weighted residual methods based on the Point Collocation and Bubnov-Galerkin were the numerical techniques used to approximate the solution reducing the errors of the global problem to a minimum. The numerical model developed to solve the weak form of boundary integral equations was based on the Boundary Element Method. This *boundary* technique is adequate to solve the problem studied since it is not necessary to mesh unbounded domains as the ground, and it allows to reduce the dimensionality of the problem by one. In order to simplify the model, the leakage current in the electrodes was considered constant around the perimeter of every cross section. This assumption allowed to reduce the integrals over the surface of the electrodes into linear integrals.

From the numerical model, it was extracted that:

- Taking into account the geometry of the conductors in grounding systems, the results obtained are adequate and they are not affected by the assumption of considering the leakage current in the electrodes constant.

- The results between the Point Collocation and Bubnov-Galerkin methods present a divergence due to the different way to vanish the residual functions in the weighted residual methods. It has been showed that if the number of discretisations is increased, this divergence is decreased.

Industrial applications

At the end of this thesis, the principal applications of the numerical approaches developed have been tested. First, the model results were validated for uniform soil assumption with standards and other substations grounding programs, and then, with the software developed by Ormazabal company, which is based on the Spanish standard. Finally, the main parameters and voltage distributions that characterise a grounding system have been calculated for commercial underground electrical substations, which is the principal industrial application of this numerical approach.

The following conclusions are extracted from the industrial applications:

- The results obtained for uniform soil assumption show an excellent agreement with the TOTBEM outcomes, especially the Bubnov-Galerkin Method. Likewise, the outcomes have a good agreement with the IEEE Std 80-2013 benchmarks, and again, the Bubnov-Galerkin Method presents minor discrepancies.

- The model results attained for a commercial underground substation show a divergence between them and the outcomes of amiKIT. This divergence is due to the formulas used by amiKIT are given by the Spanish standard, which considered a uniform soil model, and they do not represent accurately the soil structure.

- The mathematical and numerical models carried out in this thesis provide a practical tool to analyse properly the grounding grid for underground substations since the developed soil model allows to obtain more realistic outcomes.

6.2 Further research

This research has open new lines that one can pursue to extend and improve the model carried out in this thesis to analyse the grounding system of underground electrical substations. A number of the most interesting activities are presented below:

Improve the soil model. A good representation of soil structure is an important point in grounding system analysis. As it was presented, the developed approach considers a uniform soil which contains buried inside it a finite volume with different electrical properties in order to perform the underground substation. The next step is to expand this model to stratified soil structures which allow to introduce more information about the soil resistivity. Due to the urban nature of the places where underground electrical substations are set up, it would be interesting to carry out a soil model that performs not only horizontal and parallel stratums, but also vertical layers. Thus, the soil model would consider urban constructions as underground ground parks, slurry walls or foundations.

Include the steel reinforcements of the precast enclosure in the mathematical model. In the physical and mathematical approach carried out in Chapter 2, the underground electrical substation is performed as a homogeneous finite volume with different electrical properties to the uniform soil. However, the enclosure of these facilities is formed by reinforced concrete structures. One interesting line for future research is to reformulate the model and introduce the steel reinforcements into the finite volume, and so, perform the underground substation as realistic as possible. With this reformulate model, it should be possible to analyse how the steel reinforcements affect the dissipation of a fault current through a grounding grid, and study if it is necessary to connect these steel elements with the grounding system or not.

Analyse the phenomenon of transferred potentials. The transferred potential problem is a serious phenomenon to keep in mind in grounding system analysis. This phenomenon is caused by the flowing of earth leakage current through metal objects located at the surroundings of the substation during a fault situation. Due to that, remote areas away from the facility may experiment induced voltages, and the potential difference may be equal or exceed the Ground Potential Rise in these locations. Thus, areas which are supposed to be safe can present voltage differences high enough to endanger a person who can suffer an electric shock accident. In these situations, the typical danger is caused by a hand-to-feet contact. In urban areas the potentials can be transmitted by elements such as metallic fences, pipes or tramway tracks. Therefore, the analysis of this phenomenon in underground electrical substations is so important since these facilities are surrounded for this kind of elements. Consequently, an interesting research line would be to carry out an approach that allows to introduce the metal elements that surrounds the substation and analyse which areas are affected by the transferred potentials.

Appendix A

Proof of directional derivatives

In this appendix, the relation between the directional derivatives used to simplify the boundary integrals Γ_I and $\Gamma_I^{'}$ in the boundary integral equation of the exterior Dirichlet problem (Subsection 3.3.1) will be proven. This relation is given by

$$\nabla\Big(\frac{1}{r(\boldsymbol{x},\boldsymbol{\xi}_I^{'})}\Big)\cdot\boldsymbol{n}(\boldsymbol{\xi}_I^{'}) = \nabla\Big(\frac{1}{r(\boldsymbol{x}^{'},\boldsymbol{\xi}_I)}\Big)\cdot\boldsymbol{n}(\boldsymbol{\xi}_I) \tag{A.1}$$

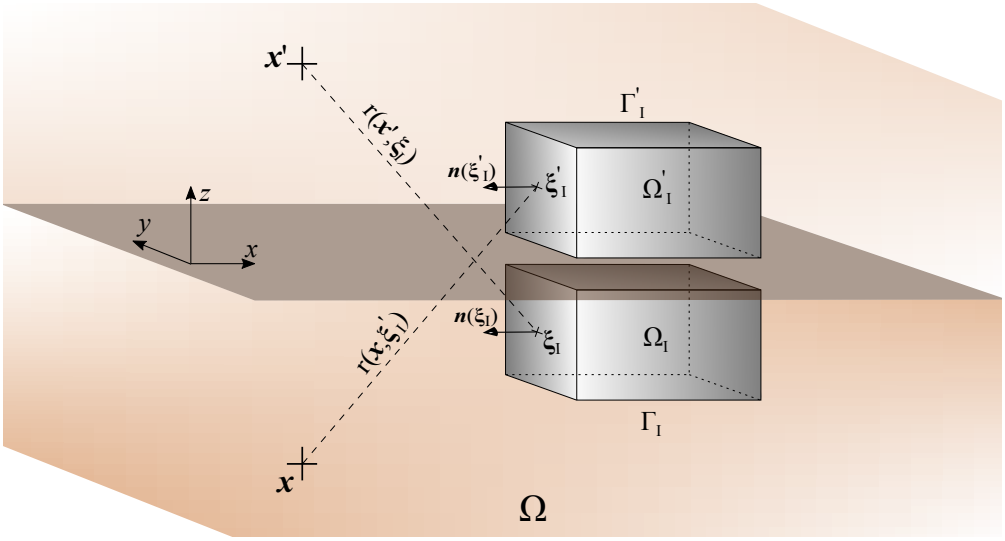

Figure A.1. Schematic representation of the distances and points to proof the relation between the directional derivatives.

In order to prove the above relation, the following is taken into account:
First, the expression on the left-hand side of equation (A.1) will be developed.

Let $\boldsymbol{x}$ be a source point located in domain Ω and $\boldsymbol{\xi}_I^{'}$ be a field point located on the surface of domain $\Omega_I^{'}$, as shown in Figure A.1.

The Euclidean distance between $\boldsymbol{\xi}_I^{'} = (\xi_{Ix}, \xi_{Iy}, \xi_{Iz})$ and any point $\boldsymbol{x} = (x, y, -z)$ is defined as

$$r(\boldsymbol{x}, \boldsymbol{\xi}_I^{'}) = \sqrt{(\xi_{Ix} - x)^2 + (\xi_{Iy} - y)^2 + (\xi_{Iz} + z)^2} \tag{A.2}$$

and its inverse is given by

$$\frac{1}{r(\boldsymbol{x}, \boldsymbol{\xi}_I^{'})} = \frac{1}{\sqrt{(\xi_{Ix} - x)^2 + (\xi_{Iy} - y)^2 + (\xi_{Iz} + z)^2}} \tag{A.3}$$

If the gradient of the inverse of the Euclidean distance (A.3) is calculated, the following vector is obtained

$$\nabla\Big(\frac{1}{r(\boldsymbol{x}, \boldsymbol{\xi}_I^{'})}\Big) = \frac{1}{\Big((\xi_{Ix} - x)^2 + (\xi_{Iy} - y)^2 + (\xi_{Iz} + z)^2\Big)^{3/2}} \Big(\xi_{Ix} - x,\ \xi_{Iy} - y,\ \xi_{Iz} + z\Big) \tag{A.4}$$

Let $\boldsymbol{n}(\boldsymbol{\xi}_I^{'})$ be the outward unit vector normal to the boundary $\Gamma_I^{'}$ (Figure A.1). Its general components are:

$$\boldsymbol{n}(\boldsymbol{\xi}_I^{'}) = (n_x^{'}, n_y^{'}, n_z^{'}) \tag{A.5}$$

Therefore, the expression of the first directional derivative can be written as

$$\nabla\Big(\frac{1}{r(\boldsymbol{x}, \boldsymbol{\xi}_I^{'})}\Big) \cdot \boldsymbol{n}(\boldsymbol{\xi}_I^{'}) = \frac{(\xi_{Ix} - x)n_x^{'} + (\xi_{Iy} - y)n_y^{'} + (\xi_{Iz} + z)n_z^{'}}{\Big((\xi_{Ix} - x)^2 + (\xi_{Iy} - y)^2 + (\xi_{Iz} + z)^2\Big)^{3/2}} \tag{A.6}$$

Now, the same procedure will be done for the expression on the right-hand side of equation (A.1).

Let $\boldsymbol{x}^{'}$ be a source point located in the domain Ω and $\boldsymbol{\xi}_I$ be a field point located on the surface of domain Γ_I, as Figure A.1 depicts.

The Euclidean distance between $\boldsymbol{\xi}_I = (\xi_{Ix}, \xi_{Iy}, -\xi_{Iz})$ and any point $\boldsymbol{x}^{'} = (x, y, z)$ is defined as

$$r(\boldsymbol{x}^{'}, \boldsymbol{\xi}_I) = \sqrt{(\xi_{Ix} - x)^2 + (\xi_{Iy} - y)^2 + (-\xi_{Iz} - z)^2} \tag{A.7}$$

and its inverse is

$$\frac{1}{r(\boldsymbol{x}^{'}, \boldsymbol{\xi}_I)} = \frac{1}{\sqrt{(\xi_{Ix} - x)^2 + (\xi_{Iy} - y)^2 + (-\xi_{Iz} - z)^2}} \tag{A.8}$$

Likewise, the gradient of the inverse of the Euclidean distance (A.8) is given by

$$\nabla\Big(\frac{1}{r(\boldsymbol{x}^{'}, \boldsymbol{\xi}_I)}\Big) = \frac{1}{\Big((\xi_{Ix} - x)^2 + (\xi_{Iy} - y)^2 + (-\xi_{Iz} - z)^2\Big)^{3/2}} \Big(\xi_{Ix} - x,\ \xi_{Iy} - y,\ -\xi_{Iz} - z\Big) \tag{A.9}$$

Let $\boldsymbol{n}(\boldsymbol{\xi}_I)$ be the outward unit vector normal to the boundary Γ_I (Figure A.1). Its general components are

$$\boldsymbol{n}(\boldsymbol{\xi}_I) = (n_x, n_y, n_z) \tag{A.10}$$

And as in the first directional derivative, the expression for the directional derivative on the right-hand side of equation (A.1) can be written as

$$\nabla\Big(\frac{1}{r(\boldsymbol{x}^{'},\boldsymbol{\xi}_I)}\Big)\cdot\boldsymbol{n}(\boldsymbol{\xi}_I)=\frac{(\xi_{Ix}-x)n_x+(\xi_{Iy}-y)n_y+(-\xi_{Iz}-z)n_z}{\Big((\xi_{Ix}-x)^2+(\xi_{Iy}-y)^2+(-\xi_{Iz}-z)^2\Big)^{3/2}} \tag{A.11}$$

As a result, the relation between the directional derivatives (A.1) can be rewritten in terms of (A.6) and (A.11) as

$$\frac{(\xi_{Ix}-x)n_x^{'}+(\xi_{Iy}-y)n_y^{'}+(\xi_{Iz}+z)n_z^{'}}{\Big((\xi_{Ix}-x)^2+(\xi_{Iy}-y)^2+(\xi_{Iz}+z)^2\Big)^{3/2}}=\frac{(\xi_{Ix}-x)n_x+(\xi_{Iy}-y)n_y+(-\xi_{Iz}-z)n_z}{\Big((\xi_{Ix}-x)^2+(\xi_{Iy}-y)^2+(-\xi_{Iz}-z)^2\Big)^{3/2}} \tag{A.12}$$

It should be noted that the equivalence between the two sides of the above relation depends on the value of z component of the unit normal vectors $\boldsymbol{n}(\boldsymbol{\xi}_I^{'})$ and $\boldsymbol{n}(\boldsymbol{\xi}_I)$. In the problem objective of this thesis, domains Ω_I and $\Omega_I^{'}$ are symmetric due to apply the method of images.

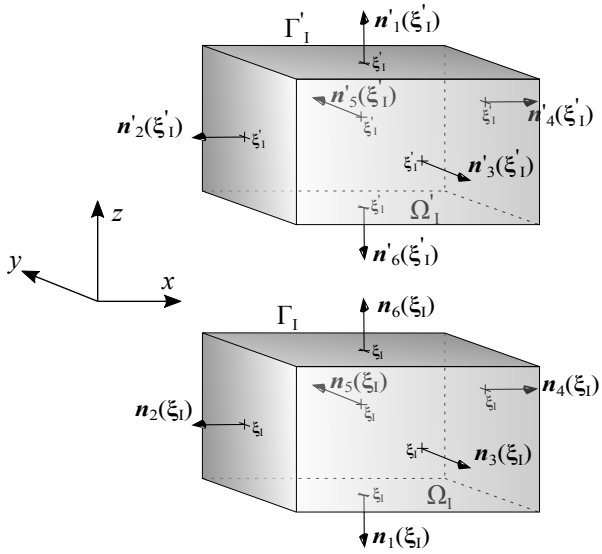

Figure A.2. Schematic representation of a parallelepiped with the vector normal for each side.

As Figure A.2 depicts, each side of the parallelepiped has associated a unit vector. As can be seen, all normal vectors present the same direction and sense between both domains, except normal vectors $\boldsymbol{n}_1$ and $\boldsymbol{n}_6$, which have different sense, and so the following relation can be stated:

$$(n_x,n_y,n_z)=(n_x^{'},n_y^{'},-n_z^{'}) \tag{A.13}$$

Consequently, if this relation is introduced into equation (A.12), the relation between the directional derivatives is verified for this problem:

$$\frac{(\xi_{Ix}-x)n_x^{'}+(\xi_{Iy}-y)n_y^{'}+(\xi_{Iz}+z)n_z^{'}}{\left((\xi_{Ix}-x)^2+(\xi_{Iy}-y)^2+(\xi_{Iz}+z)^2\right)^{3/2}}=\frac{(\xi_{Ix}-x)n_x^{'}+(\xi_{Iy}-y)n_y^{'}+(-\xi_{Iz}-z)(-n_z^{'})}{\left((\xi_{Ix}-x)^2+(\xi_{Iy}-y)^2+(-\xi_{Iz}-z)^2\right)^{3/2}} \tag{A.14}$$

And it can be used to simplify the boundary integrals Γ_I and $\Gamma_I^{'}$.

Apendix B

Extended summary in Spanish

Introducción

Desde su descubrimiento, la electricidad se ha convertido en un elemento básico en nuestro día a día, que ha cambiado y sigue cambiando y mejorando nuestro estilo de vida. En la actualidad, es un elemento indispensable en nuestra rutina diaria que empleamos para actividades tan primordiales como trabajar, comunicarnos o viajar.

La industria eléctrica es la encargada de proporcionar la electricidad a las áreas industriales, comerciales y residenciales. Se divide, fundamentalmente, en tres actividades: generación, transmisión y distribución. En la frontera entre estas actividades se encuentran las subestaciones eléctricas, instalaciones encargadas de transformar la tensión de la energía eléctrica antes de ser transportada y distribuida. Se suelen diferenciar tres tipos de subestaciones: las transformadoras elevadoras, normalmente localizadas en zonas cercanas a los puntos de generación de electricidad, y las transformadoras reductoras y subestaciones de distribución, ubicadas en áreas cercanas a los puntos de consumo. Tradicionalmente, las subestaciones eléctricas son instalaciones que ocupan grandes superficies de terreno y que normalmente presentan impactos medioambientales permanentes en sus emplazamientos.

Como es sabido, la mayoría de los consumidores de electricidad viven y trabajan en las ciudades. En las últimas décadas, las áreas urbanas han experimentado un crecimiento considerable de población llevando asociado un incremento en la demanda y consumo de energía, la necesidad de transmitir electricidad a alto voltaje hasta los centros urbanos, y garantizar en todo momento el suministro eléctrico. Como consecuencia, ha sido, y es necesaria, la construcción de nuevas subestaciones o la ampliación de las existentes. Sin embargo, la construcción de estas instalaciones eléctricas a las afueras de las ciudades se ha convertido en un reto debido a factores como la escasez de espacios libres, el coste de los terrenos urbanos, las restricciones medioambientales

en las zonas urbanas, las elevadas condiciones de seguridad o la no aceptación de este tipo de instalaciones en las cercanías de los hogares.

En vista de esta situación, los ingenieros han diseñado las subestaciones enterradas. Estas subestaciones consisten en soluciones compactas donde todos los equipos eléctricos necesarios para su funcionamiento se encuentran dentro de una envolvente de hormigón prefabricado de dimensiones reducidas. Una característica importante de este diseño de subestaciones enterradas es que el área ocupada en superficie es mínima, lo que las hace prácticamente invisibles para sus vecinos. Satisfaciendo de esta manera los requisitos tanto medioambientales como sociales exigidos actualmente en las áreas urbanas.

Un aspecto esencial a tener en cuenta en las subestaciones eléctricas es la seguridad, especialmente durante las situaciones de fallo. Durante estas situaciones, se debe de garantizar en todo momento el correcto funcionamiento del equipo eléctrico con el fin de minimizar los daños y asegurar la continuidad del suministro eléctrico, sin olvidarse de garantizar la seguridad de las personas o animales que puedan pasar o estar en sus inmediaciones. En las subestaciones eléctricas, los sistemas de tomas de tierra son los dispositivos encargados de garantizar la seguridad mediante la conducción y disipación de corriente eléctrica en el terreno.

Los sistemas de puesta a tierra siempre han tenido un papel importante en las subestaciones debido a que las descargas eléctricas que se producen durante una situación de fallo pueden ser elevadas y producir daños considerables. A consecuencia de la implantación de las subestaciones enterradas en los ámbitos urbanos, donde estas instalaciones se encuentran rodeadas de edificios residenciales, zonas verdes, parques o áreas comerciales, el correcto diseño y análisis de estos sistemas de protección se ha convertido en un elemento fundamental para la seguridad. Los sistemas de tomas de tierra están formados por un conjunto de electrodos enterrados y conectados entre sí que tienen la finalidad de unir al terreno los aparatos eléctricos o estructuras metálicas de una instalación. En general, estas mallas de electrodos conductores están complementadas con picas y electrodos auxiliares para disminuir la tensión eléctrica. Sus objetivos principales son disipar la corriente eléctrica en el terreno en condiciones normales o de fallo de la instalación, para no exceder la tensión límite de los equipos eléctricos y no afectar a la continuidad del servicio, y garantizar la seguridad de las personas y animales que estén en los alrededores de las instalaciones evitando posibles accidentes eléctricos.

Durante una situación de fallo a tierra en una subestación, la corriente eléctrica es disipada al terreno a través de los electrodos que componen el sistema de tomas de tierra, causando la aparición de gradientes de potencial sobre el área que ocupa la instalación y en sus alrededores. Esta aparición de gradientes puede provocar principalmente dos situaciones de contacto accidental. Éstas son la circulación de corriente de un pie a otro y la circulación de corriente de una mano a los pies. La primera se debe a la diferencia de potencial existente entre los pies del individuo, mientras que la segunda es causada por la diferencia de potencial que se produce entre la instalación eléctrica y

el terreno cuando la persona se encuentra sobre el terreno manteniendo algún tipo de contacto con la instalación. Estas diferencias de potencial reciben el nombre de potencial de paso y potencial de contacto, y son dos de los parámetros característicos de los sistemas de tomas de tierra. Otro de los parámetros destacables de estas instalaciones es la sobretensión de tierra (GPR), que se define como el máximo potencial que la red de tomas de tierra puede alcanzar con respecto a un punto suficientemente alejado del terreno.

En general, el análisis de los sistemas de puesta a tierra se realiza mediante las fórmulas proporcionadas por las normas, con las que se calculan las tensiones de paso y contacto de la instalación, y que posteriormente se comparan con los valores máximos tolerables para garantizar la seguridad de las personas. Además de estas fórmulas, la mayoría analíticas y obtenidas experimentalmente, a partir de los años 80 se han desarrollado programas de ordenador para el cálculo y análisis de estos sistemas de protección basadas en técnicas más sofisticadas, que permiten introducir modelos de terreno más próximos a la realidad, y por lo tanto, obtener resultados más precisos y fiables.

Objetivos

El objetivo de esta tesis es el desarrollo de una formulación matemática y numérica para el correcto diseño y análisis de los sistemas de puesta a tierra de las subestaciones eléctricas enterradas. Esta formulación está basada en las ecuaciones generales del electromagnetismo con el fin de estudiar y poder simular el fenómeno físico de la derivación de corriente eléctrica a través del sistema de tomas de tierra. La particularidad de este modelo es que permite introducir las propiedades geométricas y eléctricas de la envolvente de hormigón de las subestaciones enterradas dentro de un terreno uniforme.

Con el fin de obtener este modelo, los siguientes objetivos específicos han sido necesarios:

- Entender el fenómeno físico del problema objeto de estudio.
- Desarrollar un modelo fiable que represente el fenómeno físico estudiado en un terreno uniforme que contiene una heterogeneidad de dimensiones finitas.
- Definir un modelo matemático por medio de las técnicas más adecuadas para transformar el problema potencial descrito por el fenómeno físico.
- Determinar y desarrollar las técnicas numéricas más acordes para resolver el problema en tiempo real teniendo en cuenta las características matemáticas de la formulación.
- Validar el modelo computacional propuesto por medio de diversos casos test y resolver ejemplos reales que permitan verificar la utilidad de la formulación desarrollada.

Metodología

El correcto diseño y análisis de los sistemas de tomas de tierra ha sido objeto de estudio de los ingenieros desde los inicios de las subestaciones eléctricas. En consecuencia, numerosas formulaciones y técnicas numéricas se han desarrollado con el fin de calcular los principales parámetros de estos sistemas de protección y establecer sus niveles de seguridad. Un aspecto importante en el análisis de las tomas de tierra es disponer de modelos que permitan representar la estructura del terreno de la forma más realista posible. Con este fin, en esta tesis se ha propuesto una formulación donde el terreno se ha modelado como un suelo uniforme que contiene en su interior un volumen de dimensiones finitas y de diferentes propiedades eléctricas, que representa la subestación enterrada.

El primer paso para poder desarrollar la formulación es entender la función que realizan las tomas de tierra. Durante una situación de fallo en una subestación eléctrica, la corriente de falta que se origina es derivada al sistema de puesta a tierra y transportada por ésta hasta el terreno donde se disipará, originando como consecuencia un campo de gradientes de potencial. Sus principales parámetros, objeto de cálculo de este desarrollo, son la resistencia equivalente del sistema, las tensiones de paso, contacto y malla, y la distribución de potenciales en la superficie del terreno. Para llevar a cabo este modelo se ha considerado que la atmósfera es un aislante perfecto, que los electrodos que forman la toma de tierra son conductores perfectos, y que el terreno y el volumen que representa la subestación son dominios isótropos y homogéneos con diferentes conductividades eléctricas.

El fenómeno físico descrito se ha formulado mediante las ecuaciones generales del electromagnetismo en su estado estacionario, siendo despreciado el periodo transitorio del fenómeno por ser extremadamente corto en comparación con la duración de la falta. De esta forma, se obtienen las ecuaciones matemáticas que modelan la disipación de corriente eléctrica en un medio conductor y en la frontera entre medios no homogéneos. Estas ecuaciones son aplicadas a cada uno de los dominios que forman parte del problema a estudiar: la atmósfera, el terreno, la subestación eléctrica y el sistema de tomas de tierra. Tras introducir las hipótesis establecidas, el desarrollo de la formulación se centra en el análisis de la disipación de la corriente de falta en el terreno donde se encuentra la subestación enterrada. Al existir dos dominios conductores, el terreno y la subestación, la estrategia seguida consiste en estudiar y plantear sus ecuaciones por separado, y relacionarlos mediante las condiciones de compatibilidad que estarán aplicadas en la envolvente de la subestación. Posteriormente, los sistemas de ecuaciones obtenidos son simplificados mediante la hipótesis de asumir los medios conductores como isótropos y homogéneos, y que la superficie de terreno es horizontal. Como resultado se obtiene que el fenómeno físico objeto de esta investigación se puede formular mediante dos sistemas de ecuaciones definidos por funciones potenciales, estando relacionados entre sí por las condiciones de compatibilidad. Estas condiciones establecen que los valores de los potenciales y las densidades de corriente obtenidos por

ambos problemas deben ser iguales en la superficie de la envolvente de la subestación.

Una vez obtenida la formulación matemática, se decidió transformar el sistema acoplado de ecuaciones diferenciales con el fin de facilitar su posterior resolución mediante técnicas numéricas. Dada la naturaleza del problema, solamente se necesita calcular la densidad de corriente en la superficie de los electrodos, y el potencial y densidad de corriente en la superficie de la envolvente de la subestación. Es por esto que se han reformulado los sistemas de ecuaciones en uno formado por *boundary integral equations*, las cuales están definidas en las superficies de los dominios de los electrodos y la subestación. Esta transformación se consigue mediante la aplicación de la solución fundamental de la ecuación de Laplace y la ecuación que define la segunda identidad de Green. Mediante el empleo de esas expresiones, los sistemas de ecuaciones obtenidos para cada medio conductor son transformados de manera independiente, resultando una ecuación integral para el problema exterior y otra para el problema interior. Para poder acoplar esas ecuaciones integrales y resolver el problema es necesario introducir en ellas las condiciones de compatibilidad y la condición de contorno del problema exterior, obteniendo como resultado un sistema formado por tres *boundary integral equations* que permitirán la resolución del problema. Adicionalmente, se ha obtenido la expresión general que permite calcular el potencial en cualquier punto del terreno, la cual está formulada como una ecuación integral y permitirá calcular la distribución de potenciales en la superficie del mismo.

Finalmente, el sistema de ecuaciones integrales se ha resuelto numéricamente. El método numérico escogido para su resolución ha sido el Método de Elementos de Contorno (BEM), por ser el método más adecuado para la resolución de las *boundary integral equations*. Antes de la aplicación de este método, se han reformulado las ecuaciones a su forma débil; una forma alternativa que permite obtener soluciones aproximadas de manera precisa. Con el objetivo de simplificar estas formas débiles, se ha asumido que la densidad de corriente en los electrodos es uniforme circunferencialmente. Esta hipótesis permite reducir las integrales de superficie sobre los electrodos en integrales de línea, facilitando su posterior resolución. Como se ha indicado, la formulación débil de las *boundary integral equations* se resuelve mediante técnicas de aproximación. En este caso, se ha empleado el método de residuos ponderados, el cual se basa en reducir el error global del problema al mínimo. Entre las diferentes técnicas de residuos ponderados, en esta tesis se han formulado dos modelos numéricos, uno mediante el método de colocación puntual y otro mediante el método de Bubnov-Galerkin, los cuales han sido resueltos por medio del Método de Elementos de Contorno. Tras el desarrollo de ambas formulaciones, se llegan a sendos sistemas de ecuaciones matriciales donde se calcularán las variables densidad de corriente en la superficie de los electrodos y potencial y densidad de corriente en la envolvente de la subestación. El punto más importante en la resolución de estos sistemas matriciales ha sido el cálculo y ensamblaje de los elementos que forman la matriz, la cual está formada por las diferentes integrales de superficie y de línea. Todas las integrales se han calculado numéricamente mediante la cuadratura de Gauss-Legendre, aplicada conjuntamente con otras técnicas para calcu-

lar las integrales singulares y obtener resultados con suficiente precisión. Por último, a partir de los resultados del sistema matricial es posible calcular la distribución de potenciales en superficie, y obtener los principales parámetros que permiten analizar los sistemas de puestas a tierra de las subestaciones eléctricas enterradas.

Conclusiones

Las conclusiones extraídas de la investigación presentada en esta tesis son:

- Las ecuaciones generales del electromagnetismo, bajo la hipótesis de estado estacionario, han permitido formular matemáticamente el fenómeno físico de la disipación de corriente eléctrica a través del sistema de tomas de tierra de las subestaciones eléctricas enterradas.
- Si se suponen iguales las conductividades del terreno y de la envolvente de la subestación, es decir se transforma el problema en uno de propiedades eléctricas homogéneas, la expresión general para calcular el potencial en cualquier punto del terreno se reduce a una expresión idéntica a la desarrollada por Colominas [1995] para suelos uniformes.
- Debido a las características geométricas de los conductores que forman las tomas de tierra, los resultados del modelo no se encuentran afectados por la hipótesis de asumir que la densidad de corriente que emana del contorno de los electrodos es uniforme circunferencialmente.
- Los resultados obtenidos por los modelos desarrollados mediante colocación puntual y Bubnov-Galerkin presentan diferencias entre ellos que son debidas principalmente a la forma que tienen estos métodos de residuos ponderados de anular la función residuo. En esta tesis se ha mostrado que si el número de elementos discretizados en el método de colocación puntual aumenta, la divergencia entre ellos disminuye.
- La validación del modelo desarrollado bajo la hipótesis de suelo uniforme ofrece una excelente coincidencia con los resultados obtenidos por TOTBEM, especialmente la formulación del método de Bubnov-Galerkin. Del mismo modo, el modelo fue contrastado con los *benchmarks* descritos en la norma IEEE Std 80-2013, presentando una buena coincidencia entre los resultados y siendo de nuevo la formulación de Bubnov-Galerkin la que presenta menores discrepancias.
- Los resultados validados con el programa amiKIT para el análisis de las tomas de tierra de subestaciones compactas enterradas muestran una divergencia entre ambas aplicaciones. Esta divergencia es debida a que el software amiKIT está basado en las fórmulas de la norma española RD 337/2014 para las instalaciones de puesta a tierra, las cuales consideran el terreno como un medio uniforme y no representan con precisión el análisis de las subestaciones enterradas.

Por último, los modelos matemáticos y numéricos desarrollados en esta tesis proporcionan una herramienta práctica para analizar de manera apropiada los sistemas de puesta a tierra de las subestaciones enterradas, desarrollando un modelo que representa las heterogeneidades presentes en el terreno y proporciona resultados más ajustados a la realidad.

Futuras líneas de investigación

Esta tesis ha abierto nuevas líneas de trabajo con el fin de ampliar y mejorar el modelo matemático y numérico propuesto para el análisis de los sistemas de protección de las subestaciones eléctricas enterradas. A continuación se resumen las más interesantes.

Mejora del modelo de terreno. Disponer de una buena representación del terreno es uno de los aspectos más importantes en el análisis de las tomas de tierra. En esta tesis, el modelo desarrollado consiste en un terreno homogéneo en el que se encuentra enterrado un volumen de dimensiones finitas con diferentes propiedades eléctricas, el cual representa la subestación. El siguiente paso es mejorar este modelo de manera que se puedan representar terrenos estratificados, introduciendo de esta forma mayor información sobre la resistividad del medio. Debido al carácter urbano de este tipo de subestaciones es interesante desarrollar modelos multicapa tanto horizontales como verticales. Así, se podrá tener en cuenta en el análisis de los sistemas de protección la existencia de elementos urbanos que pueden rodear estas instalaciones eléctricas, como aparcamientos subterráneos, pantallas o cimentaciones de edificios.

Incluir las armaduras de la envolvente de hormigón en el modelo matemático. En el modelo físico-matemático desarrollado en esta investigación, la subestación compacta es modelada como un volumen homogéneo de dimensiones finitas. Sin embargo, en general, la envolvente de estas instalaciones está formada por un monobloque prefabricado de hormigón armado, es decir un volumen de propiedades heterogéneas. Una línea interesante de investigación es reformular el modelo planteado para introducir las armaduras de la estructura prefabricada. Así, se podrá analizar el efecto de dichas armaduras en la disipación de corriente a lo largo de las tomas de tierra durante una situación de fallo, y estudiar si es necesaria la conexión de estos elementos al sistema de protección o no.

Análisis del fenómeno de potenciales transferidos. La posible transferencia de potenciales es un fenómeno importante a tener en cuenta en el análisis de los sistemas de tomas de tierra. Este fenómeno está causado por el flujo de corriente eléctrica a través de objetos metálicos que se encuentran en las inmediaciones de las subestaciones, pudiendo aparecer potenciales inducidos en zonas lejanas a las instalaciones eléctricas. Estos potenciales inducidos originan diferencias de potenciales que pueden ser iguales o superiores a la sobretensión de tierra (GPR) en zonas que se suponían seguras por estar

alejadas del punto de descarga eléctrica, con la posible consecuencia de que la diferencia de potencial sea suficientemente elevada como para causar accidentes eléctricos en personas o animales. En estas situaciones, el accidente se debe normalmente al circuito mano-pie. En las zonas urbanas, ubicación preferente de las subestaciones enterradas, la corriente eléctrica disipada por los sistemas de protección puede ser transmitida por elementos metálicos como vallas, tuberías de los servicios urbanos o los raíles de los tranvías. Por ello, el análisis de potenciales transferidos en este tipo de subestaciones es importante. Por lo tanto, una línea de investigación importante es el desarrollo del modelo matemático y numérico que permita introducir elementos metálicos en las inmediaciones de las subestaciones y analizar qué áreas se ven afectadas por potenciales inducidos.

Apendix C

Extended summary in Galician

Introdución

Desde o seu descubrimento, a electricidade converteuse nun elemento básico no noso día a día, que cambiou e segue cambiando e mellorando o noso estilo de vida. Na actualidade, é un elemento indispensable na nosa rutina diaria que empregamos para actividades tan primordiais como traballar, comunicarnos ou viaxar.

A industria eléctrica é a encargada de proporcionar a electricidade ás áreas industriais, comerciais e residenciais. Divídese, fundamentalmente, en tres actividades: xeración, transmisión e distribución. Na fronteira entre estas actividades atópanse as subestacións eléctricas, instalacións encargadas de transformar a tensión da enerxía eléctrica antes de ser transportada e distribuída. Adóitanse diferenciar tres tipos de subestacións: as transformadoras elevadoras, normalmente localizadas en zonas próximas aos puntos de xeración de electricidade, e as transformadoras redutoras e subestacións de distribución, situadas en áreas próximas aos puntos de consumo. Tradicionalmente, as subestacións eléctricas son instalacións que ocupan grandes superficies de terreo e que normalmente presentan impactos ambientais permanentes nos seus emprazamentos.

Como é sabido, a maioría dos consumidores de electricidade viven e traballan nas cidades. Nas últimas décadas, as áreas urbanas experimentaron un crecemento considerable de poboación levando asociado un incremento na demanda e consumo de enerxía, a necesidade de transmitir electricidade a alto voltaxe ata os centros urbanos, e garantir en todo momento a subministración eléctrica. Como consecuencia, foi, e é necesaria, a construción de novas subestacións ou a ampliación das existentes. Con todo, a construción destas instalacións eléctricas nos arredores das cidades converteuse nun reto debido a factores como a escaseza de espazos libres, o custo dos terreos urbanos, as restricións ambientais nas zonas urbanas, as elevadas condicións de seguridade ou a non aceptación deste tipo de instalacións nas proximidades dos fogares.

En vista desta situación, os enxeñeiros deseñaron as subestacións enterradas. Estas subestacións consisten en solucións compactas onde todos os equipos eléctricos necesarios para o seu funcionamento atópanse dentro dunha envolvente de formigón prefabricado de dimensións reducidas. Unha característica importante deste deseño de subestacións enterradas é que a área ocupada en superficie é mínima, o que as fai practicamente invisibles para os seus veciños. Satisfacendo desta maneira os requisitos tanto ambientais como sociais esixidos actualmente nas áreas urbanas.

Un aspecto esencial a ter en conta nas subestacións eléctricas é a seguridade, especialmente durante as situacións de fallo. Durante estas situacións, débese de garantir en todo momento o correcto funcionamento do equipo eléctrico co fin de minimizar os danos e asegurar a continuidade da subministración eléctrica, sen esquecerse de garantir a seguridade das persoas ou animais que poidan pasar ou estar nas súas inmediacións. Nas subestacións eléctricas, os sistemas de tomas de terra son os dispositivos encargados de garantir a seguridade mediante a condución e disipación de corrente eléctrica no terreo.

Os sistemas de posta a terra sempre tiveron un papel importante nas subestacións debido a que as descargas eléctricas que se producen durante unha situación de fallo poden ser elevadas e producir danos considerables. A consecuencia da implantación das subestacións enterradas nos ámbitos urbanos, onde estas instalación atópanse rodeadas de edificios residenciais, zonas verdes, parques ou áreas comerciais, o correcto deseño e análise destes sistemas de protección converteuse nun elemento fundamental para a seguridade. Os sistemas de tomas de terra están formados por un conxunto de eléctrodos enterrados e conectados entre si que teñen a finalidade de unir ao terreo os aparellos eléctricos ou estruturas metálicas dunha instalación. En xeral, estas mallas de eléctrodos condutores están complementados con picas e eléctrodos auxiliares para diminuír a tensión eléctrica. Os seus obxectivos principais son disipar a corrente eléctrica no terreo en condicións normais ou de fallo da instalación para non exceder a tensión límite dos equipos eléctricos e non afectar á continuidade do servizo, e garantir a seguridade das persoas e animais que estean nos arredores das instalacións evitando posibles accidentes eléctricos.

Durante unha situación de fallo a terra nunha subestación, a corrente eléctrica é disipada ao terreo a través dos eléctrodos que compoñen o sistema de tomas de terra, causando a aparición de gradientes de potencial sobre a área que ocupa a instalación e nos seus arredores. Esta aparición de gradientes pode provocar principalmente dúas situacións de contacto accidental. Estas son a circulación de corrente dun pé a outro e a circulación de corrente dunha man aos pés. A primeira débese a diferenza de potencial existente entre os pés do individuo, mentres que a segunda é causada pola diferenza de potencial que se produce entre a instalación eléctrica e o terreo cando a persoa atópase sobre o terreo mantendo algún tipo de contacto coa instalación. Estas diferenzas de potencial reciben o nome de potencial de paso e potencial de contacto, e son dous dos parámetros característicos dos sistemas de tomas de terra. Outro dos parámetros destacables destas instalacións é a sobretensión de terra (GPR), que se define como o

máximo potencial que a rede de tomas de terra pode alcanzar con respecto a un punto suficientemente afastado do terreo.

En xeral, a análise dos sistemas de posta a terra realízase mediante as fórmulas proporcionadas polas normas, coas que se calculan as tensións de paso e contacto da instalación, e que posteriormente se comparan cos valores máximos tolerables para garantir a seguridade das persoas. Ademais destas fórmulas, a maioría analíticas e obtidas experimentalmente, a partir dos anos 80 desenvolvéronse programas de computador para o cálculo e análise destes sistemas de protección baseadas en técnicas máis sofisticadas, que permiten introducir modelos de terreo máis próximos á realidade, e por tanto, obter resultados máis precisos e fiables.

Obxectivos

O obxectivo desta tese é o desenvolvemento dunha formulación matemática e numérica para o correcto deseño e análise dos sistemas de posta a terra das subestacións eléctricas enterradas. Esta formulación está baseada nas ecuacións xerais do electromagnetismo co fin de estudar e poder simular o fenómeno físico da derivación de corrente eléctrica a través do sistema de tomas de terra. A particularidade deste modelo é que permite introducir as propiedades xeométricas e eléctricas da envolvente de formigón das subestacións enterradas dentro dun terreo uniforme.

Co fin de obter este modelo, os seguintes obxectivos específicos foron necesarios:

- Entender o fenómeno físico do problema obxecto de estudo.
- O desenvolvemento dun modelo fiable que represente o fenómeno físico estudado nun terreo uniforme que contén unha heteroxeneidade de dimensións finitas.
- Definir un modelo matemático por medio das técnicas máis adecuadas para transformar o problema potencial descrito polo fenómeno físico.
- Determinar e desenvolver as técnicas numéricas máis acordes para resolver o problema en tempo real tendo en conta as características matemáticas da formulación.
- Validar o modelo computacional proposto por medio de diversos casos test e resolver exemplos reais que permitan verificar a utilidade da formulación desenvolvida.

Metodoloxía

O correcto deseño e análise dos sistemas de toma de terra foi obxecto de estudo dos enxeñeiros desde os inicios das subestacións eléctricas. En consecuencia, numerosas formulacións e técnicas numéricas desenvolvéronse co fin de calcular os principais parámetros destes sistemas de protección e establecer os seus niveis de seguridade. Un aspecto

importante na análise das tomas de terra é dispoñer de modelos que permitan representar a estrutura do terreo da forma máis realista posible. Con este fin, nesta tese propúxose unha formulación onde o terreo é modelado como un solo uniforme que contén no seu interior un volume de dimensións finitas e de diferentes propiedades eléctricas que representa a subestación enterrada.

O primeiro paso para poder desenvolver a formulación é entender a función que realizan as tomas de terra. Durante unha situación de fallo nunha subestación eléctrica, a corrente de falta que se orixina é derivada ao sistema de posta a terra e transportada por esta ata o terreo onde se disipará, orixinando como consecuencia un campo de gradientes de potencial. Os seus principais parámetros, obxecto de cálculo deste desenvolvemento, son a resistencia equivalente do sistema, as tensións de paso, contacto e malla, e a distribución de potenciais na superficie do terreo. Para levar a cabo este modelo considerouse que a atmosfera é un illante perfecto, que os eléctrodos que forman a toma de terra son condutores perfectos, e que o terreo e o volume que representa a subestación son dominios isótropos e homoxéneos con diferentes condutividades eléctricas.

O fenómeno físico descrito formulouse mediante as ecuacións xerais do electromagnetismo no seu estado estacionario, sendo desprezado o período transitorio do fenómeno por ser extremadamente curto en comparación coa duración da falta. Desta forma, obtéñense as ecuacións matemáticas que modelan a disipación de corrente eléctrica nun medio condutor e na fronteira entre medios non homoxéneos. Estas ecuacións son aplicadas a cada un dos dominios que forman parte do problema a estudar: a atmosfera, o terreo, a subestación eléctrica e o sistema de tomas de terra. Tras introducir as hipóteses establecidas, o desenvolvemento da formulación céntrase na análise da disipación da corrente de falta no terreo onde se atopa a subestación enterrada. Ao existir dous dominios condutores, o terreo e a subestación, a estratexia seguida consiste en estudar e expor as súas ecuacións por separado, e relacionalos mediante as condicións de compatibilidade que estarán aplicadas na envolvente da subestación. Posteriormente, os sistemas de ecuacións obtidos son simplificados mediante a hipótese de asumir os medios condutores como isótropos e homoxéneos, e que a superficie do terreo é horizontal. Como resultado obtense que o fenómeno físico obxecto desta investigación pódese formular mediante dous sistemas de ecuacións definidos por funcións potenciais, estando relacionados entre si polas condicións de compatibilidade. Estas condicións establecen que os valores dos potenciais e as densidades de corrente obtidos por ambos problemas deben ser iguais na superficie da envolvente da subestación.

Unha vez obtida a formulación matemática, decidiuse transformar o sistema acoplado de ecuacións diferenciais co fin de facilitar a súa posterior resolución mediante técnicas numéricas. Dada a natureza do problema, soamente necesítase calcular a densidade de corrente na superficie dos eléctrodos, e o potencial e densidade de corrente na superficie da envolvente da subestación. É por isto que se reformularon os sistemas de ecuacións nun formado por *boundary integral equations*, as cales están definidas nas superficies dos dominios dos eléctrodos e da subestación. Esta transformación conséguese

mediante a aplicación da solución fundamental da ecuación de Laplace e a ecuación que define a segunda identidade de Green. Mediante o emprego desas expresións, os sistemas de ecuacións obtidos para cada medio condutor son transformados de maneira independente, resultando unha ecuación integral para o problema exterior e outra para o problema interior. Para poder acoplar esas ecuacións integrais e resolver o problema é necesario introducir nelas as condicións de compatibilidade e a condición de contorno do problema exterior, obtendo como resultado un sistema formado por tres *boundary intregral equations* que permitirán a resolución do problema. Adicionalmente, obtívose a expresión xeral que permite calcular o potencial en calquera punto do terreo, a cal está formulada como unha ecuación integral e permitirá calcular a distribución de potenciais na superficie do mesmo.

Finalmente, o sistema de ecuacións integrais resolveuse numericamente. O método numérico escollido para a súa resolución foi o Método de Elementos de Contorno (BEM), por ser o método máis adecuado para a resolución de *boundary integral equations*. Antes da aplicación deste método, reformuláronse as ecuacións na súa forma débil; unha forma alternativa que permite obter solucións aproximadas de maneira precisa. Co obxectivo de simplificar estas formas débiles, asumiuse que a densidade de corrente nos eléctrodos é uniforme circunferencialmente. Esta hipótese permite reducir as integrais de superficie sobre os eléctrodos en integrais de liña, facilitando a súa posterior resolución. Como se indicou, a formulación débil das *boundary integral equations* resólvese mediante técnicas de aproximación. Neste caso, empregouse o método de residuos ponderados, o cal se basea en reducir o erro global do problema ao mínimo. Entre as diferentes técnicas de residuos ponderados, nesta tese formuláronse dous modelos numéricos, un mediante o método de colocación puntual e outro mediante o método de Bubnov-Galerkin, os cales foron resoltos por medio do Método de Elementos de Contorno. Tras o desenvolvemento de ambas formulacións chéganse a senllos sistemas de ecuacións matriciais onde se calcularán as variables densidade de corrente na superficie dos eléctrodos e potencial e densidade de corrente na envolvente da subestación. O punto máis importante na resolución destes sistemas matriciais foi o cálculo e ensamblaxe dos elementos que forma a matriz, a cal está formada polas diferentes integrais de superficie e de liña. Toda as integrais calculáronse numericamente mediante a cuadratura de Gauss-Legendre, aplicada conxuntamente con outras técnicas para calcular as integrais singulares e obter resultados con suficiente precisión. Por último, a partir dos resultados do sistema matricial é posible calcular a distribución de potenciais en superficie, e obter os principais parámetros que permiten analizar os sistemas de posta a terra das subestacións eléctricas enterradas.

Conclusións

As conclusións extraídas da investigación presentada nesta tese son:

- As ecuacións xerais do electromagnetismo, baixo a hipótese de estado estacionario, permitiron formular matematicamente o fenómeno físico da disipación de

corrente eléctrica a través do sistema de tomas de terra das subestacións eléctricas enterradas.

- Se se supoñen iguais as condutividades do terreo e da envolvente da subestación, é dicir transfórmase o problema nun de propiedades eléctricas homoxéneas, a expresión xeral para calcular o potencial en calquera punto do terreo redúcese a unha expresión idéntica á desenvolvida por Colominas [1995] para solos uniformes.

- Debido ás características xeométricas dos condutores que forman as tomas de terra, os resultados do modelo non se atopan afectados pola hipótese de asumir que a densidade de corrente que emana do contorno dos eléctrodos é uniforme circunferencialmente.

- Os resultado obtidos polos modelos desenvolvidos mediante colocación puntual e Bubnov-Galerkin presentan diferenzas entre eles que son debidas principalmente á forma que teñen este métodos de residuos ponderados de anular a función residuo. Nesta tese mostrouse que se o número de elementos discretizados no método de colocación puntual aumenta, a diverxencia entre eles diminúe.

- A validación do modelo desenvolvido baixo a hipótese de solo uniforme ofrece unha excelente coincidencia cos resultados obtidos por TOTBEM, especialmente a formulación do método de Bubnov-Galerkin. Do mesmo xeito, o modelo foi contrastado cos *benchmarks* descritos na norma IEEE Std 80-2013, presentando unha boa coincidencia entre os resultados e sendo de novo a formulación de Bubnov-Galerkin a que presenta menores discrepancias.

- Os resultados validados co programa amiKIT para a análise das tomas de terra de subestacións compactas enterradas mostran unha diverxencia entre ambas aplicacións. Esta diverxencia é debida a que o software amiKIT está baseado nas fórmulas da norma española RD 337/2014 para as instalacións de posta a terra, as cales consideran o terreo como un medio uniforme e non representan con precisión a análise das subestacións enterradas.

Por último, os modelos matemáticos e numéricos desenvolvidos nesta tese proporcionan unha ferramenta práctica para analizar de maneira apropiada os sistemas de posta a terra das subestacións enterradas, desenvolvendo un modelo que representa as heteroxeneidades presentes no terreo e proporciona resultados máis axustados á realidade.

Futuras liñas de investigación

Esta tese abre novas liñas de traballo co fin de ampliar e mellorar o modelo matemático e numérico proposto para a análise dos sistemas de protección das subestacións eléctricas enterradas. A continuación resúmense as máis interesantes.

Mellora do modelo de terreo. Dispoñer dunha boa representación do terreo é un dos aspectos máis importantes na análise das tomas de terra. Nesta tese, o modelo desenvolvido consiste nun terreo homoxéneo no que se atopa enterrado un volume de dimensións finitas con diferentes propiedades eléctricas, o cal representa a subestación. O seguinte paso é mellorar este modelo de maneira que se poidan representar terreos estratificados, introducindo desta forma maior información sobre a resistividade do medio. Debido ao carácter urbano deste tipo de subestacións é interesante desenvolver modelos multicapa tanto horizontais como verticais. Así, poderase ter en conta na análise dos sistemas de protección a existencia de elementos urbanos que poden rodear estas instalacións eléctricas, como aparcadoiros subterráneos, pantallas ou cimentacións de edificios.

Incluír as armaduras da envolvente de formigón no modelo matemático. No modelo físico-matemático desenvolvido nesta investigación, a subestación compacta é modelada como un volume homoxéneo de dimensións finitas. Con todo, en xeral, a envolvente destas instalacións está formada por un monobloque prefabricado de formigón armado, é dicir un volume de propiedades heteroxéneas. Unha liña interesante de investigación é reformular o modelo exposto para introducir as armaduras da estrutura prefabricada. Así, poderase analizar o efecto das devanditas armaduras na disipación de corrente ao longo das tomas de terra durante unha situación de fallo, e estudar se é necesaria a conexión destes elementos ao sistema de protección ou non.

Análise do fenómeno de potenciais transferidos. A posible transferencia de potenciais é un fenómeno importante a ter en conta na análise dos sistemas de tomas de terra. Este fenómeno está causado polo fluxo de corrente eléctrica a través de obxectos metálicos que se atopan nas inmediacións das subestacións, podendo aparecer potenciais inducidos en zonas afastadas ás instalacións eléctricas. Estes potenciais inducidos orixinan diferenzas de potenciais que poden ser iguais ou superiores á sobretensión de terra (GPR) en zonas que se supoñían seguras por estar afastadas do punto de descarga eléctrica, coa posible consecuencia de que a diferenza de potencial sexa suficientemente elevada como para causar accidentes eléctricos en persoas ou animais. Nestas situacións, o accidente débese normalmente ao circuíto man-pé. Nas zonas urbanas, localización preferente das subestacións enterradas, a corrente eléctrica disipada polos sistemas de protección pode ser transmitida por elementos metálicos como valos, tubaxes dos servizos urbanos ou os raís dos tranvías. Por iso, a análise de potenciais transferidos neste tipo de subestacións é importante. Por tanto, unha liña de investigación importante é o desenvolvemento do modelo matemático e numérico que permita introducir elementos metálicos nas inmediacións das subestacións e analizar que áreas se ven afectadas por potenciais inducidos.

Bibliography

Aliabadi, M. H. (2002). *The Boundary Element Method. Volume 2: Applications in Solids and Structures*. Wiley. ↑86 , ↑90

Aneiros Blanco, J. M. (1996). Desarrollo de una formulación numérica para el cálculo y diseño de tomas de tierra de subestaciones eléctricas incorporando un modelo de terreno de dos capas. Master's thesis, Universidade da Coruña. ↑118

Beer, G. (2001). *Programming the boundary element method: An introduction for Engineers*. Wiley. ↑38

Beer, G., Smith, I., & Duenser, C. (2008). *The Boundary Element Method with Programming: For Engineers and Scientists*. Springer. ↑87

Bertolini, L., Carsana, M., & Pedeferri, P. (2007). Corrosion behaviour of steel in concrete in the presence of stray current. *Corrosion Science*, 49(3), 1056–1068. ↑151

Bertolini, L., Elsener, B., Pedeferri, P., Redaellu, E., & Polder, R. B. (2013). *Corrosion of Steel in Concrete: Prevention, Diagnosis, Repair*. Wiley. ↑151 , ↑153

Brebbia, C. A. & Dominguez, J. (1992). *Boundary elements: An introductory course*. WIT Press. ↑38 , ↑75

Cheng, A. H.-D. & Cheng, D. T. (2005). Heritage and early history of the boundary element method. *Engineering Analysis with Boundary Elements*, 29(3), 268–302. ↑77

Colominas, I. (1995). *Cálculo y diseño asistido por ordenador de tomas de tierra en instalaciones elèctricas: una formulación numérica basada en el método integral de elementos de contorno*. PhD thesis, Universidade da Coruña. ↑27 , ↑28 , ↑61 , ↑62 , ↑66 , ↑69 , ↑72 , ↑90 , ↑116 , ↑118 , ↑123 , ↑172 , ↑180

Colominas, I., Gómez-Calviño, J., Navarrina, F., & Casteleiro, M. (2001). Computer analysis of earthing systems in horizontally or vertically layered soils. *Electric Power Systems Research*, 59(3), 149–156. ↑9

Colominas, I., Navarrina, F., & Casteleiro, M. (1999). A boundary element numerical approach for grounding grid computation. *Computer Methods in Applied Mechanics and Engineering*, 174(1-2), 73–90. ↑8

Colominas, I., Navarrina, F., & Casteleiro, M. (2002). A numerical formulation for grounding analysis in stratified soils. *IEEE Transactions on Power Delivery*, 17(2), 587–595. ↑9

Colominas, I., Navarrina, F., & Casteleiro, M. (2007). Numerical simulation of transferred potentials in earthing grids considering layered soil models. *IEEE Transactions on Power Delivery*, 22(3), 1514–1522. ↑8

Dalziel, C. F. (1946). Dangerous electric currents. *AIEE Transactions on Power Apparatus and Systems*, 65(8), 579–585. ↑5

Dalziel, C. F. (1953). A study of the hazards of impulse currents. *AIEE Transactions on Power Apparatus and Systems*, 72(2), 1032–1043. ↑5

Dalziel, C. F. (1972). Electric shock hazard. *IEEE Spectrum*, 9(2), 41–50. ↑5

Dalziel, C. F. & Lee, W. R. (1969). Lethal electric currents. *IEEE Spectrum*, 6(2), 44–50. ↑5

Dawalibi, F. & Mukhedkar, D. (1975). Optimum design of substation grounding in a two layer earth structure. part i - analytical study. *IEEE Transactions on Power Apparatus and Systems*, 94(2), 252–261. ↑8

Dawalibi, F. & Mukhedkar, D. (1976). Multi step analysis of interconnected grounding electrodes. *IEEE Transactions on Power Apparatus and Systems*, 95(1), 113–119. ↑8

Dawalibi, F. & Mukhedkar, D. (1977). Resistance calculation of interconnected grounding electrodes. *IEEE Transactions on Power Apparatus and Systems*, 96(1), 59–65. ↑7

Dawalibi, F. & Mukhedkar, D. (1979). Influence of ground rods on grounding grids. *IEEE Transactions on Power Apparatus and Systems*, PAS-98(6), 2089–2098. ↑8

Dawalibi, F. P. & Blattner, C. J. (1984). Earth resistivity measurement interpretation techniques. *IEEE Transactions on Power Apparatus and Systems*, PAS-103(2), 374–382. ↑26

Dawalibi, F. P. & Donoso, F. (1993). Integrated analysis software for grounding, emf, and emi. *IEEE Computer Applications in Power*, 6(2), 19–24. ↑8

Dawalibi, F. P., Ma, J., & Southey, R. D. (1994). Behaviour of grounding systems in multilayer soils: a parametric analysis. *IEEE Transactions on Power Delivery*, 9(1), 334–342. ↑9

Dawalibi, F. P., Southey, R. D., & Baishiki, R. S. (1990). Validity of conventional approaches for calculating body currents resulting from electric shocks. *IEEE Transactions on Power Delibery*, 5(2), 613–626. ↑5

Dwight, H. B. (1936). Calculation of resistances to ground. *AIEE Transactions (Electrical Engineering)*, 55(12), 1319–1328. ↑7

Fischnaller, H. (2009). Numerical integration - an introduction for the boundary element method. Master project, Institute for Structural Analysis. Graz University of Technology. ↑93

Fortin, S., Mitskevitch, N., & Dawalibi, F. P. (2015). Analysis of grounding systems in horizontal multilayer soils containing finite heterogeneities. *IEEE Transactions on Industry Applications*, 51(6), 5095–5100. ↑9

Freschi, F. & Mitolo, M. (2017). Currents passing through the human body: The numerical viewpoint. *IEEE Transactions on Industry Applications*, 53(2), 826–832. ↑5

Freschi, F., Mitolo, M., & Tartaglia, M. (2013). An effective semianalytical method for simulating grounding grids. *IEEE Transactions on Industry Applications*, 49(1), 256–263. ↑8

General Instructions for PFS-62 (2008). *General instructions for PFS-62 underground transformer substations*. Ormazabal's Technical-Commercial department. ↑128

Ghoneim, S. S. M. (2013). Charge and current simulation method with boundary element method for grounding system calculations in case of multi-layer soil. *IOSR Journal of Engineering (IOSR-JEN)*, 3(6), 14–22. ↑8

Ghoneim, S. S. M. & Shoush, K. A. (2013). Analytical methods for earth surface potential calculation for grounding grids. *International Journal of Engineering and Computer Science IJECS-IJENS*, 13(3), 47–53. ↑8

Güemes-Alonso, J. A. & Hernando-Fernández, F. E. (2004). Method for calculating the ground resistance of grounding grids using FEM. *IEEE Transactions on Power Delivery*, 19(2), 595–600. ↑8

Güemes-Alonso, J. A., Hernando-Fernández, F. E., Rodríguez-Bona, F., & Ruiz-Moll, J. M. (2006). A practical approach for determining the ground resistance of grounding grids. *IEEE Transactions on Power Delivery*, 21(3), 1261–1266. ↑8

Guzina, B. B., Pak, R. Y., & Martínez-Castro, A. E. (2006). Singular boundary elements for three-dimensional elasticity problems. *Engineering Analysis with Boundary Elements*, 30(8), 623–639. ↑87 , ↑89

Hajiaboli, A., Fortin, S., Dawalibi, F. P., Zhao, H., & Ngoly, A. (2015). Analysis of grounding systems in the vicinity of hemispheroidal heterogeneities. *IEEE Transactions on Industry Applications*, 51(6), 5070–5077. ↑9

Hansen, G. A., Douglass, R. W., & Zardecki, A. (2005). *Mesh Enhancement: Selected Elliptic Methods, Foundations and Applications*. Imperial College Press. ↑75

Hughes, T. J. R. (1987). *The finite element method.* Prentice-Hall,Inc. ↑32 , ↑65 , ↑76

IEC TS 60479-1 (2016). *Effects of current on human beings and livestock - Part 1: General aspects.* International Electrotechnical Comission. ↑6

IEC TS 60479-2 (2017). *Effects of current on human beings and livestock - Part 2: Special aspects.* International Electrotechnical Comission. ↑6

IEEE 100 (2000). *IEEE 100 The Authoritative Dictionay of IEEE Standards Terms.* IEEE Power and Energy Society. ↑1 , ↑5

IEEE Std 80 (2013). *IEEE Guide for Safety in AC Substation Grounding.* IEEE Power and Energy Society. ↑XI , ↑5 , ↑6 , ↑7 , ↑18 , ↑26 , ↑123 , ↑124 , ↑125 , ↑126 , ↑127

IEEE Std 81 (2012). *IEEE Guide for Measuring Earth Resistivity, Ground Impedance, and Earth Surface Potentials of a Grounding System.* IEEE Power and Energy Society. ↑26

Kellogg, O. D. (1929). *Foundations of potential theory.* Springer. ↑32 , ↑34

Kouwenhoven, W. B., Knickerbocker, G. G., Chesnut, R. W., Milnor, W. R., & Sass, D. J. (1959). Ac shocks of varying parameters affecting the heart. *AIEE Transactions on Power Apparatus and Systems*, 78(2), 163–169. ↑5

Lachat, J. C. & Watson, J. O. (1976). Effective numerical treatment of boundary integral equations: a formulation for three-dimensional elastostatics. *International Journal for Numerical Methods in Engineering*, 10(5), 991–1005. ↑93

Lagace, P. J., Fortin, J., & Crainic, E. D. (1996). Interpretation of resistivity sounding measurements in N-layer soil using electrostatic images. *IEEE Transactions on Power Delivery*, 11(3), 1349–1354. ↑26

Lagace, P. J., Vuong, M. H., Lefebvre, M., & Fortin, J. (2006). Multilayer resistivity interpretation and error estimation using electrostatic images. *IEEE Transactions on Power Delivery*, 21(4), 1954–1960. ↑26

Lee, H.-S., Kim, J.-H., Dawalibi, F. P., & Ma, J. (1998). Efficient ground grid designs in layered soils. *IEEE Transactions on Power Delivery*, 13(3), 745–751. ↑9

Lee, W. R. (1966). Death from electric shock. *Proceedings of the IEEE*, 113(1), 144–148. ↑6

Li, Z.-X., Fan, J.-B., & Chen, W.-J. (2007). Numerical simulation of substation grounding grids buried in both horizontal and vertical multilayer earth model. *International Journal for Numerical Methods in Engineering*, 69(11), 2359–2380. ↑9

Liu, Y. (2009). *Fast multipole boundary element method*. Cambridge. ↑38

Lorrain, P., Corson, D. R., & Lorrain, F. (1988). *Electromagnetic Fields and Waves*, chapter Maxwell's Equations. W. H. Freeman and Company. ↑16 , ↑28

Ma, J. & Dawalibi, F. P. (2000). Analysis of grounding systems in soils with cylindrical soil volumes. *IEEE Transactions on Power Delivery*, 15(3), 913–918. ↑9

Ma, J. & Dawalibi, F. P. (2002). Analysis of grounding systems in soils with finite volumes of different resistivities. *IEEE Transactions on Power Delivery*, 17(2), 596–602. ↑9

Ma, J., Dawalibi, F. P., & Daily, W. K. (1993). Analysis of grounding systems in soils with hemispherical layering. *IEEE Transactions on Power Delivery*, 8(4), 1773–1781. ↑9

Ma, J., Dawalibi, F. P., & Southey, R. D. (1996). On the equivalence of uniform and two-layer soils to multilayer soils in the analysis of grounding systems. *IEE Proceedings - Generation, Transmission and Distribution*, 143(1), 49–55. ↑9

Maxwell, J. C. (1873). *A treatise of electricity and magnetism*. Oxford. ↑28

Meliopoulos, A. P. & Papalexpoulos, A. D. (1986). Interpretation of soil resistivity measurements: Experience with the model SOMIP. *IEEE Transactions on Power Delivery*, 1(4), 142–151. ↑26

Melipoulos, A. P. S., Xia, F., Joy, E. B., & Cokkinides, G. J. (1993). An advanced computer model for grounding system analysis. *IEEE Transactions on Power Delivery*, 8(1), 13–23. ↑8

Nahman, J. & Salamon, D. (1984). Analytical expressions for the resistance of grounding grids in nonuniform soil. *IEEE Transactions on Power Apparatus and Systems*, PAS-103(4), 880–885. ↑7

Nahman, J. & Salamon, D. (1988). A practical method for the interpretation of earth resistivity data obtained from driven rod tests. *IEEE Transactions on Power Delivery*, 3(4), 1375–1379. ↑26

Ong, E. T. & Lim, K. M. (2005). Three-dimensional singular boundary elements for corner and edge singularities in potential problems. *Engineering Analysis with Boundary Elements*, 29(2), 175–189. ↑87

Patterson, C. & Sheikh, M. (1984). *Topics in Boundary Element Research*, chapter Interelement Continuity in the Boundary Element Method. Springer US. ↑86 , ↑87

Pérez-Gavilán, J. J. (2004). Cubaturas para integrales singulares e hipersingulares del tipo de galerkin. In *III Congreso Internacional sobre Métodos Numéricos en Ingeniería y Ciencias Aplicadas*. ↑112

RD 337/2014 (2014). *Reglamento sobre condicione técnicas y garantías de seguridad en instalaciones eléctricas de alta tensión y sus Instrucciones Técnicas Complementarias ITC-RAT 01 a 23*. Ministerio de Industria, Energía y Turismo. ↑XIII , ↑6 , ↑26 , ↑123 , ↑128 , ↑129 , ↑138 , ↑140 , ↑145 , ↑148

Rüdenberg, R. (1945). Grounding principles and practice I- fundamental considerations on ground currents. *Electrical Engineering*, 64(1), 1–13. ↑26

Schwarz, S. J. (1954). Analytical expressions for the resistance of grounding systems. *AIEE Transactions on Power Apparatus and Systems*, 73(13), 1011–1016. ↑7

Shen, J. & Sterz, O. (1998). A mixed galerkin and collocation approach for treating edge and corner problems in the boundary element method. *IEEE Transactions on Magnetics*, 34(5), 3296–3299. ↑86

Southey, R. D., Siahrang, M., Fortin, S., & Dawalibi, F. P. (2015). Using Fall-of-Potential measurements to improve deep soil resistivity estimates. *IEEE Transactions on Industry Applications*, 51(6), 5023–5029. ↑26

Staelin, D. H. (2011). *Electromagnetics and Applications*, chapter Introduction to Electrodynamics. MIT. ↑17

Subia, S. R. & Ingber, M. S. (1995). A comparison of the semidiscontinuous element and multiple node with auxiliary boundary collocation approaches for the boundary element method. *Engineering Analysis with Boundary Elements*, 15(1), 19–27. ↑86

Sverak, J. G. (1998). Progress in step and touch voltage equations of ansi/ieee std 80-historical perspective. *IEEE Transactions on Power Delivery*, 13(3), 762–767. ↑7

Sverak, J. G., Dick, W. K., Dodds, T. H., & Heppe, R. H. (1981). Safe substation grounding-part I. *IEEE Transactions on Power Apparatus and Systems*, PAS-100(9), 4281–4291. ↑7

Trlep, M., Hamler, A., & Hribernik, B. (1998). The analysis of complex grounding systems by FEM. *IEEE Transactions on Magnetics*, 34(5), 2521–2524. ↑8

Trlep, M., Hamler, A., Jesenik, M., & Stumberger, B. (2003). The fem-bem analysis of complex grounding systems. *IEEE Transactions on Magnetics*, 39(3), 1155–1158. ↑8

UNESA (1989). *Método de cálculo y proyecto de instalaciones de puesta a tierra para centros de transformación conectados a redes de tercera categoría.* ↑129 , ↑130 , ↑131 , ↑137 , ↑140 , ↑148 , ↑152 , ↑153

Wenner, F. (1916). A method of measuring earth resistivity. *Bulletin of the Bureau of Standards*, 12(3), 469–482. ↑26

Wrobel, L. C. (2002). *The Boundary Element Method. Volume 1: Applications in Thermo-Fluids and Acoustics*. Wiley. ↑34 , ↑38

Zienkiewicz, O. C., Taylor, R. L., & Zhu, J. Z. (2013). *The Finite Element Method: Its Basis and Fundamentals*. Elservier. ↑64 , ↑75